2015

Experimental and numerical analysis of thin spray-on liner materials for use in underground mines

Qiuqiu Qiao
University of Wollongong

Experimental and numerical analysis of thin spray-on liner materials for use in underground mines

A thesis submitted in fulfilment of the

requirements for the award of the degree

DOCTOR OF PHILOSOPHY

from

UNIVERSITY OF WOLLONGONG

By

Qiuqiu Qiao

School of Civil, Mining and Environmental Engineering

Faculty of Engineering and Information Sciences

2015

CERTIFICATION

I, Qiuqiu Qiao, declare that this thesis, submitted in fulfilment of the requirements for the award of Doctor of Philosophy, in the School of Civil, Mining and Environmental Engineering, Faculty of Engineering and Information Sciences, University of Wollongong, is wholly my own work except where specific references or acknowledgements are made. The thesis has not been submitted for qualifications at any other academic institution.

Qiuqiu Qiao

June 2015

LIST OF Publications

Journal articles:

- **Qiao Q,** Nemcik J, and Porter I (2015). A new approach for determination of the shear bond strength of thin spray-on liners. *International Journal of Rock Mechanics and Mining Science* **73**: 54-61. http://dx.doi.org/10.1016/j.ijrmms.2014.09.23.
- **Qiao Q,** Nemcik J, and Porter I (2014). Shear strength testing of glass fibre reinforced thin spray-on liner. *Geotechnique Letters* **4**: 250-254, http://dx.doi.org/10.1680/geolett.14.00057.
- **Qiao Q,** Nemcik J, Porter I and Baafi E (2014). Laboratory investigation on support mechanism of thin spray-on liner for pillar reinforcement. *Geotechnique Letters* **4**: 317-321, http://dx.doi.org/10.1680/geolett.14.00076.
- **Qiao Q,** Nemcik J, Porter I and Baafi E (2014). Laboratory tests on thin spray-on liner penetrated rock joints in direct shear. *Rock Mechanics and Rock Engineering*, http://dx.doi.org/10.1007/s00603-014-0669-7.
- Zhang Z, Nemcik J, **Qiao Q** and Geng X. (2014). A model for water flow through rock fractures based on friction factor. *Rock Mechanics and Rock Engineering*, http://dx.doi.org/10.1007/s00603-014-0562-4.

Conference articles:

- **Qiao Q,** Nemcik J, Porter I, and Baafi E (2015). Compressive strength testing of thin spray-on liner. 15th Coal Operators Conference (pp. 199-204). Australia: University of Wollongong.
- **Qiao Q**, Nemcik J, Porter I, Baafi E, Zhang Z and Shan Z (2014). Development of testing methods of thin spray-on liner shear-bond strength. In R. Alejano, A. Perucho, C. Olalla & R. Jimenez (Eds.), Proceedings of EUROROCK: Rock Engineering and Rock Mechanics: Structures in and on Rock Masses (pp. 125-130). United Kingdom: Taylor & Francis Group.
- Shan Z, Porter I, Nemcik J and **Qiao Q** (2014). Effect of different curing conditions on the compressive and flexural properties of Plaster of Paris, 14th Coal Operators' Conference, University of Wollongong, The Australasian Institute of Mining and Metallurgy & Mine Managers Association of Australia, 103-108.

ACKNOWLEDGEMENTS

I wish to express my sincere gratitude to my thesis supervisor Dr Jan Nemcik, Faculty of Engineering and Information Sciences, University of Wollongong, for his supervision, generous support, encouragement, and guidance provided during the research.

I would also like to express my sincere thanks to Associate Professor Ian Porter, my thesis co-supervisor for his helpful advice in this thesis, and also providing the necessary support to conduct my research during my studies in Australia. I am also grateful for the support and help of Professor Naj. I. Aziz, Associate Professor Ernest Baafi, and Associate Professor Ting Ren.

I also would like to thank the technical staff in the School of Civil, Mining and Environmental Engineering, especially Col Devenish and Alan Grant, for their laboratory assistance.

A special thank is given to Bob Kininmonth for his final correction of grammatical and spelling errors.

Forever, I am indebted to my family members my father, mother and, especially my beloved wife. Without their love and support, I would never reach this point.

ABSTRACT

Steel mesh that is currently used in underground coal mines is of a passive nature and in most cases does not contribute to roadway skin reinforcement. Steel mesh is a safety device that is only effective in supporting detached pieces of rock or severely fractured rock mass experiencing large displacements. As a relatively new form of rock support Thin Spray-on Liners (TSLs) are currently being investigated as an effective skin support technology. Research indicates that TSLs may provide superior rock skin control. Being a pro-active support technique, it is known that a TSL is able to provide resistance to even small rock movements and thus significantly improve rock skin stability.

TSLs have the potential to increase roadway development rates because their application in conjunction with rock bolts can be automated. In addition, TSLs can be sprayed remotely, thereby improving personnel safety while providing resistance to small rock deformations. TSL materials have thus been attracting attention from both research organisations and industry.

In order to investigate and compare the compressive strength of glass fibre reinforced TSL developed at the University of Wollongong, a compression test was developed using cube samples of 40 mm in size. The effect of a small amount of glass fibre in the polymer matrix was tested. The test results indicate that the compressive strength and the material stiffness of the cube samples increased with the increase of glass fibre. All samples exhibited a ductile stress strain curve as they had a yield point and a fracture point. The ductile TSL yield characteristics are very important as sudden brittle failure is considered unsafe for mining practices.

In order to investigate the shear strength of glass fibre reinforced TSLs, an improved punch test was developed. The steel ring was replaced by the TSL plates, and four screws were used to tighten the TSL sample between the clamping plates to ensure stable and symmetrical loading. Four different glass fibre contents were tested to evaluate the effect of glass fibre reinforcement on the shear strength of TSLs. The effect of loading rate was also studied. The results suggest that the steel punch can shear through the polymer sheet and the failure mode is easily identified. The results are consistent and easily calculated. The shear strength increased as the glass fibre content increased. The TSL material samples showed good linear behaviour prior to reaching the ultimate load and post failure behaviour that reflects the fibre reinforcement of failed resin during the yielding stage of the sample which is beneficial to the support in underground mines. Although there may be some impact of the shearing rate on the shear strength, the effect is negligible for the loading rates used.

Shear bond strength is one of the most important properties for TSLs. The adhesion between the polymer liner and rock surface can confine the rock movement immediately after spraying. In order to better evaluate the shear bond strength of polymer liner and thereby assess its geotechnical function in strata skin reinforcement, an innovative testing method was proposed, and compared with two previous testing methods. The shear bond strength test included a polymer ring 5 mm thick and 15 mm wide coated on the periphery of each cored sample. In order to eliminate the effect of normal stress onto the substrate, the polymer ring was partitioned into four segments. The polymer ring was then sheared off each rock core with a steel sleeve and shear bond strength determined. The test results indicate that this testing procedure enable even loading of all TSL segments until failure, which can minimize the effect of

normal stress induced by shrinkage on the shear bond strength, thereby improving the accuracy in assessing the shear bond strength of TSL materials. In this study, three types of substrate and two TSL products were selected when performing the tests.

To assess its geotechnical function in strata surface reinforcement, tensile bond strength must be evaluated as it is one of the most important TSL properties that contribute to the quality of reinforcement. The adhesion between the polymer liner and the rock surface can confine the rock movement immediately after the TLS sets forming a composite layer that reinforces the rock skin. In this study, modifications and improvements were made in the process of sample preparation. The effect of loading rates, TSL thickness, rock types and environmental conditions on the tensile bond strength of polyester-based TSL material were investigated. The test results indicate that for low loading rates ranging from 0.5 mm/min to 2 mm/min the effect of loading rates can be ignored while for higher loading rates of up to 10 mm/min, the tensile bond strength increases. The data analyses indicate that the tensile bond strength of the polymer-based TSL material is inversely proportional to the square root of the TSL thickness. The results also demonstrate that TSL material adheres better to dry rocks while adhesion to wet rocks decreased to approximately 65-75% of the dry adhesion. The TSL can bond to the surface of rock or coal forming a composite layer that reinforces the rock skin. The data indicate that the tensile bond strength may increase with the tensile strength of rock substrates.

To assess its geotechnical function in rock skin reinforcement, shear behaviour of TSL that penetrated rock joints was evaluated as it is one of the important TSL properties that contribute to the quality of reinforcement. The adhesion between the fast setting polymer TSL liner and the rock surface can confine the rock movement immediately

after the TLS sets. To test this the polymeric TSL was bonded to high strength gypsum plaster samples of various surface asperities representing surface roughness and sheared under the constant normal stiffness load. All of the tested samples failed in shear through the high strength gypsum plaster rather than along the plaster-polymer interface indicating a very strong shear bond between the materials. Test results revealed that for all tested roughness the shear stress increases with the applied normal stress. In addition, the shear strength decreased as the TSL thickness increased. The investigation also showed that the shear stress decreased with the increase of shear rate. Surfaces of higher roughness indicated a slight increase in shear strength.

To study the reinforcement provided by TSL when applied onto the strata surface, the support mechanism of TSL coated rock samples was investigated thereby providing a basis for studying the effect of TSL confinement of pillars. A polymeric material liner was applied to three types of rock, siltstone, sandstone and granite. The detailed procedure for sample preparation and loading procedures are described. Results of rock failure tests indicated that significant strength improvement and enhancement of post failure characteristics developed for the TSL encapsulated samples. The TSL reinforcement of the weaker rocks appears to be better than reinforcement of the stronger rocks. It is concluded that the case when the tensile strength of the TSL material is greater than the tensile strength of rock leads to an effective rock reinforcement. In contrast, the TSL reinforcement of stronger rock types may not be as effective.

A 3-dimensional numerical model was used to simulate the TSL reinforcement of coal pillar corner with and without the TSL reinforcement. The modelling results show that

the modelled maximum displacement of the unreinforced pillar corner was almost three times higher than that observed at the TSL reinforced corner.

Vertical stress in the yielded part of the coal pillar reinforced with TSL was significantly higher than vertical stress in the unreinforced pillar. This is due to the effectiveness of the TSL generating confining stress at the pillar surface. Thus TSL makes the pillar significantly stronger especially at the pillar corner. This is important not only for the pillar design and rib stability but also for minimising the roadway intersection spans and thus providing better roof stability above the intersections.

TABLE OF CONTENTS

LIST OF FIGURES

LIST OF TABLES

CHAPTER 1 INTRODUCTION

1.1 Background

Mining plays an important role in Australian economy with up to 60 % of exports being from mining resources. To meet the increasing needs of coal for export and local industry, and to maintain high profit margins, it is essential to increase productivity. Many mining systems need to be improved however some improvements are essential if production is to increase. One of the key systems to improve production in underground coal mines is gate roadway development rates which often lag behind the retreating longwall face leading to significant financial losses.

When mine roadways are excavated, the *in situ* stress equilibrium is disturbed and strata displacement takes place until a new equilibrium is reached. Stress concentrations or relief around mine roadways can cause significant displacements of strata that need to be controlled. The magnitudes of stress can be controlled by orienting the roadways in a desirable direction however, some strata damage will always occur especially at great depth. Strata movement cannot be prevented but can be controlled. Strata control usually consists of rock bolt reinforcement as the primary support while steel mesh is used as a skin support. Secondary support consists mainly of cable bolts and other systems specific to each mine.

For the safety of personnel working at the face, the severely fractured roof needs to be supported as soon as possible. According to Hoek and Brown (1980), it is difficult to support the dead weight of rocks when the rock mass has loosened. The main aim of modern support is to reinforce the fractured rock to prevent large displacements and enable the strata to support itself. Rock bolts are very efficient in reinforcing the rock

mass however the bolt plates cannot always provide effective support to the exposed rock skin. If the unsupported rock skin is fractured, it can readily fall causing a safety hazard. Loss of rock skin that occurs between the bolts can also undermine the integrity of rock bolting. The current most widely used skin support method is steel wire mesh which has been successfully used in underground coal mines for many years. The purpose of the steel mesh is to support the fractured rock fragments when they part from the strata. According to Villaecusa (2004), steel mesh acts as a passive skin support that restricts fall of loose rocks in order to protect the safety of personnel working at the face. However, as a passive support method, it can be effective in supporting the roof only when the roof deforms and large displacements occur. In underground coal mines the installation of steel mesh is labour intensive, and is difficult to automate. In addition, underground personnel are frequently injured while installing rock support. While the installation of rock bolts or other tendon support elements can be mechanized, mesh installation still requires manual labour. One effective method for overcoming disadvantages of mesh is the use of shotcrete, in particular, steel fibre reinforced shotcrete. The use of shotcrete rapidly gained acceptance within many Canadian mines in the 1990's and is now commonly used elsewhere. However, shotcrete is very slow to cure and therefore not suitable for rock surface support in the fast advancing coal mine roadways.

In order to solve this problem, the application of Thin Spray-on Liner (TSL) has been proposed by many researchers. This type of support material can be sprayed onto a rock surface and thus it can be automated. The advantage of TSL is the strong bond to the surface of rock or coal forming a composite layer that reinforces the rock skin as

shown in Figure 1.1. Therefore, TSL is a pro-active support method and can restrict the movement of fractured rock fragments immediately.

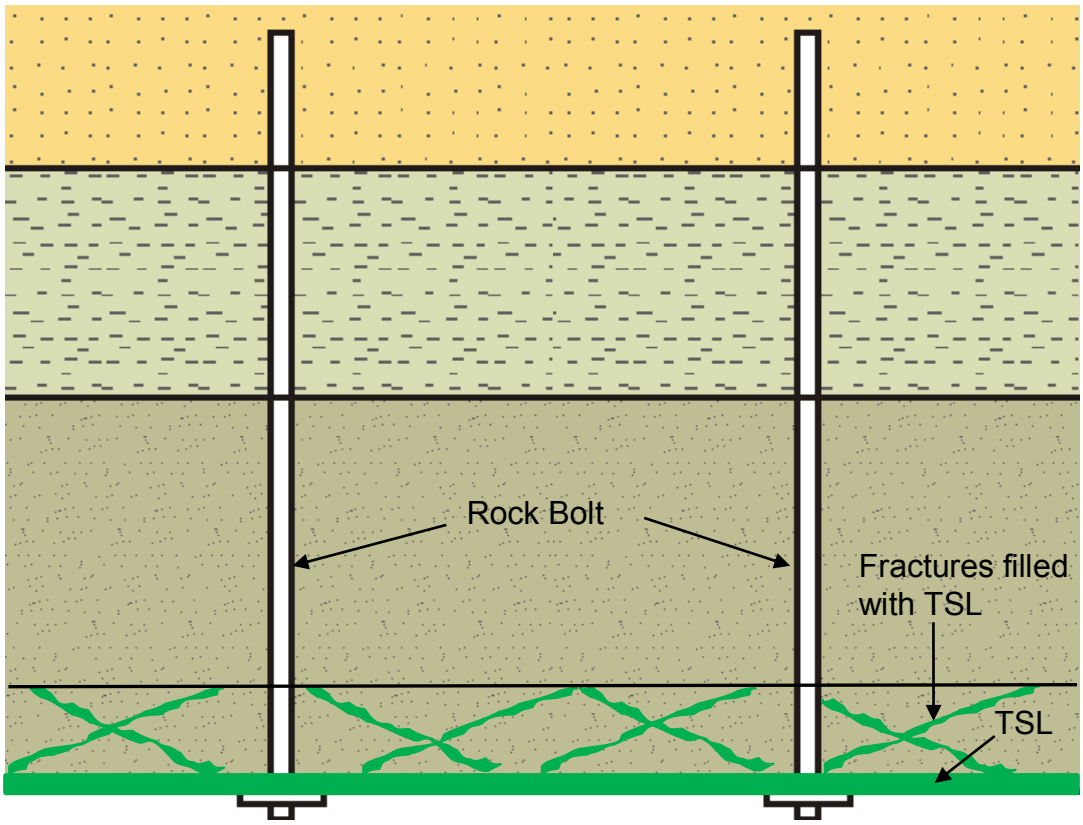

Figure 1. 1 Schematic representation of the reinforced TSL-Rock composite layer in roof strata

As an alternative to rock bolts, mesh or shotcrete, Mining Industry Research Organization of Canada (MIROC) began an investigation of rapid setting, TSL materials for ground support. The first tests on TSL rock support technology were initiated in Canada in the late 1980's (Archibald *et al.* 1992).

Conventional support in the hard-rock mining industry makes use of rock bolts or other tendon support to hold large key blocks in place while wire mesh is used to retain the small rock pieces between the tendons. In some cases, shotcrete is used in a dual

role for supporting both larger rock blocks keyed together as well as smaller pieces of loose rock.

Shotcrete, polymer liners, and steel mesh mobilize support resistance at different displacements. Materials that are sprayed onto the rock such as shotcrete or liners are able to generate support resistance at small rock deformations (in the order of mm). Mesh it a truly passive support and requires substantial displacement (in the order of 100's of mm) before it offers a support resistance (Tannant 1995, Tannant et al. 1997). Mesh is effective at catching and holding small rock falls, but it provides minimal resistance to the initiation of the rock fall itself. Sprayed materials operate differently because they are able to offer support resistance at small displacements. They minimise fracture opening and unravelling of broken rock mass and therefore can prevent rock falls from occurring in the first place. Shotcrete, especially reinforced shotcrete, can generate much higher support resistance than thin polymer liners, however, in situations where large ground convergence occurs, the more flexible thin liners may provide better support over the full range of rock deformations. According to Tannant (2001), TSL materials are receiving attention from the mining industry around the world as an emerging alternative skin support for underground mines. He stated that the characteristics of a TSL lie between steel mesh and shotcrete.

For automation of underground coal mine roadways fast set TSL curing time is essential. While the polymeric materials can set in seconds, shotcrete takes hours to harden. Smaller quantities of material are brought underground in comparison to shotcrete. Reduced usage of TSL materials results in less material handling and thus reduced logistical problems of transport and handling. Application time is shorter as compared to shotcrete.

A decision was made to study the suitability of TSL for Australian coal mines.

1.2 Key Objectives of this Research

- Investigate the weakness and limitations of currently available TSLs through literature review.
- Review and evaluate the past experiments devised to test the newly developed skin reinforcement TSL material at the University of Wollongong (UOW).
- Develop a new shear strength testing method for determining the shear strength of the TSL.
- Refine the tensile bond strength by testing the adhesion of fibre reinforced polymer liner to various types of rock under wet and dry conditions.
- Develop a new shear bond strength testing method for determining the shear-bond strength of fibre reinforced polymer liner by testings the adhesion to various types of rock under wet and dry conditions.
- Conduct laboratory tests on TSL infilled rock joints in direct shear.
- Conduct laboratory investigation on support mechanism of TSL for pillar reinforcement.
- Numerical study on the coal pillar corner reinforced with TSL material.

1.3 Thesis layout

Chapter 1 presents the general introduction and key objectives of this thesis.

Chapter 2 reviews the stress in underground roadways, the roadway failure modes in underground mines, strata support of mining, and the research related to TSLs.

Chapter 3 describes the testing of compressive and shear strength of TSL. A new shear strength testing method was developed and is discussed.

Chapter 4 presents the tensile bond and shear bond strength of TSL. A new testing approach to determine the shear and tensile bond strength of TSL materials is detailed.

Chapter 5 presents the laboratory tests on TSL infilled joints in direct shear.

Chapter 6 discusses the laboratory investigation on support mechanism of TSL for pillar reinforcement.

Chapter 7 presents the numerical simulation of a coal pillar corner comparing the unsupported and TSL reinforced coal surface displacements.

Chapter 8 presents conclusions drawn in this thesis and recommendations for future research.

CHAPTER 2 LITERATURE REVIEW

2.1 Stress in underground mines

To identify the effect and the role of TSLs as a viable method to support the roadways in underground coal mines it is essential to understand stress environments that exist within the mine. Strata underground are subjected to the gravitational (vertical) and horizontal stresses. Figure 2.1 shows a typical *in situ* stress field as experienced underground.

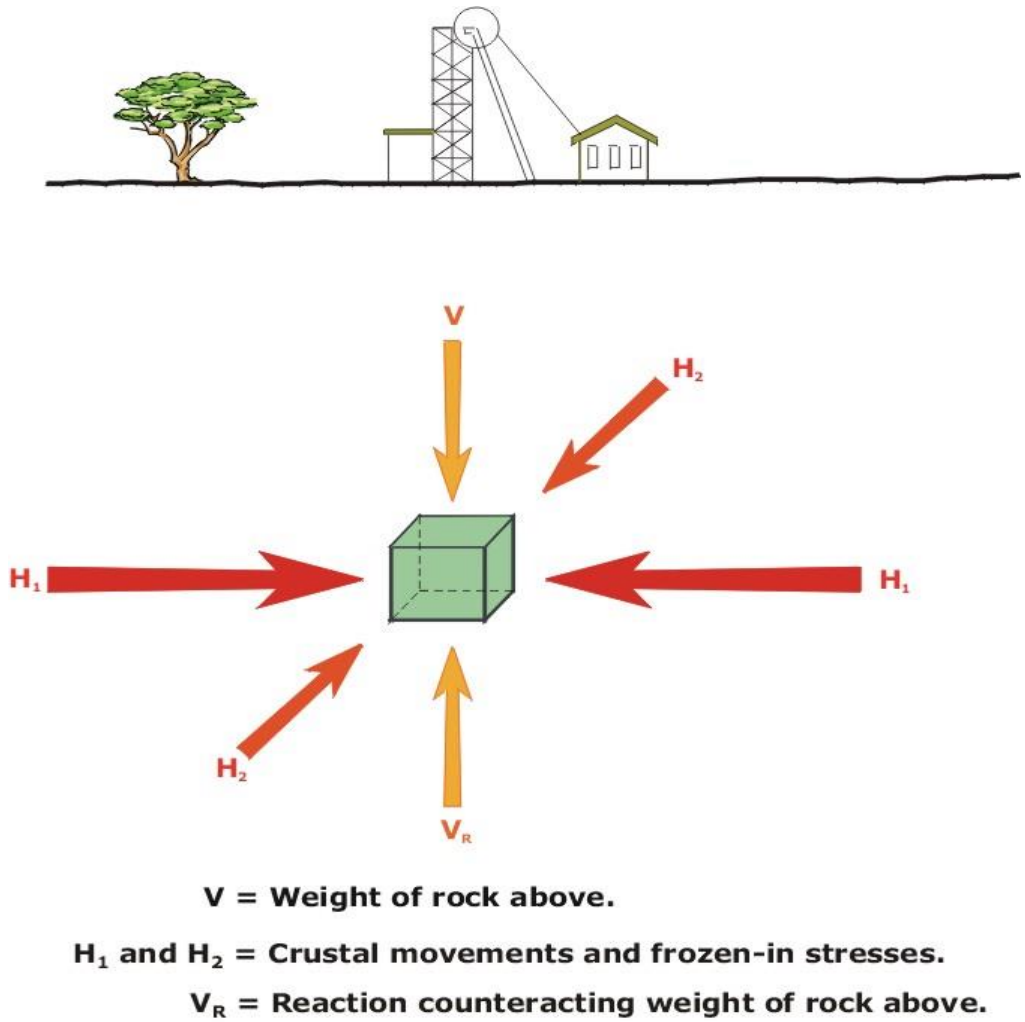

Figure 2. 1 A typical *in situ* stress field as experienced underground (Nemcik 2014)

2.1.1 Gravitational (Vertical) stress

Gravitational stresses are the stresses caused by the weight of the overlying rock mass (Nemcik, 2014). The magnitude of the gravitational stress depends on the depth and the density of the overlying rock and in general can be calculated using the following equation:

$$\sigma_v = \sum_{i=1}^{i=n} \gamma_i h_i \tag{2.1}$$

Where σ_v = Vertical Stress

γ = unit weight of the individual rock layer

h = rock layer thickness

The Earth's crust consists of sedimentary and igneous rocks of which the sedimentary strata form about 70%. Both rock types consist mainly of silica with density of 2.65 and therefore the *in situ* weight of both rocks is close to 25 kN/m^3. The weight of rock layers is in most cases similar and it is possible to use the average unit weight of the rock layers to describe the magnitude of the vertical stress under the overlying rock using Equation (2.1).

From the above equation, it can be seen that the magnitude of vertical stress increases with depth. The vertical stresses caused by the overlying rocks concentrate at the excavation sides and thus affect the ribs of the underground roadways. Relief of the vertical stress is experienced at the roof level of the mine roadway due to redirection of the vertical stress around the roadway. Figure 2.2 shows the stress path around underground openings.

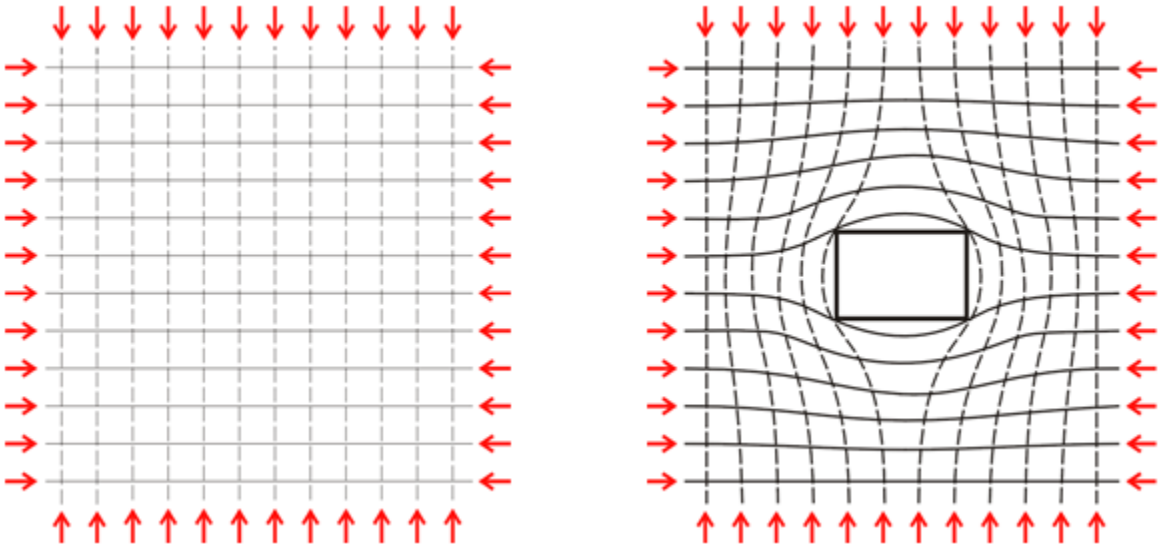

(a) No opening (before mining) (b) Opening (after mining)

Figure 2. 2 Stresses around an underground opening (Nemcik 2014)

2.1.2 Horizontal Stress

In most cases the *in situ* horizontal stress has two components. The smaller component is due to the Poisson's ratio effect of stresses in other directions while the larger component is typically contributed by the tectonic stress. The components of the horizontal stress in the Earth's crust are shown in Figure 2.3.

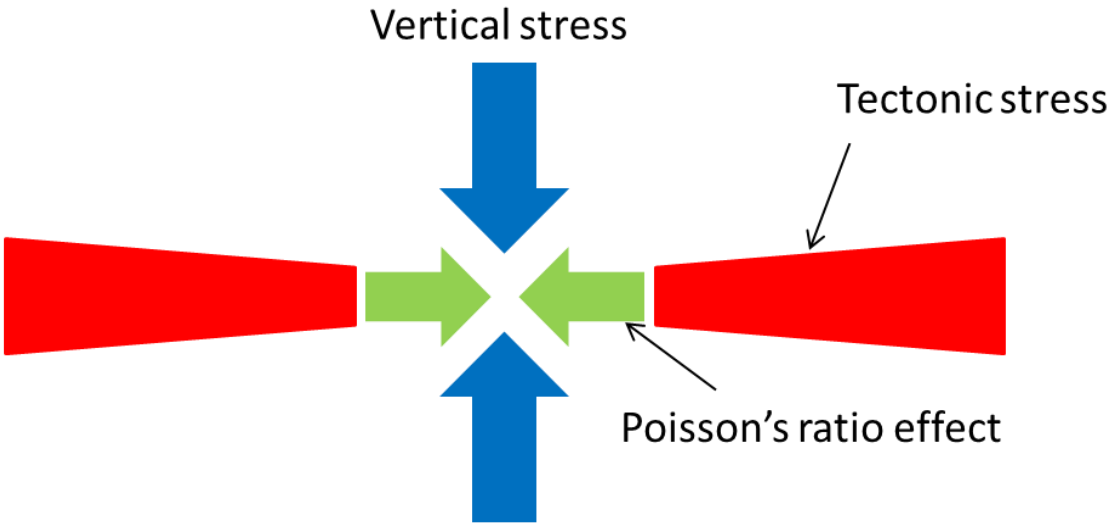

Figure 2. 3 Typical components of the horizontal stress in Earth's crust

The horizontal stress magnitudes vary with direction and in most cases around the world the maximum horizontal stress in rock is larger than the vertical stress.

Tectonic stresses are the stresses caused by the lateral movement of the continental plates which form the earth's crust (Nemcik, 2014). The force that propels the plate movement, which can cause separation, shearing or collision of the crustal plate boundaries, is caused by the convectional currents of hot mantle which rise from many stationary hotspots deep within the Earth.

The horizontal stress component caused by the Poisson's effect can be approximately determined from the following:

$$\sigma_h = \sigma_v \frac{\nu}{1-\nu} \tag{2.2}$$

Where σ_h = Horizontal stress caused by the Poisson's ratio

ν = Poisson's ratio

σ_v = Vertical stress

The magnitudes of the maximum stress (σ_1) oriented usually close to the horizontal plane varies with direction. The maximum horizontal stress is oriented in a certain direction that often coincides with the tectonic plate movement unless deviated by faulted ground while the minor horizontal stress is orientated at 90 ° to the maximum horizontal stress. Similarly to the vertical stress the magnitudes of the maximum lateral stress (σ_1) also increase with depth.

In order to explain why the horizontal stress increases with depth, it is necessary to understand the process of triaxial rock strength. The *in situ* strata are subjected to a continuous triaxial loading of broken ground. This concept is essentially identical to a laboratory triaxial strength testing procedure of broken rock. The increase in horizontal

stress with depth can be observed in Figure 2.4 showing the results of stress measurements in Australian underground coal mines.

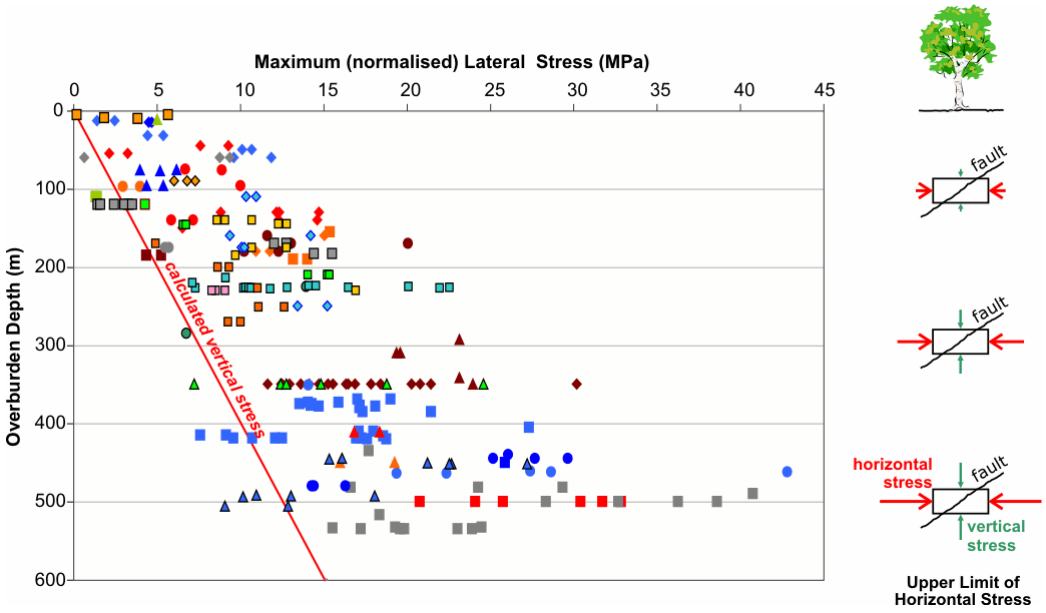

Figure 2. 4 Increase of horizontal stress with depth in Australian coal mines as measured underground by SCT (Nemcik 2014)

Note that the *in situ* ground is usually intercepted with many fault zones and discontinuities and therefore the ground strength can be described by the residual strength curve (broken curve) plotted on the maximum principal stress σ_1 versus minimum principal stress σ_3 graph shown in Figure 2.5 and also shown on the right side of Figure 2.4.

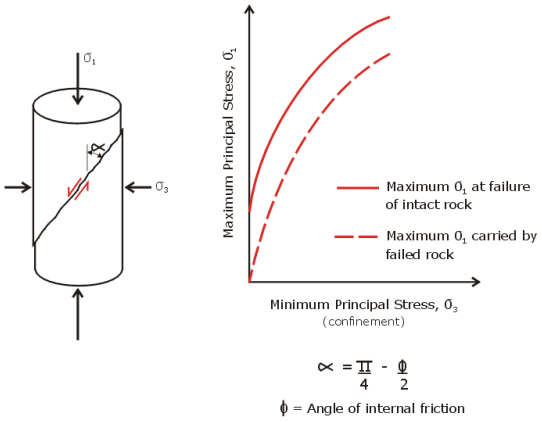

Figure 2. 5 Triaxial rock strength test (Nemcik 2014)

Typically the horizontal stress is predominately greater than the vertical stress in terms of magnitude. In general, the lateral stresses are concentrated above and below any excavation therefore elevated lateral stress field can be expected in the roof and floor above and below the mine roadways causing strata to fail. With this in mind, the role of roof support is to reinforce, conserve and maintain the residual strength of the fractured roof resulting from mining in a high horizontal stress environment.

2.1.3 Variation of strata stiffness and its effect on stress

The stress underground can also be affected by stiffness of rock. Vertical stress is mainly driven by gravitational load, taking into consideration only the unit weight of the rock and the depth of cover. According to Nemcik (2014) "horizontally bedded strata of different stiffness compress fully until they are able to carry the full weight of the overburden" and hence the vertical stress within the sedimentary layers will be the same in rock types of any stiffness. This is because the vertical stress has nowhere else to transmit but through each layer irrespective of their stiffness.

On the other hand, rock stiffness affects the amount of horizontal stress that passes through the rock. A stiffer rock layer will attract a greater amount of horizontal stress than a rock of a lower stiffness. This is because the tectonic stress compresses the layers of variable rock stiffness by the same amount. The stress endured by each layer is proportional to the stiffness of the rock. This idea was reported by Nemcik (2014) and demonstrated in Figure 2.6 where the weight of a heavy block carried by rubber and steel is predominantly carried by the steel because it is much stiffer than the easily compressible rubber. As the ground with varying stiffness is compressed by the same

amount (experiencing the same strain) the lateral stresses will be grater in the stiffer rock.

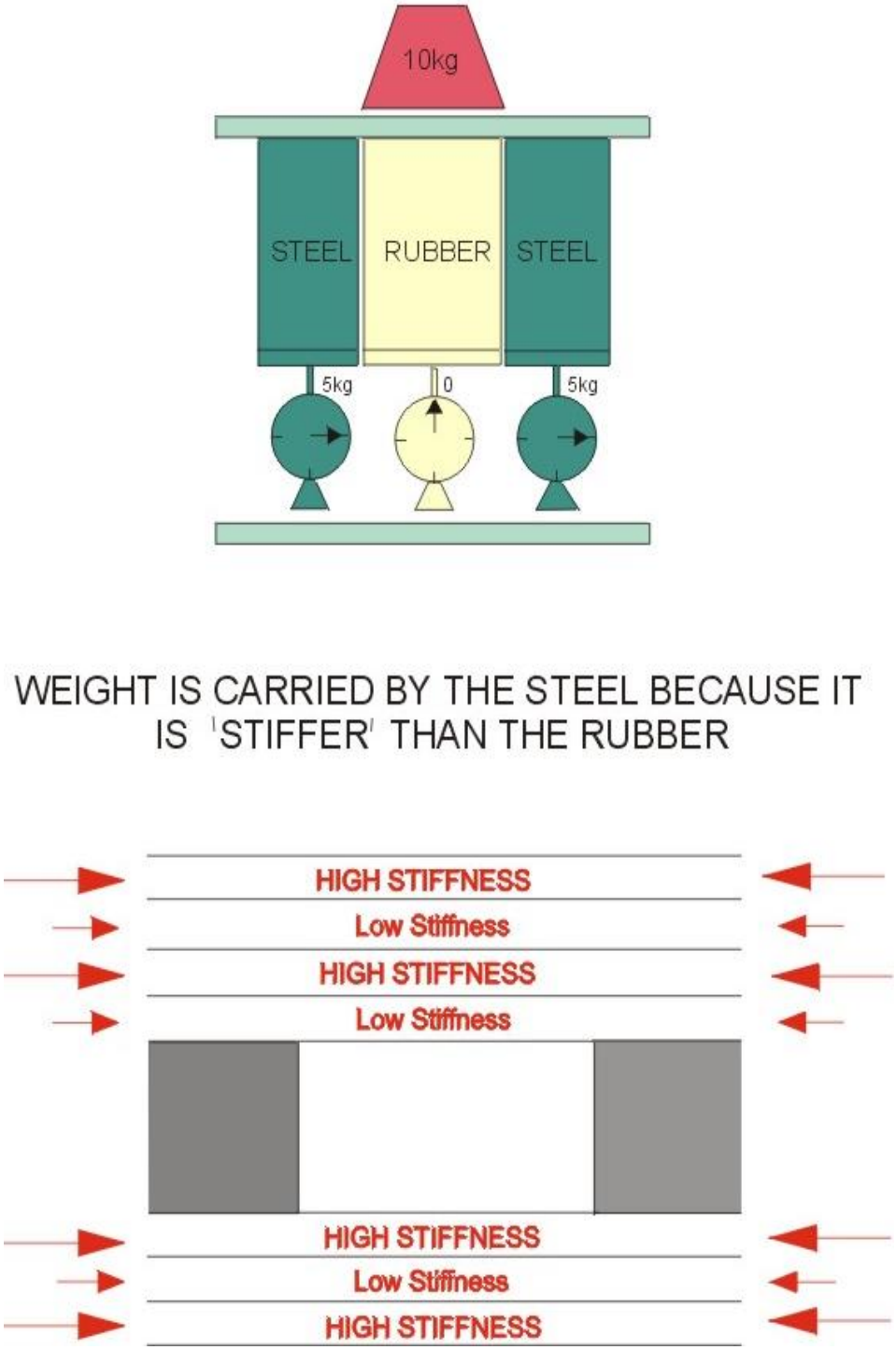

Figure 2. 6 Influence of rock stiffness on stress (Nemcik 2014)

Stress measurements are usually conducted in a competent rock that is in general stiffer than the surrounding weaker rocks. The relative stress differences in other layers of various stiffness can be calculated using Equation (2.3) (Nemcik, 2014)

$$\sigma_{NL} = E_N/E_M[\sigma_{ML} - \sigma_V \nu/(1-\nu)] + \sigma_V \nu/(1-\nu) \quad (2.3)$$

Where σ_{NL} = Normalised lateral stress

E_N/E_M = Ratio of normalised and measured Young's modulus

σ_{ML} = Measured lateral stress

σ_v = Measured vertical stress

ν = Poisson's ratio

2.1.4 Geological structures and their effect on stress

Geological structures that exist within the strata may influence the stress magnitudes and directions affecting the overall stability of the mine excavations. Geological structures such as discontinuities can be a source of localised stress concentrations underground. The geological structures may redirect the stress field to concentrate in a particular area. If these new stress distributions are higher than the *in situ* strength of rock, then the rock will fail. The failure will continue until the stress state no longer exceeds the strength of the affected rock. The use of bolts, as the primary support and steel mesh aims to control this failure and maintain the residual strength of the strata.

2.1.5 Stress orientation and its effect on roadway direction

Underground excavations and the surrounding fracture zones redirect the stresses around the mine roadways as shown in Figure 2.7. In coal mine roadways, the vertical stress concentrates mainly within the coal ribs as shown in Figure 2.2 while the lateral

stress is redirected mainly into the mine roof and the floor. When the stress field exceeds the strength of the particular rock the strata will yield forming "softened zones". As expected, when the stress concentrations are higher, the mine excavations will suffer greater damage.

The direction in which a mine roadway is driven with respect to the stress orientations is crucial for the roof and rib conditions. Roadways that are driven at a low angle to the maximum lateral stress direction experience smaller lateral stress concentrations in the roadway roof and the floor and therefore roof and floor deformations are minimised. However, mine roadways that are driven at a high angle to the stress direction experience high deformation and become less stable, as stress concentrations are maximised across the roadway. Furthermore, roadways that are driven at an angle to the maximum horizontal stress direction experience stress concentrations at one corner of the mined roadway face. This can cause biased roof or floor failure to one side of the roadway and can lead to extensive roof guttering. The floor failure is less visible and in most cases does not cause any problems. These cases are shown in Figures 2.7 and 2.8.

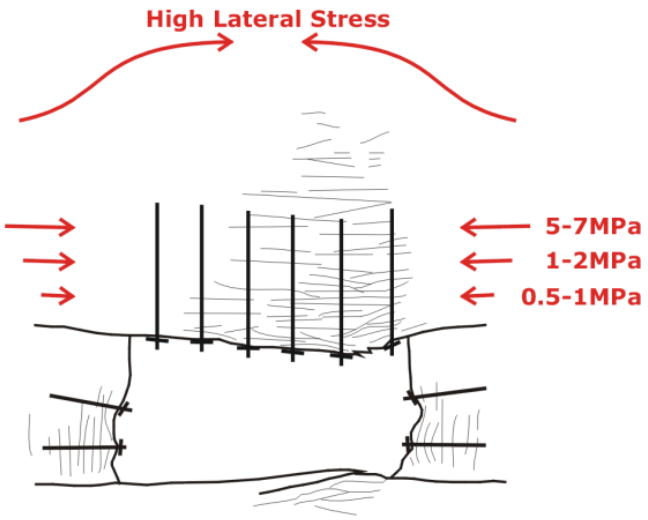

Figure 2. 7 Typical strata failure induced by lateral stress (Nemcik 2014)

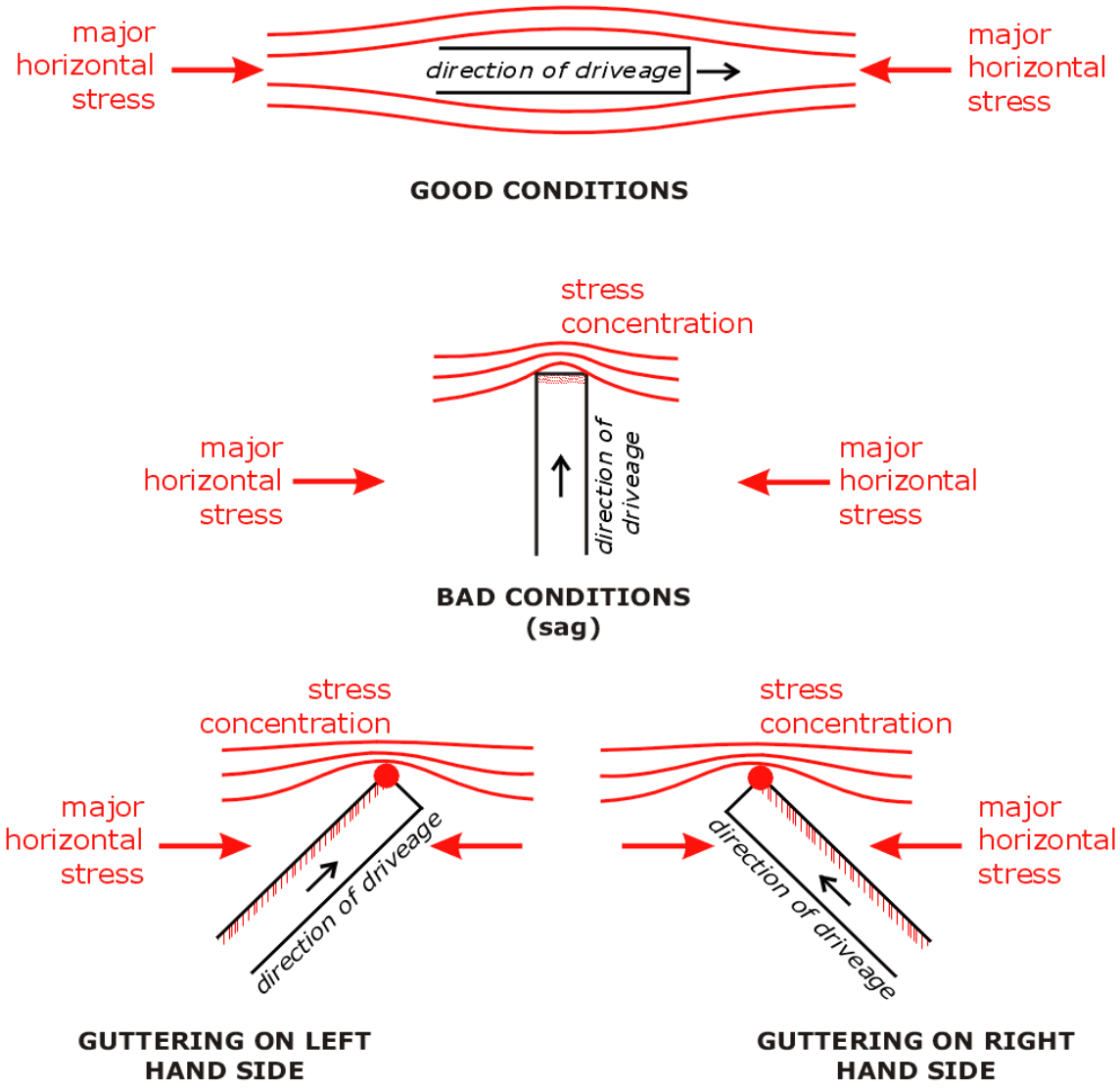

Figure 2. 8 Roadway directions versus stress orientation and the effect on strata conditions (Nemcik 2014)

The importance of recognising the roadway direction compared to the stress orientation is vital for determining how the roof may fail. In some cases, it is not possible to avoid high lateral stress situations and the roof conditions may suffer. However, knowledge of this relationship will enable prediction of strata deformation and allow for reinforcement design of the mine roadways to control bad roof conditions caused by high stress concentrations.

2.1.6 Strata reinforcement

Over the years ineffective strata support consisting of wooden props and beams has been gradually replaced with more effective strata reinforcement. Rock bolts have taken the role of the primary reinforcement and has dramatically changed the strata conditions, improved safety and increased productivity of the mines. High capacity pre-tensioned rock bolts have replaced passive strata support to provide active fracture reinforcement. Fully encapsulated rock bolts together with secondary support consisting mainly of high capacity cable bolts are the most favoured supports in Australian coal mines.

As the bolts are unable to fully control stability of the roadway skin, steel mesh was introduced to arrest any loose rock from falling into the mine roadways. Steel mesh is primarily a passive support system that is manually handled and takes time to install.

The current drive to automate installation of roof reinforcement has been an incentive to look for alternative ways to install the primary roof reinforcement and support the roadway skin. Steel mesh is of a passive nature and does not contribute to roadway skin reinforcement while via the adhesion and a small shrinkage TSLs can provide pro-active support. This makes the TSL products attractive as an effective technology.

2.2 Underground mining failures

Some typical roadway failure modes in underground coal mines are demonstrated here. These failures are mainly caused by inappropriate roadway orientations, stress concentrations, insufficient roadway supporting systems, and rock strength. According to Singh and Ghose (2006), the common underground roadway failure modes mainly

consist of guttering failure, span failure, strata skin failure, cantilever failure and rib failure.

2.2.1 Guttering Failure

Guttering failure is the rock failure that occurs at the side of coal mine roadways. As mentioned in section 2.1.5, rectangular roadways are subject to stress concentrations around the roadway corner within the roof strata as shown in Figure 2.9.

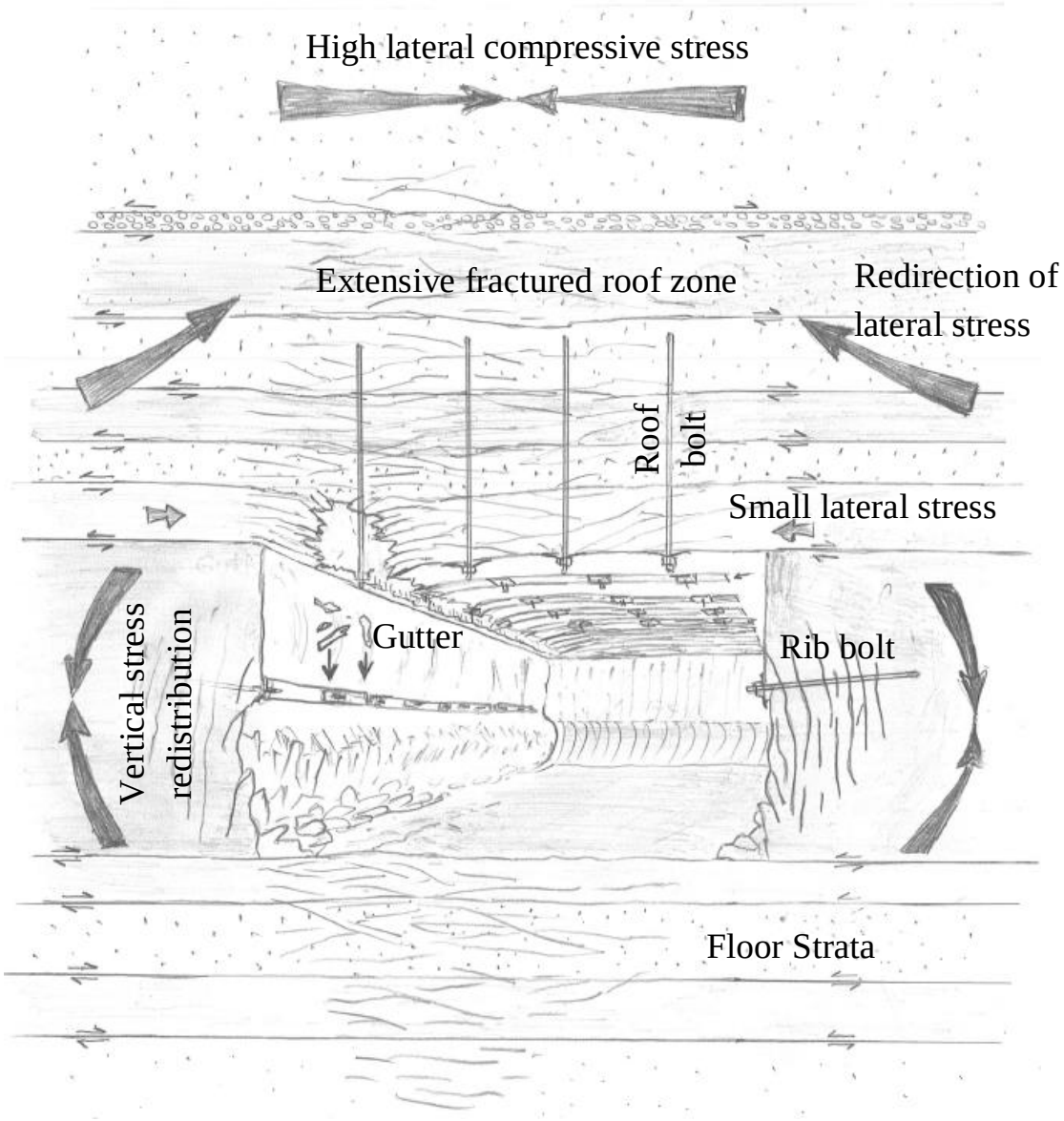

Figure 2. 9 Guttering failure

In a high lateral stress environment mine roadways can sustain significant roof and floor damage if oriented at a high angle to the maximum horizontal stress as shown in Figure 2.10. Roof tends to develop gutters on the side of the roadway where severely damaged and unsupported rock may fall out. In order to minimise the possibility of guttering occurrence, roadways should be developed at a small angle to the maximum horizontal stress. However, if roadways located in a high lateral stress environment are developed at an angle approaching $45°$ to the maximum horizontal stress, severe damage will occur at one side of the roadway.

Figure 2. 10 Rectangular coal mine roadway - strata conditions in high lateral stress field

2.2.2 Span Failure

When the coal mine roadway is at a greater width, and the capacity of the supporting system is lower than the weight of the immediate roof strata, span failure can occur. According to Singh and Ghose (2006), there are two failure modes: tensile and shear

mode. As shown in Figure 2.11(a), under the gravitational load the roof strata develops tensile fractures and bends often resulting in roof falls. The shear failure mode is illustrated in Figure 2.11(b), where shear occurs at the sides of the displacing roof. To control span failure, it is necessary (if possible) to increase the rock bolt length to anchor the lower strata horizon into the competent rock above and/or increase the rock bolt capacity to maintain high shear strength along the bedding planes.

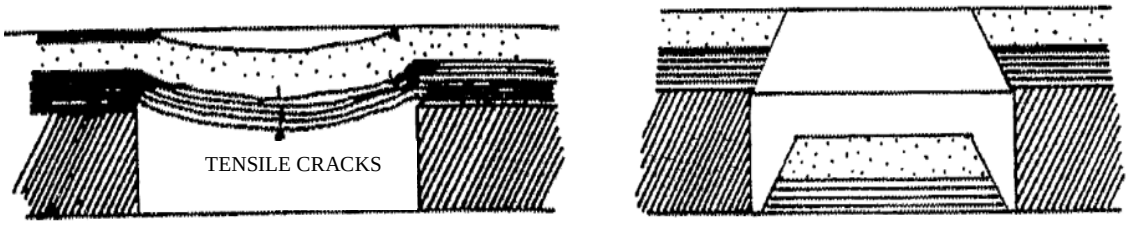

(b) Span failure – tensile mode **(a) Span failure – shear mode**

Figure 2. 11 Span failure (Singh and Ghose 2006)

2.2.3 Skin Failure

Roadway skin failure often occurs when the rock is weak or sustains significant damage (Figure 2.12).

Skin Failure

Figure 2. 12 Skin failure (Singh and Ghose 2006)

This failure mode is characterised by either shear fractures in rock or weak bedded or laminated sections causing lower unsupported sections to part and fall from the roof. In order to prevent this type of failure, extra supporting elements such as mesh need to be implemented. According to Singh and Ghose (2006), when mining, 0.3 m to 0.5 m of coal could be left in the roof where brittle or weak roof conditions prevail to provide more stable and safer working environment.

2.2.4 Cantilever Failure

When guttering failure or shear in the damaged rock at the roadway side propagates higher into the roof, cantilever roof failure can occur as shown in Figure 2.13(a), (Singh and Ghose, 2006). As guttering propagates, an arch is created as a result of stress increase in compression and thus an unstable cantilever is formed due to the lower roof being in an unconfined state. This is illustrated in Figure 2.13(b). This type of failure usually occurs at the roadway intersections where roof spans are large. For safety, these large roof spans are usually monitored using various extensometer type instruments such as Tell-Tales.

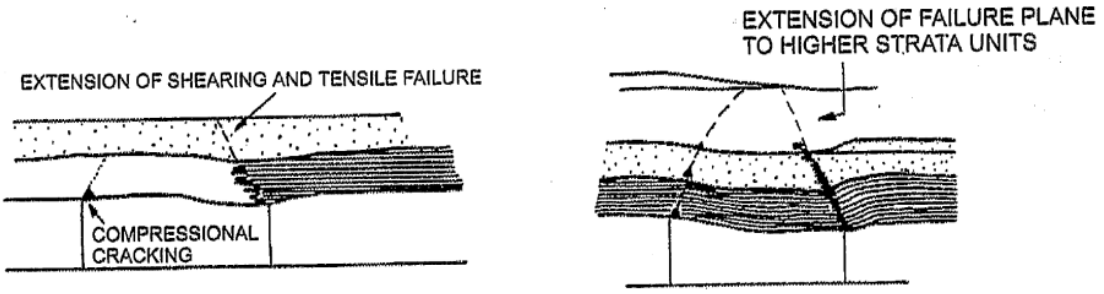

(b) Cantilever failure **(a) Shear failure in higher strata units**

Figure 2. 13 Cantilever Failure (Singh and Ghose 2006)

2.2.5 Rib Failure

Mine roadway rib failure typically occurs in deeper mines where high vertical stress concentrations yield the coal seam. This failure is characterised by coal cleat opening and buckling with large lateral displacements towards the centre of the roadway as shown in Figure 2.14.

This kind of failure can be prevented and controlled by increasing the rock blot intensity and implementing the surface support.

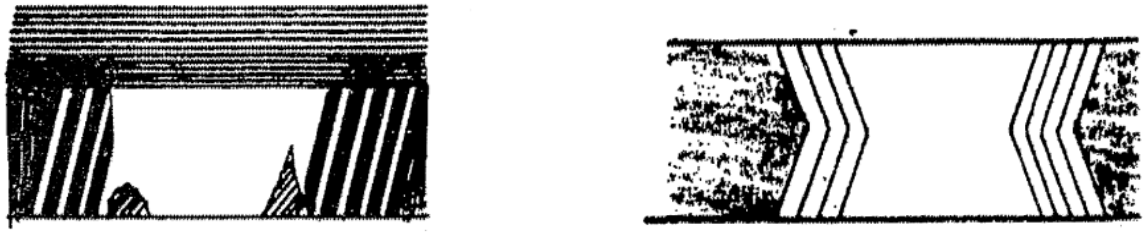

(b) Side failure due to presence of cleats **(a) Rib side buckling failure**

Figure 2. 14 Buckling Failure (Singh and Ghose 2006)

2.2.6 Measurements and monitoring of strata conditions

To ensure successful strata support design it is essential to quantify ground behaviour in the field. Measurements are necessary to define:

- Roof failure
- Rib failure
- Floor failure
- Pillar failure
- Roof reinforcement failure
- Rib reinforcement failure

- Water and gas inflow

To understand the ground behaviour we need to measure all parameters that can cause strata problems. These are:

- Pre-mining stress
- Stress changes
- Strength of rock
- Displacements of: roof, ribs, floor and pillars
- Bolt loads
- Reinforcement installation procedures
- Permeability of strata

The instruments needed for the monitoring programme include:

- 3-dimensional stress cells to establish the pre-mining stress magnitudes and orientations of the principal stresses σ_1, σ_2 and σ_3. These cells can also be used to measure the stress changes during mining. The geophysical logging of the borehole breakout within the numerous exploration holes can also be used to obtain directions of the pre-mining maximum lateral stress within the mining lease. The visual stress mapping is also a useful technique to estimate the stress directions and magnitudes within the nominated mining area.

- Extensometry to measure displacements of surrounding strata such as the Sonic or Gell extensometers and various types of readily available Tell-tales. The interpretation of these measurements should include the extent of strata

softening, detailed displacements within the strata at all depths and total displacements at the excavation surface.

- Geological data to establish the rock type of individual horizons. These include rock cores obtained from the exploration drill holes and interpretations from the geophysical logs detailing of the overburden strata.

- Strength of the individual rock beds.

  These include direct rock testing of the geological cores that may include the Uniaxial Compressive Strength (UCS), tensile strength, and the triaxial strength of chosen rocks. These values can be used to calibrate the data from geophysical logs to further enhance the rock strength properties database typically obtained from a larger area.

- Monitoring of the reinforcement performance. This may include monitoring of strain gauged instrumented rock bolts and rock bolt installation procedures such as hole size, resin encapsulation, short encapsulation pull out tests, measurements of resin strength etc.

A typical monitoring site showing various instruments is shown in Figure 2.15.

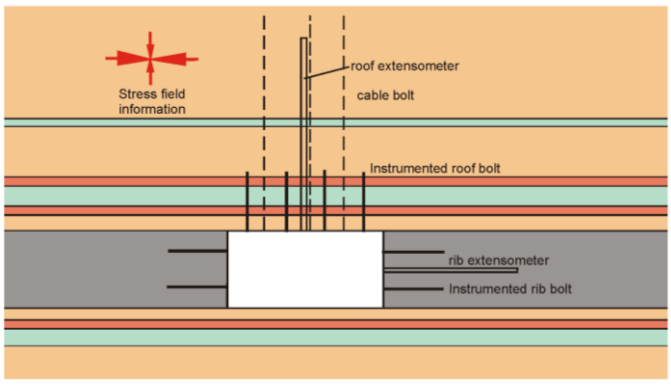

Figure 2. 15 A typical monitoring of coal mine roadway site showing various geotechnical instruments

2.3 Strata Support Systems

Strata support consists of many engineering methods to minimise displacements of fractured rocks in underground mining roadways. Rock bolts, cable bolts and strata skin confinement can effectively reinforce mine roadways, improve the productivity and safety underground.

2.3.1 Rock bolting

Rock bolting has been considered as the most significant ground control technology in the development of mining and is often used as the primary support underground. Rock bolts can provide confinement and reinforcement to roof and ribs of the roadway and minimise vertical and lateral displacements.

2.3.2 Theories of rock bolting support

Rock bolts reinforce rock strata by providing confining stress to fractures within the broken strata. The rock bolts are able to provide both normal and shear resistance to fracture displacements. This action decreases movement within the broken rock, minimises unravelling of the fragmented rock and increases the overall residual strength of rock mass. Peng (1978) described four types of rock bolts support mechanism.

2.3.2.1 Simple Skin Support

When the *in situ* lateral stresses are low, a strong roof stratum has the potential to support itself and the roof failure is unlikely to occur. However, in this case, geological rock discontinuities can make the roof conditions unsafe and a minimum roof support is required to secure any loose rock material. When the roof is strong, short and low

capacity rock bolts can be adopted to support the roof as illustrated in Figure 2.16 (Peng, 1978). In Australian coal mines minimum support rules apply for these conditions.

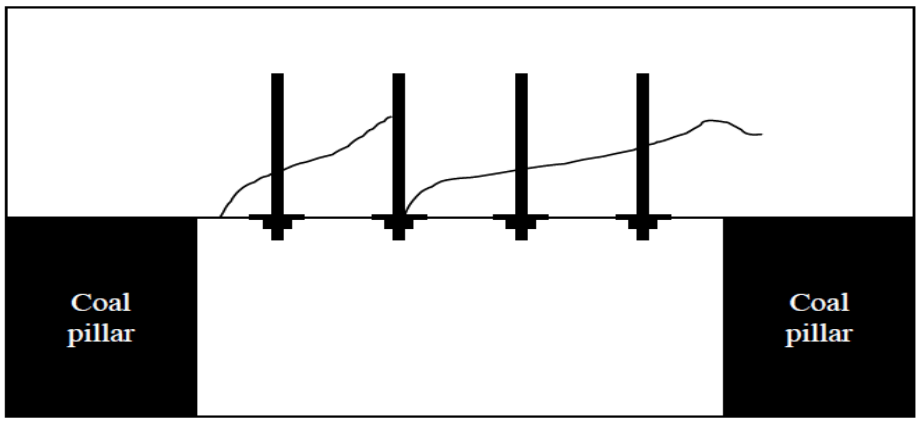

Figure 2. 16 Simple Skin Support (Peng 1978)

2.3.2.2 Suspension of a roof layer from massive bedding

When a weak immediate roof in the lower horizon exists as shown in Figure 2.17, the immediate roof can separate and fall. The failure can be controlled by bolting weak strata to the strong rock strata above. In this case, mechanical and point anchor bolts may be sufficient. The installation spacing between the bolts and their length depend on the weight of the weak beds, strength of rock bolts and thickness of the weak layer (Peng, 1978).

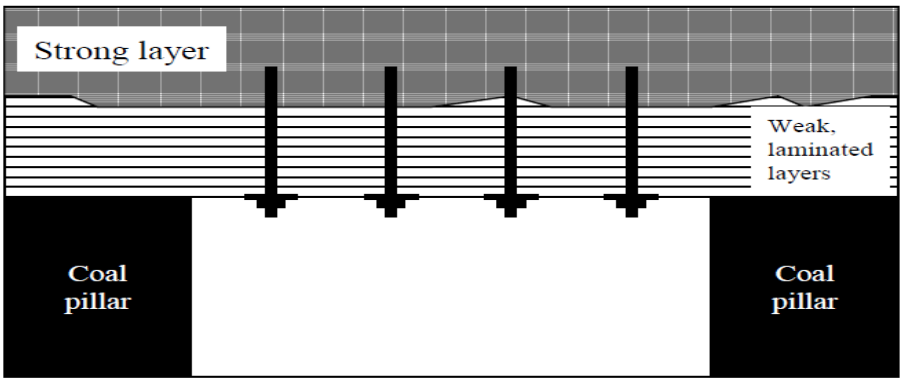

Figure 2. 17 Suspension mechanism (Peng 1978)

2.3.2.3 Beam Building of Strata

When the rock bolt length is shorter than the thickness of weak layers, beam building mechanism will play an important role in supporting the roof as shown in Figure 2.18. In this case, fully encapsulated rock bolts and close spacing need to be implemented to minimise the lateral movements of weak rock layers and combine weak planes into a thick stable beam (Peng 1978).

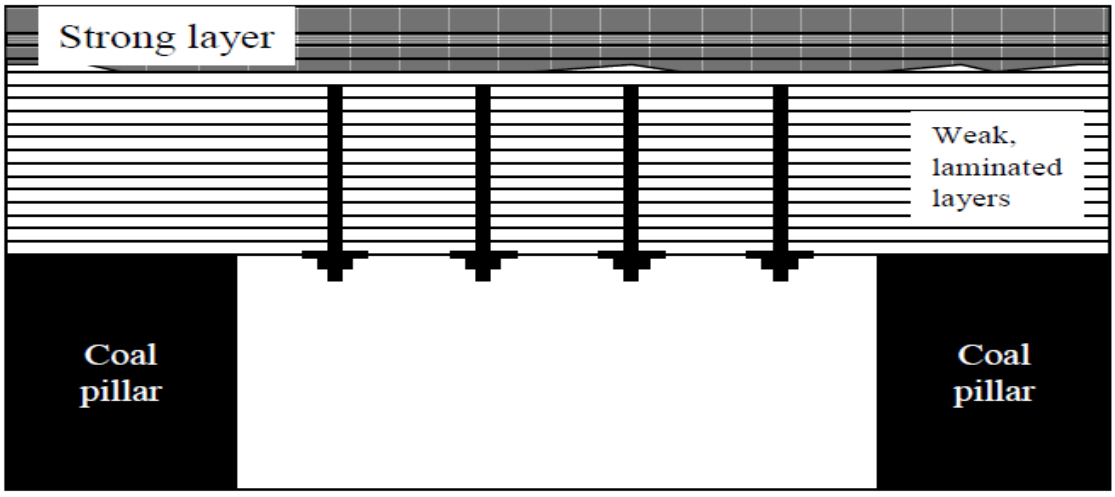

Figure 2. 18 Beam Building mechanism (Peng 1978)

2.3.2.4 Keying of Highly Fractured Rock Mass

When the roof layers are severely fractured, roof bolts can effectively hold the broken fragments together by increasing normal stress between the fractures or joints and minimising fracture displacements. In this situation, keying effect plays a vital role in supporting roof as demonstrated in Figure 2.19. The keying effect is improved by minimising the unravelling of broken rock pieces. Rock bolts are effective in preventing excessive movement in the rock mass by providing axial and shear resistance to fracture movement that can be enhanced by bolt pre-tensioning. If the

rock bolts cannot offer adequate support capacity, secondary support methods need to be implemented such as cable bolts (Peng, 1978).

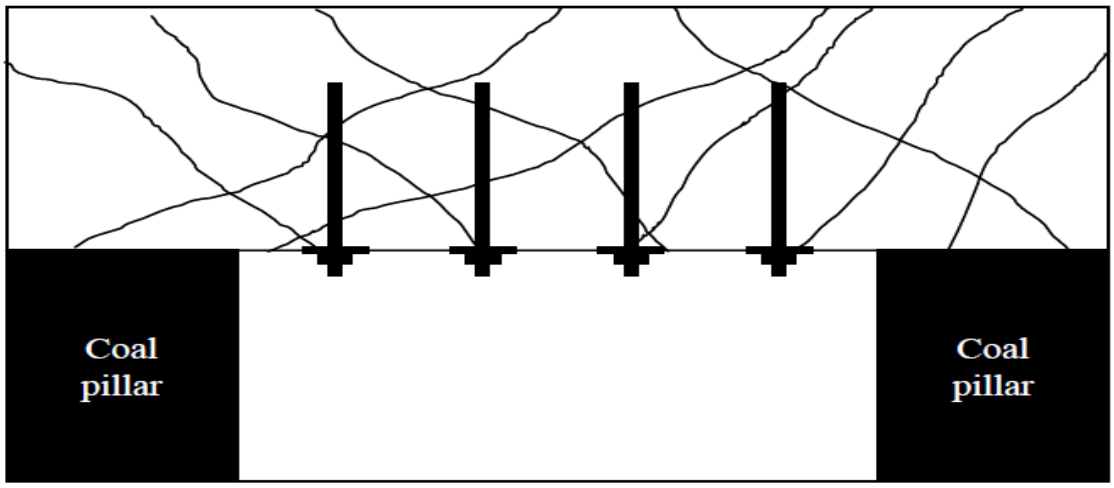

Figure 2. 19 Keying effect of bolting (Peng 1978)

2.4 Strata Skin Support

Steel mesh that is currently used in underground coal mines is of a passive nature and in most cases does not contribute to roadway skin reinforcement. Steel mesh is a safety device that is only effective in supporting detached pieces of rock or severely fractured rock mass experiencing large displacements. As a relatively new form of rock support TSLs are currently being investigated as an effective skin support technology. Research indicates that TSLs may provide superior rock skin control. Being a pro-active support technique, it is known that a TSL is able to provide resistance to even small rock movements and thus significantly improve rock skin stability.

TSLs have the potential to increase roadway development rates because their application in conjunction with rock bolts can be automated. In addition, TSLs can be sprayed remotely, thereby improving personnel safety while providing resistance to

small rock deformations. TSL materials have thus been attracting attention from both research organisations and industry.

2.4.1 Mechanisms of thin liner support

Stacey (2001) described a series of mechanisms of loading behaviour and surface support behaviour of TSL. The support mechanisms considered to be especially relevant to thin liners are analysed below.

2.4.1.1 Promotion of block interlock

The aim of this mechanism described by Stacey (2001) is mainly to keep the rock mass in a stable and unloosened condition. More specifically, this mechanism consists of several sub-mechanisms promoting block interlock as follows:

1) Bonding between the TSL and the rock surface can promote block interlock which can keep the broken blocks in place and restrict blocks rotation and shear, Figure 2.20.

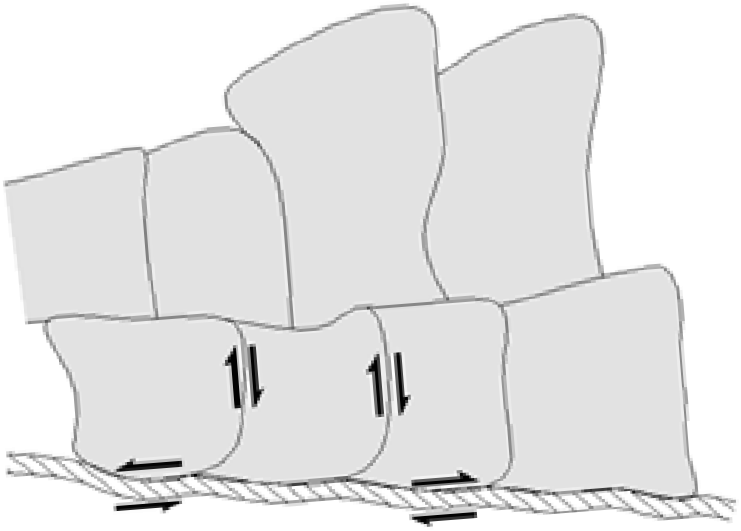

Figure 2. 20 Shear and rotational resistance with a bonded membrane (Stacey 2001)

2) Poor bond along the contact surface between the TSL and rock may result in reduced resistance to shear and rotation (Figure 2.21).

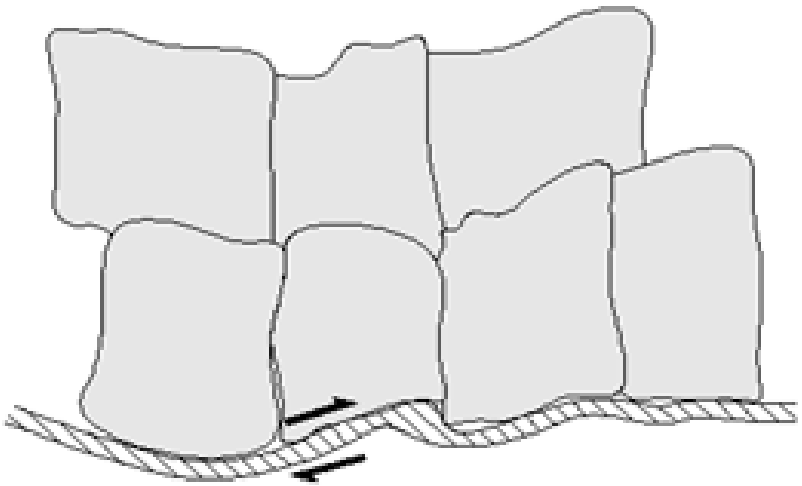

Figure 2. 21 Physical shear interlock with poorly bonded membrane providing reduced shear and rotation resistance (Stacey 2001)

3) In the process of high pressure spraying, the materials will penetrate into the fractures and joints before curing, therefore, the bond strength can prevent fractured rocks from moving which can make the surface more stable through reducing the displacement and rotation as shown in Figure 2.22.

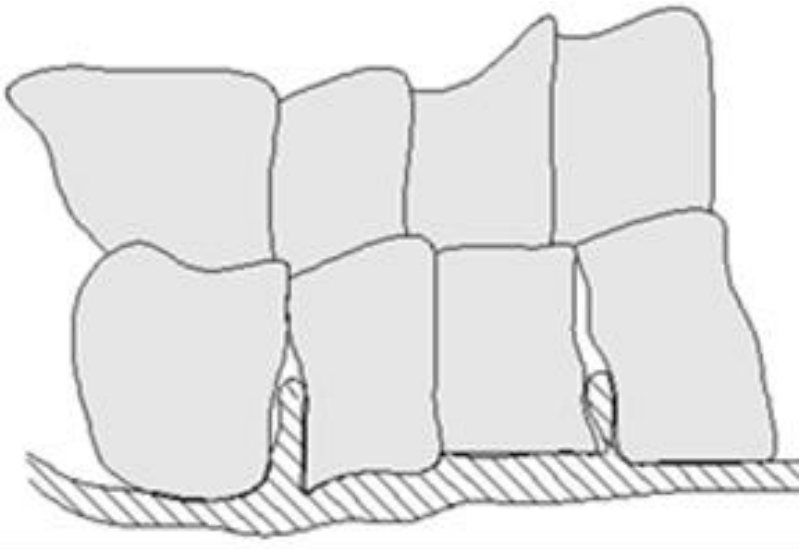

Figure 2. 22 Plugging of open joints and fractures (Stacey 2001)

4) If a thin membrane is applied to the rock early, it may be able to arrest movement of the fractured rocks, or at least minimise the process of deformation shown in Figure 2.23.

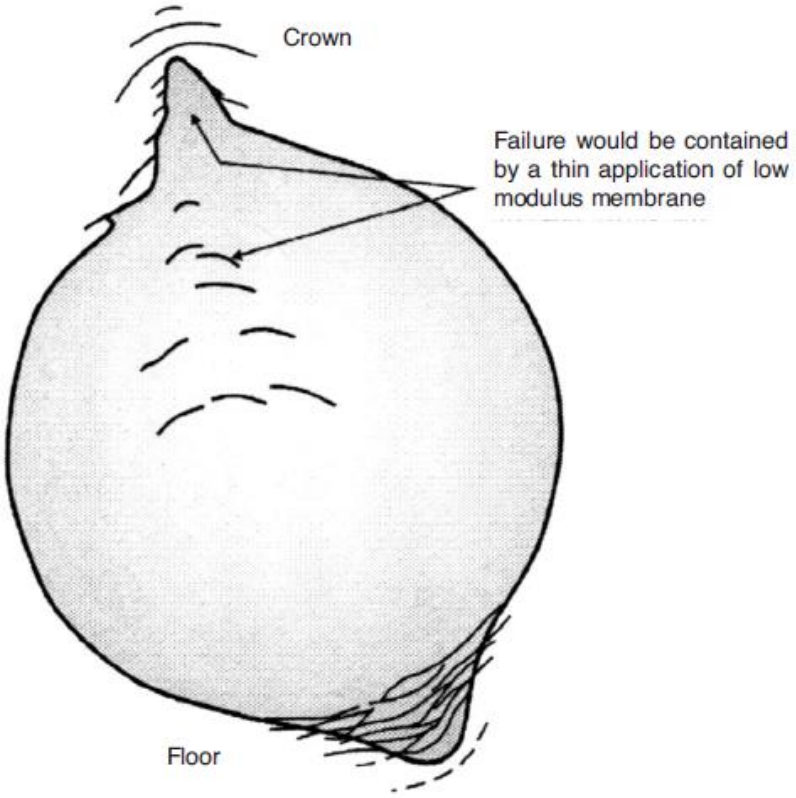

Figure 2. 23 Stress-induced spalling likely to be contained by low modulus membrane (Stacey 2001)

5) As shown in Figure 2.24, there are two mechanisms that can occur behind the TSL surface. When the bond strength between the rock and the membrane is strong enough, the support mechanism is provided by the TSL-rock composite layer. If the bond between rock and TSL fails due to excessive loading then the tensile strength of TSL material will play the main role in providing confinement to fractured rock mass.

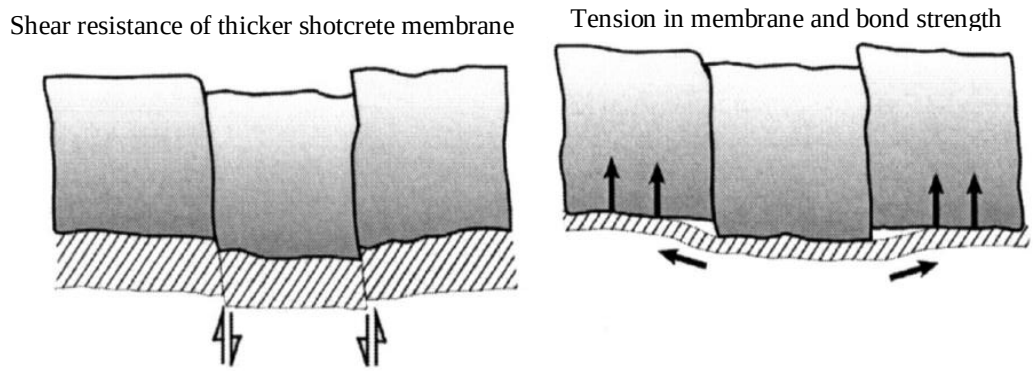

Figure 2. 24 Physical shear interlock with poorly bonded membrane (Stacey 2001)

2.4.1.2 Air tightness

When the rock mass begins to fail, the rotation and dilation of rock blocks opens the cavities among the cracks and fissures producing suction if no air is able to infiltrate the broken rock. Therefore, it is possible to inhibit the failure by providing an air tight surface and thus restrict the dilation. Coates (1970) stated that this problem could be solved by applying the air tight membrane shown in Figure 2.25 and Finn et al. (1999) identified this mechanism as a type of support mechanism which can be effectively used by TSLs. The author's opinion is that this suction is very difficult to achieve in coal mines as the strata conditions are usually too permeable to water ingress and air flow.

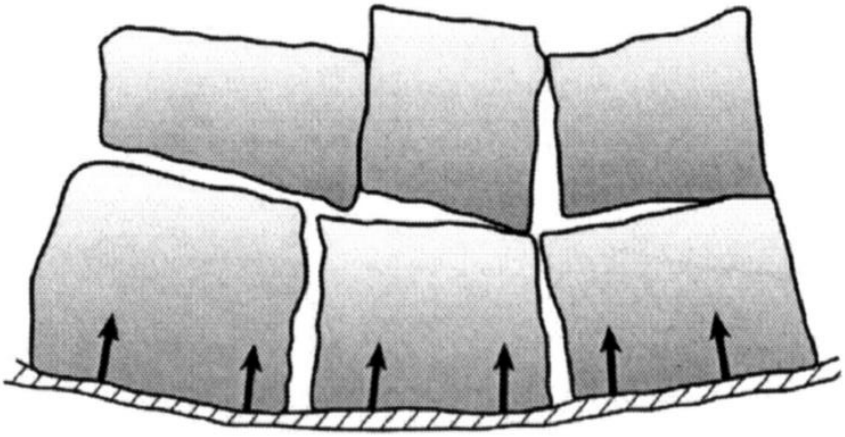

Figure 2. 25 Air-tight membrane 'suction' support pressure (Stacey 2001)

2.4.1.3 Basket mechanism

In this mechanism, the loosening fractured rocks are supported by a basket which is formed by the membrane, as shown in Figure 2.26. In fact, three considerations need to be taken into account: (a) the flexural properties or ductility of the membrane will determine the membrane deflection when forming the basket; (b) when the basket begins to form the tensile strength of the material plays the main role in supporting the basket; (c) in the case of a two-component liner, for example fibre reinforced liner, both the tensile strength of fibres and the polymer matrix will have an influence on the performance of the membranes. In addition, if the reinforcing fibres and the matrix materials de-bond, there will be a consequential reduction in load capacity.

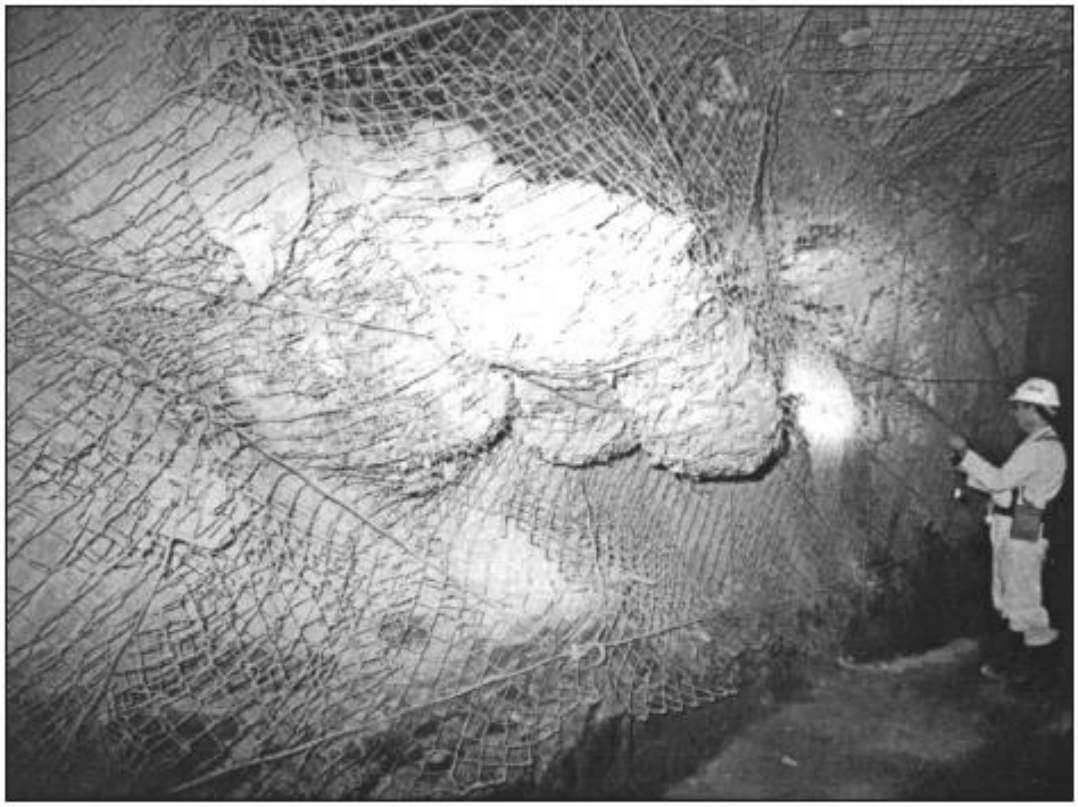

Figure 2. 26 Basket mechanism of support (Stacey 2001)

2.4.1.4 Slab enhancement

When brittle rock is under high stress, rock slabs are usually formed at the surface areas of openings. These slabs may fail and fall because of buckling caused by increasing deformation. The membrane which bonds to the fractured rock surface can effectively increase the thickness of the slab, and thus the slenderness of the slab will decrease and the resistance to buckling can increase as shown in Figure 2.27.

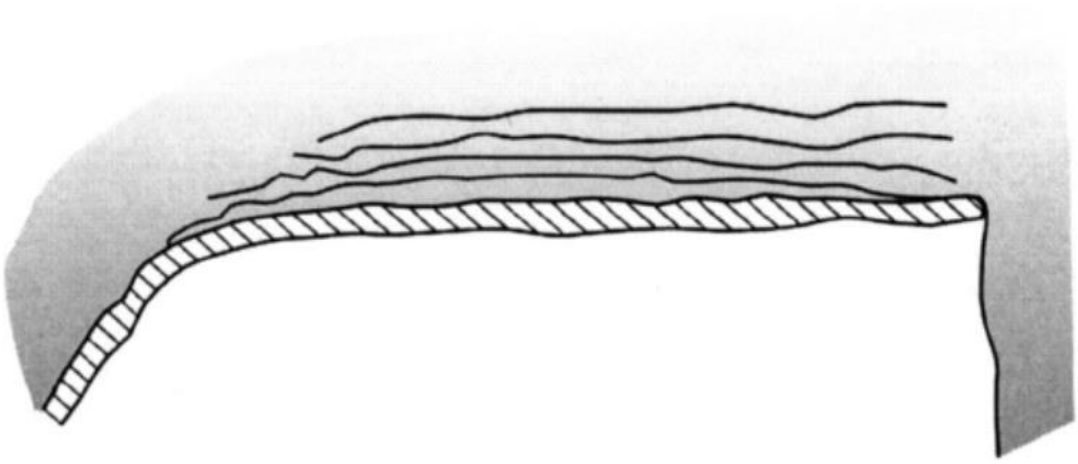

Figure 2. 27 TSL contribution to the effective slab thickness (Stacey 2001)

2.4.1.5 Beam enhancement

Similar to slab enhancement, by applying the TSL the mechanism of beam enhancement increases the bending performance of the slab through. In this case, the TSL not only improves the ability to restrict the movement of the fractured rock, but also increases the slab width and thus increases the bending strength of the slab.

2.4.1.6 Extended 'faceplate'

This mechanism extends the area of the rock bolt faceplate influence on the rock surface when using TSL as shown in Figure 2.28. This area of influence can be extended further with stiffer and thicker membranes.

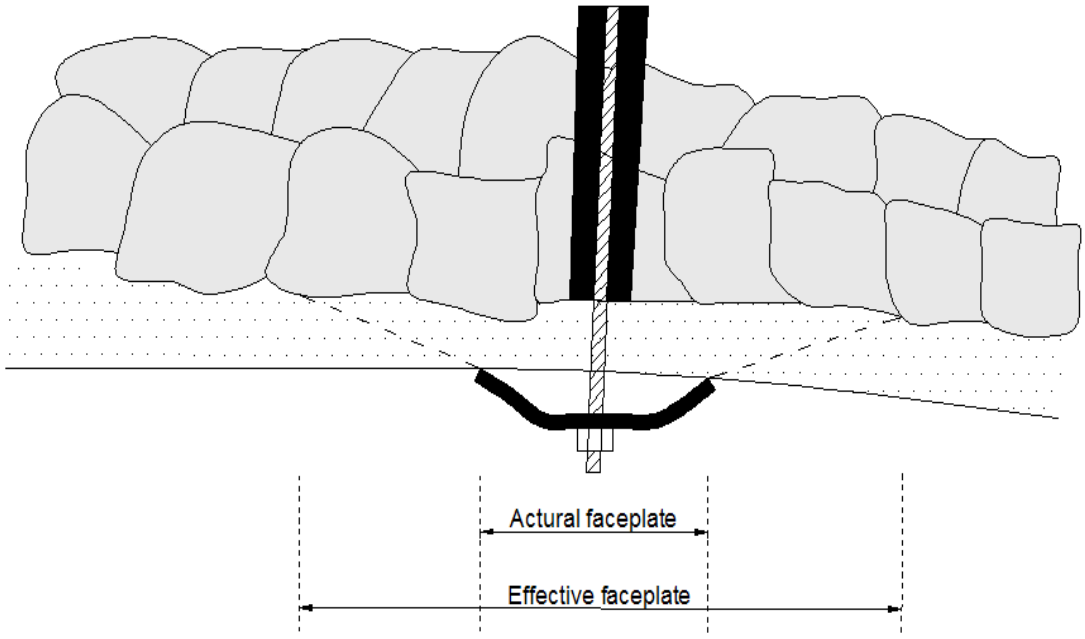

Figure 2. 28 Extended faceplate action (Stacey 2001)

2.4.2 Determination of mechanical properties of thin spray on lines

2.4.2.1 Bond (Adhesion) strength of Thin Spray-on Liners

The bond strength of TSL is very important and is different from other support methods. Once the fast curing TSL is sprayed on the rock surface, it can resist displacements almost immediately. In general, there are two types of bond strength: tensile bond strength and shear bond strength.

2.4.2.1.1 Tensile bond strength of thin spray-on liners

Ozturk and Tannant (2010) developed a new method to calculate the value of tensile-bond strength using the data of pull-out load-displacement between the TSL called Tekflex and a substrate (concrete, granite and sandstone substrates). The pull-out test fixture is shown in Figure 2.29.

Figure 2. 29 Pull-out test fixtures (Ozturk and Tannant 2010)

Based on the tensile-bond strength testing method proposed by Ozturk and Tannant (2010), Yilmaz (2013) made some modifications in the test setup using Perspex moulds in the specimen preparation instead of overcoring of the TSL to isolate the testing area, as shown in Figure 2.30.

The aim of these tests is to evaluate the value of tensile bond. The bond can be calculated from the results using the simple relationship presented in Equation (2.5).

$$\sigma_{TB} = \frac{F}{A} = \frac{F}{\pi \times r^2} \qquad (2.5)$$

Where σ_{TB} = the tensile bond strength

F = the load at failure

A = the contact surface area between TSL and substrate

r = the radius of the contact surface area between TSL and substrate.

Yilmaz (2013) stated that there are four types of possible failure locations as shown in Figure 2.31. The four failure modes can be demonstrated as follows:

Failure type I: This type of failure shown in Figure 2.31(a) takes place within the substrate because of the high bonding strength and tensile strength of the liner which exceeds the tensile strength of the substrate and causes failure within the rock.

Failure type II: This type of failure is the true tensile-bond strength. In this case, the de-bonding takes place between the TSL and rock substrate as illustrated in Figure 2.31(b).

Failure type III: This type of failure occurs within the TSL material. This is due to the fact that the tension-bond strength of the TSL to the substrate is higher than the TSL tensile strength as demonstrated in Figure 2.31(c).

Failure type IV: This type of failure indicates that the de-bonding takes place between steel dolly/epoxy and epoxy/TSL interface as shown in Figure 2.31(d). This case shows that the bonding strength between the TSL and substrate is stronger than the bonding strength both between epoxy/TSL and metal plug/epoxy. When this failure occurs, the result should be rejected and a stronger epoxy utilized.

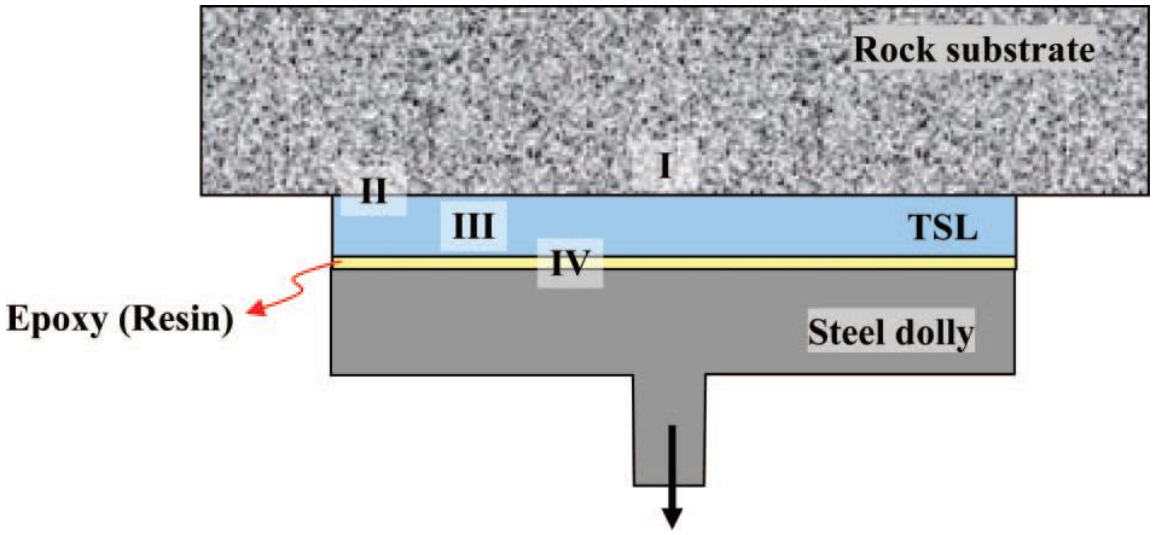

Figure 2. 30 Tensile bond-strength test set up and possible failure locations (Yilmaz 2013)

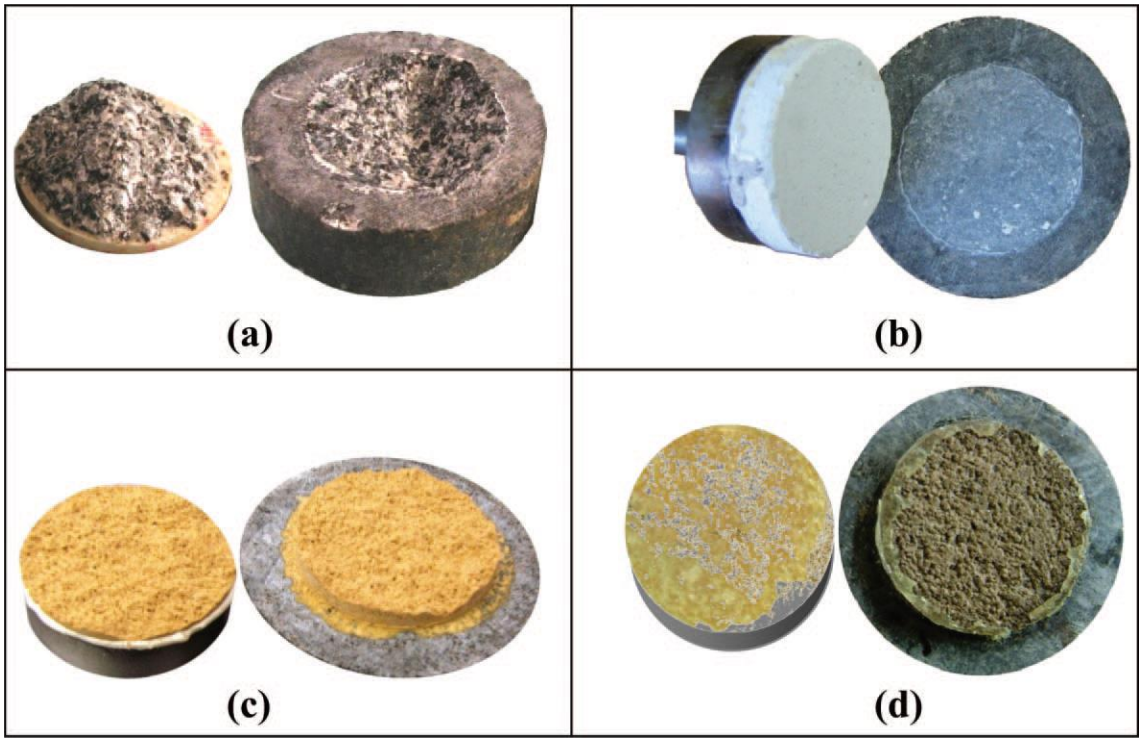

Figure 2. 31 Failure types: (a) Type I, (b) Type II, (c) Type III, (d) Type IV (Yilmaz 2013)

2.4.2.1.2 Shear bond strength of thin spray-on liners

Despite the TSL shear bond strength being important, the research on it is limited. Yilmaz (2007) developed a testing method to determine the shear-bond strength of TSLs which used a 20 mm thick steel ring with a 52.5 mm diameter hole. In the test, a diameter of 27.5 mm rock core was placed in the hole as shown in Figure 2.32 and the TSL was poured into the gap between the rock core and the steel ring. The steel base ring was fixed while the rock core was loaded until the TSL sheared off the rock surface.

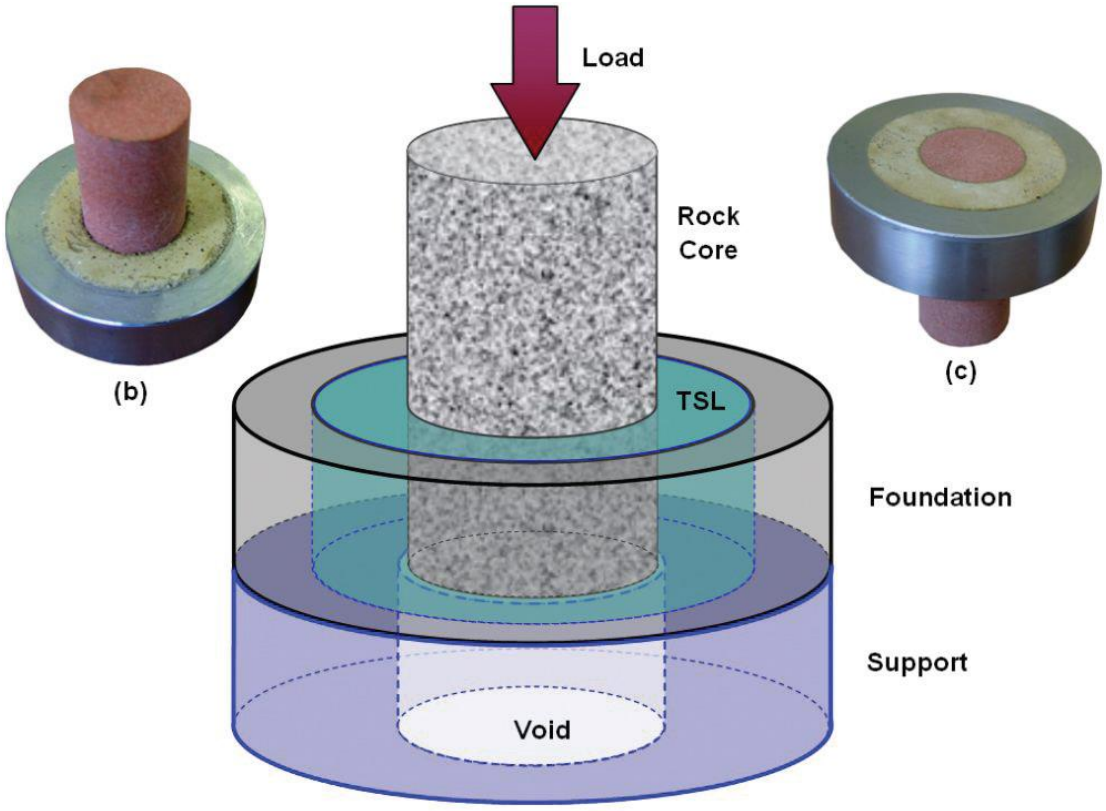

Figure 2.32 (a) Illustration of shear bond testing, (b) specimen top view, (c) specimen bottom view (Yilmaz 2007)

The aim of the shear-bond strength tests is to obtain the value of shear-bond strength which can be calculated using the following Equation (2.6):

$$\tau = \frac{F}{\pi D t} \tag{2.6}$$

Where τ = the shear-bond strength

F = the load at failure

D = the diameter of rock core

t = the ring thickness or TSL depth.

Equation (2.6) could be simplified as shown below:

$$\tau = \frac{F}{A} \tag{2.7}$$

Where, A is the contact surface area between TSL and substrate.

The author's opinion is that this test has an inherent problem with the polymer shrinkage that can significantly influence the test data.

2.4.2.2 Tensile strength of Thin Spray-on Liners

It is reported by Kuijpers *et al.* (2004) that the tensile strength testing method was chosen as a preliminary test of liner characterisation by many researchers (Tannant et al, 1999; Archibald, 2004; Spearing and Gelson, 2002). In general, the prepared samples for these tests are of "dog bone" shapes that are tensioned to failure. These tests are performed on pure resins and fibre reinforced TSL materials. It is commonly accepted by the researchers and manufacturers that the tensile strength can be tested using the American Society for Testing Materials (ASTM) D638-14 and ASTM D412-06a standards with some modifications.

2.4.2.3 Shear strength of Thin Spray-on Liners

Shear strength is another important property of TSL. However, there is only limited research in this topic. According to Hadjigeorgiou and Grenon (2002), it is assumed that the tensile strength and the shear strength had almost the same value when used to analyse the TSL support capacity. Lacerda and Rispin (2002) thought that the compressive strength could indicate the shear strength. However, Tannant (2001) stated that the support capacity of TSLs mainly rely on the loss of adhesion and shear or tensile rupture. Therefore, it is important to determine the shear property of the TSLs through reviewing the relevant literature and testing.

Yilmaz (2009) developed a testing method to determine the shear strength of TSLs. His testing setup and a failed specimen are shown in Figure 2.33.

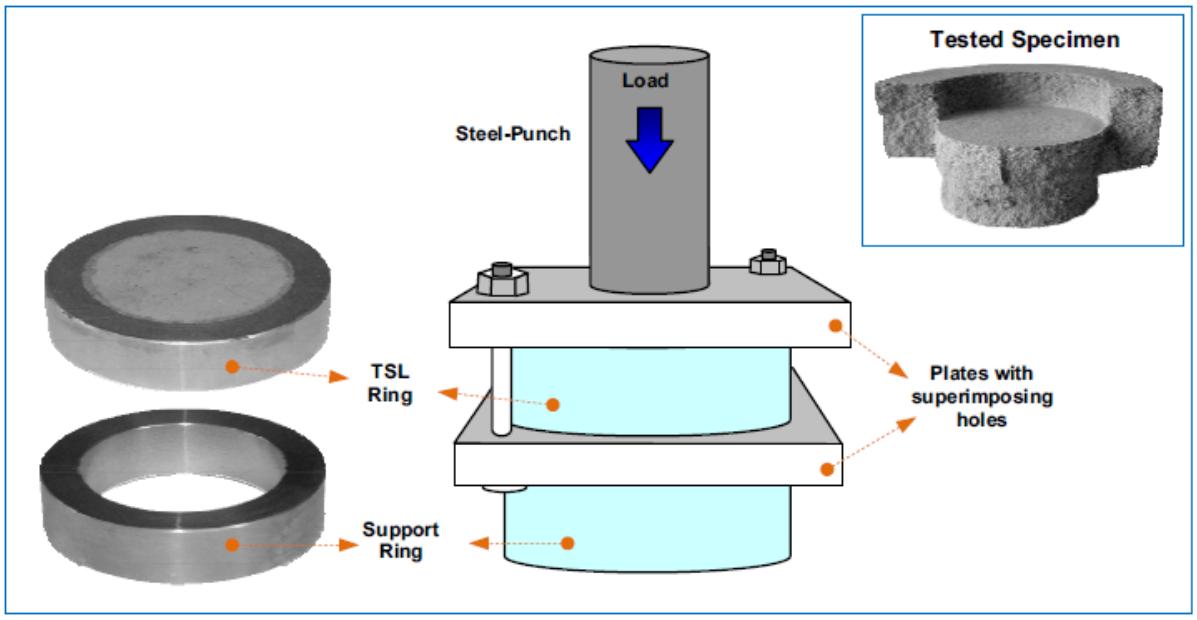

Figure 2.33 Shear strength test setup and a failed specimen (Yilmaz 2009)

The shear strength can be calculated from the tests using Equation (2.8).

$$\sigma_s = \frac{F}{A} = \frac{F}{\pi \times D \times t} \tag{2.8}$$

Where σ_s = the shear strength

F = the load at failure

D = the diameter of steel-punch

t = the ring thickness or TSL depth.

2.4.3 Desirable properties of thin spray on lines

It is known that ground conditions depend on many factors, such as rock type, geological structures and stress properties. The ideal TSL has many desirable properties. A range of ideal TSL properties was established by Espley-Boudreau (1999) and is documented in Table 2.1.

Table 2.1 The ideal TSL properties (Espley-Boudreau (1999)

Property or characteristic	Reccommended range
Non-combustible	Flame spread rating<200
High tensile strength	>5 MPa
High adhesive strength	>1 MPa on rock substrates
Tough (hardness)	Shore A, hardness 80
Elasticity	100% to 150% elongation
High shear strength	>1 MPa
Rapid cure time	<1 hour
Water resistant	Able to be sprayed onto humid/wet surfaces
Temperature tolerant	0 ℃ to 40 ℃
Rapid application rates	>1 m^2 /minute
Long pot life	>2 hours
Environtmently friendly	Only mild solvents
Low cost	<\$15/m^2
Simple application	Minimal surface preparation

Swan and Henderson (1999) developed a ranking system (Table 2.2) of the desirable properties in an attempt to highlight the relative importance of various factors when replacing steel mesh as the primary ground support.

Table 2.2 TSL ranking system (Swan and Henderson 1999)

Quality	Description	Ranking (1 to 4)
Net cost	Cost should justify change from mesh	4
Bagging strength	Initial objective to replace #7 gauge weld-mesh	3.8
Environmental	MSDS; Health & Safety; minimal protective equipment requirements	3.8
Fire retardency	Must not continue to burn after flame removal	3.5
Adhesion	Must adhere to friable ore; should bond with multiple applications	3.5
Flexible	Must deform as failing rock bulks; should resist blast damage	3.0
Sprayability	Should use standard spraying equipment; minimise losses; mix at nozzle	2.8
Humidity	Must work in relative humidity that exceeds 90%	2.8
Set-up time	Quick-setting, achieving minimum required strength after 8 hrs	2.8
Product life	Must be stable in presence of acid, alkaline, co_2 gas and diesel emissions	2.6

2.5 TSL experiments conducted at UOW

A fibre glass reinforced polymeric TSL is being developed at UOW. It has the properties that satisfy the specified Mine Occupational Health and Safety (MOHS) requirements. The formation of the composite layer between the TSL and the rock skin

via adhesion is one of the most desirable properties that enable stiff and durable rock skin reinforcement. The adhesion between the polymer liner and rock surface can confine the rock movement within seconds after spray application. This composite layer can significantly improve rock confinement of the area between the bolts and thus improve the integrity of a rock bolting system that can otherwise be undermined by the unravelling of fractured rock or coal skin. An improvement to strata skin control, namely the roof and the rib integrity can be expected when using the TSL product. This will lead to safer roadways and roadway intersections and possibly higher pillar strength as the friable coal and overstressed rock mass will remain confined.

2.5.1 Bearing Capacity of TSL

Currently, almost all steel bolt plates are designed for steel mesh support however, they can cause a TSL tear failure around the sharp metal edges. Ultimately, they can affect the support capacity of the polymer liners. The bearing capacity test aims to determine how the bearing plates and their shape influence the TSL polymer liner bearing capacity. A puncture test was designed and tested using the 500 kN Instron servo-hydraulic universal testing machine and the 5000 kN Avery compression machine. The ultimate compressive strength of the fibre glass reinforced polymer liner was measured as illustrated in Figure 2.34 (Nemcik *et al.*, 2011a). In this test, a series of steel discs shown in Figure 2.35 were utilised to load the TSL material to failure.

According to the test results, it can be seen that the bearing plate and polymer material began to bend upward when the compressive load was increased. When the maximum bearing capacity of the TSL was reached, the polymer layers began to separate and shear took place under the loaded area. The permanent damage occurred when the steel

plates punctured through the TSL. Once the steel disk penetrated the polymer, the measured loading rate rapidly increased with a minimal displacement. At that point the test was terminated.

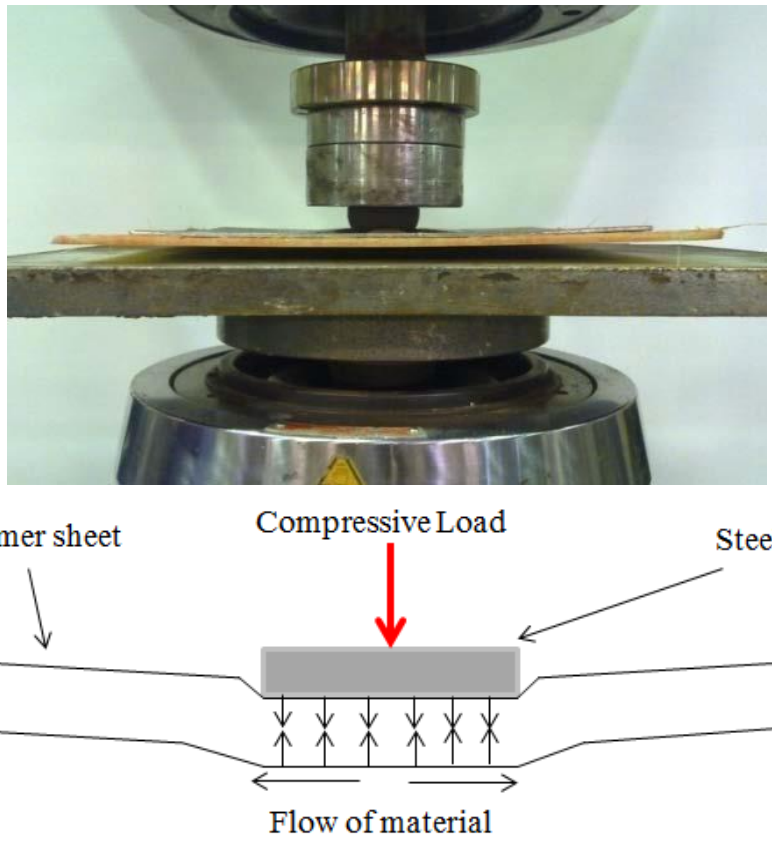

Figure 2.34 Loading of a steel disk compressed into a glass fibre reinforced polymer liner (Nemcik *et al.* 2011a)

Diameter (mm)	Thickness (mm)
10	17
20	17
30	20
40	20
50	20
60	20
80	20
100	20
120	20

Figure 2.35 A series of steel disc sizes used to load the polymer TSL to failure (Nemcik *et al.* 2011a)

As the size of the bearing plates increased, the bearing capacity also increased as shown in Figure 2.36.

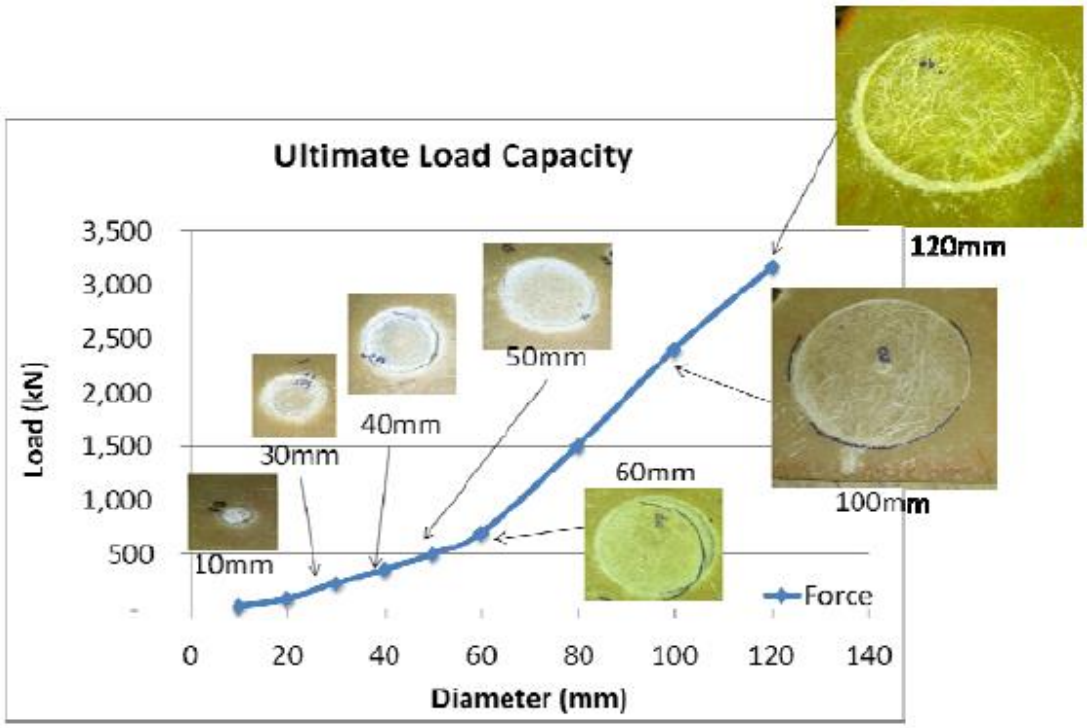

Figure 2.36 Summary of the load bearing capacity tests (Nemcik *et al.* 2011a)

As can be seen from the test results the bearing loads were linearly proportional to the diameter of the bearing plates for plate sizes from 10 mm to 60 mm in diameter. This punch failure was primarily a puncture failure through the material. For the larger plates the loading rate increased as the polymer did not experience a puncture failure. It must be pointed out that these preliminary puncture tests were conducted on smooth, flat and hard surfaces that do not represent the underground conditions where the puncture loads may be much smaller when installed on softer and irregular surfaces. It would be expected that on the softer and irregular surfaces the puncture failure mode and loads would be very different. Additional tests are planned to clarify this.

In order to optimise the bearing capacity of the steel plates, the plates must meet some requirements (Nemcik *et al.*, 2011a): (1) In order to minimise the stress concentrations, the steel plates should preferably be circular as the currently used rectangular steel plates can easily cause stress concentrations at the sharp corners; (2) The steel plates should have a thickness of 3 mm which can allow for some deformation; (3) To achieve effective bearing capacity, the steel plates should be quite large with a minimum suggested diameter of about 250 mm; (4) In order to install the bolt on uneven surface, the plate edges should be rolled or bent up; (5) The plates should be made stiffer at the plate centre; (6) Drainage holes around the collar of the steel plates should be implemented. An example of a stiffened plate can be seen in Figure 2.37.

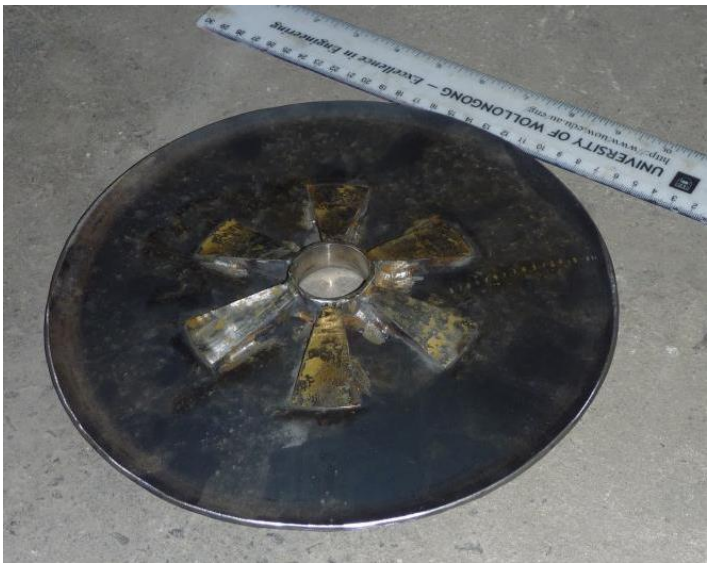

Figure 2.37 Example of a circular bearing plate for polymer bearing capacity testing (Nemcik *et al.* 2011a)

2.5.2 TSL Strength Testing

2.5.2.1 Estimated strata loads on TSL liner

The primary role of the TSL is to support the maximum strata loads that may develop in the unsupported area located between the bolts in the coal mine roadway. To

establish the maximum loads of the fractured and unsupported roof in a loose state located between the bolts, the following assumptions were made:

- The geometry of a typical rectangular coal mine roadway is 5.5 m wide or less.
- From a typical pattern of inclined bolts installed by the mine bolting system it is assumed that the spacing between the 4 bolts across the roadway does not exceed 1.5 m.
- The rows of bolts are typically spaced at not more than 2 m along the roadway.
- The severe damage that usually occurs within the immediate roof is caused by either weak geology fractured by lateral stress concentrations or geological structures such as joints or weak bedding planes.
- The unsupported roof between the bolts takes a shape of the pyramid as shown in Figure 2.38 with the base at the roof level and the central point at a height established by angle α.
- In the first assumption the angle α (see Figure 2.38) of severely fractured roof between the bolts that can unravel and fall out may not be greater than 30^{o}. This angle α is based on several assumptions. In response to high lateral stress, low angle fractures develop at approximately 30^{o} to the direction of the lateral stress. This has been taken from the basic rock mechanics where α represents the angle between the axis of the cylindrical specimen loaded to failure and the failure plane calculated to be $\pi/4 - \varphi/2$, where φ = angle of friction. The angle φ typically ranges between 30^{o}- 40^{o} with the angle α ranging 25-30^{o}. Thus 30^{o} was chosen for this case.

- The density of rock is assumed to be approximately 2.5 kg/m^3.

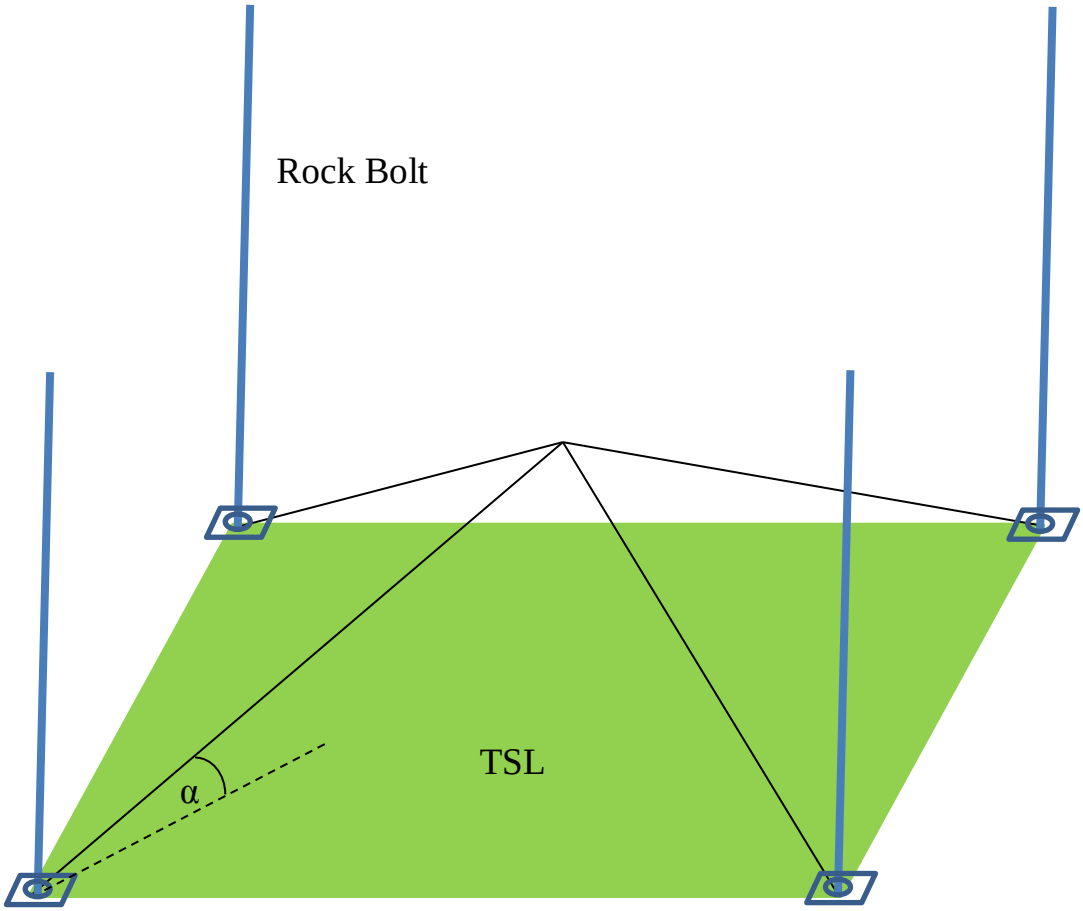

Figure 2.38 Expected strata loads on the TSL

Based on the above assumptions, the calculated maximum load of the pyramid is approximately 1.8 tonnes.

In the second assumption, if the weak rock fractures totally into small particles and separates from the reinforced strata, a steeper arch like volume of rock may need to be considered. Lack of resin encapsulation in the lower bolt section adjacent to the bolt plate can also increase the failure height. However, such deformations do not represent the typical failure in bolted roadways and therefore may not represent the normal

conditions where the TSLs may be used. Never the less the assumed potential weight that can be carried by the TSL was raised to 4 tonnes for several reasons:

- The capacity of the typical roof steel mesh used underground is around 4 tonnes.
- Strength of the TSL ≥ 4 tonnes is based on a 5 mm thick liner.
- The profile of loose failed rock that needs to be supported by the TSL in some mines may exceed 1.8 tonnes in weight.

2.5.2.2 Non-destructive Tests

Polymer sheet and steel mesh non-destructive experimental tests were carried out by placing 1 tonne load using the terracotta pavers on a 1 m by 0.8 m polymer sheet and a steel mesh (Nemcik *et al.*, 2011b) as shown in Figure 2.39. It is clear that the recorded defection of the loaded polymer sheet was 40% lower than the deflection of the steel mesh using the same load.

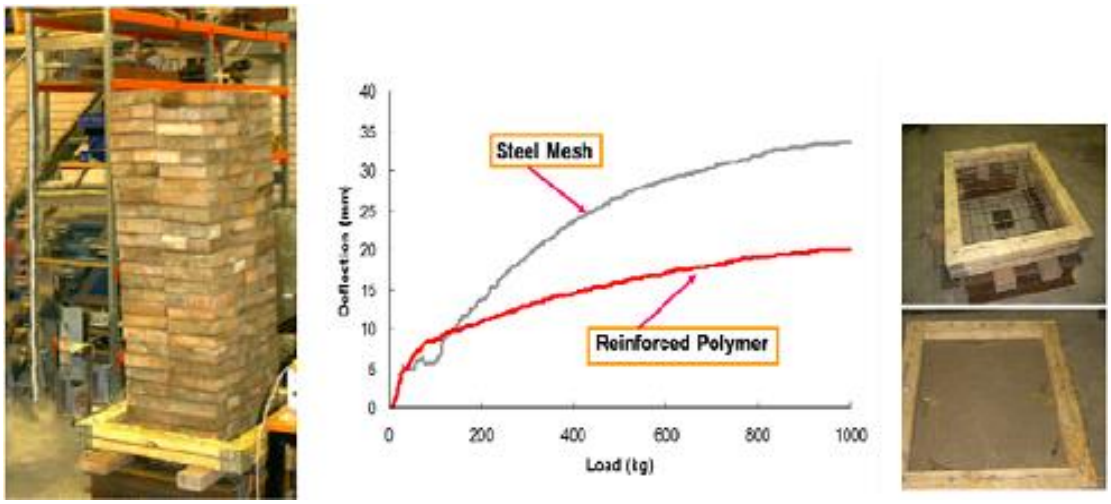

Figure 2.39 Glass fibre reinforced polymer skin and steel mesh with 1 tonne of evenly distributed load (Nemcik *et al.* 2011b)

2.5.2.3 Ultimate Strength Testing

In order to investigate the ultimate strength of the polymer liners, a number of polymer sheets were used to conduct the test. Because the 1 tonne load was not enough to fail the glass reinforced polymeric sheets in the previous tests, a greater load was applied onto the tested sheets. The steel frame was built to conduct the tests in a 500 t Avery compressive machine. The test sample size was 0.8 m by 0.6 m because of the loading machine restrictions.

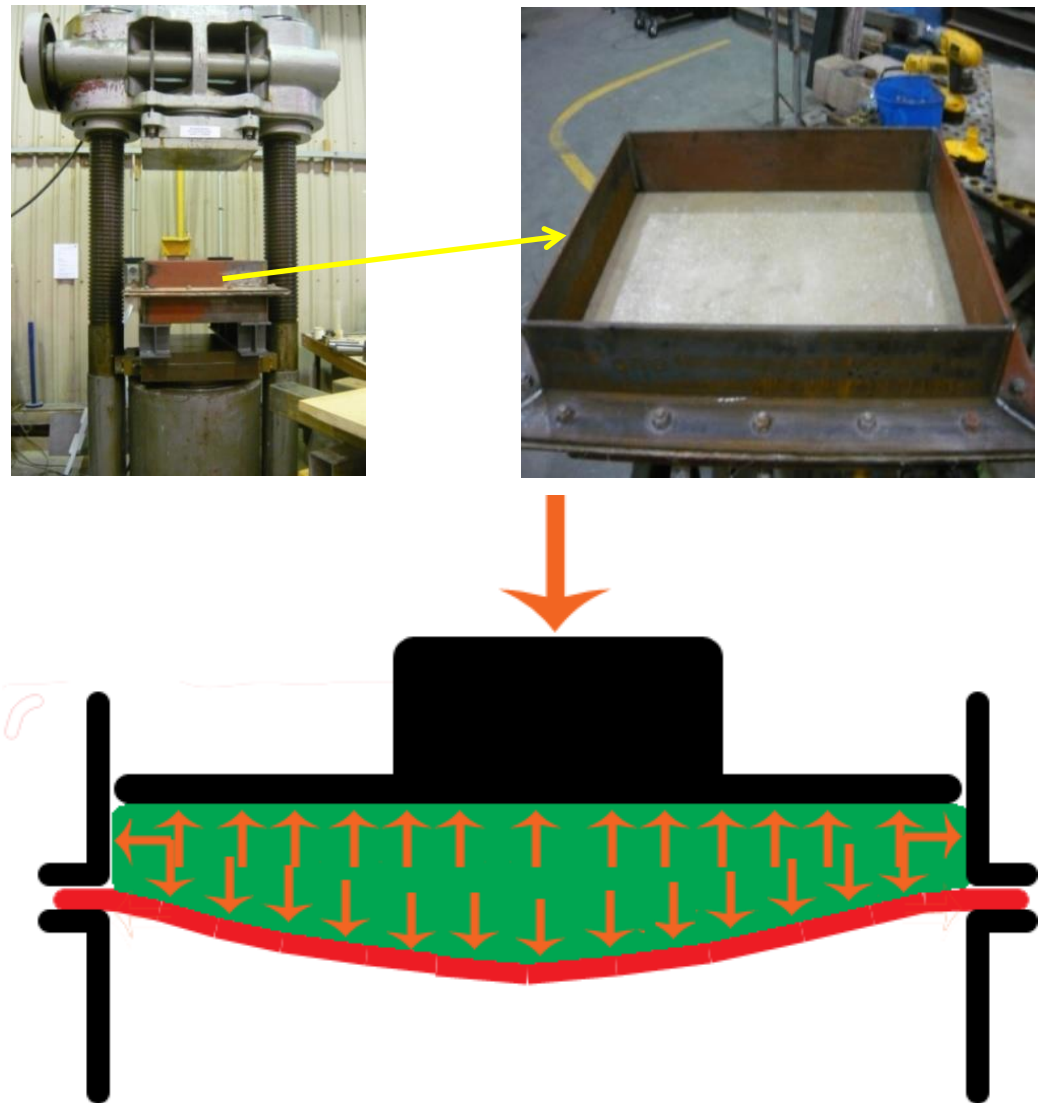

Figure 2.40 Polymer sheet loaded with the assistance of an air bag (Nemcik *et al.* 2011b)

Four types of tests discussed below were conducted. An evenly distributed load was trialled using a semi inflated airbag placed onto the polymer sheet sample. The airbag was inflated without protruding out of the steel enclosure, covered with a steel plate and loaded as shown in Figure 2.40.

The puncture and deflation of several air bags occurred prior to reaching the ultimate load. Despite the early failure of air bags, the tests revealed some important results indicating that: the polymer sheet did not fail when an evenly distributed load of up to 69 kN was applied onto the tested sample sheet. The achieved load was relatively high when considering the required capacity of skin support underground.

Three other tests were carried out to get the ultimate strength of the glass reinforced polymer liner. A circular steel seat 150 mm in diameter with a 5 mm rubber matt at the contact surface was used to load the sheet as shown in Figure 2.41. The failure occurred below the contact point at the load of 45 kN at a maximum deflection of 52 mm.

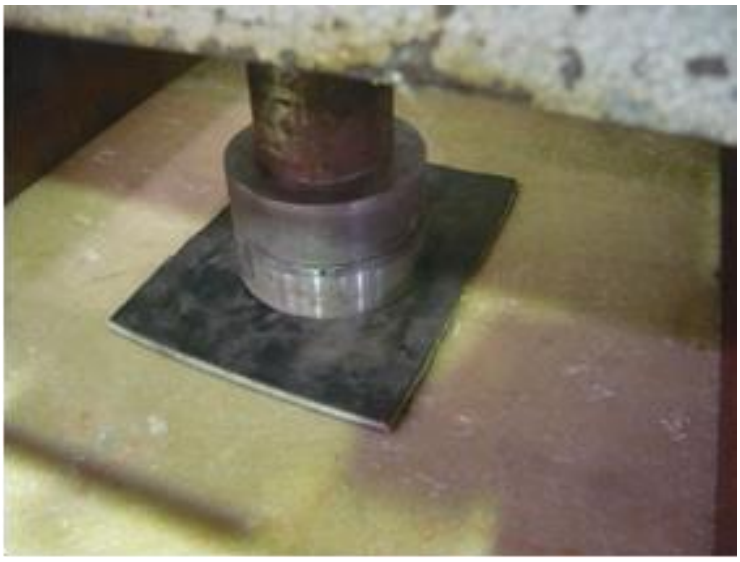

Figure 2.41 Loading of the polymer sheet to failure with a 150 mm diameter steel plate (Nemcik *et al.* 2011b)

Based on the previous tests, the following test was conducted by bonding terracotta pavers to the TSL polymer sheet. In this test, a load of 100 kN was applied and a deflection of 38 mm measured without failure. The last test was based on the second test, using a rubber mat buffer over the TSL polymer to minimise problems of the steel loading plate sharp edge as shown in Figure 2.42. The adhesion was lost between the pavers and the specimens in the process of testing.

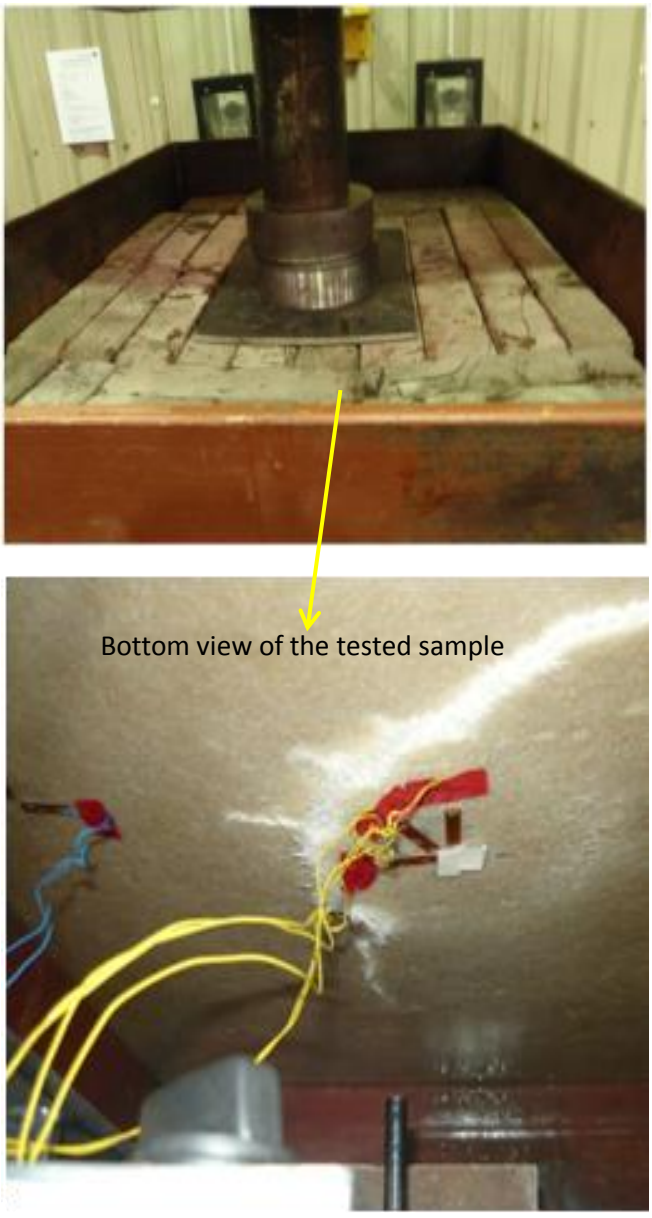

Figure 2.42 The TSL sheet loaded with the 150 mm steel cylinder on pavers (Nemcik *et al.* 2011b)

The four test results were compared in Figure 2.43. Through the tests it was shown that the samples can resist loads from 4 to 10 tonnes which was more than the maximum *in situ* load conditions calculated to be not more than 4 tonnes. Therefore, the test data indicate that the polymeric TSL is an effective support method.

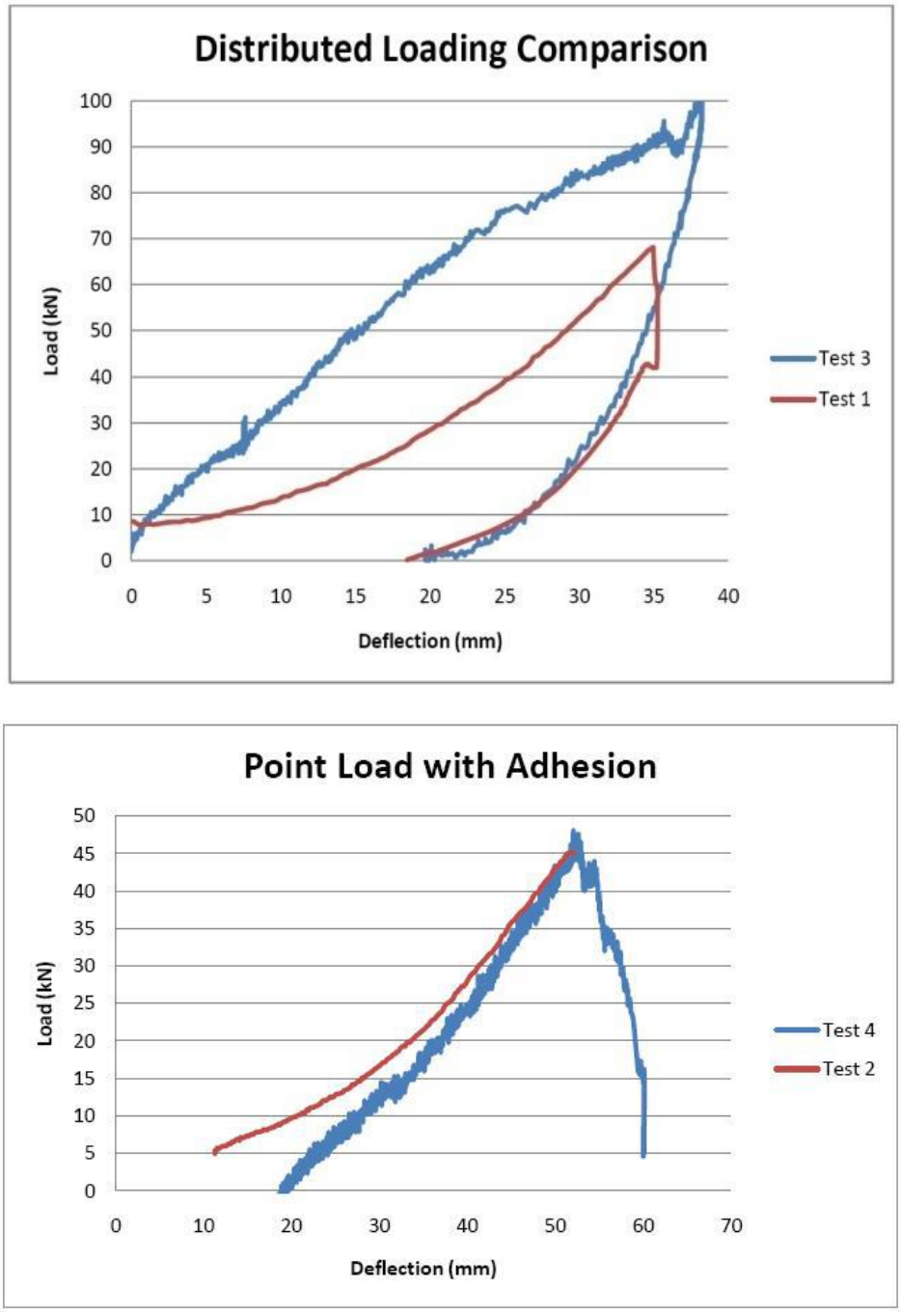

Figure 2.43 Summary of the TSL load vs displacement of all four tests (Nemcik *et al.* 2011b)

2.5.3 Tear strength of TSL

In order to investigate the tear strength of the TSL materials, it is essential to understand the mode of tear failure in underground roadways. According to Nemcik *et al.* (2013a), there are two main failure types, one is the tear failure due to the lateral movement of TSL through the rock bolts installed underground and the other is the trouser tear due to the differential movement of the supported strata both shown in Figures 2.44(a) and 2.44(b) respectively. He carried out two types of experiments using the fibre glass reinforced TSL. The tests are described below.

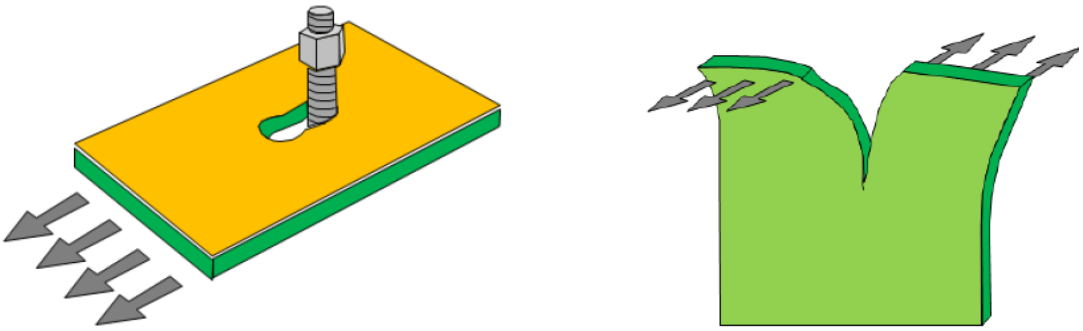

Figure 2.44 Schematic diagram of the TSL tearing test (Nemcik *et al.* 2013a)

2.5.3.1 Bolt tear test

Six polymer sheets 300 mm in length, 150 mm in width and 5 mm thick, were used to conduct the rock bolt-TSL tear test. Three samples were reinforced with two layers of glass fibre and the other three were reinforced with three layers of glass fibre. A hole with the diameter of 27 mm was drilled through the polymer sheet, and a steel rock bolt 22 mm in diameter (a standard rock bolt diameter in Australia) was placed in the hole. The 500 kN Instron servo-hydraulic universal testing machine was used to induce

bolt shear as shown in Figure 2.45. The displacement rate of 5 mm/minute was adopted to load the samples.

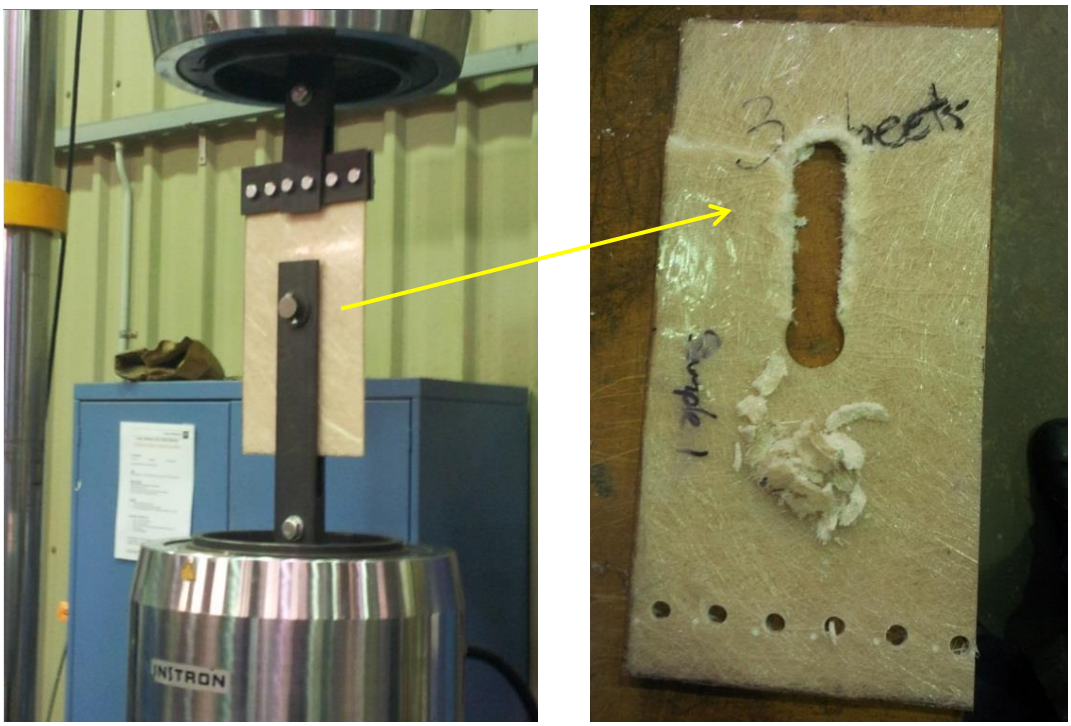

Figure 2.45 The polymer sheet with steel rock bolt clamped into the 500 kN Instron servo-hydraulic universal testing machine and torn apart (Nemcik *et al.* 2013a)

The samples reinforced with two layers of glass fibre failed at the tear strength ranging from 4 kN to 8 kN while the samples reinforced with three layers of glass fibre failed within the range of 6 kN to 12 kN. The load versus displacement graphs were plotted in Figure 2.46 and Figure 2.47 respectively for two and three layers of glass fibre reinforced polymer sheets.

Results show that the tear strength of the bolt-TSL may not be sufficient for resisting the tear action at high loads however the tear itself may not seriously influence the TSL support capacity. The tests of currently used steel mesh indicate that the mesh is stiff and yields quickly when loaded parallel to the steel strands. However in the

diagonal direction it begins to deform at a relatively low load that increases sharply as the deformation reaches critical values prior to failure.

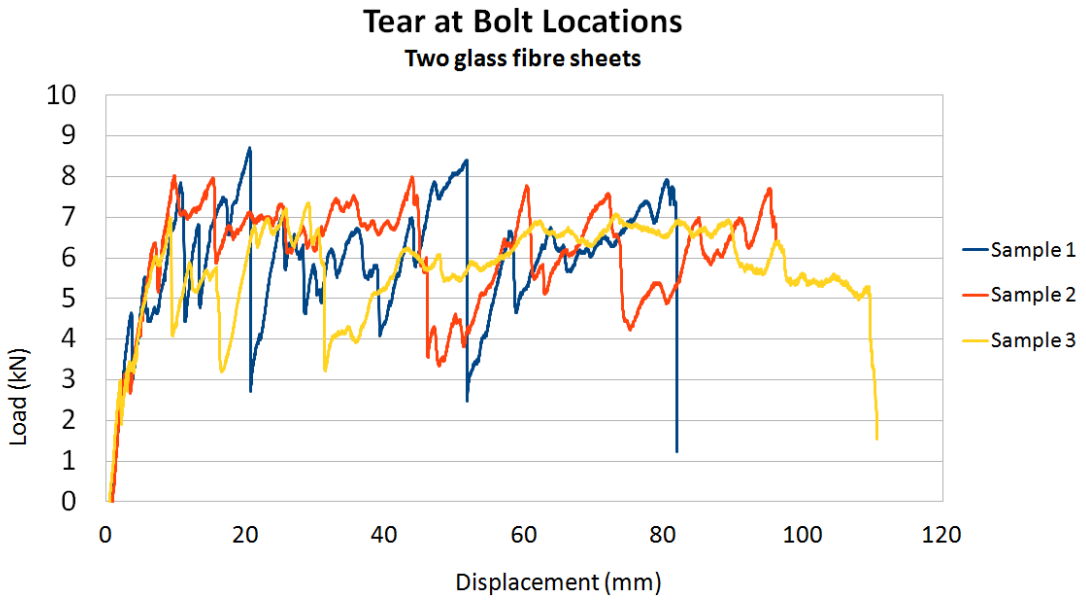

Figure 2. 46 Measured bolt tearing capacity of polymer samples reinforced with two glass fibre sheets (Nemcik *et al.* 2013a)

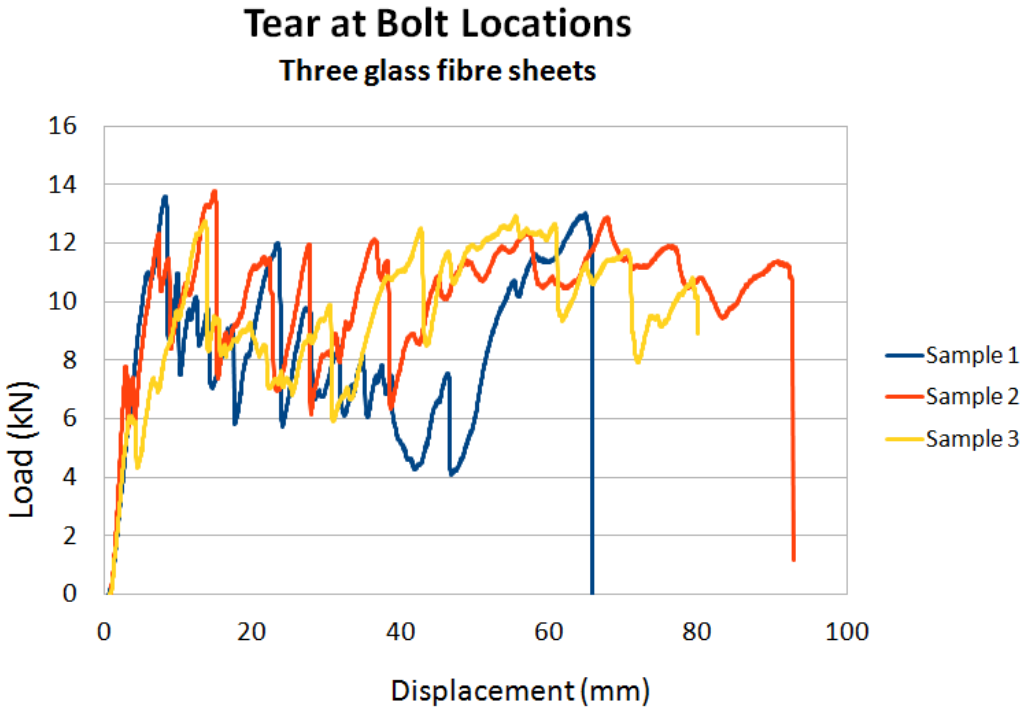

Figure 2.47 Measured bolt tearing capacity of polymer samples reinforced with three glass fibre sheets (Nemcik *et al.* 2013a)

2.5.3.2 Trouser tear test

Six polymer sheets 200 mm in length, 100 mm in width and 5 mm in thickness, were used to conduct the trouser tear test. Three samples were reinforced with two layers of glass fibre and the other three were reinforced with three layers of glass fibre. In order to enable the tear to propagate, a 50 mm long cut was prepared in each polymer sheet. To enable the tests (shown in Figure 2.44b), the edges of the samples were clamped and pulled in the opposite directions normal to the polymer sheet. The 500 kN Instron servo-hydraulic universal testing machine was used to tear the prepared sheet apart (Figure 2.48).

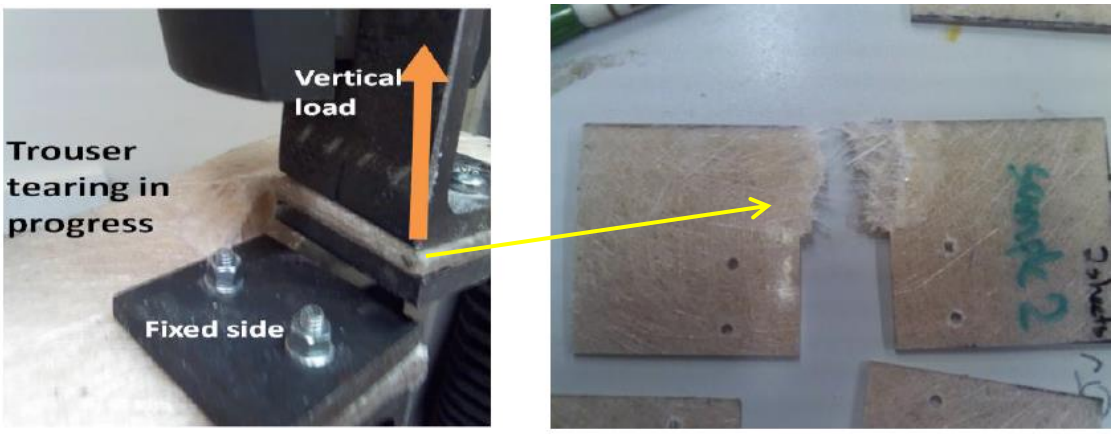

Figure 2.48 TSL sample clamped in the 500 kN Instron servo-hydraulic universal testing machine and torn apart (Nemcik *et al.* 2013a)

The trouser tear resistance of samples reinforced with two glass fibre layers peaked at an average of about 0.4 kN while the samples with three glass fibre layers tore at a higher load averaging approximately 1 kN. The load versus displacement graphs were plotted in Figure 2.49 and Figure 2.50 respectively for two and three layers of glass fibre reinforced polymer sheets.

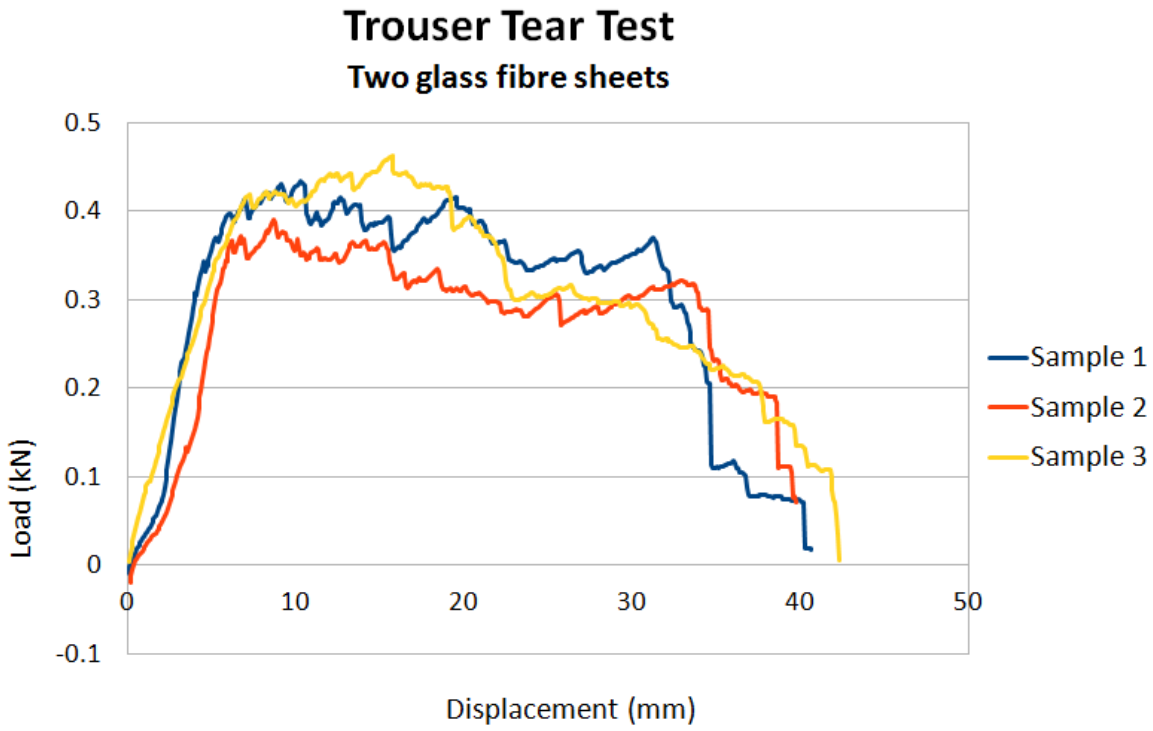

Figure 2.49 Measured trouser tearing capacity of polymer samples reinforced with two glass fibre sheets (Nemcik *et al.* 2013a)

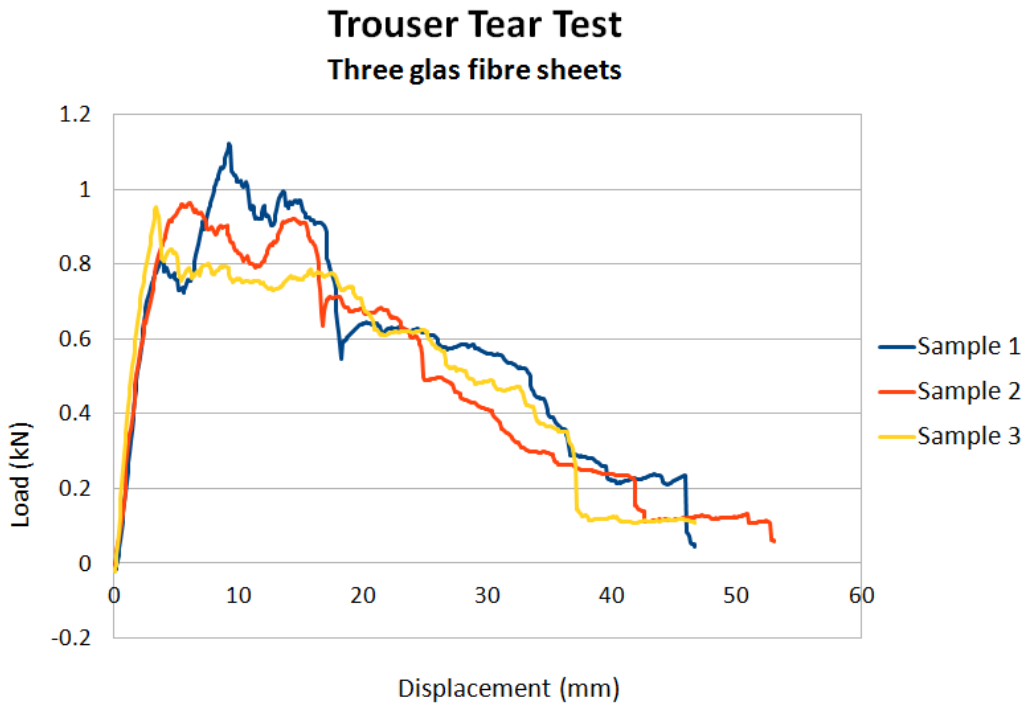

Figure 2.50 Measured trouser tearing capacity of polymer samples reinforced with three glass fibre sheets (Nemcik *et al.* 2013a)

A delamination problem occurred in some tests where the TSL separated along the glass fibre layers as shown in Figure 2.51. This occurred due to the nature of laying the fibre during sample preparation. Delamination is unlikely to occur during TSL spray application where the individual fibres would orient in a more random pattern. Further tests need to be carried out with sprayed fibre reinforced product.

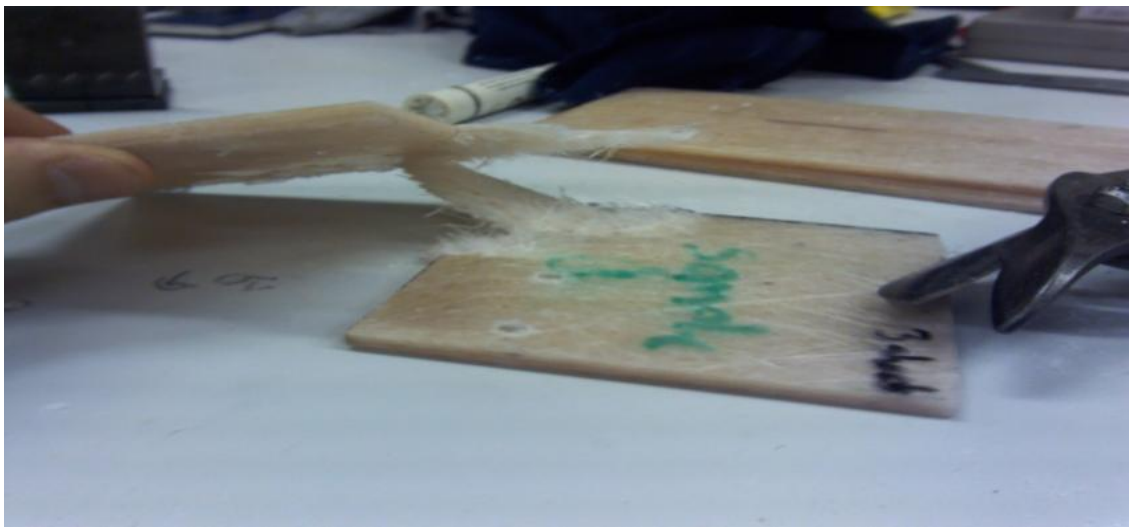

Figure 2.51 Delamination along the glass fibre layers (Nemcik *et al.* 2013a)

2.5.4 Guttering experiment

In a high lateral stress environment mine roadways can sustain significant roof and floor damage if oriented at a high angle to the maximum horizontal stress. Roof tends to develop gutters on the side of the roadway where severely damaged and unsupported rock may fall out as shown in Figure 2.52.

To assess the reinforcing capabilities of glass reinforced polymer skin supporting damaged sedimentary strata a 5mm polymer layer was bonded to a concrete block formed from a number of small triangular prisms to simulate fractured strata. The concrete prisms within the block were oriented as shown in Figure 2.53 to simulate

failed bedding planes and low angle shear fractures that often form in response to high lateral stress.

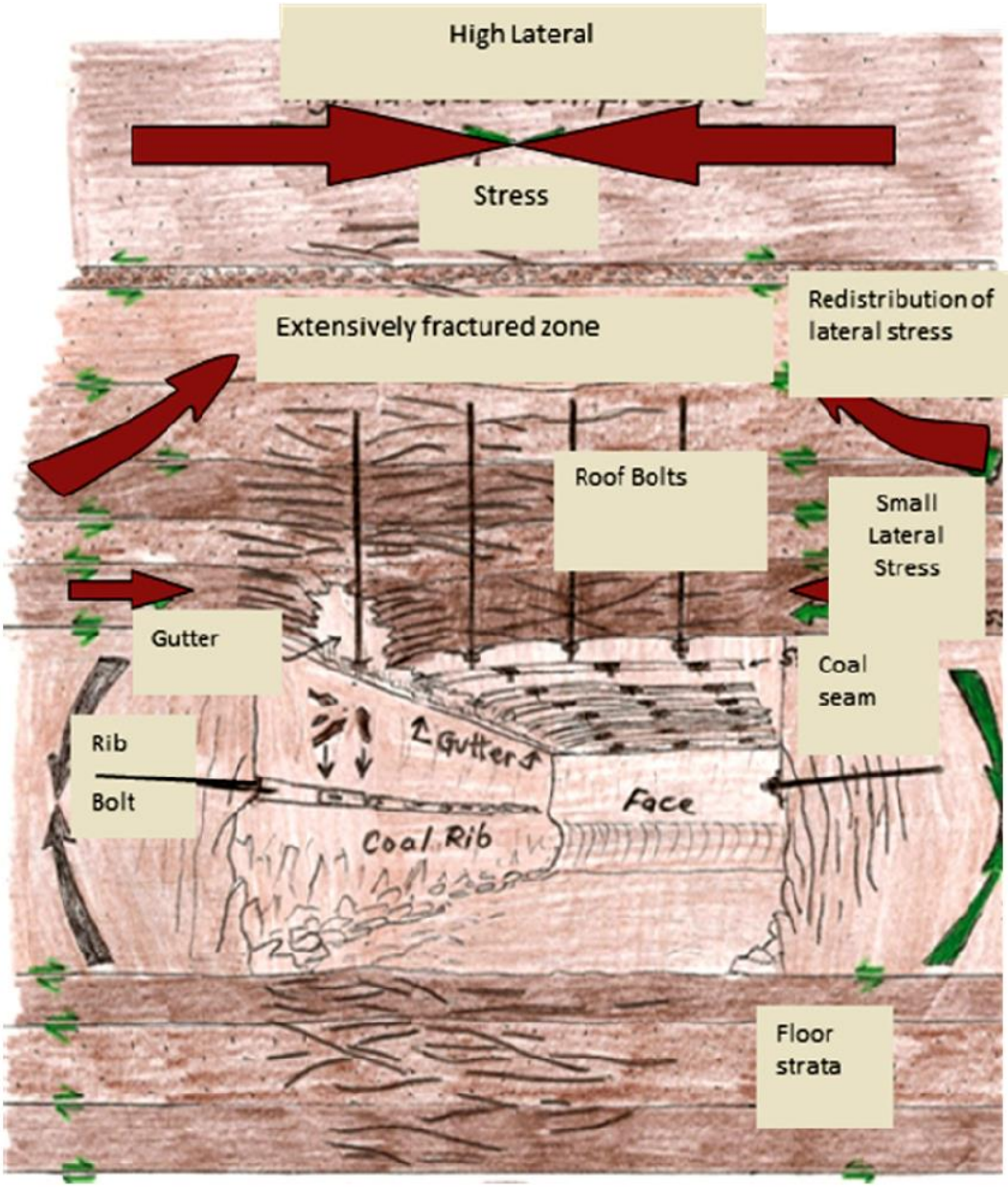

Figure 2.52 Typical roof conditions in coal mine roadway in a high lateral stress environment (Nemcik *et al.* 2013b)

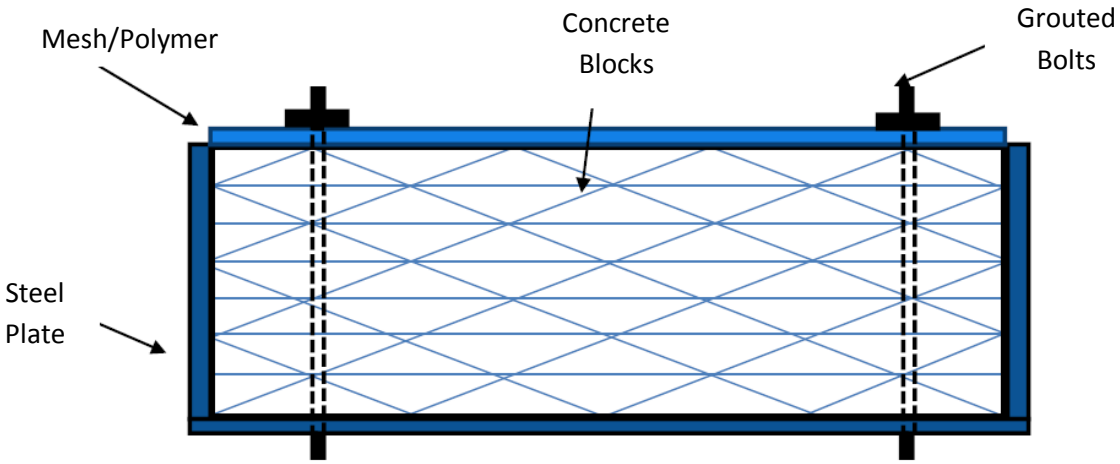

Figure 2.53 Test specimen assembled from concrete prisms to imitate fractured strata (Nemcik *et al.* 2013b)

Three of these large scale tests were conducted. In addition to a test with no skin reinforcement, which produced predictable results, a second test used the glass fibre reinforced polymer for skin support and another used steel mesh. The block dimensions were restricted to 800 x 400 x 400 mm in size due to the loading machine size. The three sides were confined with steel plates and bolts while one side was a free face reinforced first with the polymer reinforcement and then with the steel wire mesh. The 5 mm glass reinforced polymer sheet was bonded (using the same polymer) to the exposed concrete face to simulate adhesion of the sprayed polymer to the concrete prisms. The confined concrete block was then mounted into the Instron machine and loaded at a rate of 0.5 mm per minute while the load and displacements were monitored.

As the load increased, slip along the concrete prisms dilated the concrete loading the reinforcing polymer sheet. The polymer sheet gradually de-bonded but continued to resist the substantial concrete skin movement (Figure 2.54) with the maximum load

and deflection as shown in Figure 2.56. The test was stopped prior to polymer failure as unsafe conditions due to excessive block displacement were experienced.

Figure 2.54 Loading of the concrete specimen reinforced with polymer sheet showing dilation of the concrete prisms (Nemcik *et al.* 2013b)

To compare the effectiveness of the polymer skin reinforcement versus the steel wire mesh support, the experiment was repeated with 5 mm thick 100 mm x 100 mm steel wire mesh attached to the concrete face with four bolts and plates. The concrete specimen was loaded at the same rate as before and the block behaviour was monitored. The loaded specimen supported with the steel wire mesh and polymer is shown in Figure 2.55. As the load on the sample increased, the blocks began to slide along the discontinuities and rotate, displacing and loading the wire mesh. As before the test was not loaded to failure as the displacements of the specimen exceeded the safe limits.

The maximum stress and the associated deflections were 1.58 MPa and 107 mm for steel mesh and 3.15 MPa and 94.3 mm for TSL as shown in Figure 2.56.

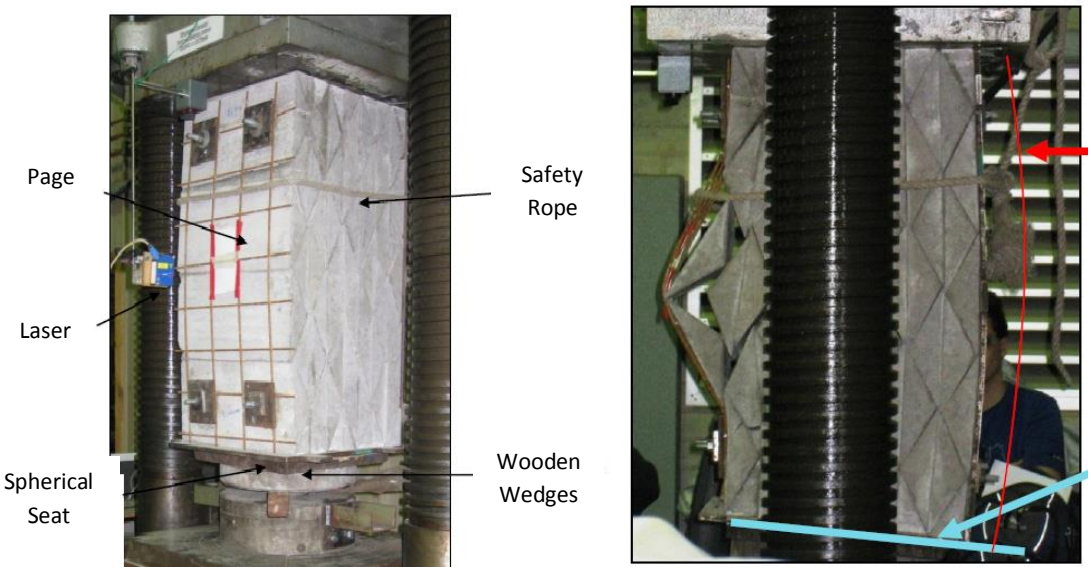

Figure 2.55 Loading of the concrete specimen reinforced with steel wire mesh showing displacement and rotation of the prisms (Nemcik *et al.* 2013b).

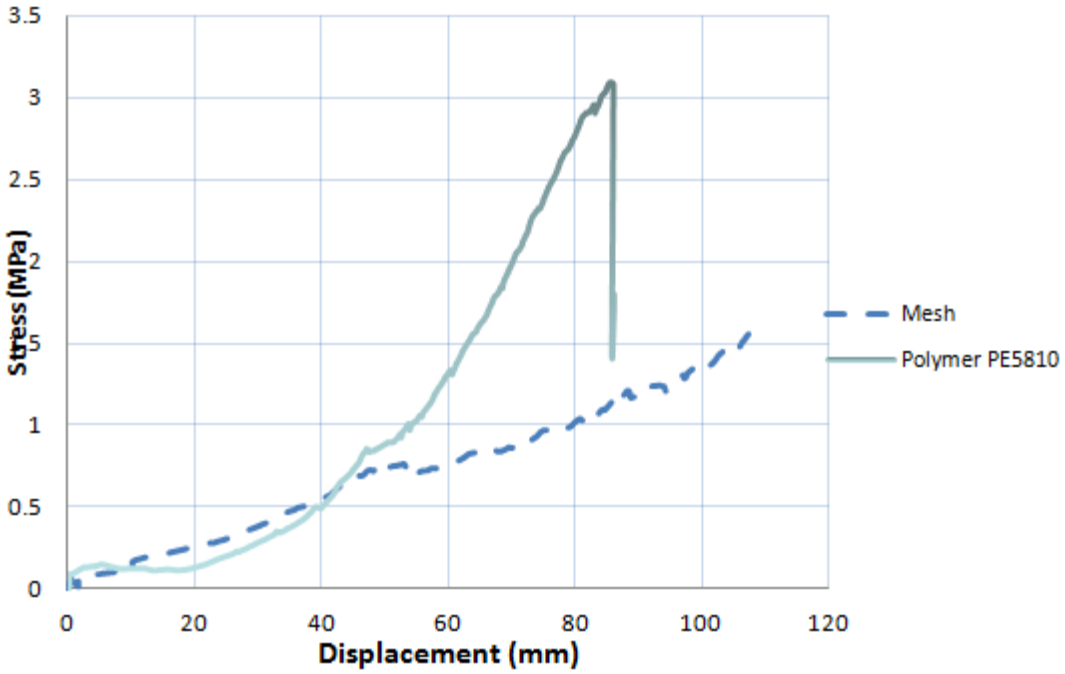

Figure 2.56 Load vs displacement results for tested concrete specimen reinforced with the polymer skin and steel wire mesh (Nemcik *et al.* 2013b).

2.5.5 Strata with weak bedding planes

To compare the performance of TSL and steel mesh in reinforcing strata with weak bedding planes, three laboratory experiments were made, one was a control sample without any skin support and the other two samples were supported with the TSL reinforcement and steel mesh respectively as shown in Figure 2.57.

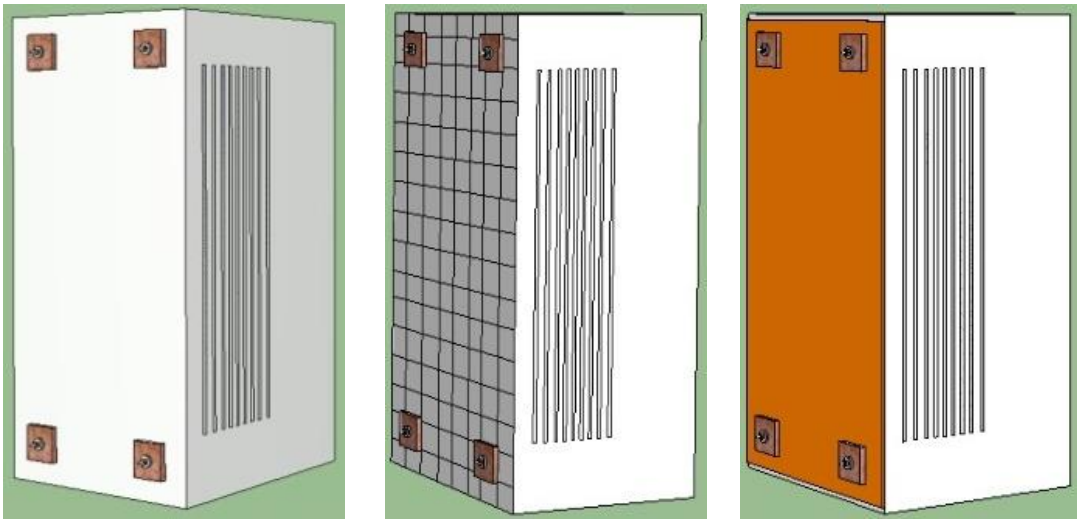

(a) Control sample (b) Steel mesh reinforced sample (c) TSL reinforced sample
Figure 2.57 Schematic diagrams of the samples (Shan *et al.* 2014a)

The control sample was made of concrete 400 mm in length, 400 mm in width and 800 mm in height. The bedding planes were simulated with thin plastic sheets. The cement, sand and water were mixed before pouring into the mould as shown in Figure 2.58a, while thin plastic sheets were placed at planned positions as illustrated in Figure 2.58b. The sample was left three to four days to set. To attach a steel frame to the back of the sample with rock bolts, four holes were made through the concrete. The TSL reinforced sample was prepared in a similar manner with 5 mm thick glass fibre reinforced polymer liner adhered to the front surface. In order to guarantee that the polymer liner was not loaded axially in the process of loading, the polymer liner was

made to be a little shorter than the height of the concrete surface. The last sample with steel mesh reinforcement was prepared in the same way with the steel mesh bolted to the front surface.

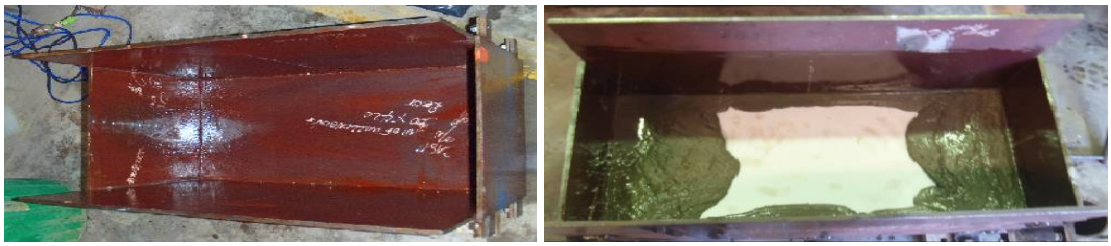

(a) (b)

Figure 2.58 Procedures for sample preparation (Shan *et al.* 2014a)

A 500 t compressive testing machine was used to conduct the tests. The tests were carried out at a loading rate of 0.5 mm/min. During the tests, the load and displacement were recorded. The normal displacement at the centre of the sample was measured with a laser. The test setup and TSL reinforced sample are shown in Figure 2.59 (a) and (b), respectively.

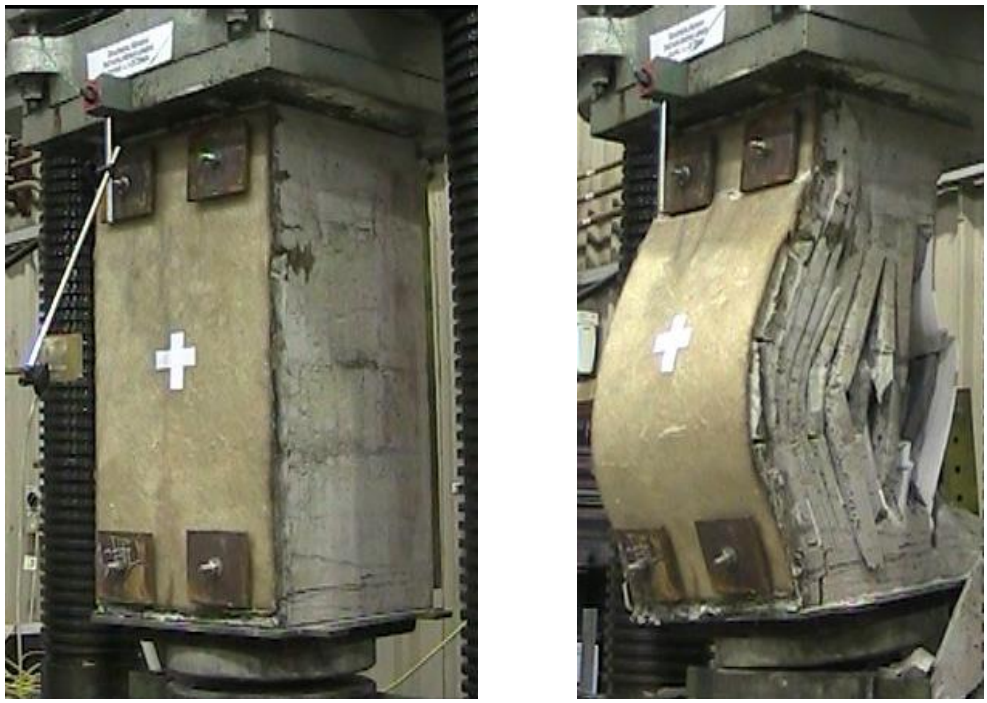

(a) (b)

Figure 2.59 (a) Test setup, (b) TSL reinforced sample after failure (Shan *et al.* 2014a)

The test results were summarised in Table 2.3. For the control sample, the sample cracked and concrete blocks dislodged when loaded. As expected, most cracks occurred near the weak bedding planes. The normal and axial displacements were 0.4 mm and 3.1 mm respectively at the peak load of 2494 KN. For the steel mesh reinforced sample, the peak load was 2321 KN. The load was lower than the control sample, and the reason for that is that one rock bolt broke during the loading which reduced the bearing capacity of the sample. The normal and axial displacements were 1.9 mm and 3.1 mm respectively at the peak load. As for the TSL reinforced sample, the bonded surface de-bonded in the process of loading at first, and then concrete carried the compressive load. As the concrete deformed, the TSL confined the sample and resisted the load until failure. The maximum load was 2856 KN, and the normal and axial displacements were 2 mm and 3.1 mm respectively at the peak load.

Table 2.3 Summary of test results (Shan *et al.* 2014a)

Sample	Peak Load (KN)	Vertical displacement (mm)	Horizontal displacement (mm)
Control sample	2494	3.1	0.4
Steel mesh reinforcement	2321	3.1	1.9
TSL reinforced sample	2856	3.1	2

Figure 2.60 and Figure 2.61 shows the graphs of load versus normal displacement and load versus axial displacement respectively. It can be seen that the TSL reinforced sample gave the largest peak load, and the steel mesh reinforced sample exhibited the smallest peak load because of rock bolt failure. However, the difference between the three tests was not significant and the results were not conclusive. Therefore, this test had to be modified and redesigned. A new revised test was conducted and is analysed in the next section.

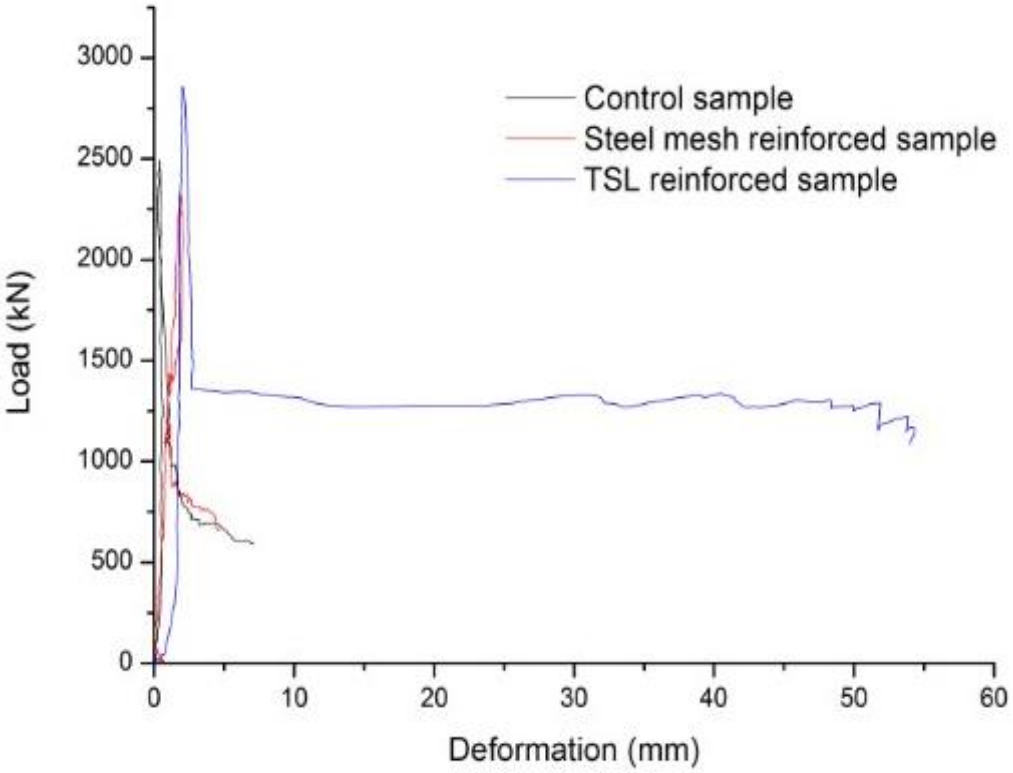

Figure 2.60 Load versus normal deformation (Shan *et al.* 2014a)

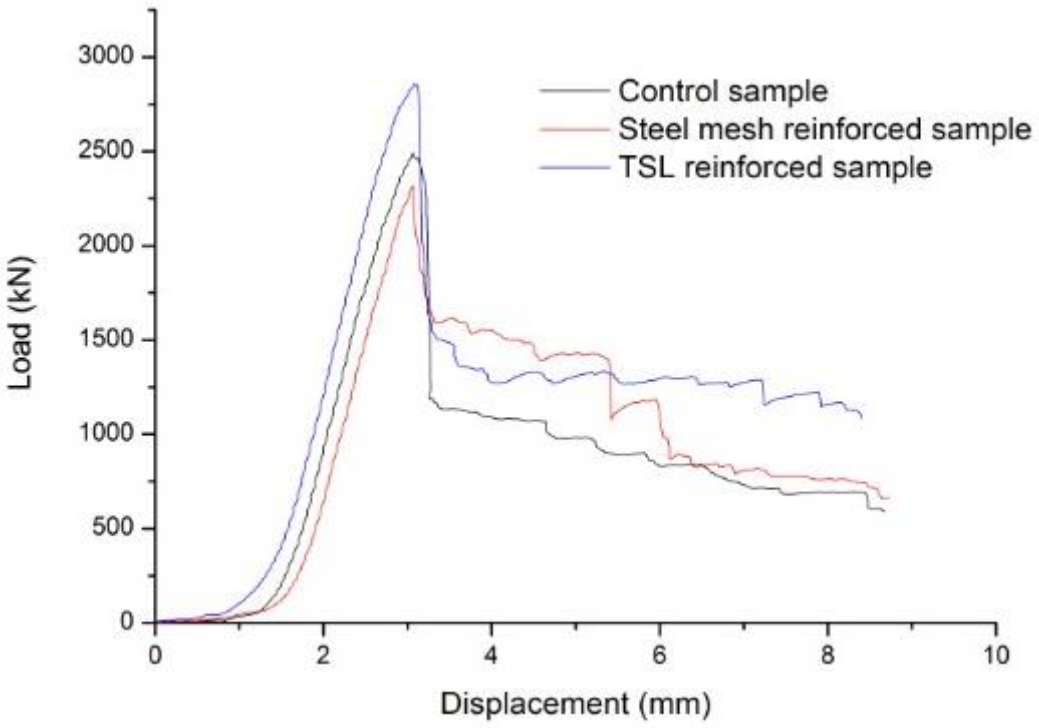

Figure 2.61 Load versus axial deformation (Shan *et al.* 2014a)

In hard rock mines dynamic loads must be considered and therefore the strata support design can be very different from that used in underground coal mines. In soft rock conditions encountered in Australian coal mines with depth not exceeding 600 m, the rock usually fails in a gradual manner ahead of the coal mining face. Therefore the strata support is normally installed in already fractured rock. Therefore the support is not subjected to any major dynamic loads. When designing the support for the stratified strata in coal mines, in most cases the geotechnical engineer is dealing with the post failure properties of rock. It is therefore important that in all tests undertaken in the laboratory, not only the maximum loads but the post failure loads need to be measured. As can be seen from Figures 2.60 and 2.61, after reaching the sample peak strength, the TSL reinforced sample can still resist a significant load up to around 1300 kN even with large displacements over 50 mm. However, the unreinforced sample and the steel mesh reinforced sample exhibited similar post failure behaviour with the residual strength of approximately 750 kN at the displacement of 9 mm only. Although these two tests were stopped early for safety reasons, it could be predicted that the residual strength would not increase with the additional displacement. Therefore, it can be concluded that the TSL material is better than steel mesh in reinforcing the tested sample in terms of residual strength which is critical in the coal mine roadway support.

2.5.6 Buckling strength of TSL

The buckling failure test represents the commonly observed failure in both roof and rib strata. In order to investigate the TSL-rock composite buckling strength, a buckling experiment was designed at UOW where the TSL was bonded to the pre-cast high strength plaster plates of a specific geometry to encourage buckling (Figure 2.62) and loaded to failure. Due to its bonding properties the TSL forms a composite layer with

the rock substrate that becomes significantly stronger than the unreinforced rock skin. The tests showed superior performance of the TSL bonded to the plaster plates in contrast to the unreinforced plates.

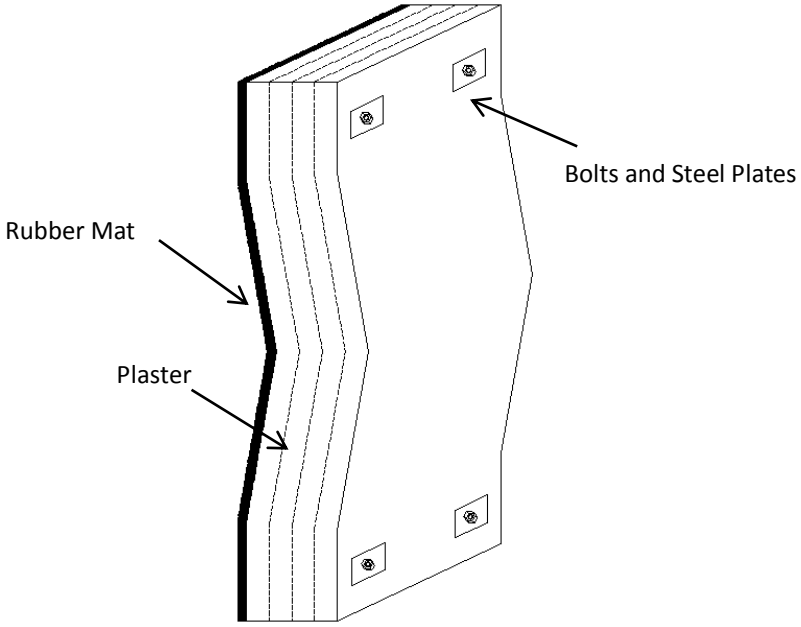

Figure 2.62 Schematic diagram of the buckling test (Mirsepassi 2013)

Figure 2.63 shows the failure mode of plaster samples with different support methods. The first test was conducted as a control test (Figure 2.63a) where the sample had no reinforcement on the outside surface. When the load was applied onto the sample, the tensile stress developed on the outside of each plate at the mid-span of the sample. The plates began to fail when the stress exceeded the tensile strength of the plaster. Calculations of the tensile stress indicate that the plaster tensile failure occurred at 7.4 MPa. The failure occurred at an axial load of 41.2 kN and the relevant normal displacement was 1.8 mm as shown in Figure 2.64.

The second sample was supported by steel mesh as shown in Figure 2.63b. The test result indicated that the plaster failure mode in tension was similar as in the previous test with no support. The axial load at failure was 78.5 kN and the relevant normal displacement was 3.1 mm. As expected, the steel mesh has significantly improved the bearing capacity of the plaster sample where the axial load increased from 41.2 kN to 78.5 kN. The results are shown in Figure 2.64.

(a) (b) (c)

Figure 2.63 Samples (a) without support, (b) with steel mesh support and (c) with polymer support after failure (Mirsepassi 2013)

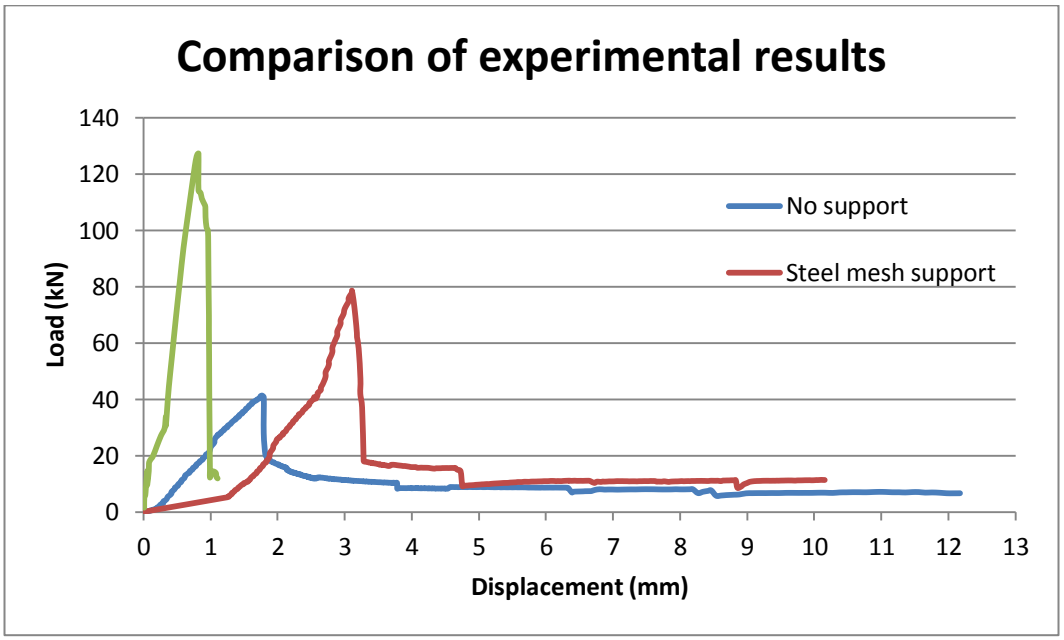

Figure 2.64 Testing results under different support conditions (Mirsepassi 2013)

Due to the TSL bonding characteristics the TSL forms a composite layer with the plaster plates that becomes significantly stronger than the unreinforced plaster plates. When bonded to the plaster surface, the polymer based TSL provides a confining stress to the adjacent plaster plate. Under this condition, the tensile stress at the TSL-plaster interface was lower, and the plaster failed in compression (shear), not in tension. However, the other adjacent plates failed in tension due to bending. In the tests, each mode of failure was clearly demonstrated in Figure 2.65. The sample reinforced with the TSL (shown enlarged in Figure 2.66) clearly shows the shear fracture that typically occurs in confined rock material where the tensile fractures cannot develop.

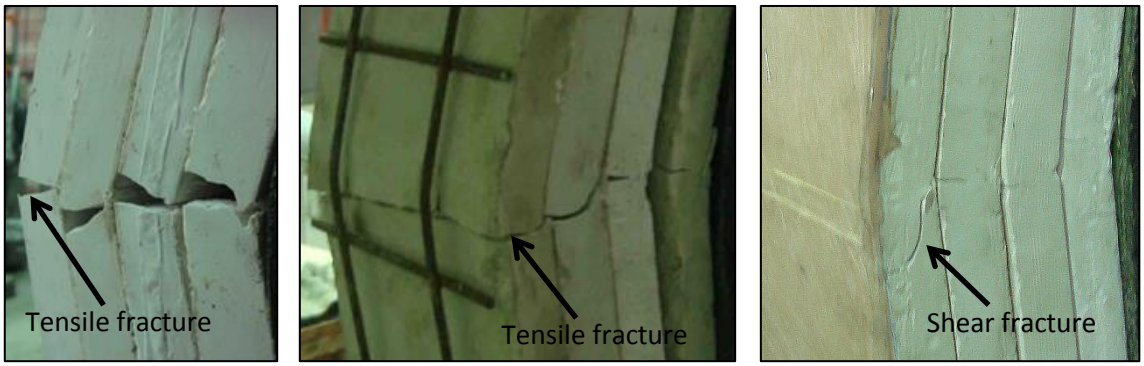

Figure 2.65 Fracture patterns of tested samples without support (a), with steel mesh support (b), and with polymer support (c)

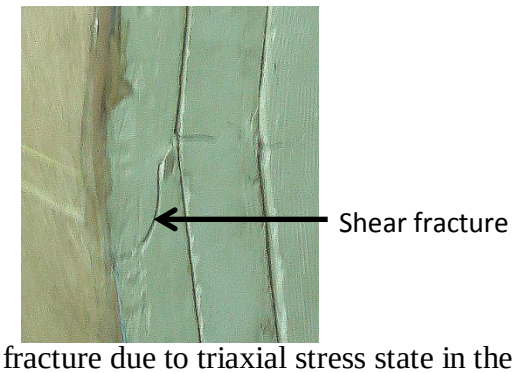

Figure 2.66 Shear fracture due to triaxial stress state in the reinforced plaster plate

This is evidence that the plaster plate reinforced with the TSL was loaded to a significantly higher value than the non-reinforced plaster. The failure load was 127.2

kN and the relevant loading displacement was 0.8 mm as shown in Figure 2.64. The tests showed superior performance of the TSL bonded to the plaster plates in contrast to the unreinforced and steel mesh reinforced plates.

2.5.7 Three Point Flexural Testing

When sprayed on roadway walls close to the underground coal mine face, the TSL material bonds to the rock skin and shortly after, rock bolts are installed through the cured TSL. When strata displacements occur during further mining, roof and coal ribs tend to buckle outwards into the mine opening bending the TSL material. The three-point bending test was designed to measure the TSL flexural strength. The TSL flexural testing setup is illustrated in Figure 2.67.

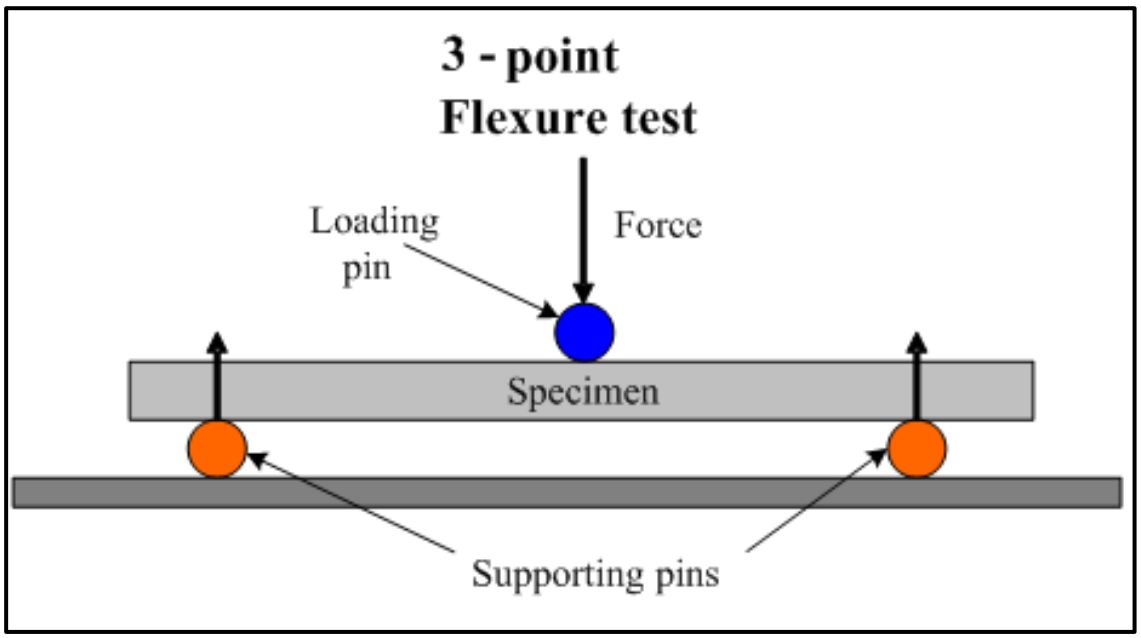

Figure 2.67 Three point flexure testing (Rolls 2008)

The flexural strength of TSL is obtained using Equation 2.9:

$$\sigma = \frac{3FL}{BH^2} \tag{2.9}$$

Where σ = Flexural strength

F = Peak load applied

L = Distance between two supporting pins

B = Sample width

H = Thickness of the sample

The Young's modulus E_b is calculated using Equation 2.10 :

$$E_b = \frac{L^3}{4BH^4} * \frac{F}{Y} \tag{2.10}$$

Where F = Applied peak load

L = Distance Between two supporting pins

B = Sample width

H = Thickness of the sample

Y = Deflection at the position of loading

To conduct the three-point bending test, the samples were placed on two supporting pins with 120 mm separation. The loading was applied at a rate of 2 mm/min. Rolls (2008) tested twenty samples. Among these eight samples were without fibre reinforcement and the remaining 12 samples were reinforced with glass fibre. The test results were averaged and shown in Figure 2.68.

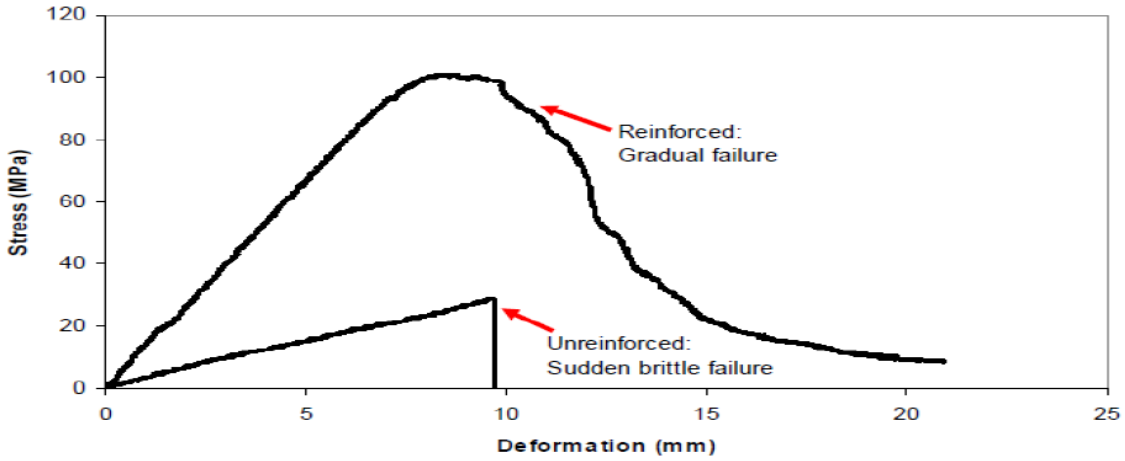

Figure 2.68 Three-point flexural test results of 5mm thick samples unreinforced and reinforced with glass fibre (Rolls 2008)

It can be clearly seen that the reinforced TSL can sustain a significantly higher resistance capacity than the unreinforced samples (around five times higher). Also it is shown that the reinforced samples failed gradually after reaching the peak load and exhibited ductile post failure behaviour. In contrast, the unreinforced samples broke suddenly after reaching the peak load and exhibited brittle failure behaviour. During excessive yielding the glass reinforced samples also exhibited an audible cracking noise which is beneficial in underground mining as it provides audible warning for safety when excessive strata displacements occur.

Dear (2010) studied the effect of different fibre types on the flexural strength of TSL samples using 6 mm long carbon fibre, 6 mm long glass fibre and 12 mm long glass fibre respectively. The testing results were presented in Table 2.4.

It is clear that the flexural strength and Young's modulus of the control sample without reinforcement was lower than the reinforced samples. Compared to the other samples, the sample reinforced with 12 mm long glass fibre exhibited the largest flexural strength and Young's modulus. It can also be seen that the length of glass fibre

affected the flexural strength. As shown in Table 2.4, the maximum strength of 12 mm glass fibre reinforced sample was twice the maximum strength of 6 mm long glass fibre reinforced samples. This is due to better cross-linking between longer fibres thereby making them harder to be pulled out of the polymer resin.

Table 2.4 Summary of flexural strength testing results (Dear 2010)

Definition	Control (unreinforced)	6 mm carbon fibre	6 mm glass fibre	12 mm glass fibre
Maximum deflection (mm)	17.8	9.4	11.9	15.9
Maximum Load (N)	85.4	138.7	162.6	330.2
Maximum stress (MPa)	13.6	22.1	25.9	52.6
Young's Modulus (MPa)	444	1881	1781	1952

2.5.8 Desirable Properties of the Polymeric TSL Material

The desirable properties of TSL developed by UOW listed in Table 2.5.

Table 2.5 Desirable properties of TSL (Presentation by Nemcik to ACARP 2012)

Mechanical Property	**Unreinforced**	**Glass Fibre Reinforced**
Tensile Strength	>10 MPa	>25 MPa
Elasticity (Young's Mod.)	>500 MPa	>10,000 MPa
Yield Strain	>1%	>5%
Ultimate Strain	>3%	>10%
Adhesion - Tensile (sandstone substrate)	>0.1 MPa (dry) >0.05 MPa (wet)	>0.1 MPa (dry) >0.05 MPa (wet)
Adhesion - Shear (sandstone substrate)	>1 MPa (dry) >0.2MPa (wet)	>1 MPa (dry) >0.2 MPa (wet)

The aim of the tests and research is to obtain the properties of the glass reinforced polymeric TSL and to match the desirable TSL properties listed in Table 2.5 developed by the UOW.

2.6 Summary

In general, it is accepted that high stresses underground are a dominant factor controlling the design and reinforcement of mine excavations. Primarily the high lateral stresses and their directions with respect to the orientation of mine excavations must be considered. Other factors that influence the reinforcement designs are the rock geology, intact and residual rock properties and geological structures.

To successfully estimate rock behaviour surrounding mine excavations it is necessary to quantify the stress conditions, geology, and rock properties. A suitable measuring and monitoring program of strata and the response of the reinforcement system described here must therefore be implemented.

Previous research has detailed many types of strata behaviour and discussed the suitable reinforcement systems to control strata failure. In coal mines where a soft bedded rock is present, these failures vary considerably. This chapter details the understanding of these variations that are essential to enable successful design of the reinforcing system for each condition.

Historical experience with strata support in coal mines has identified that rock and cable bolts are probably the most efficient roof support systems currently available. Furthermore the improvement in implementing TSLs in strata skin control in coal mines has been identified and proven to be more effective support than the currently

used steel mesh. One of the most desirable properties of the TSL materials described here include tensile and shear bonding to the substrate forming a composite layer of reinforced rock skin and the TSL. The spray system of applying the TSL materials to the substrate enables full automation of the process and thus can improve the productivity and safety in coal mines.

Steel bolt plates designed primarily for the mesh application are too stiff and can cause TSL puncture failure around the sharp metal edges. This can affect the support capacity of the polymer liners. A puncture test designed to measure the ultimate compressive strength of the fibre glass reinforced polymer liner established that TSL is able to withstand large loads ranging from 100 kN to 3000 kN for plate diameter ranging from 10 mm to 120 mm. These preliminary puncture tests were conducted on smooth, flat and hard surfaces that do not represent the underground conditions where the puncture loads may be much smaller when installed on the softer and irregular surface. Additional tests need to be performed to clarify this. The suggested improvements to the ordinary steel plates are larger more flexible plates with rounded edges that can distribute the loads more evenly to minimise TSL failure.

The lateral bolt tear tests of the reinforced TSL indicated a strength range of 4 kN to 8 kN for the samples reinforced with two layers of glass fibre while the samples reinforced with three layers of glass fibre failed within the range of 6 kN to 12 kN. It is envisaged that the tear induced by the bolt may not seriously influence the TSL support capacity. The trouser tear resistance of samples reinforced with two glass fibre layers peaked at an average of about 0.4 kN while the samples with three glass fibre layers tore at a higher load averaging approximately 1 kN. A delamination problem occurred in some tests where the TSL separated along the glass fibre layers due to the

nature of laying the fibre during sample preparation. Delamination is unlikely to occur during TSL spray application where the individual fibres would orient in a more random pattern.

The guttering experiment using the pre-jointed concrete sample reinforced with the 5 mm thick polymer TSL indicated a higher strength when compared to no support and the sample supported with 5 mm thick steel mesh. The sample reinforced with TSL failed at 496 kN and deflection of 94 mm while the sample supported with steel mesh failed at 248 kN and displacement of 107 mm.

The bedded strata support experiment was inconclusive as the bolts used to confine the large sample broke during loading. It is suggested to repeat these experiments in the future to establish the strength of each support mechanism.

The buckling test designed to the specific geometry that represents the commonly observed failure in both mine roof and rib strata was tested without and with the steel mesh support and also with the TSL reinforcement. The tests showed superior performance of the TSL bonded to the plaster plates in contrast to the steel mesh support or no support. For no support the sample failed at an axial load of 41.2 kN and 1.8 mm displacement, while the sample supported with steel mesh loaded to a maximum of 78.5 kN and displacement of 3.1mm and the TSL reinforced sample performed significantly better at a maximum load of 127.2 kN and 0.8 mm displacement.

The three point bending test clearly indicates that the fibre reinforced TSL samples are superior in bending with larger displacements, higher peak and post-failure loads and

associated audible warnings. The unreinforced TSL resin has a lower strength and behaves in a brittle manner with no post-failure strength.

Compared to the other samples, the sample reinforced with 12 mm long glass fibre exhibited the largest flexural strength of 52.6 MPa and Young's modulus of 1.95 GPa when compared to shorter fibres. The maximum strength of 12 mm glass fibre reinforced sample was twice the maximum strength of 6 mm long glass fibre reinforced samples.

CHAPTER 3 COMPRESSIVE AND SHEAR STRENGTH TESTING OF GLASS FIBRE REINFORCED POLYMERIC THIN SPRAY-ON LINERS

3.1 Introduction

This study addresses the development of TSL materials at the University of Wollongong. The compressive strength is one of the TSL properties that contribute to the quality of reinforcement, and therefore it must be known. However, there are limited research studies to date on the compressive strength of TSL. When developing the TSL material, many prototypes are routinely tested in tension and its flexural strength measured to select the best suited material. Currently there is no standard testing method to determine the compressive strength of the TSL materials. When considering usefulness of the compressive test, it is evident that the tests are complicated and may not be directly applicable to the TSL strength investigations. The compressive tests based on the cube samples used here are relevant mainly for TSL comparison purposes.

Likewise the shear strength of the TSL material is not routinely studied and only a limited number of research studies have been reported to date. When analysing the support capacity of TSL, Hadjigeorgiou and Grenon (2002) assumed that the shear strength of TSL is equal to its tensile strength. Tannant (2001) thought that the loss in support capacity of a TSL depends on the adhesion loss and tensile or shear rupture. With this in mind a testing system based on the shear punch method was developed to investigate the shear strength of TSL prototypes.

3.2 Compressive strength testing of thin spray-on liners

The aim of this test is to determine the compressive strength of TSL and attempt to establish a standard testing method for the compression test of TSL materials.

3.2.1 Sample preparation

3.2.1.1 Selection of sample shape and size

For comparison, it is desirable to perform compressive testing of the TSL prototypes with and without fibre reinforcement. Preparation of the fibre reinforced samples has proven difficult as the polymeric material is usually not viscous enough to evenly distribute the fibre within the large sample. In the process of preparation, ideally the glass fibre should be distributed evenly within the samples without air bubbles. The initial mould chosen to prepare the TSL samples was a plastic cylindrical tube with a height to diameter ratio of 2:1 shown in Figure 3.1.

Figure 3.1 Cylindrical mould to prepare TSL samples

However, the investigation showed that this mould was not suitable as the exothermic reaction caused by the resin heating producing excessive heat that melted the plastic mould and formed cracks in the sample. The main problem of the cylindrical bottle mould was the deformation under the exothermic reaction therefore the plastic mould was discarded. It was decided to use the steel cube moulds that are commonly used in the industry to test resins and other materials. The selected 40 mm steel cube mould assembly is shown in Figure 3.2.

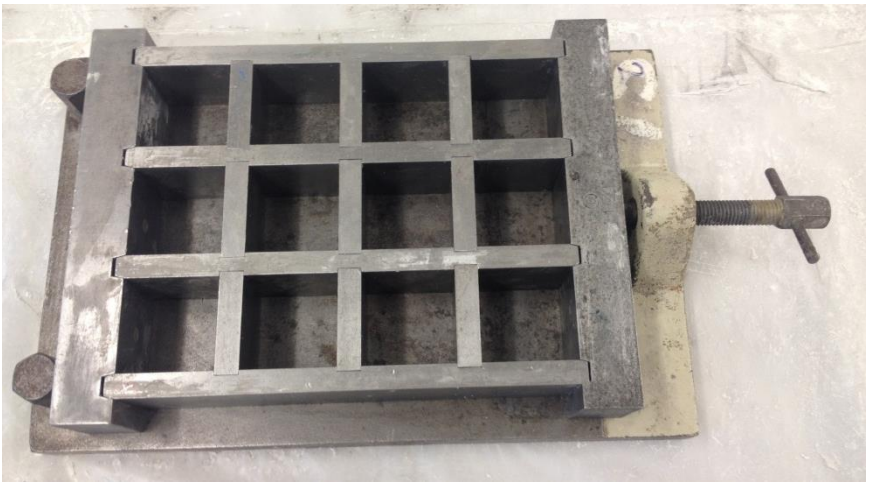

Figure 3.2 Steel cubical mould to prepare TSL samples

Compared with the plastic cylindrical mould, a steel mould assembly consisted of 12 small cubical moulds placed on a metal block. The dimensions of the multiple moulds were cubes of 40 mm side. This setup had an extra advantage over the previous mould as multiple samples can be poured at the same time reducing the sample preparation time. The cube has the further advantage that its sides do not need to be machined prior to testing as the steel plates make five out of six sides perfectly smooth ready for the compressive test. Being a steel mould, it does not deform or crack during the TSL

sample preparation and curing time. In addition, it is easy to grease the mould which makes the process of removing samples easy.

3.2.1.2 Procedure of sample preparation

The procedure to prepare the 40 mm cubical samples is:

a) Apply grease to all contact surfaces in the mould to ensure samples can be easily removed from the mould.

b) The polymer components are mixed evenly according to the research chemists' recommended ratio using a plastic cup and a wooden spatula.

c) Add the glass fibre as required into the solution and mix evenly.

d) Pour the solution into the mould and ensure it fills the mould and is distributed evenly as shown in Figure 3.3.

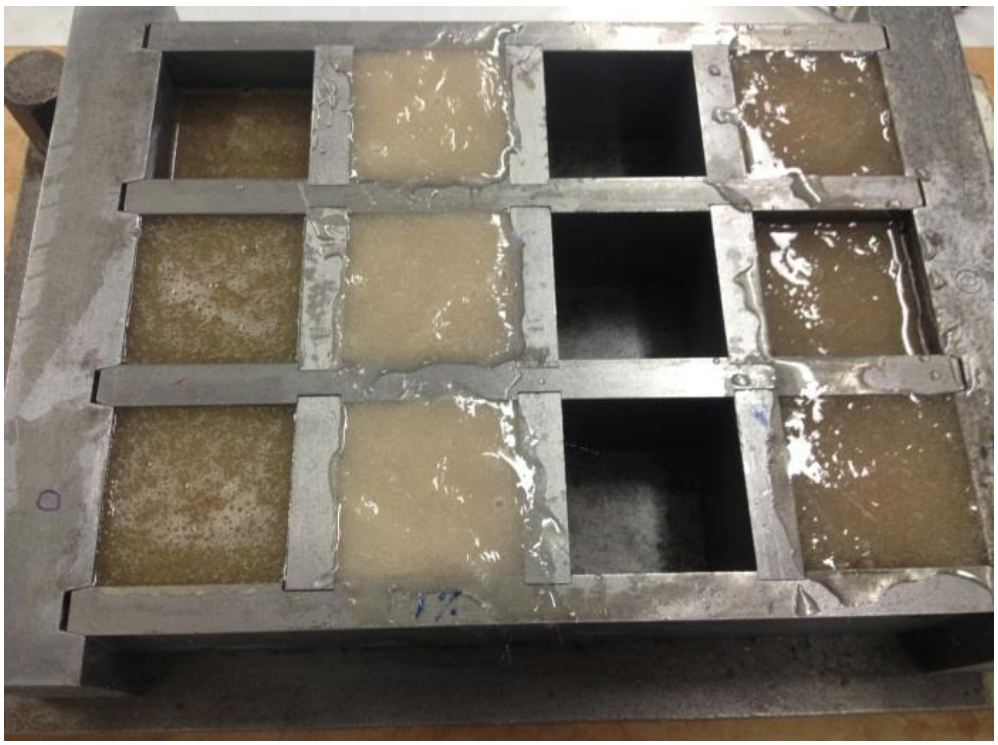

Figure 3.3 TSL samples after pouring

e) Repeat the previous steps for all samples within the mould assembly.

f) Put the mould with the TSL samples in the oven at 60℃ overnight to standardise the polymer curing process.

g) Remove the samples carefully and sand down the sharp surfaces until smooth as shown in Figure 3.4.

Figure 3.4 Completed TSL samples ready for testing

The chosen mould enabled quick sample preparation for the compressive tests however, several problems occurred in the process of pouring samples. The polymer became difficult to mix as the glass fibre content increased. It was practically impossible to mix more than 1% of glass fibre into the mould. This amount of fibre is far less than needed and other methods must be trialled to achieve much greater percentage for testing. The sprayed product may consist of more than 30% of glass fibre by volume. Therefore, in the future, a new method needs to be devised to enable mixing a greater proportion of the fibre material into the samples. Other problem was

air bubbles entrapped within the solution during polymer mixing. This problem can be partially overcome using vibration or a vacuum chamber treatment.

Since the high fibre content mix was not possible, three low glass fibre contents were chosen to be tested. Nine samples were prepared. The first three had no glass fibre, the second three had 0.5% glass fibre and the last three samples had 1% of glass fibre mixed in.

3.2.2 Test setup

The Instron hydraulic testing rig was used for the compressive testing. A compressive load was applied onto the polymer samples and loaded to failure, while load and deformation measurements were recorded. The Instron testing device is shown in Figure 3.5 below.

Figure 3.5 Compression strength testing setup

3.2.3 Test results

Testing of the samples showed that the polymer samples gradually failed with violent outbursts of small debris flying at considerable velocities away from the sample. This made the experiment unsafe so the initial test ended prematurely. This can be seen in the graph of the first sample with 1% of glass fibre and the third sample without glass fibre where testing stopped much earlier. The solution to the flying debris was to wrap a rag around the samples. All remaining samples with and without the added fibre were successfully tested.

The third sample of three with 0.5% glass fibre and the first sample of three with 1% glass fibre had a higher yield point than the other two samples with the same fibre content, respectively. The reason for this difference may be because not all samples came from the same mixture. The two samples with 0.5% glass fibre were made from the same batch, whereas the third sample was made separately. Also the last two samples with 1% glass fibre were made from the same batch, whereas the first sample was made separately. Therefore it seems that there could be some minor differences in the samples resulting in small TSL strength variation. Another likely reason in strength variation is the unknown presence of small bubbles trapped in the samples. It appears that the increase in fibre content also increases the amount of air bubbles in the samples. The stress versus strain graphs for all the tested samples with 0%, 0.5% and 1% glass fibre reinforcement respectively are plotted in Figure 3.6. From the graphs it can be observed that all samples exhibited ductile behaviour as they had a yield point and a fracture point. The routine dog bone tensile tests indicate that the increase in fibre content reduces brittle failure. It is therefore probable that the brittle failure experienced in the compressive tests would be minimised with high fibre content.

This is important as having brittle failure characteristics would mean that failure would be sudden and unsafe for mining practices.

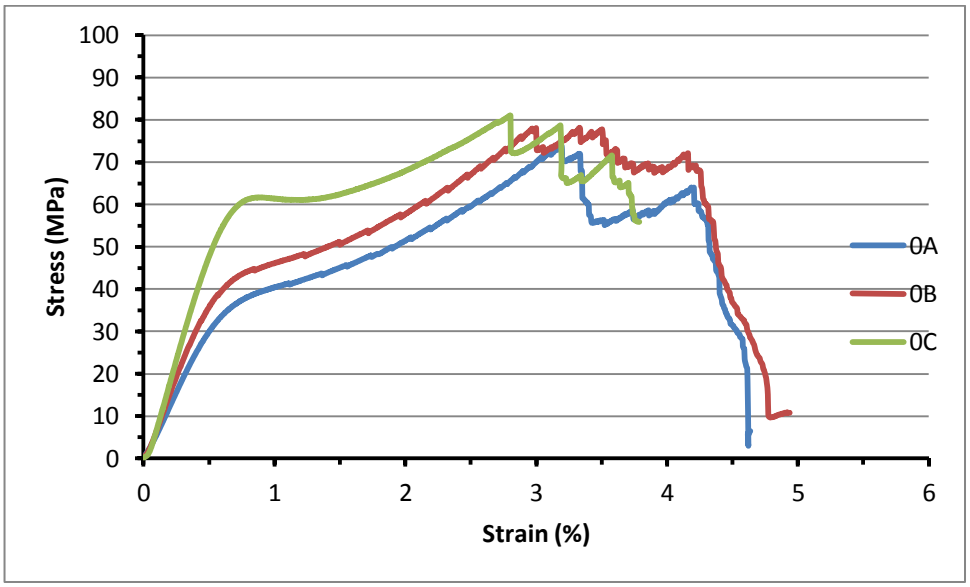

(a) 0% glass fibre reinforcement

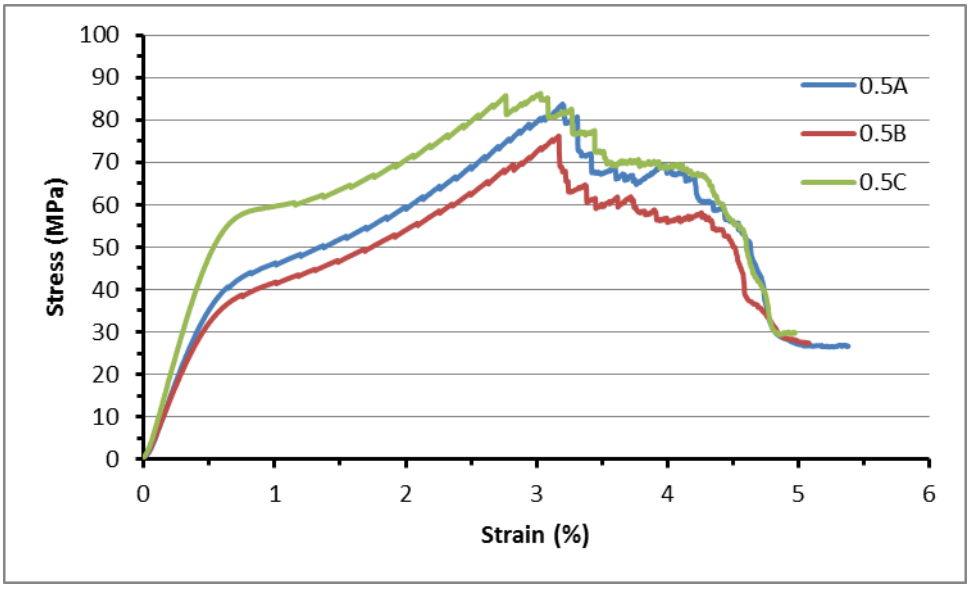

(b) 0.5% glass fibre reinforcement

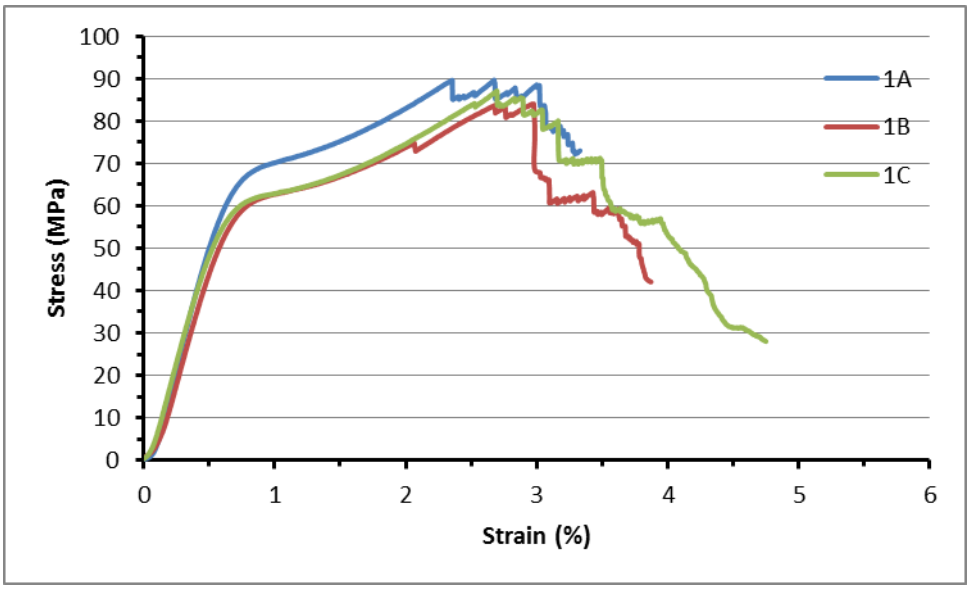

(c) 1% glass fibre reinforcement

Figure 3.6 Stress versus strain graphs for all the samples with different glass fibre content: (a) 0%, (b) 0.5%, and (c) 1%

Despite the small fibre content in the samples the data indicate that the compressive strength of cube samples increased with the increase of glass fibre content. The average compressive strength was measured to be 77.7 MPa for the samples without glass fibre reinforcement, 82.1 MPa with 0.5% glass fibre reinforcement and 86.9 MPa with 1% glass fibre reinforcement as shown in Table 3.1. The compressive test results indicate two distinct elastic zones. Within the first 6% of strain the material Young's modulus was approximately 8 GPa after which strain softening occurred reducing the modulus to approximately 1.4 GPa. Thus a small increase of the fibre glass content has slightly increased the overall material stiffness.

It can also be observed from Figure 3.6 that as the glass fibre content increases, the strain decreases at the location of peak stress. This indicates a rapid increase in loading when displacements occur. In general, high TSL strength and initial stiffness together

with high residual strength and high deformation capabilities are beneficial to underground roadway support. These benefits can be achieved using the polymer material that is reinforced with high glass or other type of fibre content. It is interesting to note that the failure behaviour of all samples demonstrated post failure strength probably caused by the low width to height ratio of the cube samples. It may be expected that the samples of high width to height ratio and low fibre content would probably show a brittle failure mode.

Table 3.1 Summary of all tests

Glass fibre content	Test Number	Compressive strength	Mean strength	STDEV (MPa)
0%	A	73.84	77.67	2.96
	B	78.15		
	C	81.04		
0.5%	A	83.79	82.09	4.28
	B	76.21		
	C	86.27		
1%	A	89.64	86.91	2.29
	B	84.04		
	C	87.07		

The test results indicate that as expected the averaged compressive strength values were similar as the glass fibre concentration in the reinforced samples was low. Despite this the samples with 1% of fibre were on average 11% stronger than the samples with no fibre. These results indicate that the compressive strength of the TSL samples with larger fibre content should dramatically increase the material stiffness,

strength and improve the post failure properties. Further compressive tests of samples with higher glass fibre content are recommended to enable strength determination of the sprayed TSL material. This can be achieved by repetitive spraying of the material components to build up a thick layer of material that can be cut and tested.

The measured strain softening of the material prior to peak load appears to be significant and independent on the glass fibre content probably due to softening of the resin. This behaviour can be desirable for material formulations with low glass fibre content as the material provides a significant reinforcement at the initial stage of loading and retains relatively high loads at higher strains. This behaviour is further complemented by high strains during the post failure loading. Higher glass fibre contents within the polymeric material may produce much higher stiffness of the material in compression. Further tests need to be undertaken for formulations with higher fibre (approximately 30%) to quantify the results.

The stress-strain test data shown in Figure 4.6 indicate that after the peak strength is exceeded there is a gradual reduction of the load. No abrupt failure of the material was observed until the load reduced significantly. A gradual reduction in post-failure strength is desirable in underground application. It is expected that an increase of the glass fibre would further improve the post failure behaviour with large strains before the total separation of the material occurs. This can be confirmed by testing the sprayed material. Brittle failure characteristics of the TSL would be sudden and unsafe for mining practices.

The violent outbursts of small debris flying at considerable velocities away from the yielding samples need to be studied further to ensure safety. This may be overcome by

toughening the prototypes of the polymeric material. It is also envisaged that large amounts of the glass fibre within the loaded material would eliminate such brittle failure mechanism. Further tests are necessary to validate this comment.

The glass fibre percentage and the air entrapment within the polymer mixture need to be researched as they can significantly affect the compressive strength. When spraying the material onto the rock surface, the external mixing and the air assist spray stream can produce variable outcomes. Observations indicate that the great speed of the sprayed material assisted with the air blasts tend to reduce the presence of surface water or dirt, minimises air entrapment and aligns the fibre parallel to the substrate. These effects need to be quantified once the sprayed samples are available.

3.3 Shear strength – punch tests of thin spray-on liners

Yilmaz (2009) developed a punch test composed of a steel ring, a steel punch and clamping fixture to determine the shear strength of TSLs. A 20 mm high and 10 mm thick steel ring with the inner diameter of 52 mm was used to house the TSL. The clamping fixture was used to clamp the steel ring with TSL. A 29.6 mm diameter steel punch was used to shear through the polymer sheet. The test results indicated that this test method is effective and suitable to evaluate the shear strength of TSLs. However, this testing procedure is difficult and inconvenient to determine the glass fibre reinforced TSL materials' shear strength.

The new UOW testing approach discussed here is simpler in TSL sample preparation while it reduces the testing cost by replacing the disposable steel ring with TSL sheets. In addition, it can ensure stable and symmetrical loading thereby improving the accuracy of testing results. In this chapter, the punch shear strength of two TSLs with

four different glass fibre contents was investigated. The effect of loading rate on the shear strength of TSLs was evaluated and reported here.

3.3.1 In-situ shear loading mechanism

Yilmaz (2009) described three possible shear mechanisms that may take place in underground as shown in Figure 3.7.

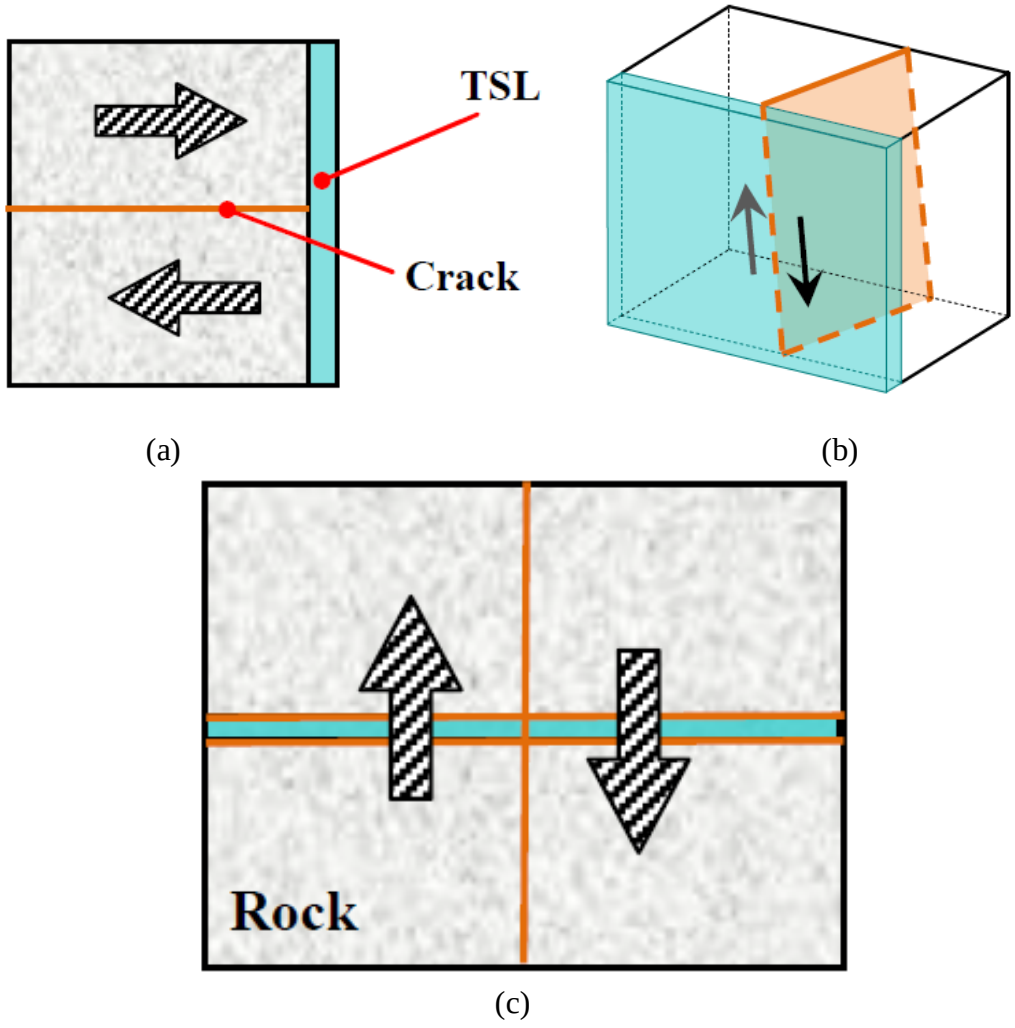

Figure 3.7 Possible shear mechanisms of TSL materials: a) shear perpendicular to the roadway surface; b) shear parallel to the roadway surface; and c) shear through TSL materials that penetrated into the fractured rock (Yilmaz 2009)

The TSL materials bonded to the substrate can be either debonded or sheared across the polymer due to the fracture movement within the rock as shown in Figures 3.7a.

Another shear mechanism of fracture displacement acting parallel to the roadway surface can tear the TSL material as shown in Figure 3.7b. The TSL material that permeates into the joints or cracks around the roadway may be sheared through during fracture displacements as illustrated in Figure 3.7c.

3.3.2 Sample preparation

Two TSL products, Prototype A and Prototype B were used to conduct the Shear strength punch tests. The procedures for preparing the samples for the TSL shear strength testing are shown in Figure 3.8. Four groups of samples were prepared for each prototype. Each group of four samples was reinforced with no fibre, one fibre sheet, two fibre sheets and three fibre sheets respectively.

The procedure is as follows:

a) Using several plastic plates glued together a mould 250 mm long by 85 mm wide and 5 mm thick was prepared as shown in Figure 3.8a. This geometry makes a rectangular TSL sheet that can be cut into four pieces suitable for punch testing. Each test piece has to be big enough to eliminate the boundary affects to improve the accuracy of evaluating the shear strength. The mould was placed onto the smooth glass plate and all components were lightly greased using Vaseline to make the samples when cured, easy to remove.

b) The polymer components were mixed evenly according to the research chemist's recommended ratio using a plastic cup and a wooden stick.

c) The TSL mixture was poured into the plastic mould. The TSL viscosity was high and it was difficult to pour directly, and a wooden stick was used to assist placing the TSL evenly into the mould.

d) Once the TSL was poured as shown in Figure 3.8b, it was left to cure for approximately four hours. The sample was then removed from the plastic mould and was left at room temperature to cure for five days.

e) When making the sample reinforced with one sheet of the glass fibre, one half of the mixture was poured into mould and the glass fibre sheet was placed on top before the remaining mixture was poured to complete the 5 mm thick sample. Finally, the procedure (d) was repeated.

f) When making the sample reinforced with two sheets of glass fibre, one-third of the mixture was poured into the mould, the fibre sheet was placed on top. The second third of the mix was then poured into mould and the procedure repeated. The sample was finished as described in section (d) and (e). The aim here was to ensure that the two fibre layers were evenly spaced within the sample.

g) The TSL sample with three layers was prepared in a similar manner. All four types of prepared polymer sheets are shown in Figure 3.8c.

h) When preparing the samples it is important to ensure that an even spacing of the fibre sheet material is achieved within each sample.

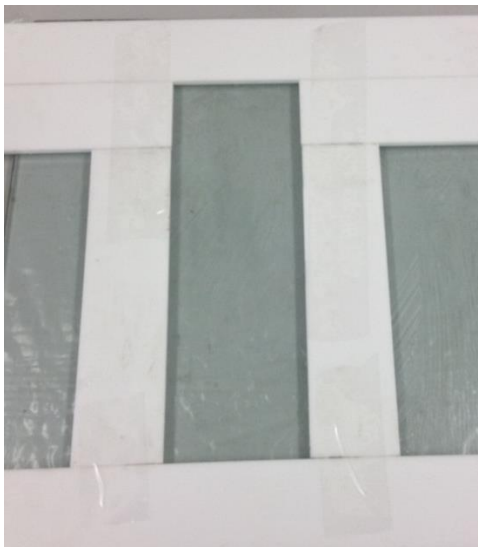

(a)

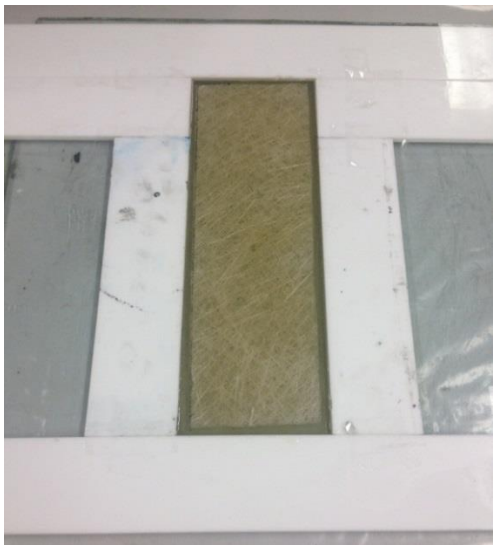

(b)

(c)

Figure 3.8 Sample preparations for shear (punch) test: (a) mould, (b) sample in the mould, and (c) prepared samples

3.3.3 Description of shear testing using steel punch

The testing apparatus consists of two parts: steel punch and clamping fixture as shown in Figure 3.9. The cylindrical steel punch 29.9 mm in diameter was used to puncture the TSL material. The clamping components were made of two steel plates with

threaded holes for four screws. The central diameter of the holes within both clamping plates was also 30 mm in diameter to accommodate the steel punch. The thickness of both the top and bottom steel plates were 20 mm providing sufficient clamping strength for the polymer sample for testing. The thickness of the bottom steel plate was also sufficient to accommodate the polymer residue produced in the test. Four screws were used to tighten the polymer sample between the clamping plates to ensure stable and symmetrical loading.

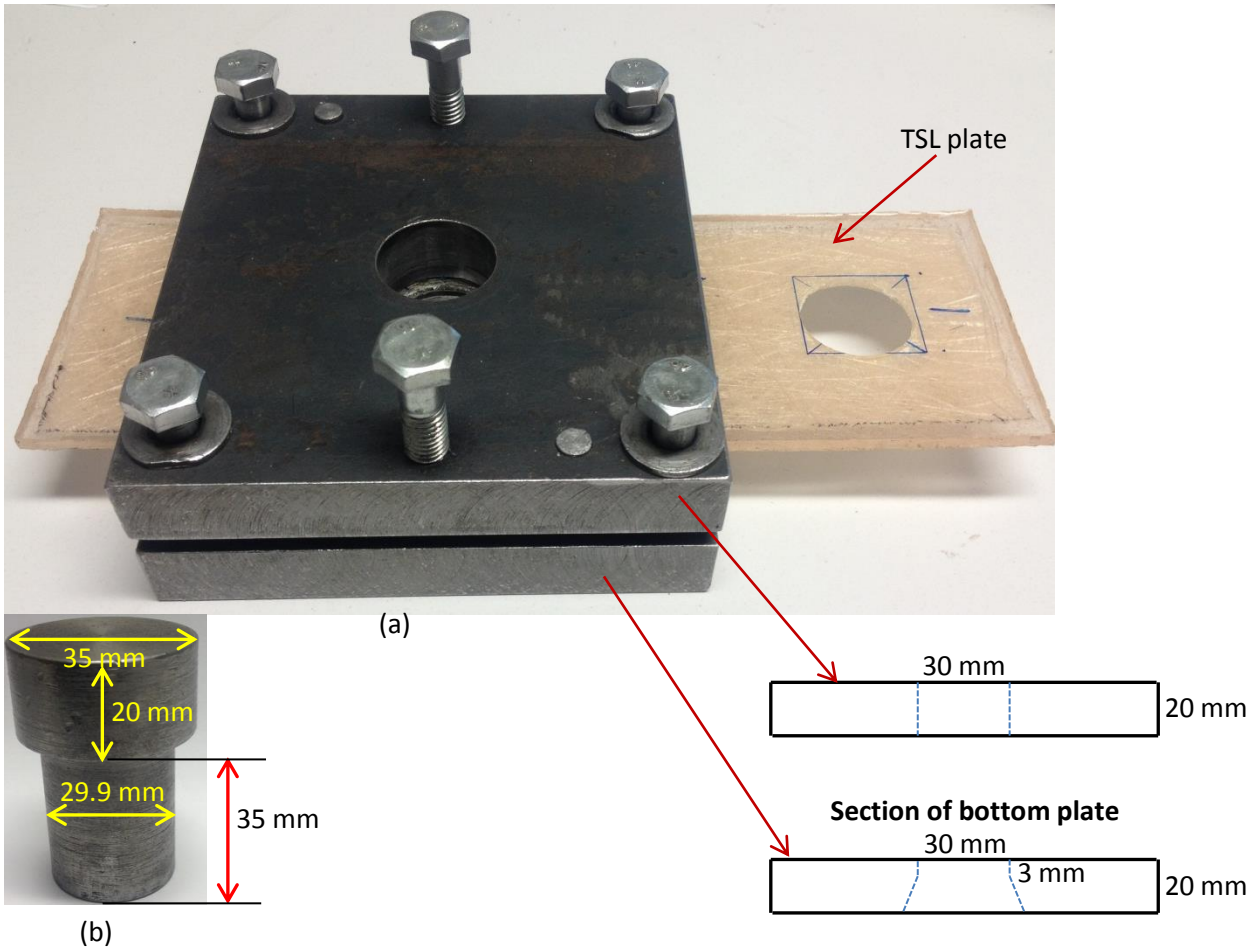

Figure 3.9 Material shear strength testing apparatus: (a) Clamping fixture and (b) Steel punch

3.3.4 Test setup and execution

After the sample was cured for the pre-determined period under the laboratory conditions, the tests were executed. Each type of a polymer sheet requires a number of tests (four suggested). Figure 3.10 demonstrates the material shear strength testing setup. The tested samples at the University of Wollongong laboratory were 250 mm in length, 85 mm in width and 5 mm in thickness. Before commencing the TSL punch shear strength tests, the exact thickness of the material was measured at the test location as presented in Table 3.2. The sample was put into the test rig clamped by two steel plates. In order to avoid the bending or sample tilting, the test rig clamped the sample symmetrically by tightening the four screws. A 29.9 mm diameter steel punch was used to shear through the polymer sheet. It was important to ensure that there was no gap or clearance between the two steel plates and the tested sample to prevent sample bending or other dislodgement. The shear test assembly was placed in the Instron compression machine. In the process of puncturing the TSL material, the TSL shearing rate used (punch displacement speed) was 1.5 mm/min. At this speed, the 5 mm thick TSL test was completed within two minutes as the peak shear strength was reached at displacements of approximately 1.4 mm. The residual strength was obtained at displacements of 2-3 mm depending on the amount of fibre reinforcement. The load was applied to the steel punch until the polymer sheet sheared through. During the test, the load and displacements were recorded.

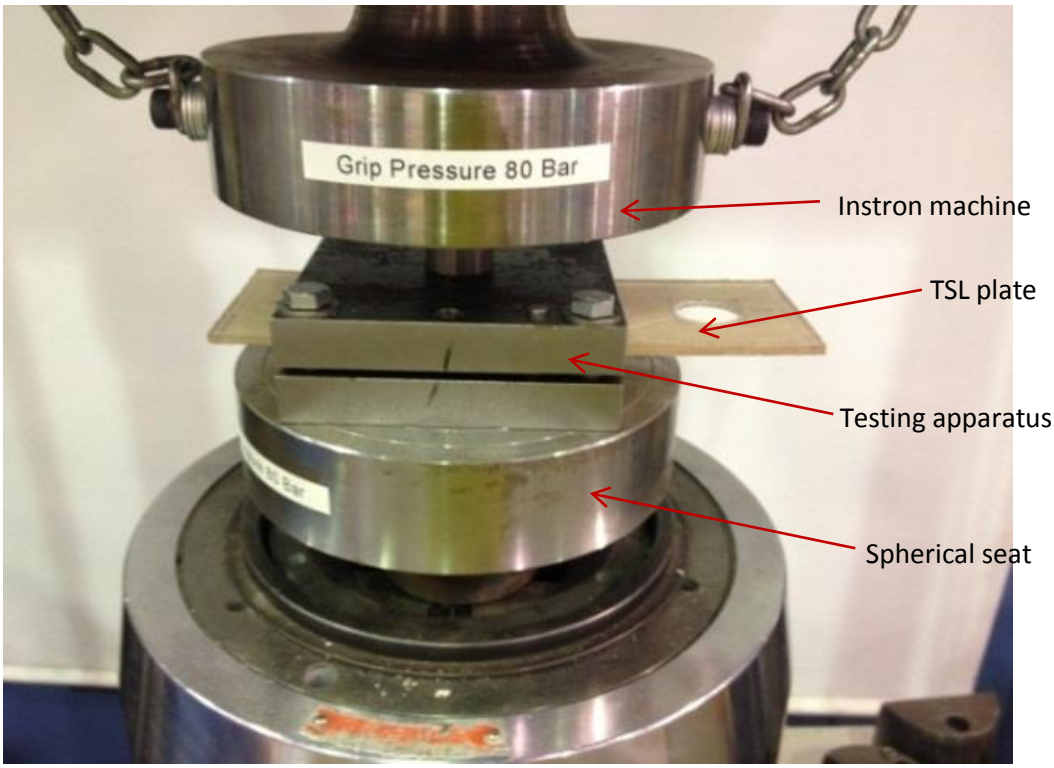

Figure 3.10 Material (punch) shear strength testing setup

3.3.5 Failure mode and calculations

In the punch shear strength test, the failure of TSL materials took place perpendicular to the TSL material surface by punching through the TSL sheets. The punctured TSL samples shown in Figure 3.11 indicate that the failure plane is regular and consistent for two different TSL prototypes A and B except that the TSL prototype B sheet without glass fibre reinforcement exhibited very brittle behaviour breaking into small pieces as shown in Figure 3.12. Therefore, the results for unreinforced TSL prototype B were limited.

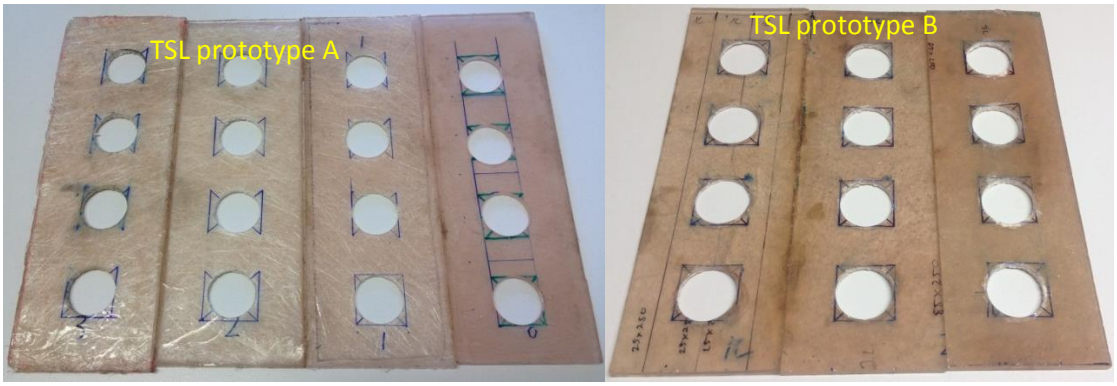

Figure 3. 11 TSL material sheets after punch testing

Figure 3.12 TSL B material without glass fibre reinforcement after punch failure

The material shear strength perpendicular to the TSL sheet can be calculated by Equation (3.1). The strength can be obtained by dividing the force at failure by the area along which the TSL material shears:

$$\sigma_s = \frac{F}{A} = \frac{F}{\pi \times d \times t} \tag{3.1}$$

Where F = applied force at failure

σ_s = shear strength of the TSL material

d = diameter of steel punch

t = thickness of the TSL material

3.3.6 Analysis of test results

3.3.6.1 Effect of loading rate on punch shear strength

To evaluate the effect of loading rate on the shear strength and select an appropriate loading rate for the tests, four different loading rates were used: 0.5, 1.0, 1.5, and 2.0 mm/min. The strength versus loading rate graph with different glass fibre contents reinforcement is plotted in Figure 3.13.

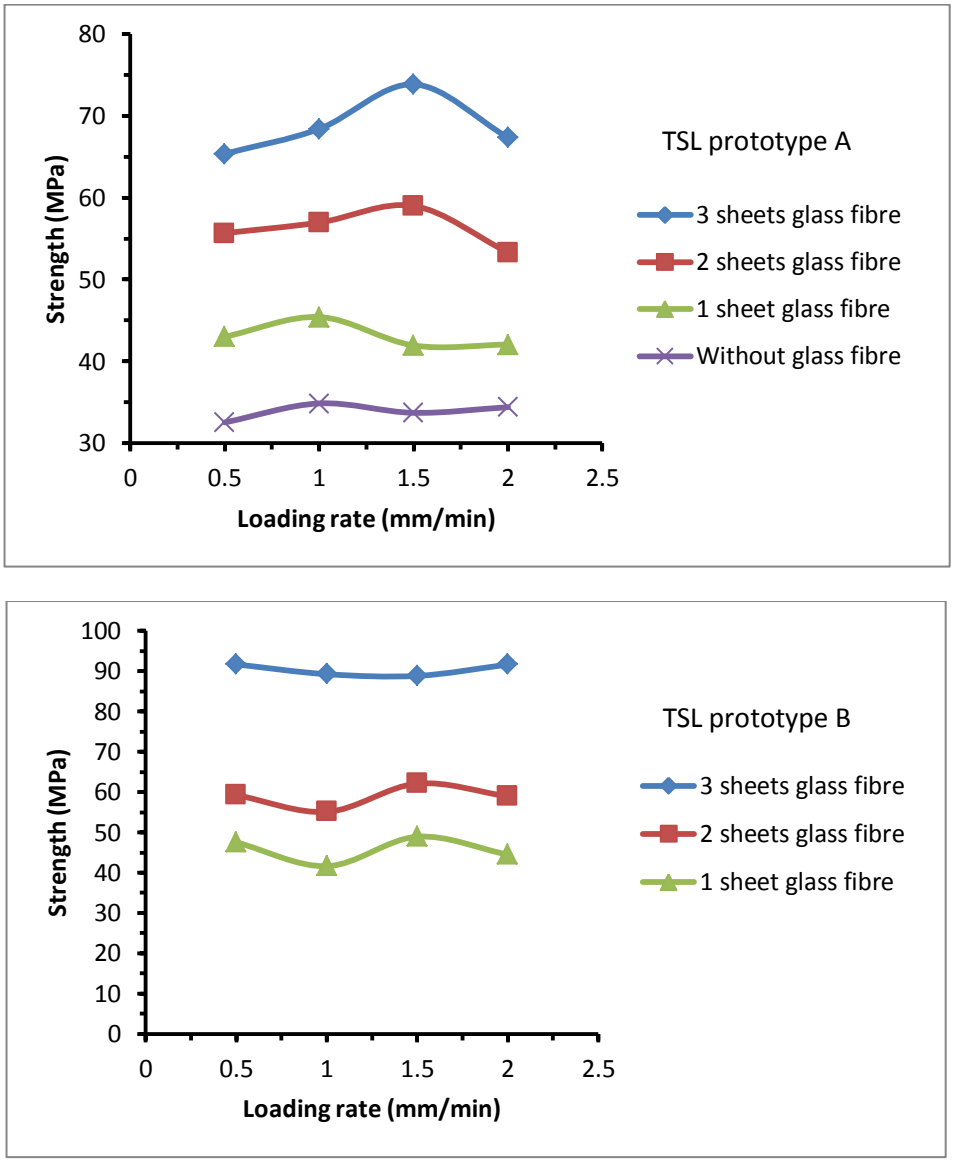

Figure 3.13 Effect of loading rate on the shear strength of TSL prototypes A and B with different sheets of glass fibre reinforcement.

The results for both TSL A and B prototypes indicated that the effect is negligible. Ozturk and Tannannt (2010) investigated the effect of loading rate on the adhesive strength, and similar results were obtained. As the peak strength can be reached at displacements of roughly 1.4 mm and the residual strength at approximately 2-3 mm, the loading rate of 1.5 mm/min was used for the subsequent shear tests of approximately two minutes duration.

3.3.6.2 Punch shear strength of TSL Prototype A

Figures 3.14 to 3.17 show the load and displacement graphs of the samples tested at the University of Wollongong laboratory. Four samples 5 mm thick were prepared without glass fibre reinforcement and also with one, two and three sheets of glass fibre reinforcement respectively. In Figures 3.14 to 3.17 it can be clearly seen that the peak load increased as the glass fibre content increased. The polymer material samples showed good linear behaviour prior to reaching the ultimate load and ductile behaviour that reflects the fibre reinforcement of failed resin during the yielding stage of the sample which is beneficial to the support in underground mines.

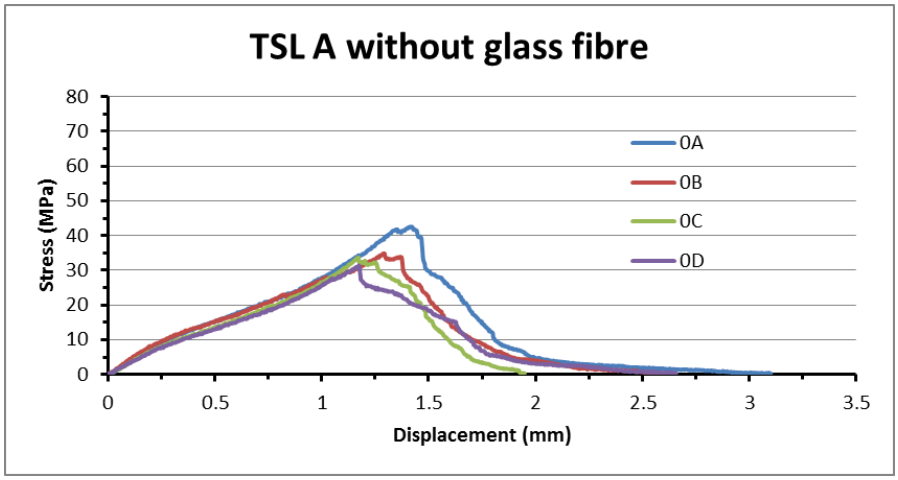

Figure 3.14 Stress vs displacement graph of four tested samples without glass fibre reinforcement

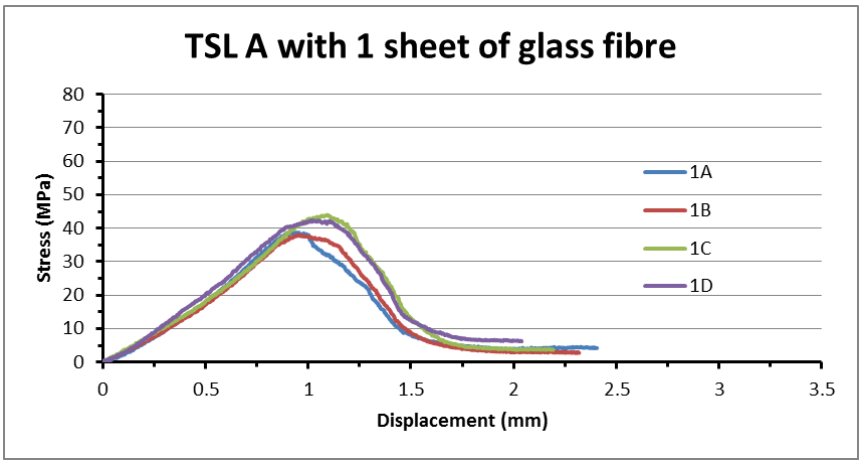

Figure 3.15 Stress vs displacement graph of four tested samples with 1 sheet of glass fibre reinforcement

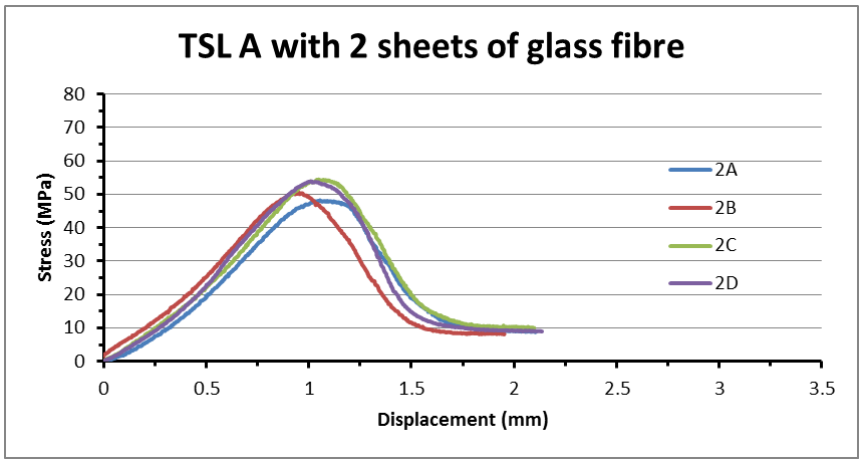

Figure 3.16 Stress vs displacement graph of four tested samples with 2 sheets of glass fibre reinforcement

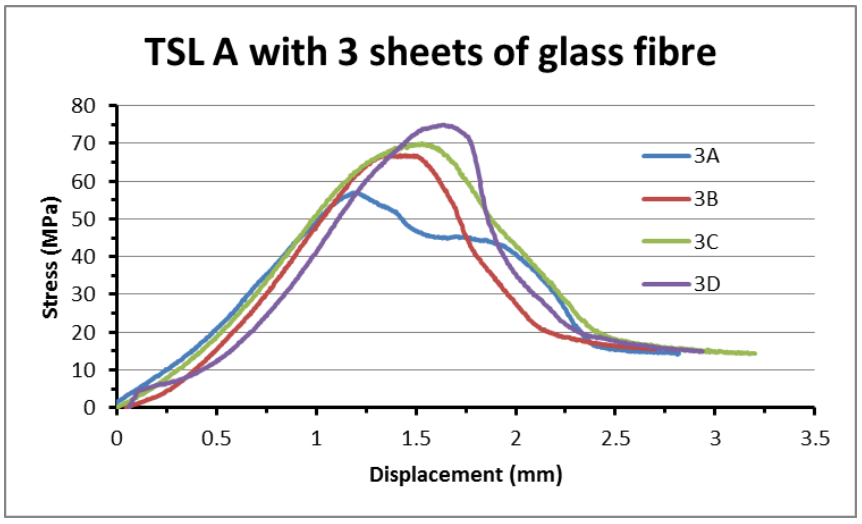

Figure 3.17 Stress vs displacement graph of four tested samples with 3 sheets of glass fibre reinforcement

Test results for TSL prototype A are summarised in Table 3.2.

Table 3.2 Summary of test results for TSL prototype A

Glass fibre content	Test Number	Thickness (mm)	Peak Strength (MPa)	Res. Strength (MPa)	STDEV (MPa)		Mean Strength (MPa)	
					Peak	Res.	Peak	Res.
Without glass fibre	0A	4.98	32.53	1.84	1.29	0.65	33.12	0.89
	0B	5.01	34.85	0.83				
	0C	4.99	33.70	0				
	0D	4.95	31.39	0.87				
1 sheet glass fibre	1A	5.02	38.72	2.13	2.47	0.78	40.76	3.26
	1B	4.97	38.00	2.97				
	1C	4.98	43.90	3.75				
	1D	5.01	42.41	4.18				
2 sheets glass fibre	2A	4.96	48.22	8.90	2.95	0.73	51.76	8.98
	2B	4.93	50.45	8.15				
	2C	4.98	54.46	9.93				
	2D	4.96	53.89	8.94				
3 sheets glass fibre	3A	5.03	65.98	14.31	1.24	0.65	67.24	14.81
	3B	4.97	66.96	15.71				
	3C	5.00	67.07	14.34				
	3D	4.99	68.95	14.87				

Note: Res.=Residual

The polymer samples without glass fibre reinforcement exhibited a larger steel punch displacement of 1.2-1.4 mm at peak load than most of the other samples reinforced with glass fibre. The majority of the glass fibre reinforced samples failed within 0.9-

1.1 mm displacement, however two samples reinforced with three sheets of fibre did not experience a linear load increase at the early stage of loading. Consequently their peak load was recorded at a higher displacement. This could have been caused by either insufficient tightness of the polymer sheet within the testing rig or debris left under the steel plate. The main aim of these tests was to compare the material shear strength with different glass fibre content.

As expected, the shear strength of the polymer material increased significantly with the increase of glass fibre content. Without glass fibre reinforcement, the mean shear strength of the polymer material was approximately 35.6 MPa; with 1, 2 and 3 sheets of glass fibre reinforcement, the mean shear strength of the polymer material was 40.8 MPa, 51.8 MPa and 67.2 MPa respectively as shown in Table 3.2. As expected, the post-failure puncture strength of the polymer TSL also increased with the glass fibre content. At a steel punch displacement of 2.5 mm the average residual strength of the TSL sheet was approximately 0.89 MPa for no fibre while for one, two and three sheets of fibre the residual strength was approximately 3.3 MPa, 9.0 MPa, and 14.8 MPa respectively.

3.3.6.3 Punch shear strength of TSL Prototype B

Figures 3.18 to 3.21 show the stress vs displacement curves of the samples tested for TSL prototype B. As for the Prototype A, 16 samples 5 mm thick were prepared for Prototype B without glass fibre reinforcement and also with one, two and three sheets of glass fibre reinforcement respectively. The unreinforced Prototype B material was extremely brittle failing at low loads. Only one sample survived to a load of 28.0 MPa before brittle failure occurred (see Figure 3.18). With increase of the glass fibre

content, the reinforced samples increased in strength. This was consistent with the Prototype A tests. The polymer material samples showed good linear behaviour prior to reaching the ultimate load and ductile behaviour that reflects the fibre reinforcement of failed resin during the yielding stage of the sample which is beneficial for the support in underground mines.

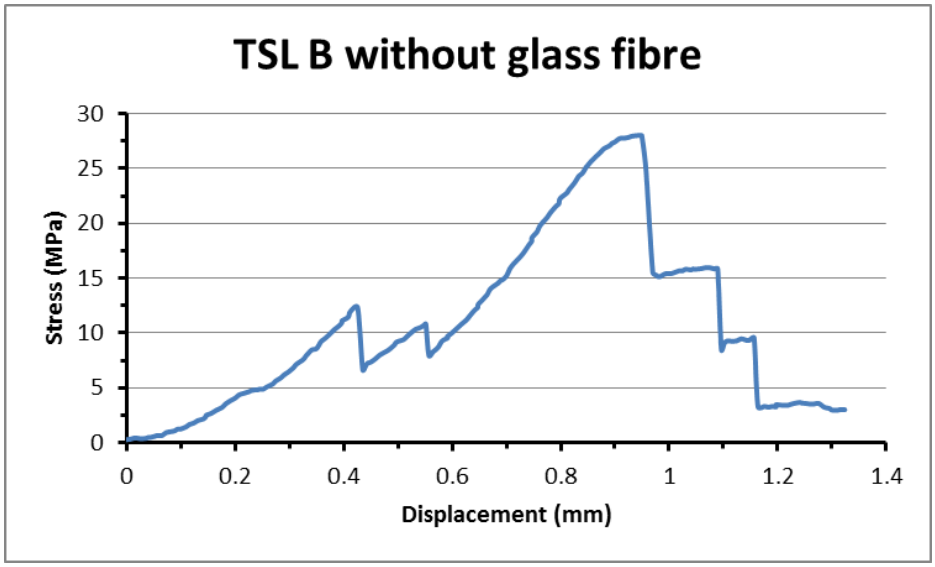

Figure 3.18 Stress vs displacement graph of four tested samples without glass fibre reinforcement

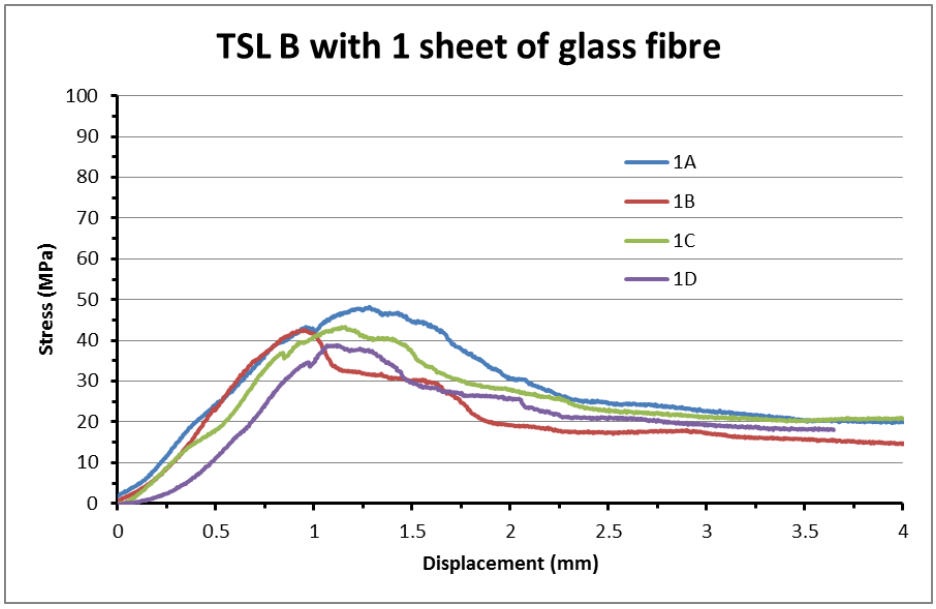

Figure 3.19 Stress vs displacement graph of four tested samples with 1 sheet of glass fibre reinforcement

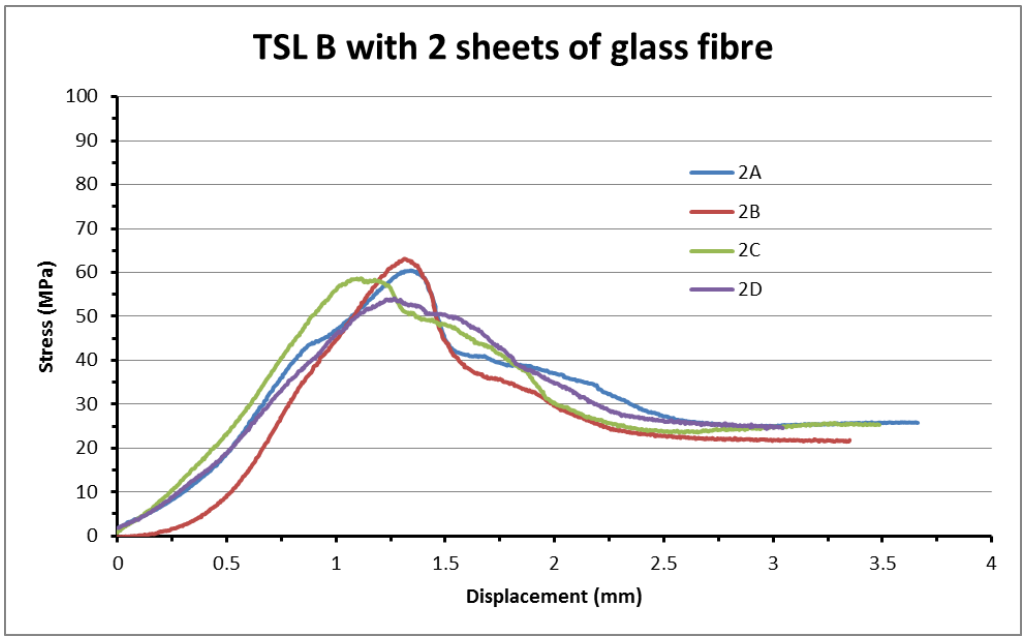

Figure 3.20 Stress vs displacement graph of four tested samples with 2 sheets of glass fibre reinforcement

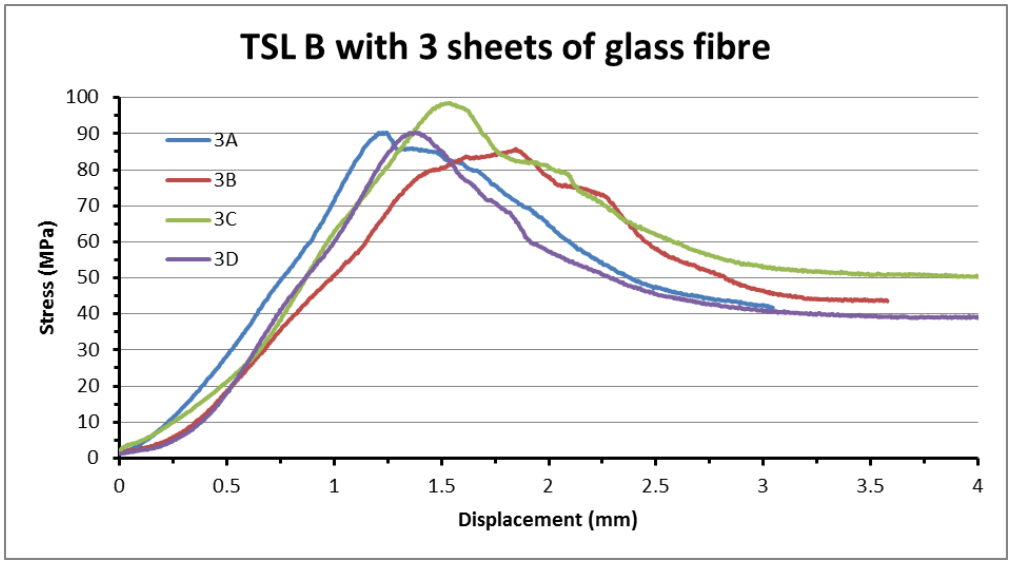

Figure 3.21 Stress vs displacement graph of four tested samples with 3 sheets of glass fibre reinforcement

The majority of the glass fibre reinforced samples failed within 1.0-1.5 mm of steel punch displacement. As expected, the shear strength of the polymer material increased significantly with the increase of glass fibre content. For glass fibre reinforcement, the mean shear strength of the polymer material with 1, 2 and 3 sheets of glass fibre were

43.2 MPa, 59.1 MPa and 91.2 MPa respectively as shown in Table 3.3. It is clear that the shear strength increased significantly with 3 sheets of glass fibre reinforcement when compared with the 2 sheets of glass fibre.

Table 3.3 Summary of test results for TSL B

Glass fibre content	Test Number	Thickness (mm)	Peak Strength (MPa)	Res. Strength (MPa)	STDEV (MPa)		Mean Strength (MPa)	
					Peak	Res.	Peak	Res.
1 sheet glass fibre	1A	4.98	38.87	17.51	3.34	2.58	43.24	16.16
	1B	5.03	43.32	11.71				
	1C	4.99	42.52	17.40				
	1D	5.00	48.25	18.03				
2 sheets glass fibre	2A	4.89	60.49	25.77	3.27	1.52	59.08	24.38
	2B	4.91	63.09	21.85				
	2C	4.95	58.64	25.31				
	2D	4.93	54.12	24.58				
3 sheets glass fibre	3A	4.99	90.32	41.70	5.30	4.85	91.23	43.64
	3B	4.97	85.80	43.55				
	3C	5.01	98.52	50.35				
	3D	5.02	90.29	38.97				

Note: Res.=Residual

When reinforced with 1 and 2 sheets of glass fibre, TSL B and TSL A had similar shear strengths although the shear strength of TSL B was slightly greater than the shear strength of TSL A. However, the shear strength of TSL B with 3 sheets of glass fibre reinforcement was significantly greater than the TSL A. In addition, TSL B exhibited larger displacement at peak load than TSL A. Therefore, this testing method has the

potential to effectively evaluate the shear strength of different TSL materials. At a steel punch displacement of 3.5 mm the average residual strength of the TSL sheet was approximately 16.2 MPa, 24.4 MPa, and 43.6 MPa for one, two and three sheets of fibre respectively.

The test results might have been affected by many parameters, such as curing time, glass fibre distribution within the TSL material, quality of the glass fibre, chosen thickness of the TSL and other surrounding conditions. In order to minimise the factors affecting the tests, the geometry and sample quality variations must be kept at a minimum. For example, the curing time and the thickness of the TSL material of all the samples were kept the same (five days and 5 mm thick respectively). In the future, different TSL thickness should also be tested. In addition, the effect of curing time and its influence on the shear strength of the TSL material should be investigated.

The testing method should be kept simple and relevant to the material tested. The choice of the punch test to measure TSL shear loads satisfies the simplicity and relevance of testing TSL materials. The advantages of the punch method are:

a) Simple, easy and quick sample preparation,

b) The test can be repeated quickly many times, as each polymer sheet can be of any length to accommodate numerous tests.

c) The testing setup is small and easy to use.

d) The complication of many variables is reduced because the substrate is not involved.

e) It is cost effective.

The up-to-date results suggest that the steel punch can shear through the polymer sheet well and the failure mode is easily identified. The data indicate that the results are consistent throughout all tests. This test method makes it easy to compare the shear tests of different thin spray on liner materials. The results indicate good ductile behaviour of the TSL samples and consistent increase of shear strength with the amount of fibre reinforcement within the samples.

3.4 Summary

To date, the compressive strength of TSL has not been researched in depth therefore the aim of this study was to develop a suitable comparative method of TSL compressive testing. The steel block cube mould was selected as it is able to withstand the heating caused by the exothermic reaction during the resin setting period. The compressive strength of one TSL product was tested. The unreinforced and glass fibre reinforced cube samples 40 mm in size were prepared and their strength tested. Due to difficulties with introducing glass fibre into the TSL matrix, the tests were conducted on samples with only a small amount of fibre. The results indicate that both the compressive and residual strength of these samples increased with increase of glass fibre content. In addition, the measured strain at the peak stress increased with higher glass fibre content. The maximum fibre content of 1% in the cube samples was actually much lower than 30% of the anticipated glass fibre in the spray application. Therefore a suitable method must be devised to enable casting polymeric samples with high fibre content to address this inequality. This could be achieved by spraying thick volumes of the TSL material and cutting it into samples for testing.

The consistent results from both Prototypes A and B shear punch tests showed a distinct increase of the TSL material strength with the increase of glass fibre reinforcement. The post failure behaviour of the samples indicated similar trend. The effect of loading rates on the shear strength of TSL materials appeared negligible.

The results indicate that while reinforced with the same amount of glass fibre, TSL prototype B had higher shear strength than TSL prototype A. Without glass fibre reinforcement, TSL A can sustain some residual strength while the TSL B exhibited brittle failure mode with no post-peak strength.

The choice of the punch test to measure TSL shear loads satisfies the simplicity and relevance of testing TSL materials as it produces consistent results and it is simple, easy, quick and cost effective.

CHAPTER 4 BOND STRENGTH TESTING OF TSL MATERIALS

4.1 Introduction

The composite layer formed by strong bond between the TSL and the rock skin is a very important property that provides stiff and durable rock skin reinforcement. This composite layer can significantly improve rock confinement to the area surrounding the bonded surfaces and thus improve the integrity of the overall rock bolting system that can otherwise be undermined by the unravelling of fractured rock or coal strata. An improvement to strata skin control, namely the roof and the rib integrity, can be expected when using the TSL product. The adhesion between the polymer liner and the rock surface can confine the rock movement immediately after spraying.

The TSL strength and ability to bond to various substrates significantly improves the reinforcing capabilities of the immediate strata surface. In softened strata, the bond can keep the fractured rock pieces together and hold the fragments in place increasing the self-supporting capacity of severely fractured strata. Without the bond strength, the TSL performance is reduced. Therefore, good bond strength of the TSL is desirable to effectively support the underground excavations.

4.2 Adhesion properties of TSL materials

The TSL adhesion to substrate can be divided into two components, the shear and the tensile bond. Both exhibit different mechanisms of bonding and as expected, they have different magnitudes of adhesion where tensile bond is usually weaker than the shear bond.

In order to assess the shear bond strength of the polymer liner and thereby evaluate its geotechnical function in strata skin reinforcement, three shear bond testing procedures were trialled. The aim of the tests was to evaluate pure unconfined shear bond strength of TSL bonded to the various strata types without the effect of normal stress onto the polymer surface and to choose the most appropriate test for this type of bond loading for future routine testing.

The first test utilized the standard double sided shear testing procedure using three rock cubes of 40 mm sides bonded together with a 5 mm thick polymer layer. The testing procedure involved clamping the two outer blocks while the load was applied onto the central block. A similar method was also trialled by Saydam and Yilmaz (2003) with different sample geometry.

The second test included a polymer ring 5 mm thick and 15 mm wide coated on the periphery of each cored sample. The idea of this method was based on Yilmaz's (2007) shear bond strength testing approach that was redesigned to suit the current research. The polymer ring was then sheared off each rock core with a steel sleeve and the shear bond strength determined. However, this way of specimen preparation can cause normal stress induced by TSL shrinkage around the rock surface affecting the shear bond strength between the interface of the rock core and the TSL.

The third test was identical to the second test except that the polymer ring was partitioned into four segments to minimise the effect of normal stress onto the substrate and thus measure true unconfined shear bond strength.

4.2.1 Mechanism of shear bond strength

In underground coal mines, the joints or fractures are ubiquitous. When the TSL is sprayed onto the rock surface, it is possible for sprayed liner to penetrate into the fractures and cracks within the rock. Stacey (2001) described a series of mechanisms of loading behaviour and surface support behaviour of TSLs and proposed the theory "Promotion of block interlock" which is related to the shear bond strength between the TSL and the rock surface. The aim of this mechanism is mainly to keep the rock mass in a stable and unloosened condition. Based on the support mechanism of Stacey (2001, 2004), Yilmaz (2007) tested the *in situ* loading mechanism of TSL relevant to shear bond strength as shown in Figure 4.1.

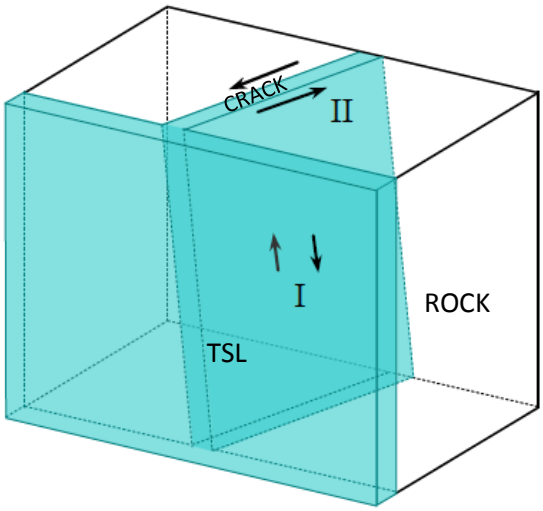

Figure 4.1 *In situ* mechanism of TSL crack penetration relevant to shear bond strength testing (after Yilmaz, 2007)

The shear bond strength between the TSL and the rock surface can promote the block interlock which can keep the broken blocks in place and minimise block rotation caused by the shear. Stacey and Yu (2004) determined the effect of various factors on the support capacity of TSL using the method of finite element stress analysis and

demonstrated that the support mechanism of TSL penetrating into the joints and fractures within the rock mass plays an important role in the supporting system.

4.2.2 Double sided shear bond strength test

4.2.2.1 Sample preparation

The test samples were made from three rock cubes of 40 mm side bonded together with 5 mm thick polymer layers. Three different rock types were tested, namely: coarse sandstone, fine sandstone and coal. Two TSL products, Prototype A and Prototype B were used to conduct the double sided shear tests.

A steel mould was used to prepare the samples as shown in Figure 4.2.

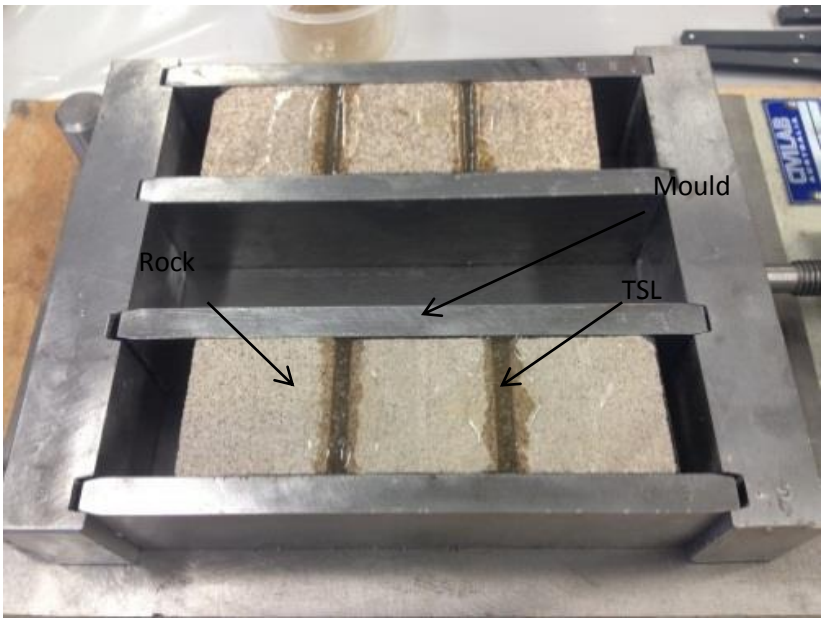

Figure 4.2 Double sided shear bond strength test - sample preparation

The procedure for preparing samples is as follows:

(a) The steel mould and rock samples were cleaned using acetone to ensure that both the rock samples and steel mould were clean. Vaseline was used to grease

the mould for easy removal of the cured samples from the mould. It should be noted that the bonding surfaces must be grease free.

(b) For testing on the wet surfaces, the samples were placed in water for 24 hours before casting the TSL onto the wet rock surface. For the dry shear bond testing, the samples were left to dry for 24 hours at room temperature before testing took place.

(c) Sticky tape was wrapped around the edges adjacent to the polymer face to prevent polymer leakage that could contaminate other rock surfaces.

(d) Samples were then placed into the mould leaving a 5 mm gap between adjacent rock cubes.

(e) The polymer components were mixed evenly according to the research chemist's recommended ratio using a plastic cup and a wooden stick.

(f) The TSL mixture was poured into the gaps between the rock cubes. If the TSL viscosity is high and difficult to pour directly, a wooden stick can be used to assist the TSL placement into the mould. In this group of samples the polymeric TSL was bonded to the dry surfaces.

(g) Once the TSL was poured, it was left to cure for approximately four hours. The sample was then removed from the mould. The sample was left at room temperature to cure for an additional five days.

(h) The procedures (a), (b), (c), (d), (e), and (f) were repeated to make the number of samples as needed.

4.2.2.2 Loading rate

In the process of conducting double sided shear bond strength tests, the displacement control mode was selected to execute the tests. The loading rate for the test used a standard displacement speed of 0.005 mm/s (0.3 mm/min). At this speed, most of the tests were expected to be finished within four minutes except for some tests with high yield characteristics.

4.2.2.3 Description of test apparatus and testing procedures used

The test apparatus for conducting the double sided shear test consisted of the bottom steel fixture and the steel top part to accommodate the sample. The sample was clamped by tightening the four screws. A steel loading platen was used to apply the load onto the sample. The test setup is shown in Figure 4.3

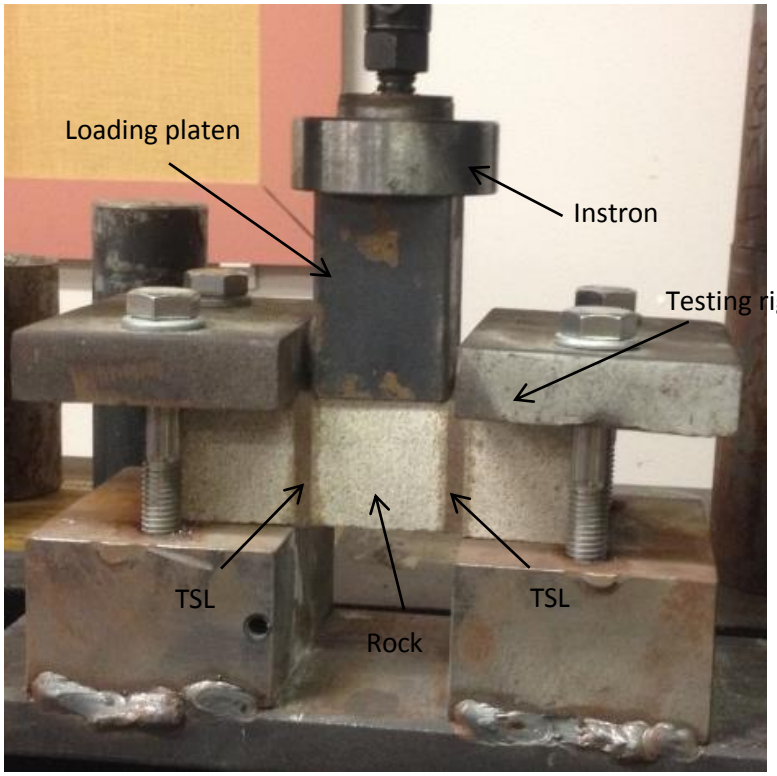

Figure 4.3 Double sided shear bond strength - test setup

The testing procedure involved clamping the two outer blocks only while the load was applied onto the central block. The TSL material was applied to the surfaces of rock samples. During the test, the load and displacements were recorded.

4.2.2.4 Calculations

The material shear bond strength of each test was calculated using Equation (4.1). The strength was obtained by dividing the force at failure by the total area (two contact surfaces) along which the TSL material failed in shear:

$$\sigma_{sb} = \frac{F}{2A} = \frac{F}{2d^2} \tag{4.1}$$

Where F = applied force at failure

σ_{sb} = shear bond strength of the TSL material

d = length of rock cube side

A = area of one contacted side

The length of rock cube side was measured before each test to establish the bonded surface areas.

4.2.2.5 Results and analysis

More than 30 double sided shear tests were performed at the University of Wollongong laboratory. Figure 4.4 shows a typical stress versus displacement graph of the double sided shear tests. The mean shear bond strength of double sided shear test results for TSL A and B are summarised in Table 4.1.

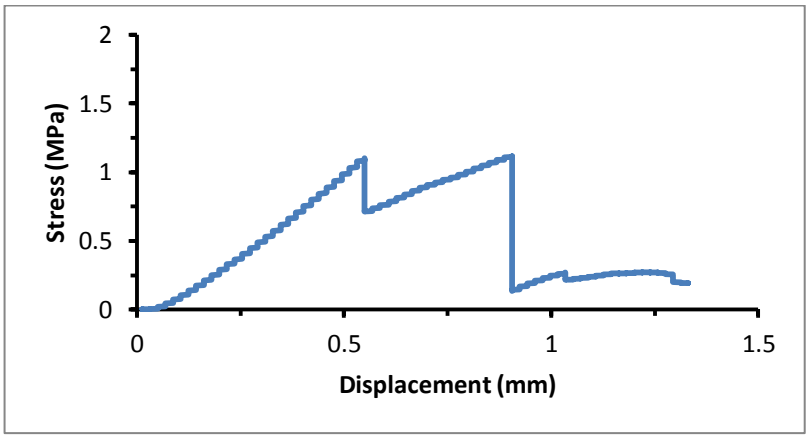

Figure 4.4 A typical stress vs displacement graph of double shear bond strength test

Table 4.1 Mean shear bond strength of double sided shear test results for TSL A and B

Sample	Mean strength for TSL A (MPa)	Mean strength for TSL B (MPa)
Dry coal	1.11	1.37
Wet coal	0.49	0.62
Dry coarse sandstone	1.57	1.96
Wet coarse sandstone	0.93	1.18
Dry fine sandstone	2.96	3.35
Wet fine sandstone	1.80	2.19

Most of the time excellent adhesion to the rock surfaces forced the shear failure to propagate through the rock rather than along the TSL surfaces. There were several peak strength points with a large scatter between the tests making the test results difficult to interpret. Therefore the results did not yield the values of the TSL shear bond strength but only indicated that the bonding values are higher than the shear strength of the intact rock. Some samples failed on one side only causing the assembly to bend and wedge. Closer examination showed that the four bolts within the steel assembly were bending in response to the loads during testing and possibly affecting

the results. On the whole the results are inconclusive. Figure 4.5 shows samples after failure for the double sided shear bond strength test.

Figure 4.5 Samples after failure for the double sided shear bond strength test

After observing the behaviour of the tested samples and examining the integrity of measured data it was decided that this test is not appropriate to measure very strong polymeric bond stresses. The following methods were trialled to improve the accuracy of these essential measurements.

4.2.3 Full TSL ring shear bond strength test

To eliminate the problems experienced in the double shear test, the full TSL ring shear test method that was first performed by Yilmaz (2007) was modified and trialled. The test preparation is set out as follows.

4.2.3.1 Sample preparation

The test included a polymer ring 5 mm thick and 15 mm wide bonded on the periphery of the cylindrical rock sample. Three different rock types were tested, namely: coarse sandstone, fine sandstone and coal. Two TSL products, Prototype A and Prototype B were used to conduct the full ring shear tests. A greased Perspex mould was used to pour the polymer ring, as shown in Figure 4.6.

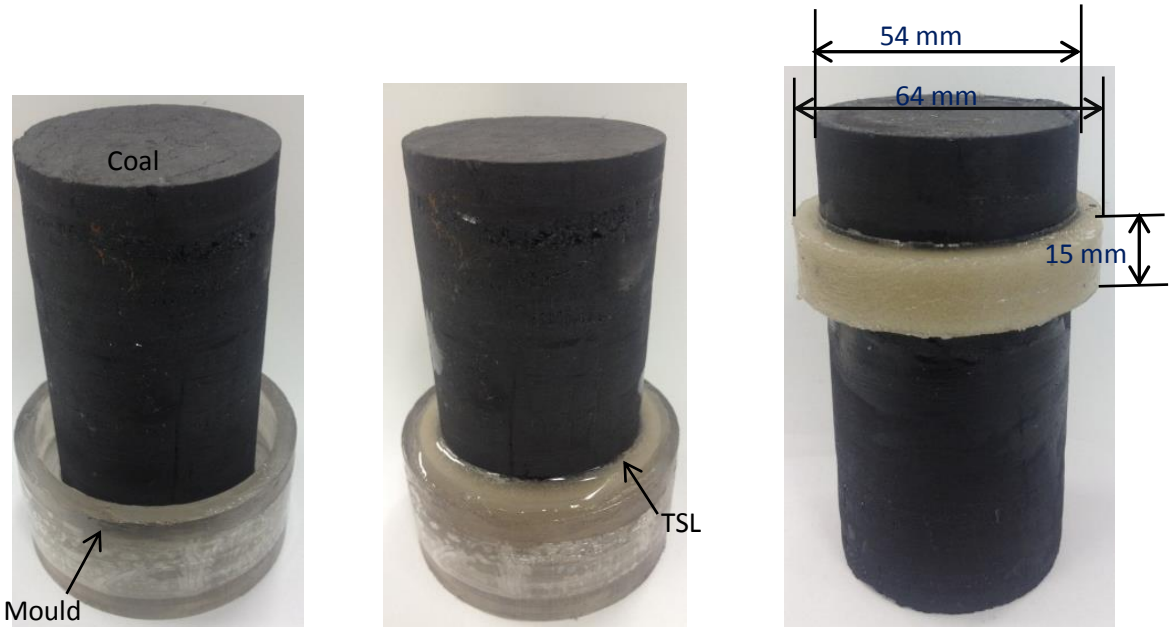

(a) (b) (c)

Figure 4.6 Sample preparations for TSL ring shear test: (a) sample inserted in the mould, (b) TSL poured in the mould and (c) a prepared sample ready for testing

The procedures for preparing samples were as follows:

(a) The Perspex mould and rock samples were cleaned using acetone to ensure that both the rock samples and Perspex mould were clean. A thin film of Vaseline was used to grease the mould for easy removal of the cured samples. It should be noted that the sample bond surfaces must be grease free. It is also essential that the working table is totally clean.

(b) To tighten the mould fit on the rock sample and prevent leakage of the polymer liquid, one or more rings of sticky tape were wound between the rock and the mould.

(c) The rock sample was inserted into the middle of the mould. The mould was raised to the attached sticky tape and forced to a tight fit. If loose, an additional

layer of sticky tape should be wrapped around the sample until tight fit is achieved.

(d) The polymer components are mixed evenly according to the research chemist's recommended ratio using a plastic cup and a wooden stick.

(e) The TSL mixture was poured into the plastic mould. If the TSL viscosity is high and difficult to pour directly, a wooden stick can be used to assist the TSL placement into the mould.

(f) Once the TSL was poured, it was left to cure for approximately four hours. The sample was then removed from the plastic mould. The sample was left at room temperature to cure for five days.

(g) The procedure was repeated for all tested samples.

4.2.3.2 Description of test apparatus and testing procedure used

The test apparatus for conducting the full TSL ring shear bond strength was an Instron compression machine that used a 5 mm thick steel sleeve to load and strip the polymer ring off the rock sample. It must be noted that there are two sides of the polymer ring, the top and the bottom. The surface formed on top when pouring the polymer was slightly irregular and not suitable for load application. However, the bottom section was precise and smooth, suitable to be evenly loaded with the assistance of the spherical seat. The spherical seat is essential to enable evenly distributed contact between the TSL ring and the steel cylinder to ensure evenly distributed shear load. The testing procedure is shown in Figure 4.7. During the test, the load and displacements were recorded.

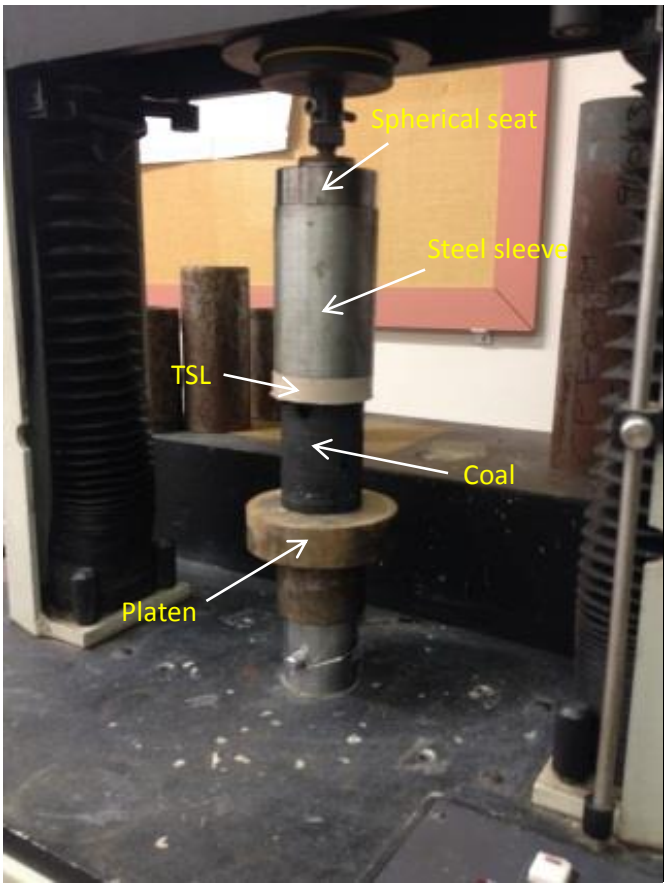

Figure 4.7 Full TSL ring shear bond strength test procedure

4.2.3.3 Loading rate

The applied rate of loading displacement of the assembly was selected to be 0.005 mm/s (0.3 mm/min) taking approximately 2-5 minutes to complete.

4.2.3.4 Calculations

The TSL shear bond strenght was calculated by Equation (4.2) where the peak load is divided by the bonded area around the sample.

$$\sigma_{sb} = \frac{F}{\pi \times D \times h} \tag{4.2}$$

Where F = applied stress at failure

σ_{sb} = shear bond strength of the TSL material

D = diameter of rock sample

h = height of TSL ring

The diameter of rock sample and the geometry of the polymer ring were measured before the test began to obtain the bonded area.

4.2.3.5 Failure mode

These tests did not yield the shear strength data as the TSL rings failed in tension as shown in Figure 4.8. The reason for this was complicated, but the resin shrinkage around the rock sample during the process of resin curing and the applied load caused high tension in the TSL and subsequent failure of the polymer ring. It was realised that this test cannot be used to measure true unconfined shear bond as the polymeric material shrinks and induces an unknown normal load onto the bond surface. The purpose of this test is to measure the unconfined shear bond between the TSL and the substrate. Any normal loads would increase this value. If the normal load is not known or difficult to measure it is better to design an experiment that overcomes this problem.

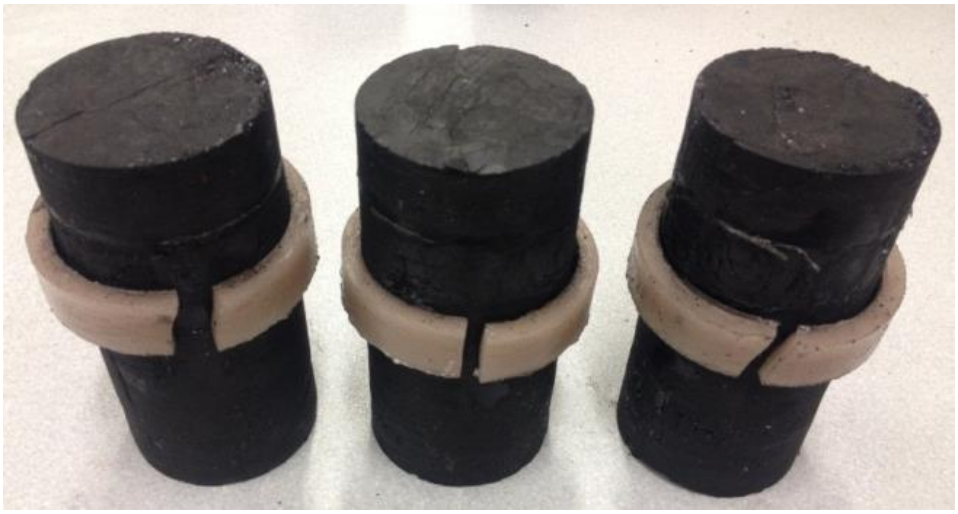

Figure 4.8 TSL ring shear bond strength test samples after failure

4.2.3.6 Results and analysis

The results of these tests are discused here as they are used in a later section of this chaper to compare all tested values derived from various experiments. Figure 4.9 shows a typical stress versus displacement graph of full TSL ring shear bond strength.

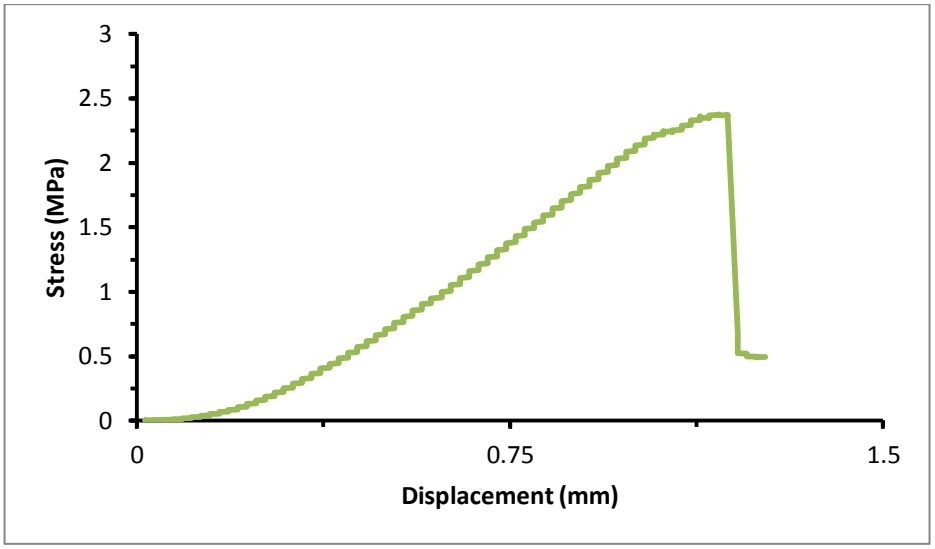

Figure 4.9 A typical stress versus displacement graph of full TSL ring shear bond strength

The mean shear bond strength of full ring shear test results for TSL A and B are summarised in Table 4.2.

Table 4.2 Mean shear bond strength of full ring shear test results for TSL A and B

Sample	Mean strength for TSL A (MPa)	Mean strength for TSL B (MPa)
Dry coal	2.19	2.53
Wet coal	-	-
Dry coarse sandstone	3.53	4.67
Wet coarse sandstone	-	-
Dry fine sandstone	6.28	7.24
Wet fine sandstone	-	-

Although these tests were more consistent than the double sided shear tests it was realised that the test results were greatly affected by tension within the polymer band that broke the TSL rings. The tension within the TSL rings applied a normal stress to the bond interface and therefore would have increased the measured shear stress. The tension was mainly caused by the resin shrinkage during the curing process and partly due to the Poisson's ratio effect during loading. The results were inconclusive as the pure shear bonding characteristics without the effect on the normal stress are required. Therefore, the full TSL ring shear bond strength testing method is not suitable to determine the shear adhesion of polymer because the failure mode was complicated and difficult to interpret.

4.2.4 Proposed test procedure for determination of the shear bond strength

The discontinuous ring shear test method was designed to overcome the shrinkage and tension problems of full ring shear test. The TSL ring was partitioned into four segments and tested.

4.2.4.1 Sample preparation

The Perspex mould (Figure 4.10a) was used to house the TSL material and rock or coal samples (Figure 4.10b).

A 5 mm thick steel sleeve (shown in Figure 4.12) was used to strip the polymer ring off the rock sample. In this study, three types of substrate: coal and two types of fine and coarse grain sandstone, were selected to perform the tests with two TSL products.

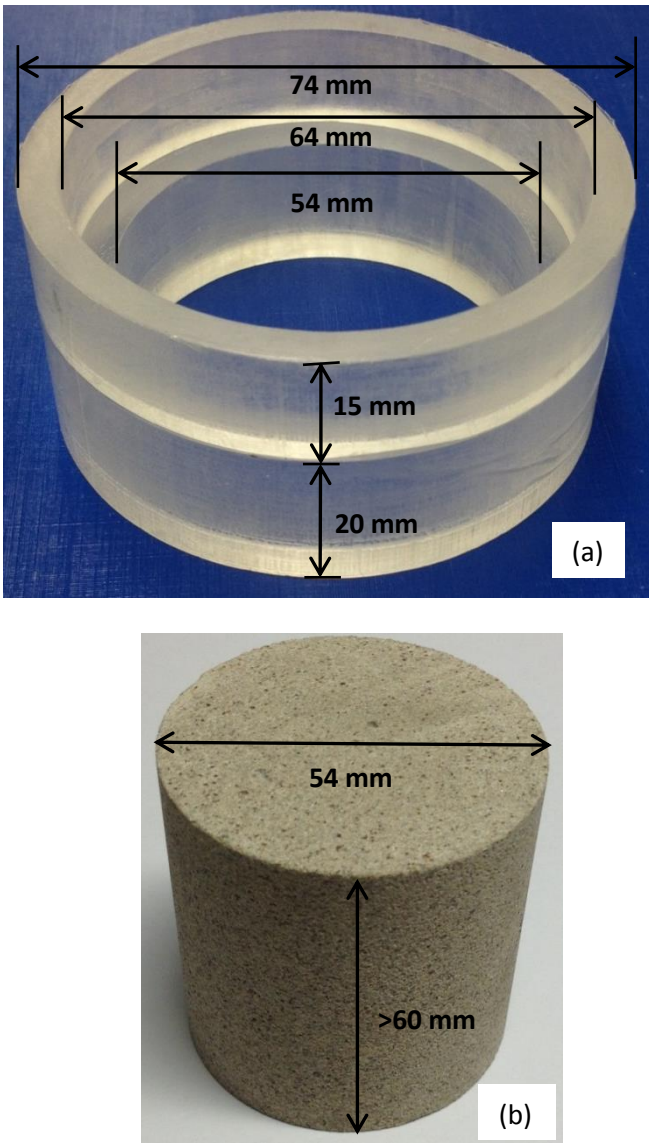

Figure 4. 10 Perspex mould (a) and a rock sample (b)

The procedures for preparing samples were the same as for preparation of full ring TSL shear bond strength test as shown in Figure 4.11 except for the step e):

e) In the process of casting the TSL ring, four pieces of rubber were used to separate the polymer segments. Thus the polymer ring was partitioned into four segments to minimise the effect of the induced normal stress onto the substrate.

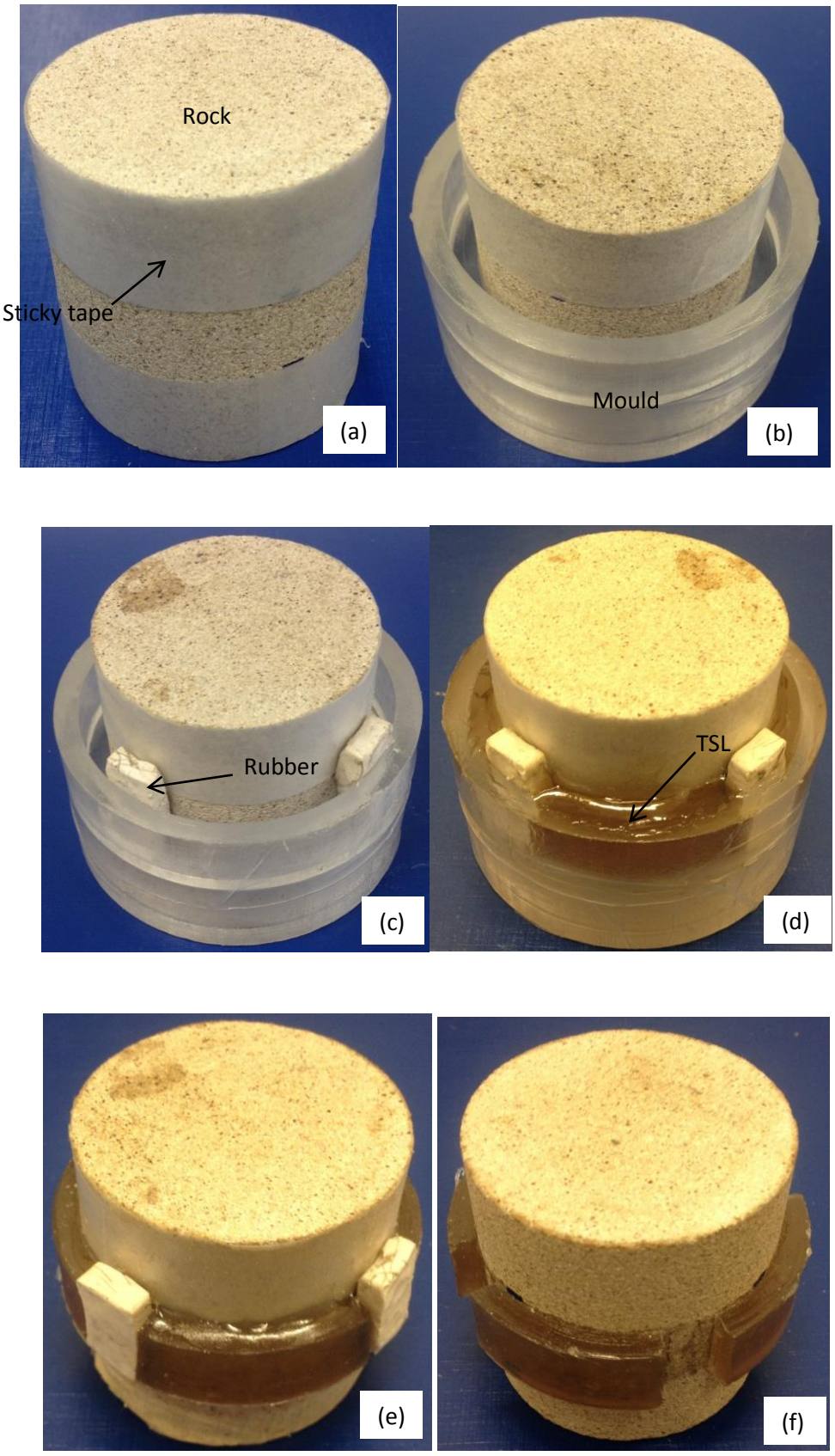

Figure 4. 11 Steps for sample preparation

4.2.4.2 Description of test apparatus and testing procedure

The test apparatus for conducting the shear bond strength test was similar to the full ring TSL shear test however the displacement rate of 1 mm/min was used to load each sample. At this speed, most of the tests were expected to be finished within two minutes except for some tests with high yield characteristics. The testing setup is shown in Figure 4.12. During the test, the load and displacements were recorded.

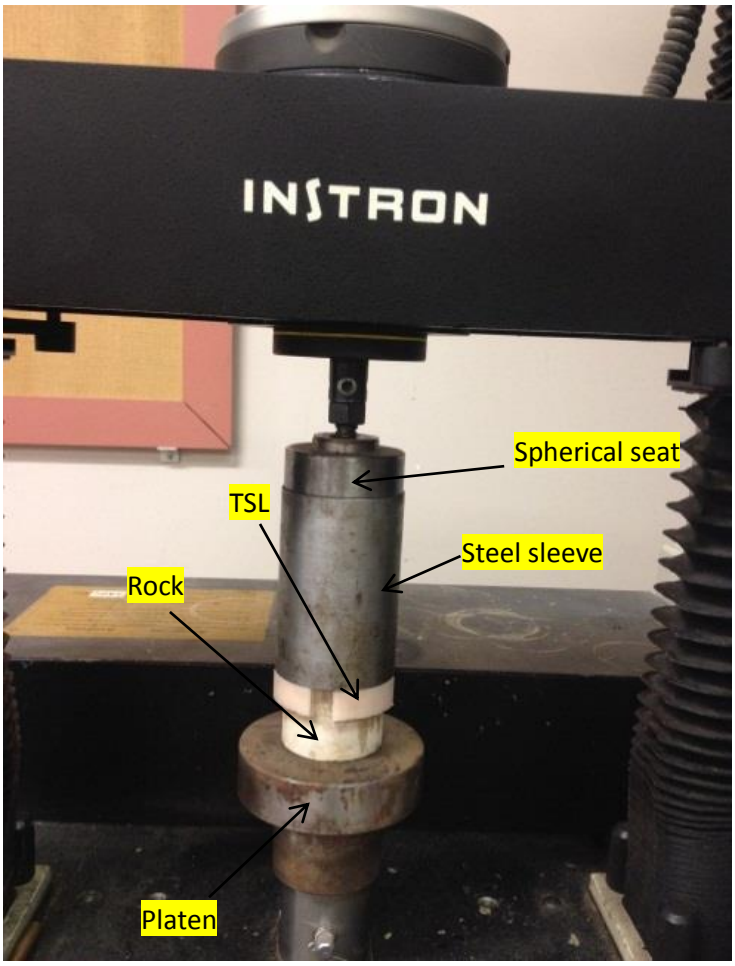

Figure 4.12 Segmented TSL ring shear bond strength testing setup

4.2.4.3 Failure mode and calculation

The aim of these tests was to measure the interface unconfined shear bond strength between the substrate and the TSL. Therefore, it was necessary to identify the location of failure after testing. In fact, there are three possible failure mechanisms:

1) failure occurs within the TSL material,

2) failure takes place within the substrate,

3) failure along both the substrate and TSL interface.

The shear bond strength can be calculated by Equation (4.3) where the maximum force is divided by the bonded area around the sample as follows:

$$\sigma_{sb} = \frac{F}{\pi \times D \times h - 4A} \tag{4.3}$$

Where F = the applied maximum force

σ_{sb} = the shear bond strength achieved at failure

D = the diameter of rock sample

h = the height of TSL segments

A = the empty area between two adjacent pieces of rubber.

To calculate the effective area, the total empty area 4A needs to be subtracted from the total ring.

If failure takes place within the substrate or TSL material other than at the TSL-rock/coal interface, the calculated TSL–substrate shear bond strength will be

underestimated. Sometimes there are some pieces of substrate left on the TSL material after testing. Based on the percentage of substrate left on the liner at the base of elevator bolt in the Ozturk and Tannant (2010) test, they proposed a method to classify the failure mode for determining the tensile bond strength of TSL materials. The shear bond failure mode for the strength test described in this thesis can also use the same assumptions that are described in Table 4.3.

Table 4.3 Classification of shear bond failure mode for shear bond strenght testing based on Ozturk and Tannant (2010)

Substrate left on liner (%)	Failure mode
0-33	Shear bond strength at TSL-substrate interface
34-66	Combination
67-100	Cohesion in the substrate

Figure 4.13 shows several shear bond strength test samples after failure. According to the above classification in Table 4.3, all of the samples failed along the TSL-substrate interface. Therefore, the testing method is suitable to determine the shear bond strength of TSL materials because the failure mode was simple, consistent and the results were easy to interpret.

Figure 4.13 Discontinuous TSL rings sheared off the tested samples

4.2.4.4 Analysis of results

In this study, two TSL product prototypes named A and B, were tested. The results for the TSL prototype A bonded to various substrates were plotted in Figure 4.14 a, b and c and summarised in Table 4.4. Likewise the results for the TSL prototype B bonded to various substrates were plotted in Figure 4.15 a, b and c and summarised in Table 4.5. When the applied load reached the shear bond strength between substrate and TSL, the polymer segments sheared off and the load dropped down abruptly.

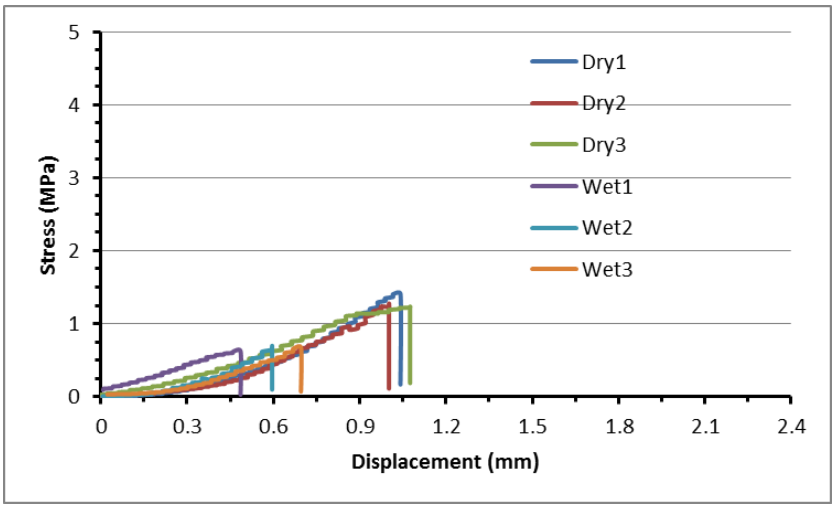

(a) TSL prototype A bonded to wet and dry coal surface

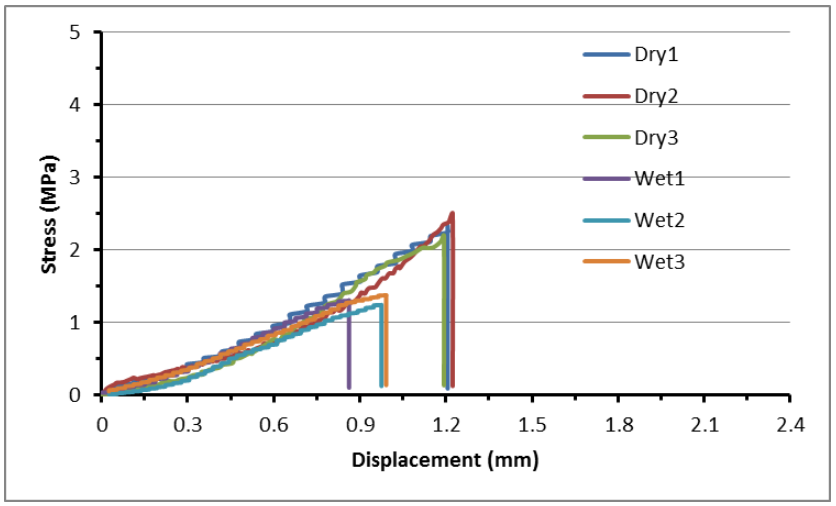

(b) TSL prototype A bonded to wet and dry coarse sandstone surface

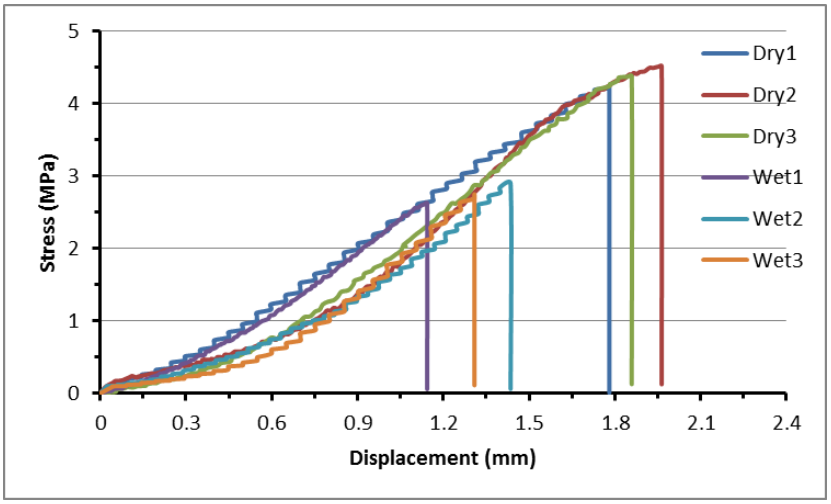

(c) TSL prototype A bonded to wet and dry fine sandstone surface

Figure 4.14 TSL prototype A bonded to various substrates

Table 4.4 Shear bond strength statistics for TSL prototype A

Sample	Failure mode	Shear bond strength (MPa)	Mean strength(MPa)	STDEV (MPa)
Dry coal 1	Interface	1.40		
Dry coal 2	Interface	1.28	1.30	0.07
Dry coal 3	Interface	1.23		
Wet coal 1	Interface	0.63		
Wet coal 2	Interface	0.69	0.66	0.02
Wet coal 3	Interface	0.67		
Dry coarse sandstone 1	Interface	2.33		
Dry coarse sandstone 2	Interface	2.49	2.34	0.12
Dry coarse sandstone 3	Interface	2.19		
Wet coarse sandstone 1	Interface	1.31		
Wet coarse sandstone 2	Interface	1.24	1.31	0.05
Wet coarse sandstone 3	Interface	1.37		
Dry fine sandstone 1	Interface	4.22		
Dry fine sandstone 2	Interface	4.51	4.37	0.12
Dry fine sandstone 3	Interface	4.37		
Wet fine sandstone1	Interface	2.62		
Wet fine sandstone 2	Interface	2.89	2.75	0.11
Wet fine sandstone 3	Interface	2.74		

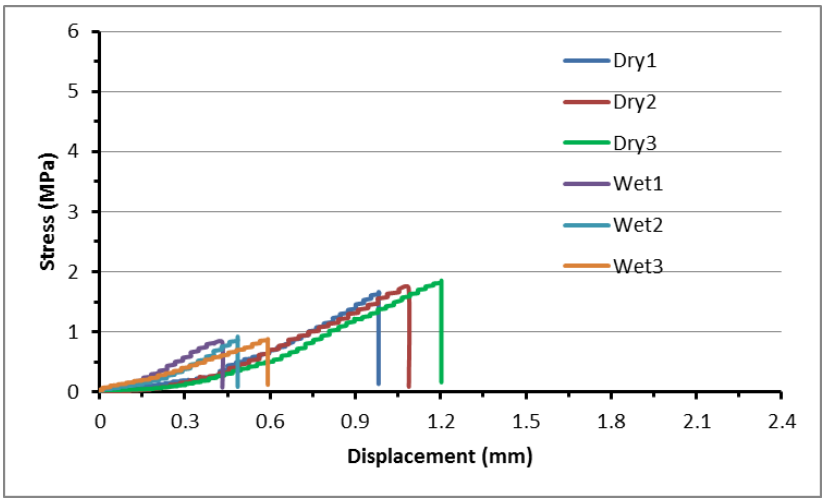

(a) TSL prototype B bonded to wet and dry coal surface

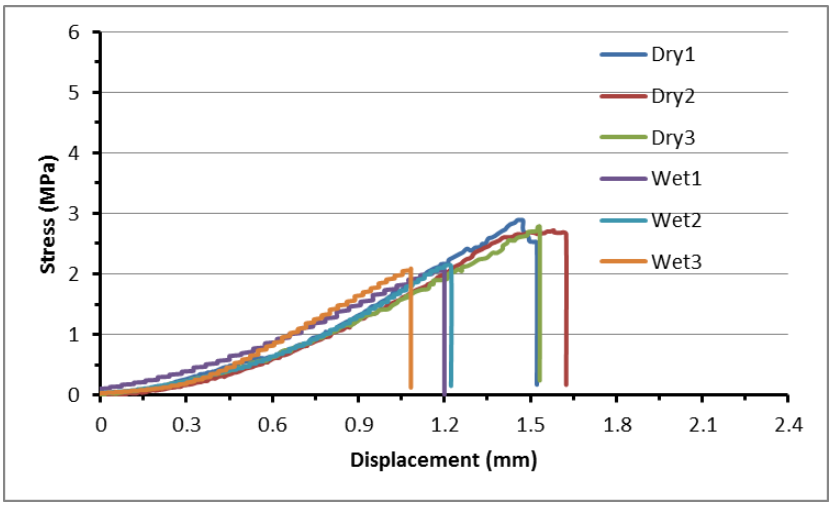

(b) TSL prototype B bonded to wet and dry coarse sandstone surface

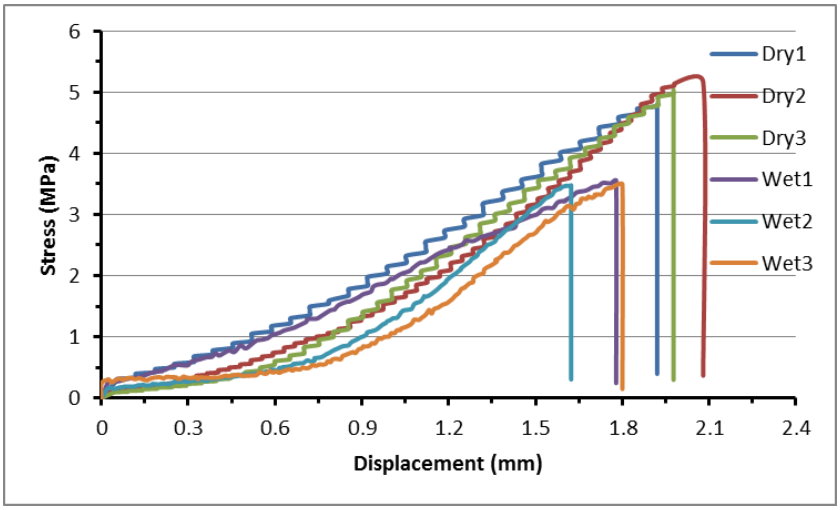

(c) TSL prototype B bonded to wet and dry fine sandstone surface

Figure 4.15 TSL prototype B bonded to various substrates

Table 4.5 Shear bond strength statistics for TSL prototype B

Sample	Failure mode	Shear bond strength (MPa)	Mean strength(MPa)	STDEV (MPa)
Dry coal 1	Interface	1.66		
Dry coal 2	Interface	1.72	1.74	0.08
Dry coal 3	Interface	1.85		
Wet coal 1	Interface	0.82		
Wet coal 2	Interface	0.92	0.87	0.04
Wet coal 3	Interface	0.88		
Dry coarse sandstone 1	Interface	2.89		
Dry coarse sandstone 2	Interface	2.72	2.82	0.07
Dry coarse sandstone 3	Interface	2.86		
Wet coarse sandstone 1	Interface	2.07		
Wet coarse sandstone 2	Interface	2.13	2.10	0.02
Wet coarse sandstone 3	Interface	2.09		
Dry fine sandstone 1	Interface	4.80		
Dry fine sandstone 2	Interface	5.16	5.00	0.15
Dry fine sandstone 3	Interface	5.03		
Wet fine sandstone 1	Interface	3.55		
Wet fine sandstone 2	Interface	3.45	3.50	0.04
Wet fine sandstone 3	Interface	3.49		

The results indicate that the shear bond strength of TSLs varies with substrate types. When bonded to coal, both TSL A and TSL B have the least shear bond strength between the contact interfaces. When applied to fine sandstone both TSL A and TSL B attain the biggest shear bond strength.

The results also demonstrate that both TSL prototypes adhered better to dry substrates than the wet ones. For the same TSL material and substrate, the shear bond strength of dry samples was measured to be almost 1.5 to 2 times greater than the bond to the wet samples. In addition, it is clear that when bonded to the same substrate, TSL B had higher shear bond strength than TSL A.

The segmented ring shear test results shown in Tables 5.4 and 5.5 appear consistent, reliable and conclusive. Therefore, it is recommended to evaluate the shear bond strength of different TSL products using this type of test.

For skin support TSL shrinkage is desirable as it will introduce compression in the substrate skin making a more durable composite layer of TSL bonded to substrate that provides resistance to fracture formation, propagation and excessive displacements.

4.2.5 Discussion

All the double-sided shear tests done in this study did not fail along the bonded TSL-rock interface, instead shear failure propagated through the rock. Therefore the results do not represent the TSL bond shear strength and this test procedure for strong shear bonds was not deemed to be appropriate. In the TSL full ring shear tests, the polymer always failed in tension caused mainly by the resin shrinkage during the curing process and partly due to the Poisson's ratio effect during loading. The tension that developed within the TSL rings applied a normal stress to the bond interface and therefore would have increased the measured shear strength. For this reason this test failed to give the true unconfined shear bond strength and therefore is not recommended. The segmented TSL ring shear bond procedure has proven to be consistent producing true unconfined shear bond strength for all tested rock types. The procedure was simple, easy and quick

to prepare, repeatable, cost effective with easy interpretation of the tested results. Therefore this procedure of testing is recommended for future tests.

Tables 4.6 and 4.7 summarise the results obtained from the three different shear test methods.

Table 4.6 Comparison of the mean shear bond strength for three different methods of testing TSL prototype A

Sample	Double-sided shear test (MPa)	Full ring shear test (MPa)	Segmented ring shear test (MPa)
Dry coal	1.11	2.19	1.30
Wet coal	0.49	-	0.66
Dry coarse sandstone	1.57	3.53	2.34
Wet coarse sandstone	0.93	-	1.31
Dry fine sandstone	2.96	6.28	4.37
Wet fine sandstone	1.80	-	2.75

Table 4.7 Comparison of the mean shear bond strength for three different methods of testing TSL prototype B

Sample	Double-sided shear test (MPa)	Full ring shear test (MPa)	Segmented ring shear test (MPa)
Dry coal	1.37	2.53	1.74
Wet coal	0.62	-	0.87
Dry coarse sandstone	1.96	4.67	2.82
Wet coarse sandstone	1.18	-	2.10
Dry fine sandstone	3.35	7.24	5.00
Wet fine sandstone	2.19	-	3.50

4.3 Tensile bond strength testing of thin spray-on liners

It is commonly accepted that adhesion loss followed by tensile rupture is an important failure process from a design point of view (Ozturk and Tannant, 2010; Oztruk, 2012). When TSL adhesion is strong enough, the TSL-rock composite layer is able to restrict opening of fractures and unravelling of broken strata. This process can minimise the chance of any broken material falling into the mine roadways. Although the tensile-bond strength test using steel dolly pull-off test (Tannant *et al.* 1999; Tannant and Ozturk 2003; Archibald 2001; Ozturk and Tannant 2004, 2010 and 2011; Yilmaz 2009) has received common acceptance by researchers and manufacturers, there are still some concerns that need to be addressed. Some factors that affect the tensile bond strength of TSLs were investigated by Ozturk and Tannant (2010). They proposed a testing method for determining the adhesive strength of TSL material, and studied the effect of liner thickness and loading rates on adhesive strength of a cement-based TSL material Tekflex that was applied to concrete and granite surfaces. Ozturk and Tannant (2011) also investigated the influence of rock properties and environmental conditions on the adhesive strength of Tekflex. Ozturk (2012) used the fracture mechanics method to interpret thin spray-on liner adhesion test data and showed that edge crack propagation is the main failure mechanism during pull-off tests, although Fowkes et al (2008) argued that cavitation being a cohesive failure of TSL resulting from growth and coalescence of micro-voids is likely to be the rupture mechanism of TSL adhesion tests. Ozturk (2012) calculated the work of thin spray-on liner adhesion using the analytical method. Yilmaz (2013) conducted research to compare the tensile bond strength of different thin spray-on liners.

Currently, the studies on polyester-based TSL materials are limited as the past research mainly focused on the cement-based TSL materials. In this tensile bond study, modifications were made to the process of sample preparation. Steel specimen housing equipment was used to ensure even load distribution. The effect of loading rates, liner thickness, rock types and environmental conditions on the tensile bond strength of polyester-based TSL material were investigated. It was observed that in most cases the polymeric material was excellent in adhering to dry, wet or dusted surfaces minimising any air bubbles forming at the substrate-TSL surfaces.

4.3.1 Description of apparatus and sample components

4.3.1.1 Properties and dimensions of rock samples

Four types of rock were used to conduct the tensile bond strength tests. To suit the rock housing equipment, the sub-cored rock diameter of 54 mm was chosen while the rock sample was cut to a thickness greater than 20 mm to maintain rock sample strength. The rock end surfaces cut with the diamond saw were relatively smooth. The tensile strength of each rock type was measured in the laboratory prior to testing. The measured tensile strength of each rock type is summarised in Table 4.8.

Table 4.8 Tensile strength of rock conducted at the University of Wollongong

Rock Type	Tensile Strength (MPa)
Coal	0.94
Marble	5.73
Granite	7.49
Sandstone	8.31

4.3.1.2 Loading fixture

Ozturk and Tannant (2010) developed an elevator bolt with a 33 mm diameter base that they used for the tensile bond tests. There are many advantages of the elevator bolt test method however, this elevator bolt had to be discarded after each test and could not be reused.

In this study, a new reusable cylindrical steel dolly was made. It is commonly accepted that the diameter of the steel dolly should be at least ten times greater than the largest grain size of the rock substrate. The diameter of the cylindrical steel dolly was 38 mm with a threaded hole on the top as shown in Figure 4.16(a). The steel loading ring (Figure 4.16b) was connected to the steel dolly. The advantage of the steel dolly is that it can be used up to five times. After each test, the end of the tested dolly (Figure 4.16c) was cut off (Figure 4.16d) and the dolly was reused (Figure 4.16e).

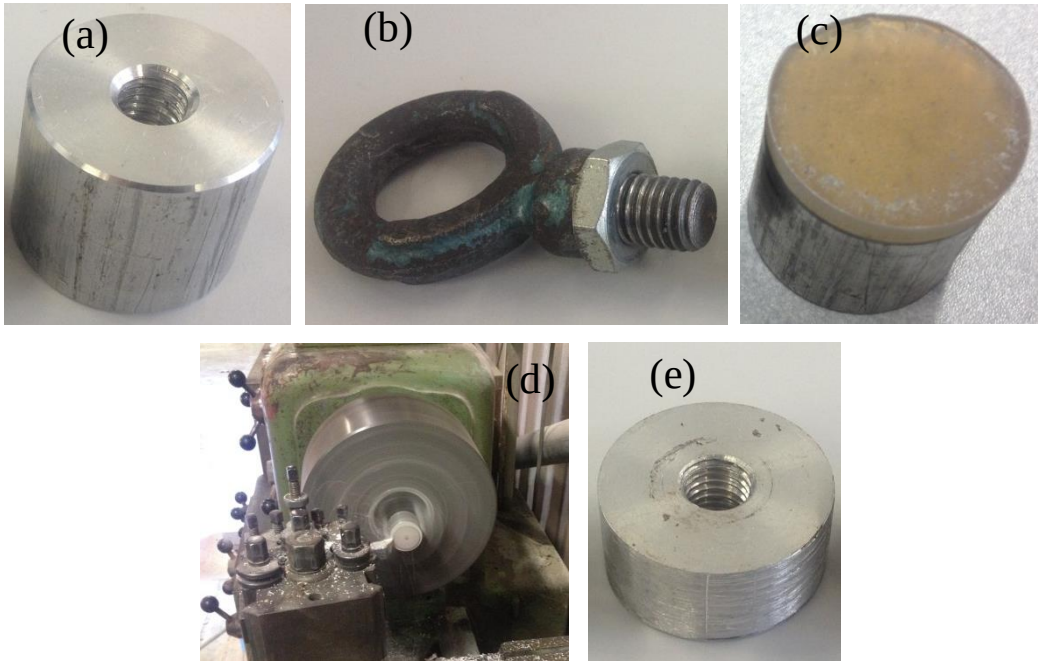

Figure 4.16 Sample components

4.3.1.3 Sample housing equipment

To minimise the effect of bending and ensure even load distribution along the bonded surface, steel equipment consisting of the top and bottom parts were developed to house the test specimens as shown in Figure 4.17. This type of design was essential as non-uniform stress distribution along the contact surface will cause stress concentrations and underestimate the tensile bond strength between TSL material and rock surface.

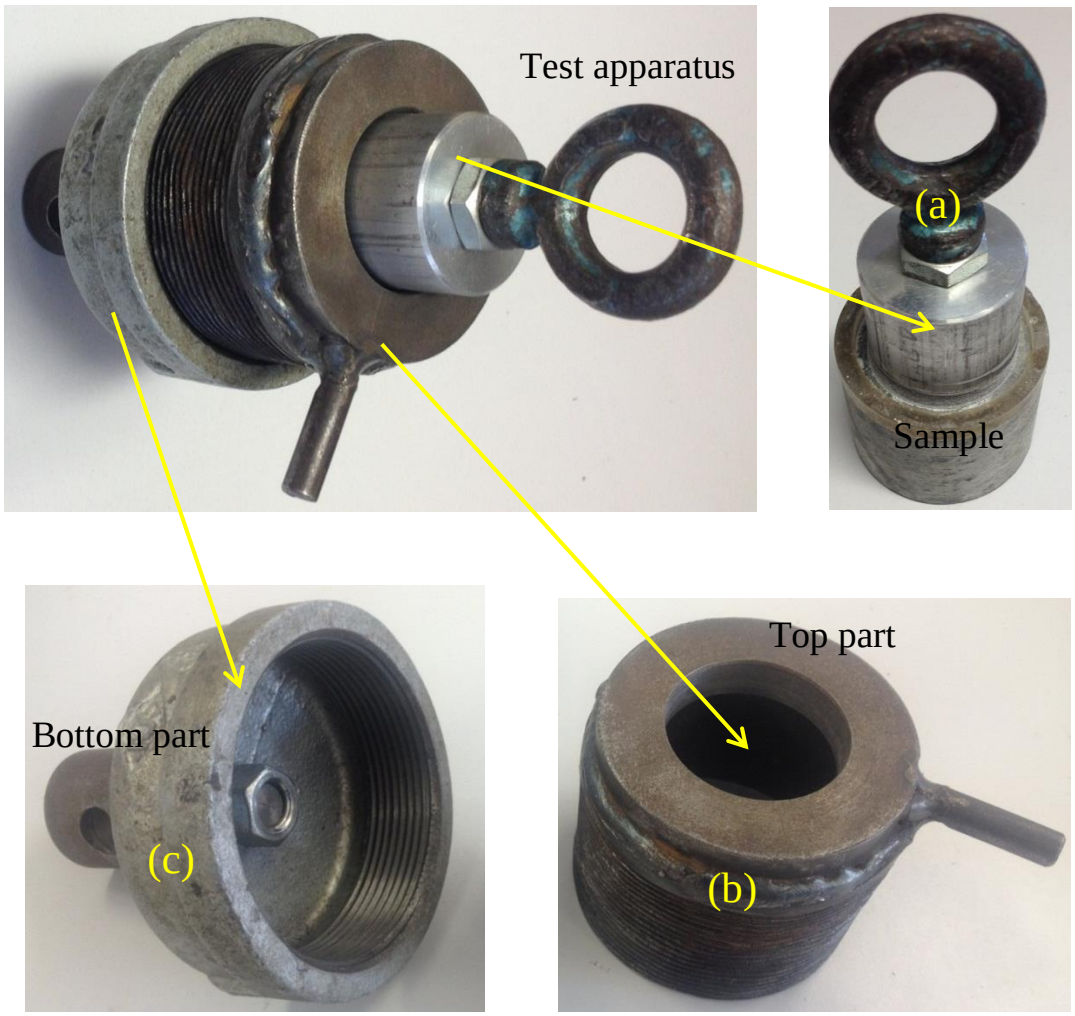

Figure 4.17 Sample housing equipment

4.3.1.4 Epoxy and overcore equipment

High strength epoxy was used to glue the steel dolly to the TSL material. The epoxy had to be very strong to prevent the failure of the epoxy bond. According to Ozturk and Tannant (2010), Araldite exhibited high adhesive strength after 24 hours of curing, and therefore Araldite was selected to attach the steel dolly to the TSL material. To separate the TSL-rock bond area beneath the steel dolly, the TSL was overcored as shown schematically in Figure 4.18. During the TSL overcoring, the sample was inserted into a thick plastic tube to prevent damage to the rock. A thin-walled core bit with the inner diameter of 40 mm was used to cut through the TSL material down to the rock substrate.

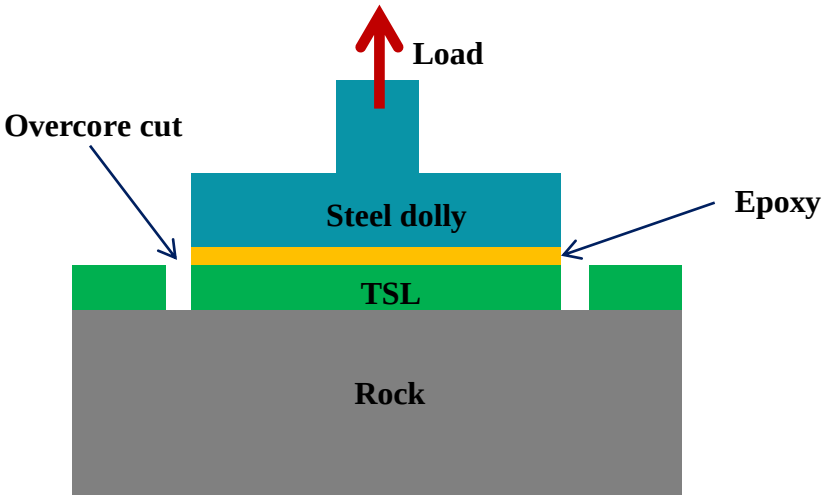

Figure 4.18 Illustration of tensile bond strength testing

To reduce the possible disturbance to the specimen during over-coring, the drill bit was gently operated using an up and down motion and a minimum thrust. Yilmaz (2013) proposed a Perspex mould to eliminate the over-coring process however his TSL material was of high viscosity while the Perspex caused persistent leakage of the TSL

in our tests, contaminating the sample surface and therefore was not used in this study. The overcoring setup is shown in Figure 4.19.

Figure 4.19 TSL overcoring setup

4.3.2 Sample preparation and test procedure

An outline of the procedure used for preparing samples is given here:

a) All rock samples were sub-cored with 54 mm diameter core barrel and cut to length with a diamond saw to fit into the testing device and provide a smooth bond surface for testing.

b) The coal samples were sub-cored parallel to the bedding planes and the core ends trimmed with a diamond saw to the required length to provide a bond surface for testing. The tested surface was perpendicular to the bedding planes to minimise failure through the rock or coal as the sedimentary strata usually part easily along the bedding planes.

c) For testing on wet surfaces, the samples were placed in water for 24 hours before casting the TSL onto the wet rock surface.

d) For the dry tensile bond, the samples were left to dry for 24 hours at room temperature before testing took place. A sample ready for testing is shown in Figure 4.20a.

e) Para film was used to wrap the rock samples and keep them clean as shown in Figure 4.20b. The role of the Para film was to prevent the leakage of the TSL materials onto the rock sample side surface. A separate plastic strip was wrapped around the sample to protrude 1 to 9 mm above the edge (Figure 4.20c) to enable a polymer layer of various thickness to be poured onto the surface for testing according to the requirement. The use of plastic strips simplifies the process of sample preparation and easy pouring of the TSL material at the expected thickness.

f) The polymer layer of required thickness was applied onto the rock surface as shown in Figure 4.20d.

g) Sufficient time was allocated to allow curing before removing the plastic film (Figure 4.20e). The steel dowel was centrally bonded to the polymer surface with the high strength araldite epoxy. A 38 mm coring bit was used to gently overcore the dowel through the polymer stopping at the rock surface. The overcored dowel is shown in Figure 4.20f.

h) The tensile bond strength of the TSL was then tested by pulling the dowel and attached central TSL ring away from the rock surface.

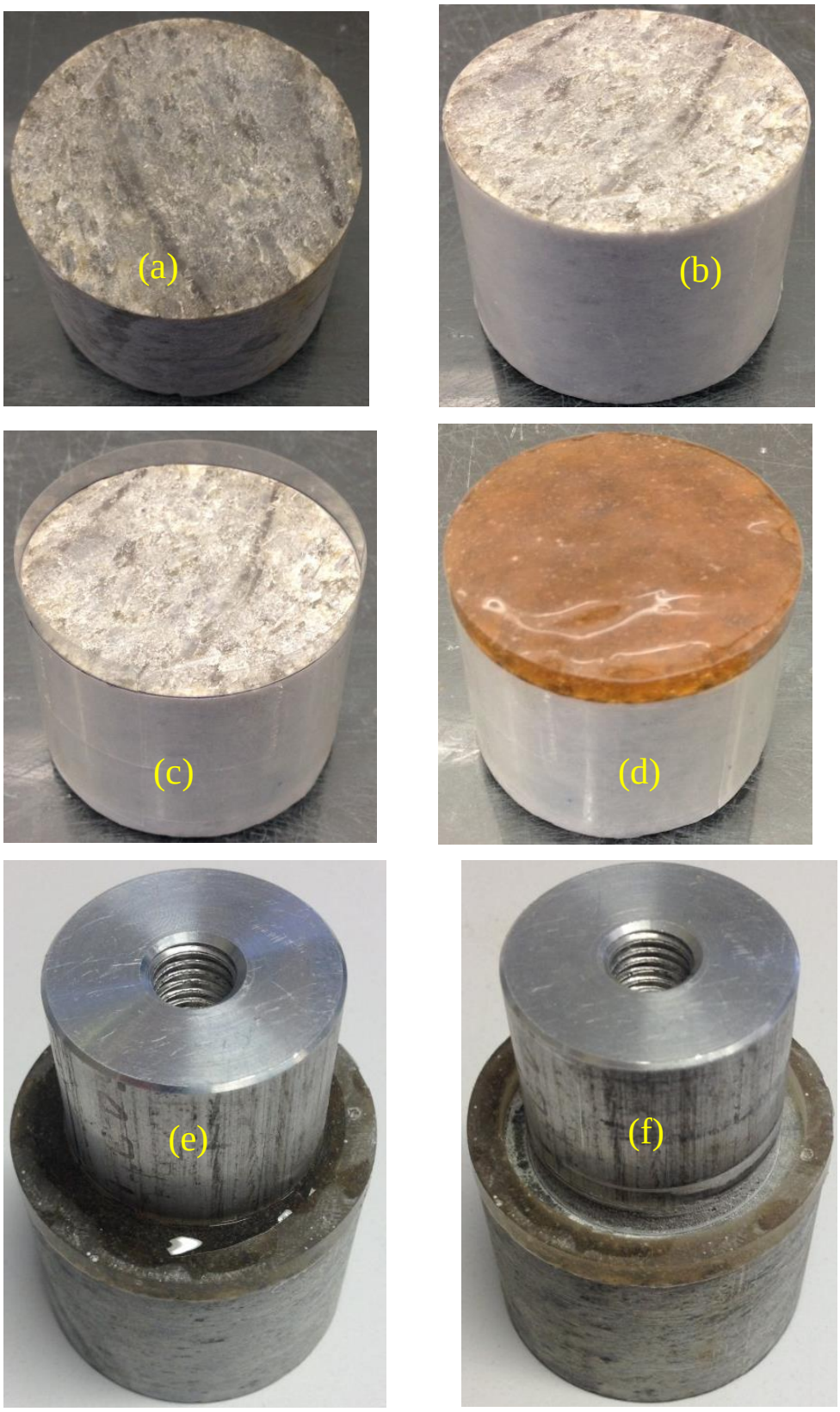

Figure 4.20 Procedures of sample preparation

An Instron loading machine was used to perform the test. Steel housing equipment was used to hold the sample and ensure an evenly distributed load. The applied load and displacements were recorded during the test. The load was applied at a displacement rate of 2 mm/min with tests completed in approximately 1minute. The testing setup is shown in Figure 4.21.

Figure 4.21 Test setup

4.3.3 Calculation and failure mode

The material tensile bond strength of each test was calculated using Equation (4.4). The strength can be obtained by dividing the force at failure by the contact area of the polymer TSL.

$$\sigma_{tb} = \frac{4F}{\pi \times d^2} \tag{4.4}$$

Where F = maximum force applied to the test surface at failure,

σ_{tb} = tensile bond strength of the TSL material at failure,

A = the contact area of steel dolly,

d = diameter of the TSL ring.

Four possible failure mechanisms for the tensile bond failure were described by Ozturk and Tannant (2010), and Yilmaz (2013). The four failure modes were presented as following:

- De-bonding on the TSL-epoxy boundary or epoxy/steel dolly interface when the epoxy bonding to TSL or steel dolly is lower than the TSL-rock bond strength.
- Failure within the rock substrate when the tensile bond strength exceeds the tensile strength of the rock material.
- Failure along the rock-TSL surface which gives the true tensile bond strength between the rock and TSL material.
- Failure taking place within the TSL material when the tensile bond strength is higher than the tensile strength of TSL material.

In some cases, there may be a combination of these failure mechanisms. Schematic of tensile bond strength testing was illustrated in Figure 4.18. To effectively evaluate and interpret the failure mode, Ozturk and Tannant (2010) visually estimated and classified the failure mode according to the percentage of substrate left on TSL material at the base of the elevator bolt as shown in Table 4.9.

Table 4.9 Classification of tensile failure mode (Ozturk and Tannant 2010)

Substrate left on the TSL liner	Failure mode
0-33%	Adhesive at interface
34-66%	Combination
67-100%	Cohesive in the substrate

4.3.4 Analysis of results

4.3.4.1 Effect of loading rate on Polymer TSL tensile bond strength

To investigate the effect of different loading rates on the tensile bond strength of the polymer TSL, the marble rock was used to conduct the tests under eight different loading rates of 0.5, 1, 1.5, 2, 3, 5, 7 and 10 mm/min. Two samples were tested at each loading rate. The curing time for the samples was seven days under room conditions and the applied thickness of TSL material was 5 mm. The graph of loading rate versus tensile bond strength tested at the University of Wollongong is plotted in Figure 4.22.

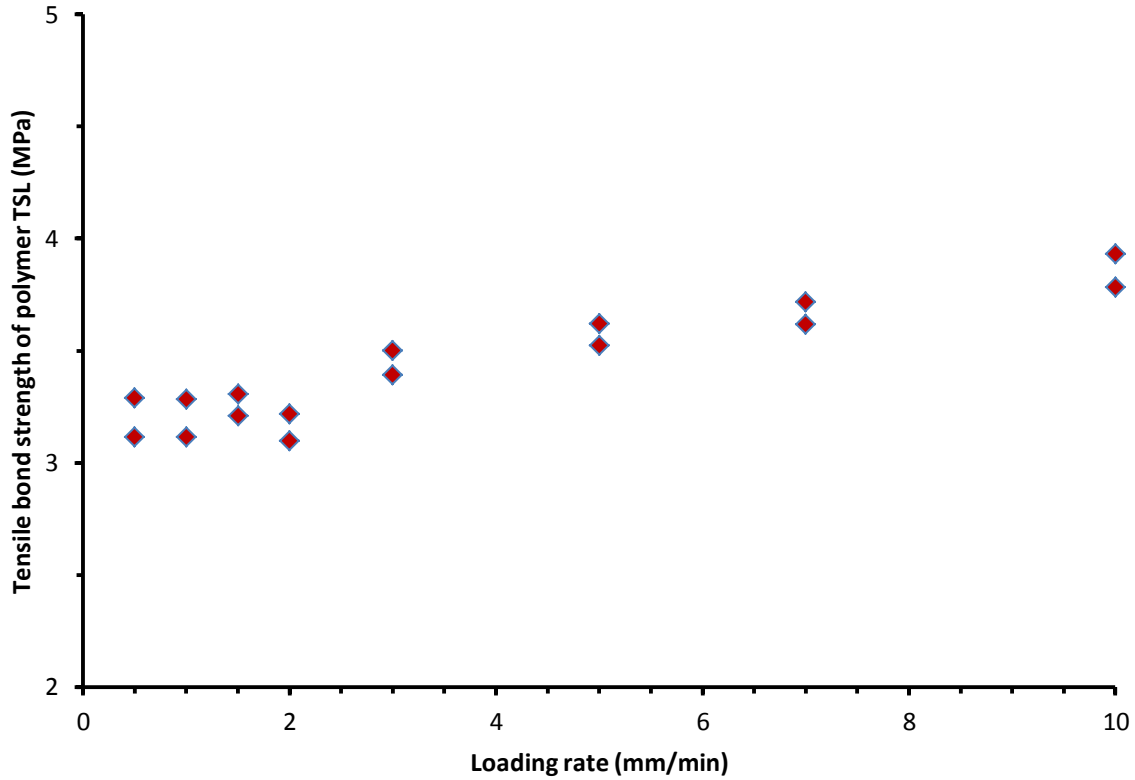

Figure 4.22 Loading rate versus tensile bond strength

It can be seen from Figure 4.22 that the lower loading rates ranging from 0.5 mm/min to 2 mm/min have little effect on the tensile bond strength while for higher loading

rates of up to 10 mm/min, the tensile bond strength increased with the increase of loading rates. Ozturk and Tannant (2010) also studied the effect of loading rates on adhesive strength between a cement-based TSL material named Tekflex and saw-cut paving stones using four loading rates of 0.1, 0.5, 1 and 2 mm/min and the similar results were obtained. Therefore, the effect of loading rate is negligible for the lower loading rates and the optimal loading rate was determined. In this study, initial tests indicated that samples failed within the displacement of 1 mm. Thus the loading rate of 2 mm/min was selected to conduct the following tests to ensure that the failure occurs at approximately half minute and the effect of loading rates on the tensile bond strength would therefore be minimised. Note that the measured displacements during loading were much larger than the actual separation displacements prior to failure. This was caused by low stiffness of the loading system. However, displacements did not play an important role in the tensile bond testing.

4.3.4.2 Effect of TSL thickness

Yang and Li (2001) studied the effect of TSL thickness on pull-off force for a thin elastic layer material sandwiched between a cylindrical indenter and a rigid substrate based on Kendal (1971). They derived the equation to calculate the pull-off force F_c:

$$F_c = \pi a^2 \sqrt{\frac{2E\gamma}{h(1-\nu^2)}} \tag{4.5}$$

Where E = Young's modulus,

ν = Poisson's ratio of thin liner,

γ = the work of adhesion,

a = the radius of the pull-off test,

h = the thickness of the liner.

The tensile bond strength σ_c can be obtained using:

$$\sigma_c = \sqrt{\frac{2E\gamma}{h(1-\nu^2)}} \tag{4.6}$$

For any type of TSL material, the Young's modulus E, Poisson's ratio ν and the work of adhesion γ are constant. The Equation (4.6) can be expressed by Equation (4.7).

$$\sigma_c = C \times h^{-0.5} \tag{4.7}$$

Where $C = \sqrt{\frac{2E\gamma}{(1-\nu^2)}}$ is a constant. It can be concluded that the tensile bond strength is inversely proportional to the square root of the thin liner thickness.

The experimental study at the University of Wollongong was conducted to evaluate the effect of TSL liner thickness on the tensile bond strength. Five different TSL thicknesses of 1 mm, 3mm, 5mm, 7mm and 9mm were applied onto the granite rock surface and loaded to failure in tension. The graph of TSL thickness versus tensile bond strength between TSL material and granite rock was plotted in Figure 4.23.

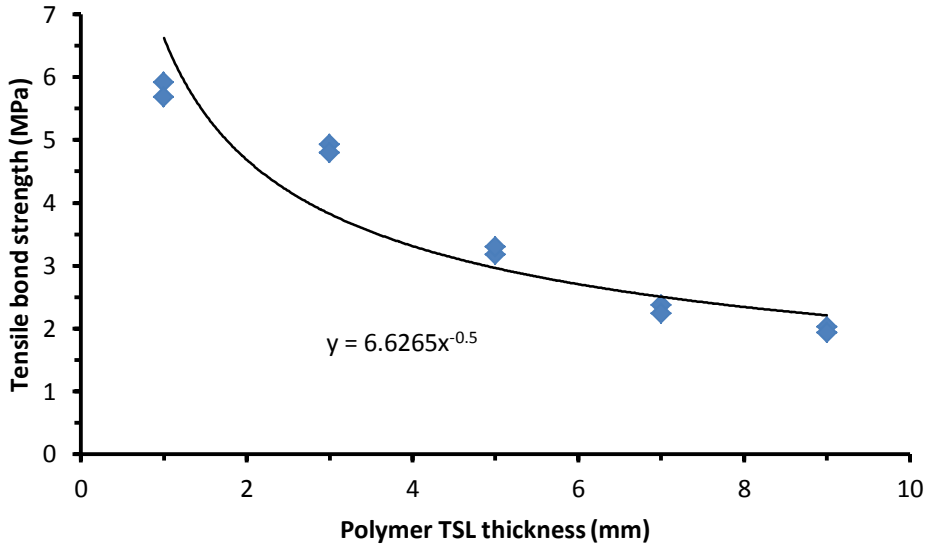

Figure 4.23 Experimental results of TSL thickness versus tensile bond strength

As can be seen in Figure 4.23 the tensile bond strength between the TSL material and granite rock is inversely proportional to the square root of the TSL thickness matching the Equation (4.7) well. Ozturk and Tannant (2010) also investigated the effect of liner thickness on the adhesive strength using the cement-based liner material applied onto saw-cut granite substrates and paving stones. Their results revealed similar conclusions with the adhesive strength displaying an inverse square root relationship with the liner thickness. Therefore, it can be concluded that the tensile bond strength of both the cement-based and polymer-based TSL material are inversely proportional to the square root of the TSL material thickness. Using Equation (5.7), the tensile bond strength of various TSL thicknesses can be converted into a specific thickness (such as 5 mm in this study) to compare the adhesive characteristics of the TSL materials.

4.3.4.3 Effect of rock types and surface conditions (wet and dry)on TSL tensile bond strength

Four types of rock were used in this study, one of which was coal. More than 60 tests were conducted, and only the samples that failed along the TSL and rock surface were analysed and summarized in Table 4.10. Some of the typical failures are shown in Figure 4.24, (a) epoxy bond failure, (b) rock failure and (c) TSL debonding.

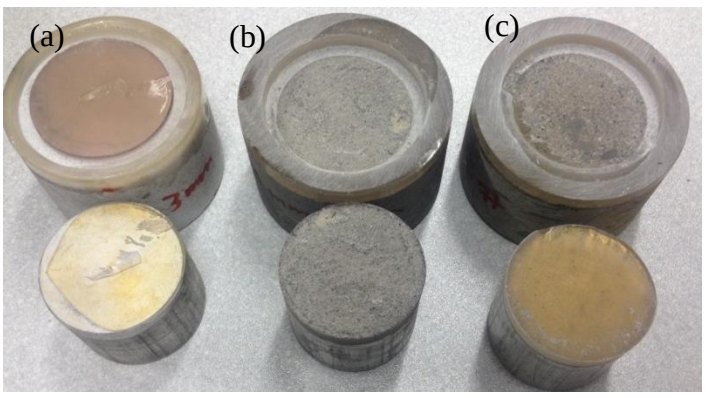

Figure 4.24 Typical failures observed during testing

Table 4.10 Summary of test results

Rock Type	Test number	Failure mode	Tensile bond strength (MPa)	Mean strength (MPa)	Standard Deviation (MPa)
Wet coal	1	Interface	0.51	0.51	0.07
Wet coal	2	Interface	0.44		
Wet coal	3	Interface	0.58		
Dry coal	1	Interface	0.81	0.76	0.06
Dry coal	2	Interface	0.76		
Dry coal	3	Interface	0.70		
Wet marble	1	Interface	2.44	2.40	0.12
Wet marble	2	Interface	2.26		
Wet marble	3	Interface	2.35		
Wet marble	4	Interface	2.53		
Dry marble	1	Interface	3.18	3.27	0.29
Dry marble	2	Interface	3.68		
Dry marble	3	Interface	3.00		
Dry marble	4	Interface	3.23		
Wet granite	1	Interface	1.70	2.01	0.32
Wet granite	2	Interface	1.86		
Wet granite	3	Interface	2.08		
Wet granite	4	Interface	2.41		
Dry granite	1	Interface	3.00	3.08	0.13
Dry granite	2	Interface	2.96		
Dry granite	3	Interface	3.11		
Dry granite	4	Interface	3.26		

Wet sandstone	1	Interface	2.70	2.48	0.21
Wet sandstone	2	Interface	2.60		
Wet sandstone	3	Interface	2.23		
Wet sandstone	4	Interface	2.38		
Dry sandstone	1	Interface	3.40	3.32	0.08
Dry sandstone	2	Interface	3.28		
Dry sandstone	3	Interface	3.26		
Dry sandstone	4	Interface	3.38		

It can be seen from Table 4.10 that the tensile bond strength varies when applied onto different rock types. The results also demonstrate that TSL material adhered better to dry substrates than to wet rocks. When applied to coal samples, the tensile bond strength was the smallest (the mean strength 0.51 MPa and 0.76 MPa for the wet and dry surface respectively). In contrast, the tensile bond strength was highest when applied to sandstone samples (the mean strength 2.48 MPa and 3.32 MPa for the wet and dry surface respectively), followed by marble samples (the mean strength 2.40 MPa and 3.27 MPa for the wet and dry surface respectively) and then granite samples (the mean strength 2.01 MPa and 3.08 MPa for the wet and dry surface respectively). It seems that the tensile bond strength increases with the tensile strength of rock. It is common that pore water pressure and fresh surface water exist in underground excavations, and therefore the excavation surfaces vary from wet to dry but in most cases at the mining face wet rock prevails. For this reason it is essential to investigate the tensile bond strength between TSL and wet rock surfaces. The presence of water significantly reduced the measured tensile bond strength when compared with the dry surface. In this study, the wet samples were submerged in the water for 24 hours and

the TSL cast onto the wet surface. Table 4.10 indicates that the test results were consistent and conclusive.

4.4 Summary

The summary and conclusions are divided into two parts for shear bond strength testing and tensile bond strength testing.

4.4.1 Shear bond strength testing

The aim of the study was to compare three different testing methods to determine the shear bond strength of TSL materials and choose the most suitable method. The double sided shear test can simulate the effect of TSL fracture penetration and reinforcement; however, if not secured properly, failure of this test can be caused by tension rather than shear due to bending of the assembly during the test. The full ring shear test can eliminate the effect of bending, however, it could cause normal stress induced by shrinkage around the rock surface, affecting the shear-bond strength between the interface of rock core and the TSL. The four ring segments test results indicated that all of the failure occurred along the TSL-substrate interface. This test minimised the TSL problems associated with the normal stress to the shear interface by leaving four gaps between the adjacent polymer segments. It must be noted that due to smooth loading surfaces and use of the spherical seat the load on all ring segments would have been approximately equal.

Therefore this test is considered acceptable to measure the unconfined shear bond strength. Other possible geometries may be trialled in the future such as a rail guided mechanism to shear a small polymer sample of known area bonded to the rock surface.

The test results indicate that the four segment ring testing method is an effective testing approach that has a lot of advantages. These are:

(a) Simple, easy and quick sample preparation (also readily available from *in situ* drilling).

(b) The test is repeatable.

(c) The testing setup is flexible and easy to operate.

(d) Easy interpretation of data and simple calculations.

(e) It is cost effective.

4.4.2 Tensile bond strength testing

In the process of sample preparation, several modifications were made. The steel dolly was used to replace the disposable elevator bolt used by Ozturk and Tannant (2010). Steel TSL housing equipment was developed to ensure the even load application thereby improving the accuracy of results. The test results indicate that for lower loading rates from 0.5 to 2 mm/min, the effect of loading rates can be ignored while for higher loading rates of up to 10 mm/min, the tensile bond strength increased with the increase of loading speed. The data clearly indicate that the tensile bond strength of the polyester-based TSL material is inversely proportional to the square root of the TSL material thickness. The results also demonstrate that TSL material adhered better to dry substrate than the wet rocks. The data also indicate that the tensile bond strength may increase with the tensile strength of rock substrate.

CHAPTER 5 DIRECT SHEAR TESTS OF JOINTS INFILLED WITH THIN SPRAY ON LINER - LABORATORY TESTS

5.1 Introduction

The shear bond strength between the TSL and the rock surface can promote block interlock which can keep broken blocks in place and minimise block rotation caused by the shear. Stacey (2001) described a series of mechanisms of loading behaviour and surface support behaviour of thin spray-on liners and proposed the theory "promotion of block interlock" which is related to the shear-bond strength between the TSL and rock surface. The aim of this mechanism is mainly to keep the rock mass in a stable and unloosened condition. Subsequently, Stacey and Yu (2004) determined the effect of various factors on the support capacity of TSL using the method of finite element stress analysis. They demonstrated that the TSL penetration into the joints and fractures within the rock mass plays an important role in the supporting system. Penetration of TSL material into the joints and fractures has the potential to inhibit the movement of fractured rock mass and consequent failure. This support mechanism is relevant in the high stress regions such as at the excavation surface where loosening and stress fracturing has occurred. The depth of penetration of the liner material depends on its consistency, the applied or sprayed pressure and the openness and orientation of the fractures and natural weak planes. For the less viscous TSLs, penetration into the fractures or joints will be much greater. Especially for the downwards inclined fractures or joints in the sidewalls of tunnels and mine roadways and shafts, they allow much greater penetration due to the influence of gravity. Mason

and Stacey (2008) used an analytical method to study the effect of the penetration of TSL into joints and fractures. The results revealed that the elastic modulus of fractured rock penetrated by liner material is the same as the elastic modulus of the rock without fractures, although the elastic modulus of the intact rock is greater than that of fractured rock at the excavation surface (Jaeger *et al.* 2009). Fowkes *et al.* (2008) studied crack repair using TSLs and the results indicated that TSL material filled the crack and can prevent crack propagation and consequent failure. Ozturk (2012) showed that edge crack propagation is the main failure mechanism during pull-off tests, although Fowkes *et al.* (2008) argued that cavitation being a cohesive failure of TSL resulting from growth and coalescence of micro-voids is likely the rupture mechanism of TSL adhesion tests.

To study the shear behaviour of TSL penetrated rock joints, the direct shear test was adopted. The effects of surface roughness, penetrated thickness to asperity height ratio, shear rate, and normal load on the shear behaviour of TSL penetrated rock joints was investigated in this study.

5.2 Experimental program

5.2.1 Test apparatus

The direct shear apparatus used consisted of two steel shear boxes that enclosed the tested samples in position for testing. The size of the top box was 250 mm in length, 150 mm in height, and 75 mm in width. The lower box was 250 mm in length, 100 mm in height, and 75 mm in width as shown in Figure 5.1.

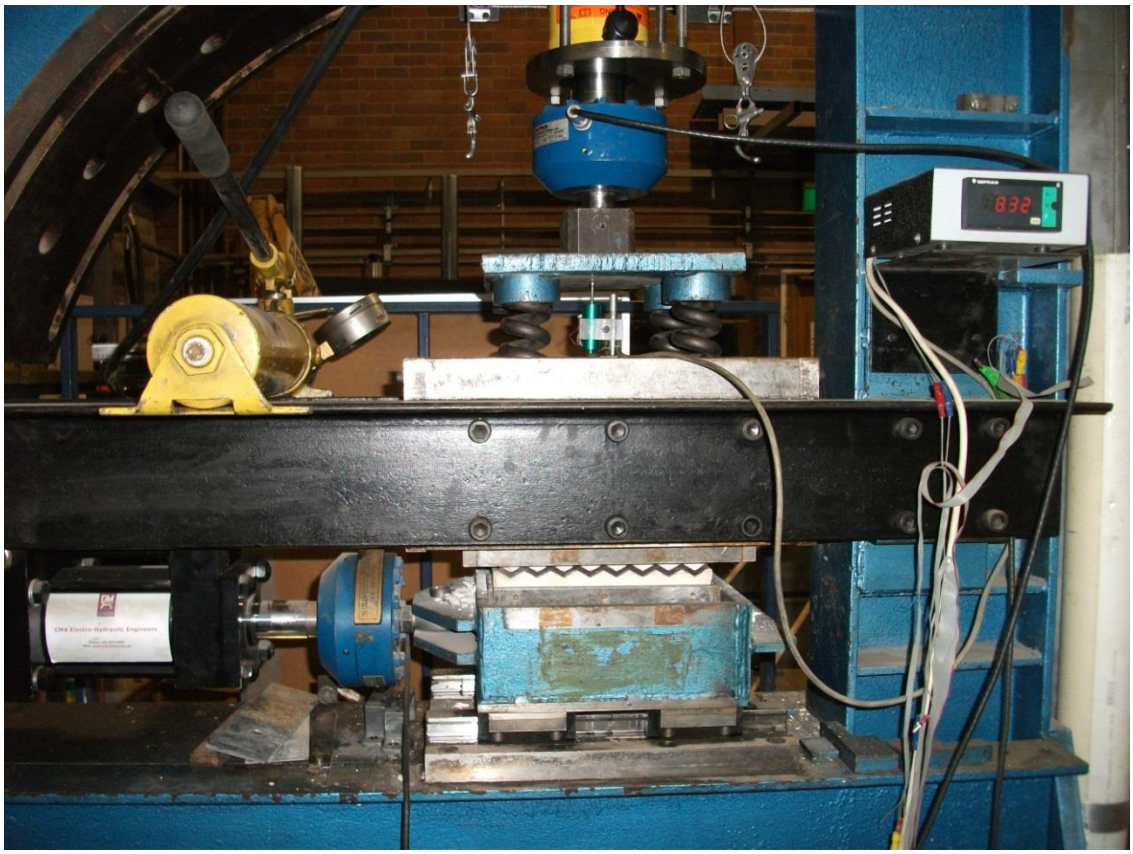

Figure 5.1 Direct shear testing apparatus

The upper box was fixed in the lateral direction while the lower shear box was loaded and allowed to move in the horizontal direction only. The top box was loaded in the vertical direction via the group of four springs to simulate the normal load and stiffness of the surrounding rock (Constant normal stiffness condition). The initial normal load to the TSL surface was applied with a hydraulic jack via the springs located above the upper box. The applied load was measured using a calibrated load cell. The lateral shear load was then applied to the lower box by a transverse hydraulic jack driven by the computerised strain-control unit. During testing, all loads and displacements were monitored by a computer system. The maximum normal and shear load capacity were 180 kN and 120 kN, respectively. The rate of applied shear displacement allowed by the system ranged from 0.35 to 1.7 mm/min.

5.2.2 Sample preparation

The top and bottom moulds were removed from the shear apparatus to cast the samples. High strength gypsum plaster ($CaSO_4.H_2O$, hemihydrate), mixed with water at the ratio of 3.5: 1 by weight, was used to make the artificial joints. Three types of 8 triangular asperities with an angle of 9.5˚ (Type I), 18.5˚ (Type II), and 26.5˚ (Type III) were cast on the gypsum plaster surfaces illustrated in Figure 5.2.

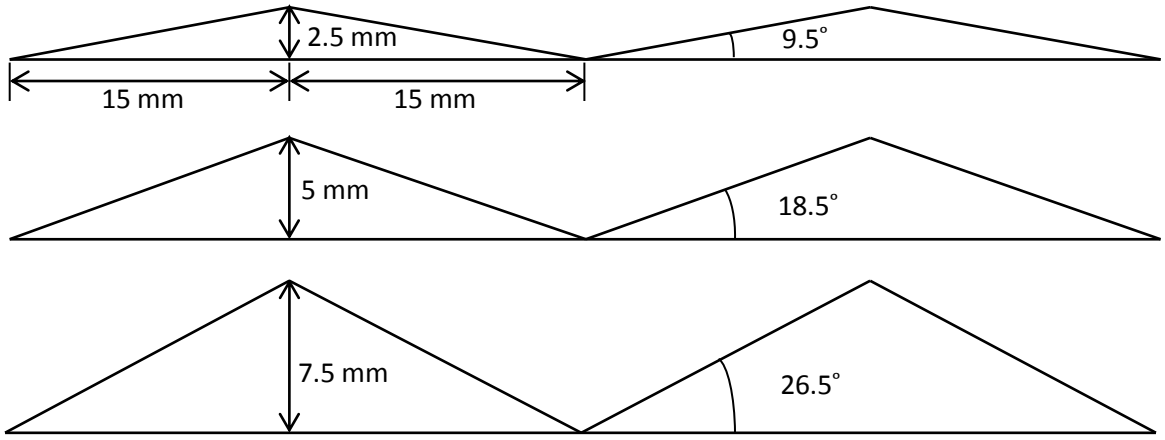

Figure 5.2 Interface profiles of Type I, II and III joints

Although triangular asperities may not represent the true roughness of the in-situ rock conditions, they can provide a simplified basis for evaluating the effect of roughness on the shear behaviour of TSL infilled rock joints. The plaster mixture was poured into the lightly greased lower mould and the asperity profile was formed using the Perspex mould located at the bottom of the box. Care was taken to mix the plaster slowly not to entrap the air bubbles within. After an hour of curing at room temperature the plaster was removed, inverted and placed back into the box on top of three steel plates for the asperities to protrude outside the mould. When casting the top specimen, the sides of

the steel box were extended, lightly greased and the plaster poured on top of the plaster asperities to form a matching specimen. To ensure separation of the two fully mated specimens, a thin plastic film was placed between the two moulds. The whole assembly was left for another hour to cure at room temperature before removing the moulds. The specimens were then placed in an oven at 50 ˚C for 2 weeks to cure. The mean uniaxial compressive stress (σ_c) and Young's modulus (E) of the cured plaster samples were approximately 60 MPa and 16 GPa, respectively (Mirzaghorbanali *et al.*, 2014a, 2014b). The average angle of friction ($\boldsymbol{\phi}_b$) for the plain interfaces without any asperities of the cured plaster sample was measured to be approximately 35˚ (Mirzaghorbanali *et al.,* 2014a, 2014b).

The key procedure in the process of bonding the plaster samples together is to fill the TSL material into the joints. The top and bottom plaster specimens were laid on their sides leaving a gap between them to accommodate the TSL. To prevent leakage, two lightly greased glass plates were used to block two ends at each side. The TSL components were mixed according to the research chemist's recommended ratios and injected into the gap using an industrial type syringe. The TSL was left to cure for approximately 5 hours at room temperature and then the sample was placed into an oven at 50 ˚C for 2 weeks to complete the cure. Figure 5.3 shows the sample preparation for pouring the TSL material.

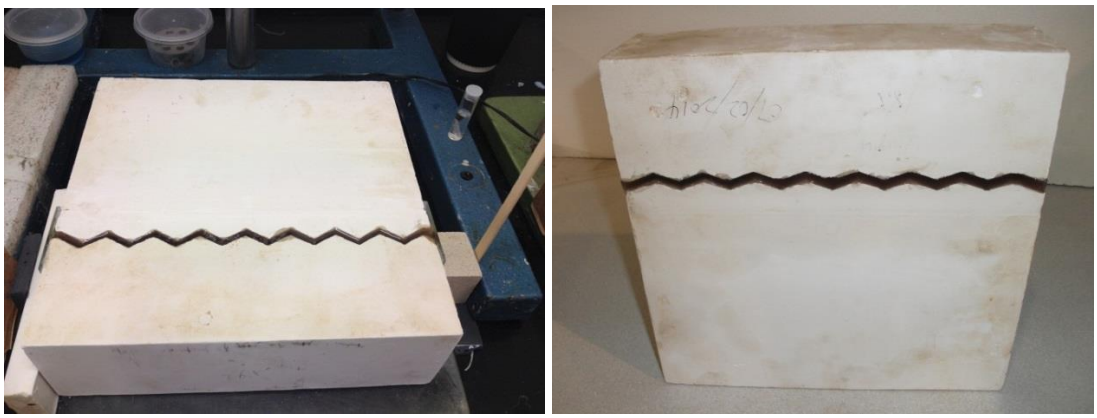

Figure 5.3 Pouring of the TSL material to bond two plaster samples

5.2.3 Test conditions

To study the influence of normal stress on the shearing strength, nine tests were tested at a shearing rate of 0.5 mm/min and the normal load of 0.13 MPa, 0.55 MPa and 1.05 MPa respectively while keeping the asperity height to TSL thickness at the ratio equal to 1. Saiang et al (2005) stated that, when used with rock bolts, the normal load on shotcrete lining seldom exceeds 0.5 MPa. Higher loads (>1 MPa) rarely exist at the shotcrete-rock interface, while they used the normal stress from 0.04 to 1.57 MPa to simulate practical cases. The normal loads of 0.13 MPa, 0.55 MPa and 1.05 MPa were selected to conduct the tests in this study.

To investigate the effect of TSL infill thickness on shear strength, three tests were performed with TSL thickness of 2.5 mm, 5 mm and 7.5 mm, keeping the shearing rate at 0.5 mm/min and using type II asperities. To investigate the effect of shearing rate on the shear stress, three different shear speeds were adopted, 0.5 mm/min, 1 mm/min and 1.5 mm/min respectively with the 5 mm thick TSL and the asperity type II.

5.3 Experimental results

It was observed from Figure 5.4 that the shear failure did not occur between the TSL and the plaster material. Instead the shear failure propagated through the plaster in a similar manner to failure that typically occurs in an intact rock. This indicates that the bond strength between the TSL and the plaster is higher than the shear strength of the plaster material.

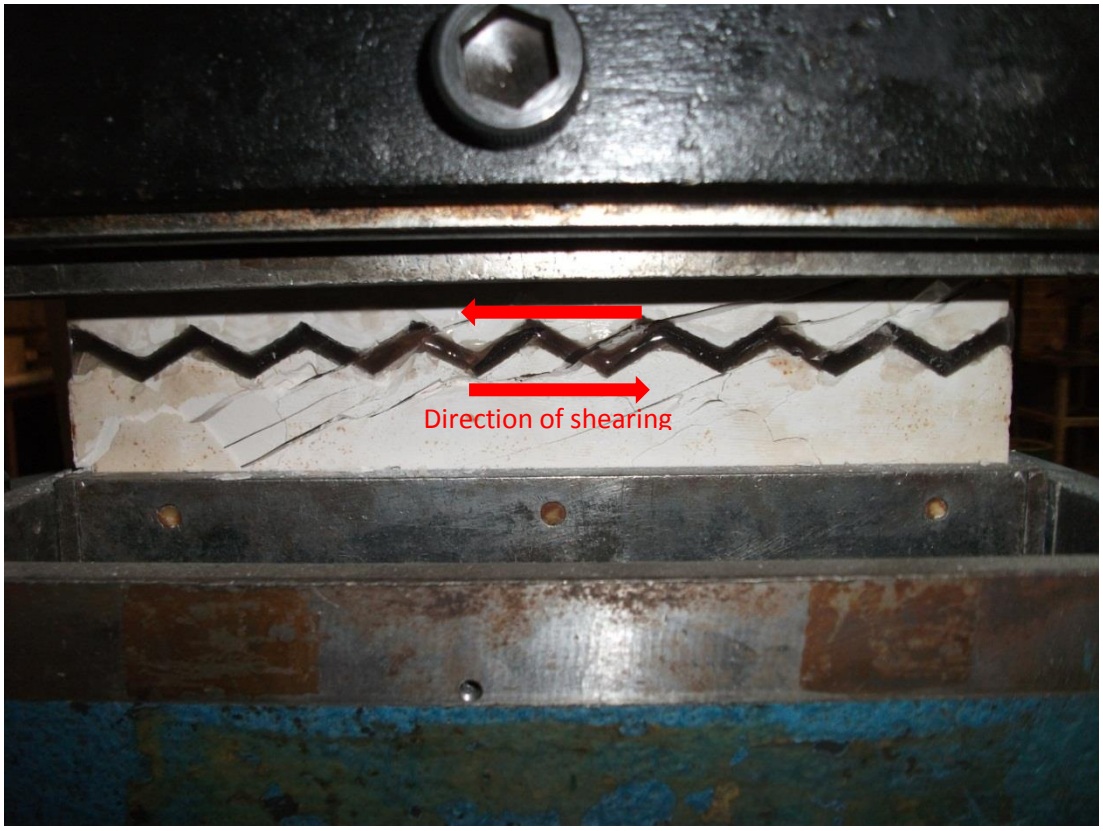

Figure 5.4 Typical shear failure mode of high strength plaster and polymeric TSL composite

5.3.1 Testing of TSL infilled Type I, II and III Joints

The three types of joints with asperity angles of 9.5˚, 18.5˚ and 26.5˚ were tested in shear. The tests were carried out under the three applied normal loads of 0.13 MPa, 0.55 MPa and 1.05 MPa. The TSL infill thickness for type I, II and III joints were 2.5

mm, 5 mm and 7.5 mm respectively with the asperity heights of 2.5 mm, 5 mm and 7.5 mm. The measured Young's modulus of the TSL material and the high strength plaster were 9 GPa and 16 GPa respectively. In all infilled joints the ratio of TSL thickness to asperity height was equal to 1. The graph of shear stress versus the horizontal displacement for the Type I, II and III joints are presented in Figures 5.5. The tested normal stress versus the shear strength for all joint types is summarised in Figure 5.6.

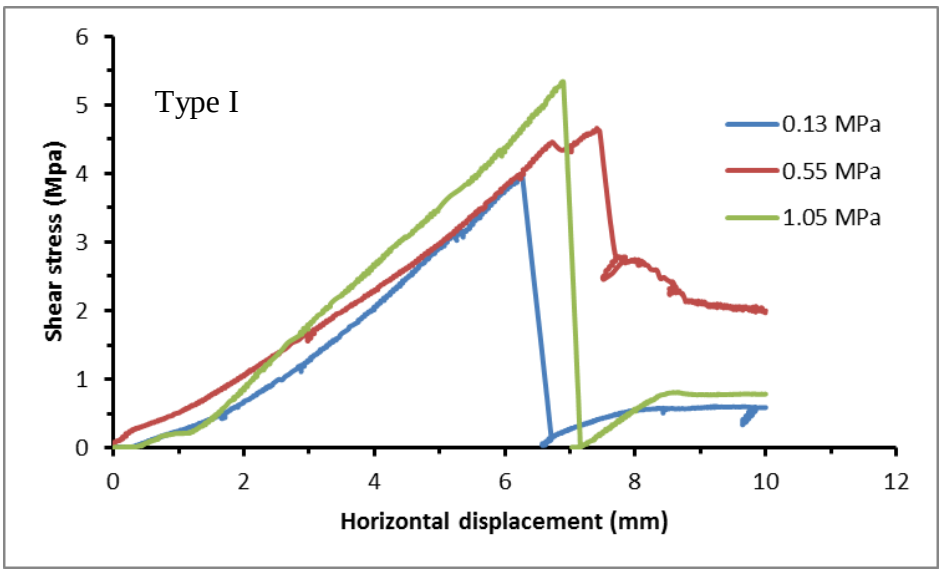

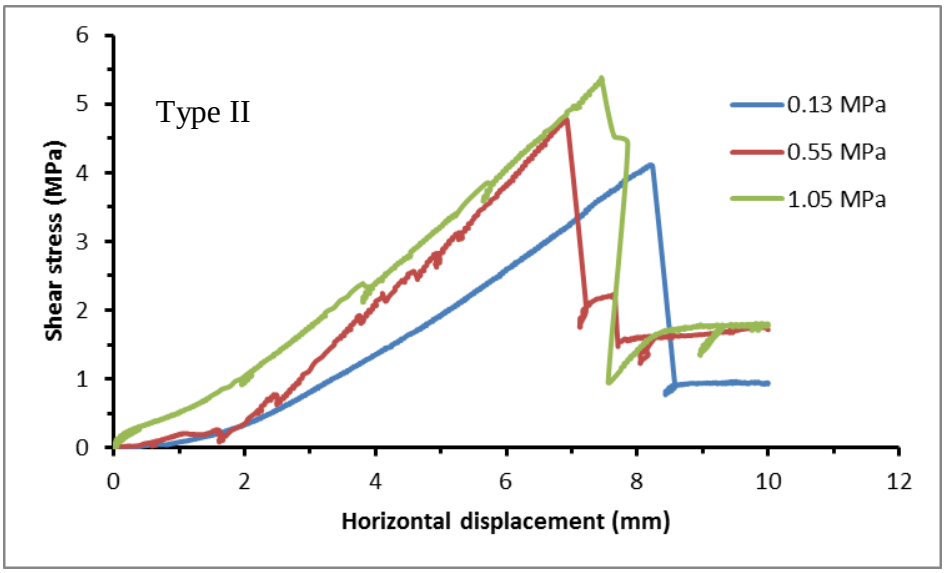

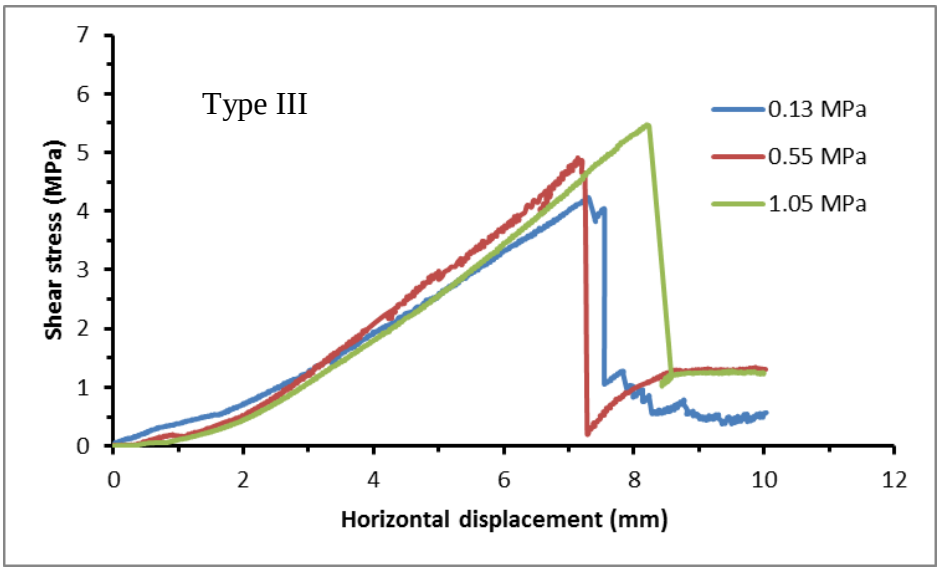

Figure 5. 5 Shear stress vs horizontal displacement for type I, II and III joints

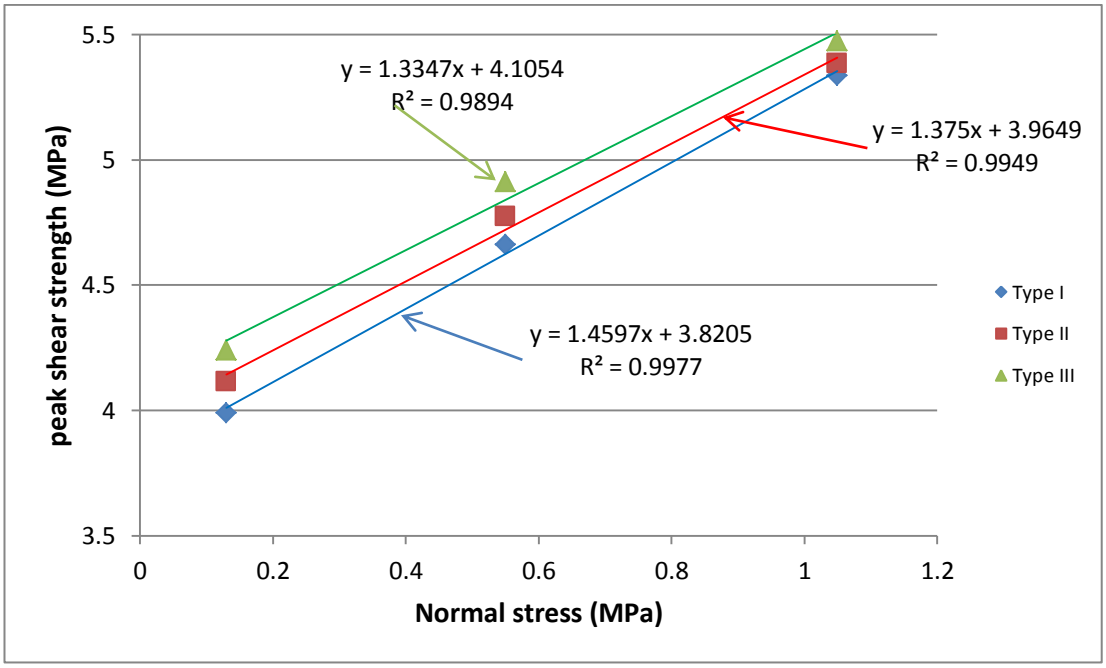

Figure 5.6 Shear peak strength vs normal stress for all joint types

The data shown in Figure 5.5 indicate that the shear load reduced suddenly after reaching the peak shear strength. This matches the observations during testing as the abrupt brittle failure propagated through both the plaster and TSL materials. After the fracture formation, the friction along the fractures played the main role. It is found

from both Figures 5.5 and 5.6 that as expected, the shear strength increased with the increase of the applied normal stress. Good correlation coefficient of the linear trend lines was indicative of the homogeneous plaster properties. The good correlation of data shown in Figure 5.5 enables extrapolation of the shear strength for different joint types and normal loads. For example, extrapolation of peak shear strength is approximately 3.8 MPa under zero normal load for type I joint. Similarly, under zero normal load for type II and III the shear strength of 3.9 MPa and 4.1 MPa can be obtained. These values are the approximate cohesion value of the composite material tested which are almost the same as the cohesion in pure plaster (Shan *et al.* 2014b). This is not surprising as the shear fractures formed primarily in the plaster. Calculations from the data shown in Figure 5.6 indicate that the angles of internal friction ($\boldsymbol{\phi}_b$) in the TSL-plaster composite are 55˚, 54˚ and 53˚ for the type I, II and III respectively. Previous measurements (Shan *et al.* 2014b) indicate that the angle of friction in the pure plaster is approximately 43˚. Therefore the measured internal angles of friction ($\boldsymbol{\phi}_b$) for the composite are significantly higher than the angle of internal friction in the pure plaster. In terms of the internal angle of friction the TSL material therefore appears to increase the strength of plaster. Some typical samples after failure are shown in Figure 5.7. For clean joints without the TSL infill the sample behaviour would probably be quite different with shear propagating through the asperities as they represent the plane of weakness.

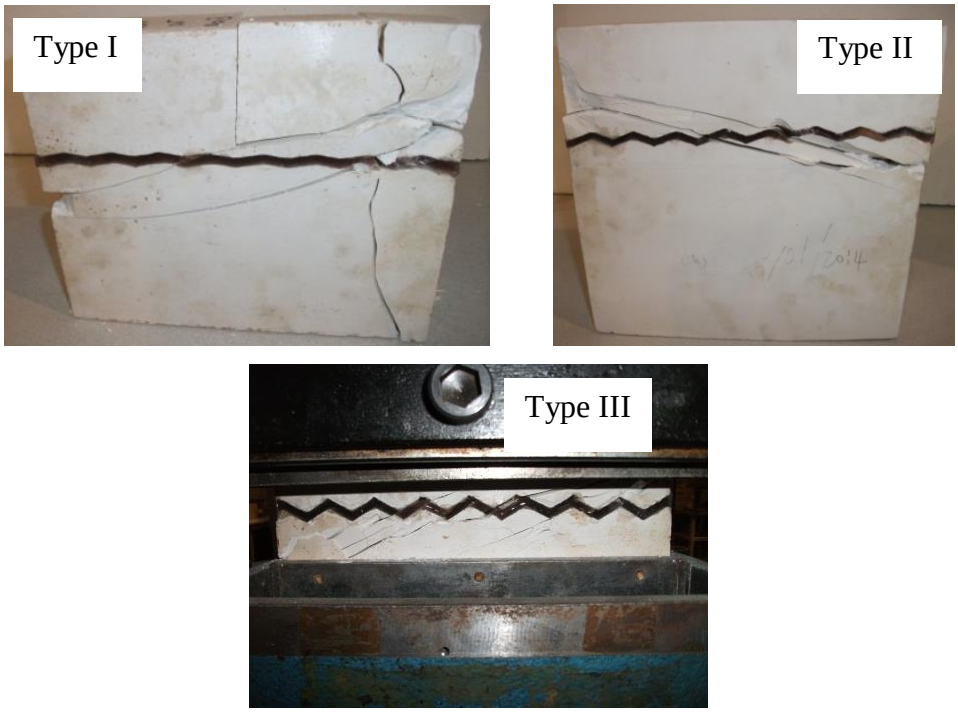

Figure 5.7 Typical samples after failure for the tested joints

5.3.2 Effect of infill thickness on shear strength

Three different rations of infill thickness to asperity height (t/a = 0.5, 1.0 and 1.5) were tested while the other conditions remained the same. To minimise the number of samples used, the type of joints used to conduct these tests was the type II joint with the inclination angle of 18.5˚. Three tests were carried out under the normal stress of 0.55 MPa with the shear rate of 0.5 mm/min. The graph of shear stress versus horizontal displacement with different infill thickness to asperity height ratios is plotted in Figure 5.8. The infill thickness to asperity height ratio versus the shear stress is shown in Figure 5.9.

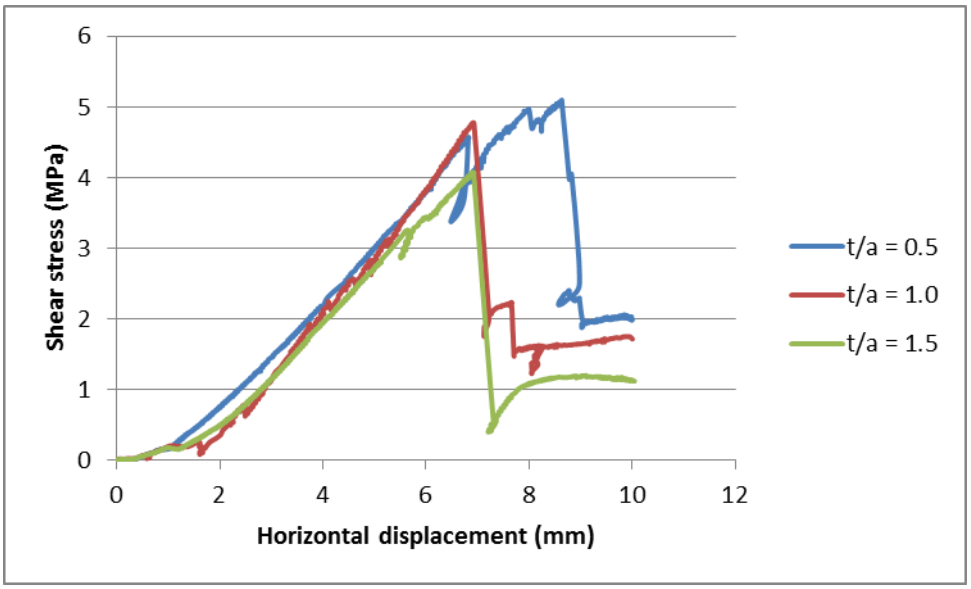

Figure 5.8 Shear stress vs horizontal displacement with different infill thickness to asperity height ratios

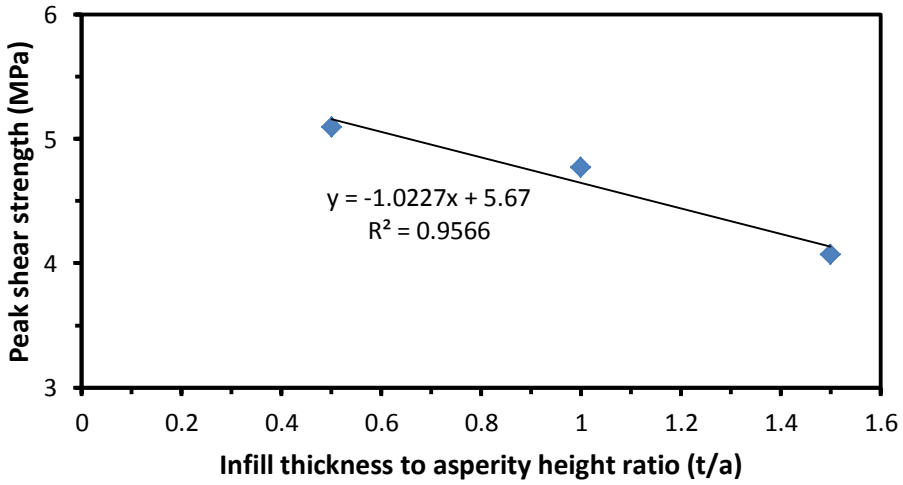

Figure 5.9 Peak shear strength vs infill thickness to asperity height ratio

It is observed from both Figures 5.8 and 5.9 that the peak shear stress decreased with the increase of the infill thickness to asperity height ratio. The linear relationship between the infill thickness to asperity height ratio and peak shear stress was obtained as shown in Figure 5.10 with the linear correlation coefficient of 0.96. Because the data indicate that the relationship may be linear, the peak shear strength can be

extrapolated to different infill thickness to asperity height ratios. Close visual examination of the broken surface (Figure 5.10) revealed that the TSL and plaster sample did not debond or fail along the interface or within the TSL material. Instead, the sample failed like an intact rock. The tests indicate that the TSL material bonded well to the plaster samples, with bond strength greater than the cohesion of the plaster.

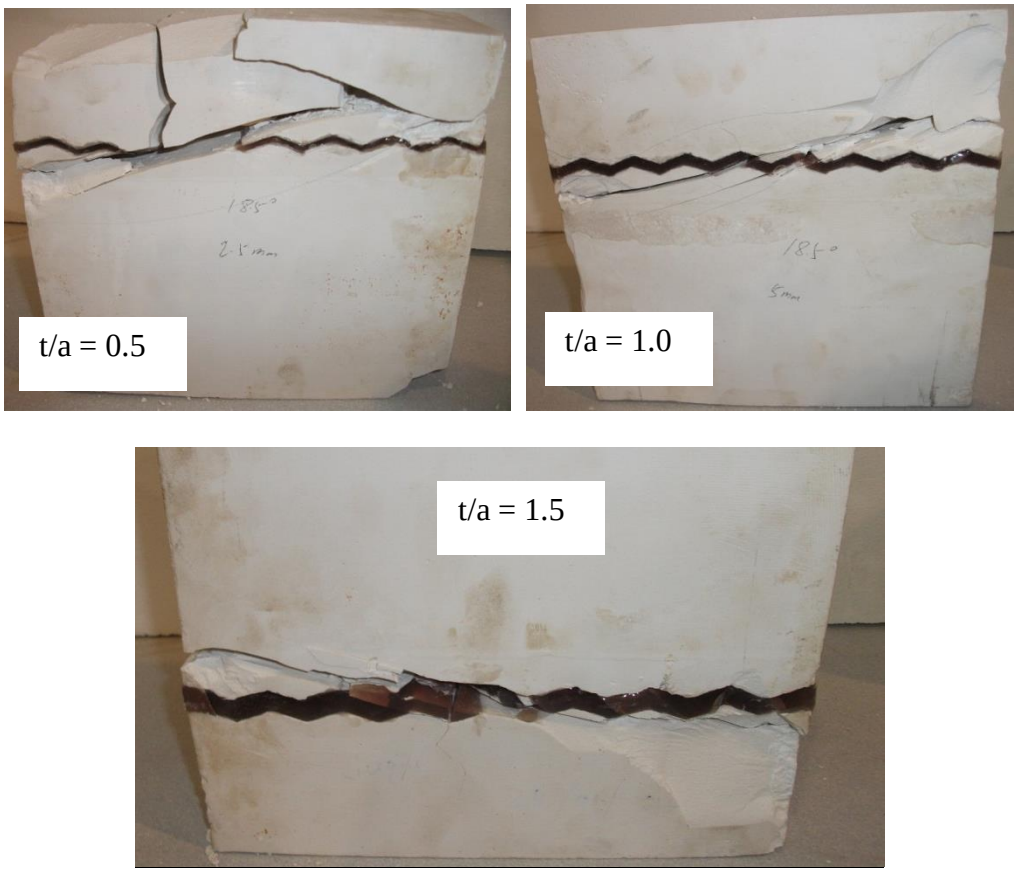

Figure 5.10 Samples with different infill thickness to asperity height ratios after failure

5.3.3 Effect of shear rate on shear strength

This study was aimed to investigate whether the increase in shearing rate may change the bonding characteristics of the polymer infill surface. Three different shear rates (0.5 mm/min, 1.0 mm/min, and 1.5 mm/min) were used. The only variable was the shear rate, while the other conditions were kept the same. To minimise the number of

samples used, the joint type II with the inclination angle of 18.5˚ was used. Three tests were carried out under the normal stress of 0.55 MPa. The shear stress versus horizontal displacement for different shear rates is plotted in Figure 5.11 while the peak strength for each case is plotted in Figure 5.12. The linear trend for shear strength was obtained as shown in Figure 5.12 however, from previous studies (Mirzaghorbanali *et al.* 2014b) the non-linear relationship was obtained for the shear strength when using a very wide range of shear rate application. Experiments by (Mirzaghorbanali *et al.* 2014b) used displacement rates from 0.5 mm per minute up to 20 mm per second and were aimed to simulate the seismic loading events. Slower rates of shear displacements reported here may be more appropriate for the failure of sedimentary strata at slow loading rates. For that reason, a linear trend within the small range of loading rates may be sufficient to depict the effect of shear rate application.

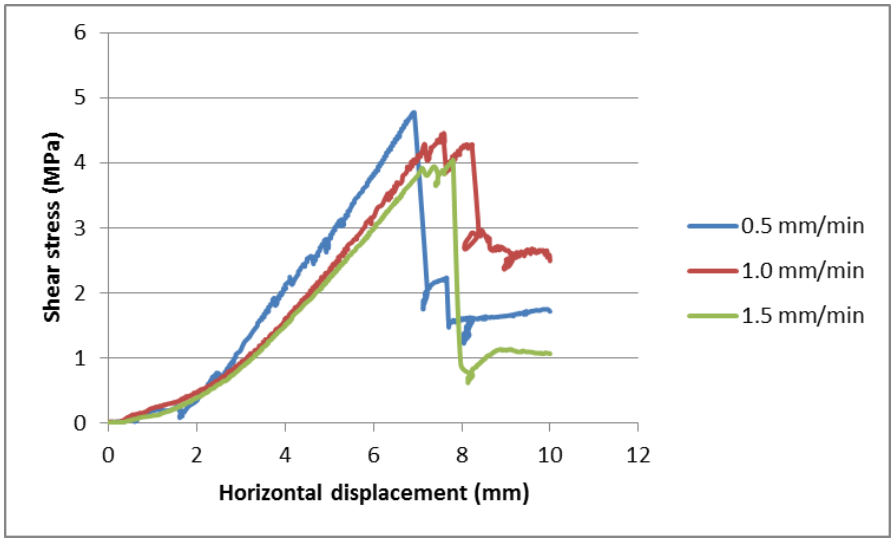

Figure 5.11 Shear stress vs horizontal displacement with different shear rates

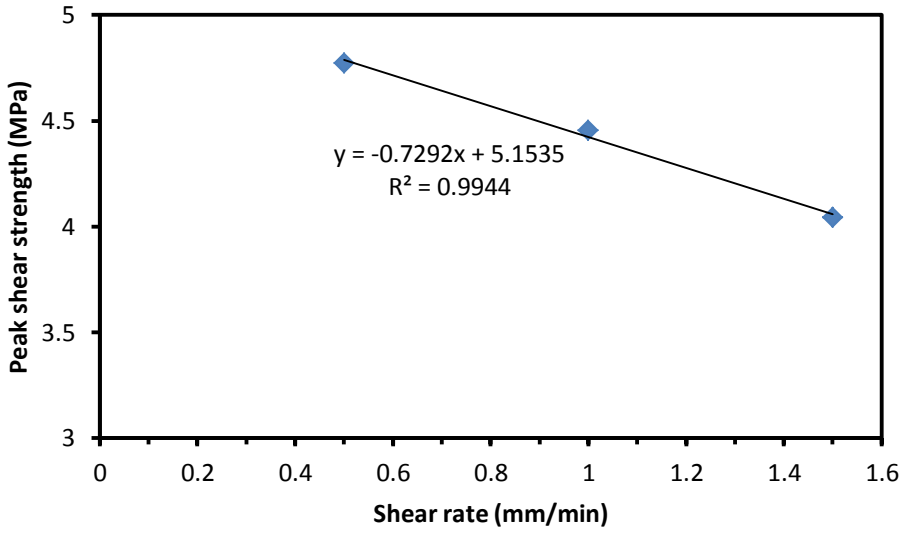

Figure 5.12 Peak shear stress vs shear rate graph

Close visual examination of the broken surfaces (Figure 5.13) revealed that the TSL-plaster interface did not debond but failure propagated through the plaster material. As in the previous tests the TSL material bonded well to the plaster samples, with bond strength greater than the cohesion of the plaster. From both Figures 5.11 and 5.12 it is observed that the peak shear stress in plaster decreased with the increase of shear rates. The relationship between the shear rate and peak shear stress was obtained as shown in Figure 5.12 with the relevant linear correlation coefficient of 0.99. The linear relationship obtained may be used to extrapolate the peak shear stress for different shear rates however, as previously mentioned, the typical strata shearing rates in Australian coal mines are relatively low. Therefore the failure may not occur along the infilled TSL-rock interfaces that are subjected to a similar normal stress used in the experiments.

Figure 5.13 Typical failure through the tested sample

5.3.4 Effect of roughness on shear strength of infilled joints

To study the influence of TSL-plaster interface roughness on shear strength, three types of joints with different roughness subjected to normal stress were tested. The test results are summarized in Figure 5.14 shown below.

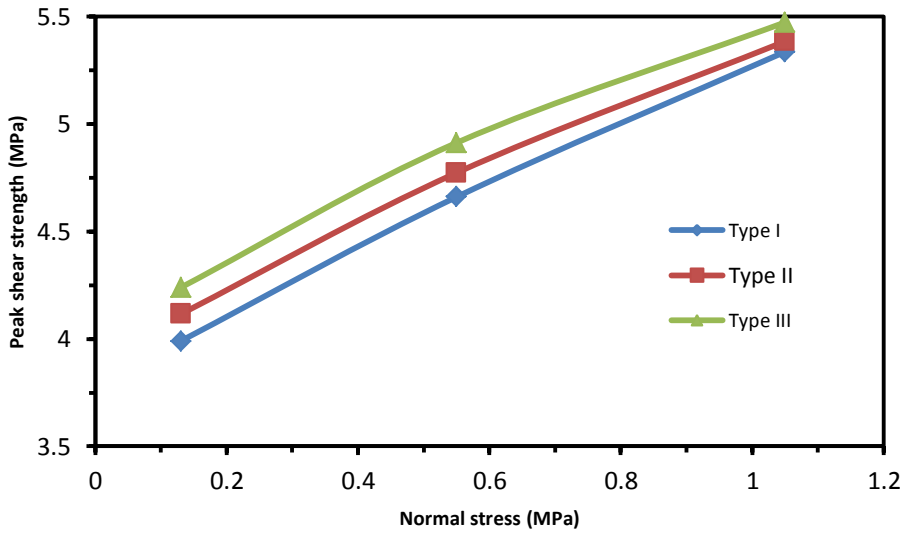

Figure 5.14 Comparison of different roughness on shear stress

The tests showed that as in previous cases the TSL-plaster interface did not debond but failure propagated through the plaster material as shown in Figure 5.7. The data indicate that despite the failure within the plaster, the angle of the TSL infilled

asperities affect the behaviour of the samples. From Figure 5.14 it is clear that the slight increase of peak shear strength occurred with the increase of the asperity inclination angle. It can be seen that the shear stress increment due to joint roughness under high normal stress (1.05 MPa) was larger than the increments under the low normal stress (0.13 MPa and 0.55 MPa) however, the differences were quite small. It can be concluded that if the failure does not occur along the TSL interface, the roughness represented by the asperity angle provide only minor increase in shear resistance. Overall, the tests indicate that the rough surfaces are more desirable than the smooth surfaces. As expected, the normal stress had a significant influence on the shear strength.

5.4 Summary

Test results presented in this study reveal that the shear strength of the polymeric TSL-plaster composite increased with the applied normal stress for the three asperity types. In addition, the shear strength decreased with the increase of the TSL infill thickness to asperity height ratio. The investigation also shows that the increase in shear rate decreased the shear strength but that may not be an issue in Australian underground coal mines with predominantly low shear displacement rates. When subject to high normal loads the joint roughness had little effect on the shear stress while for lower confinement the difference in roughness provided slightly higher shear strength of the TSL-plaster composite.

For all tested samples the shear failure did not occur between the TSL and the plaster material. Instead the shear failure propagated through the plaster in a similar manner to failure that typically occurs in an intact rock. This indicates that the bond strength

between the TSL and the plaster is higher than the shear strength of the high strength plaster material. The tests also indicate that the TSL-plaster bond is very high. The high strength plaster material is in many respects similar to homogeneous rock and much simpler to use for experimental purposes. Future studies using rock material should be undertaken to confirm the results presented here. In addition, the TSL material used in this study is under development at the University of Wollongong and it is probable that the bond characteristics may improve in time as new polymeric formulations are developed. Therefore it is essential that rock of very high strength is used to determine the actual bonding characteristics of the TSL material to the rock surface. Nevertheless this study has measured shear strength of the TSL-plaster composite subject to changes in joint properties. Understanding of joint reinforcement is essential in future studies of the TSL material reinforcing the fractures within the rock skin.

CHAPTER 6 LABORATORY INVESTIGATION ON SUPPORT MECHANISM OF THIN SPRAY-ON LINER FOR PILLAR REINFORCEMENT

6.1 Introduction

In the process of mining extraction, coal pillars are designed and used to support overburden strata and maintain stability of the roadways. It has been commonly accepted that pillar failure starts from the rib sides especially at the pillar corners, and will gradually propagate towards the pillar core. The confining stress in the pillar increases with the distance from the pillar edge towards the pillar centre. Normally there is no lateral stress confining the rib surface. When the load applied on the pillar exceeds the compressive strength of the rib, failure starts to propagate towards the pillar core. Currently, steel mesh is used to reinforce the coal pillar ribs. However, steel mesh cannot provide confinement to the pillar until large displacements occur. TSL materials are now being introduced to reinforce the ribs. If the TSL bonds to coal, it forms a strong composite layer on the rib surface. Together with rock bolts this layer can provide confining stress to the pillar surface that will reduce the yielded rib zone thereby improving the rib conditions and minimise roadway spans. This is beneficial especially at the pillar corners where deep seated failure often occurs. Minimising failure of the pillar corners may significantly improve stability of the roadway intersections.

Research on the failure mechanism of TSL coated rock sample is limited. A review of the support mechanisms provided by the TSL membrane was presented by Stacey

(2001). Kuijpers (2004) studied the confining effect of a TSL to reinforce the rock pillar. He found that a thin liner changed the post failure behaviour of pillar by providing confinement to the rock surface. However, the procedures of sample preparation and testing were not described in his study. Archibald (2004) conducted laboratory trials to substantiate the concept that TSL can improve the structural performance of rock materials when applied onto cylindrical rock core samples in a similar manner to a pillar wrap. Lau et al. (2008) conducted compression tests of the cylindrical samples using one rock type separately coated with two types of TSL material. However, the details of sample preparation, mechanical properties of rock, TSL material and loading rate, were not given and the testing results were variable and inconclusive.

To evaluate the strength of the cylindrical rock samples coated with the polymer membrane, several tests were conducted using various rock types in this study. The size of tested samples may not represent the large scale behaviour experienced underground however, the support mechanism of TSL coated materials are to some degree similar in coating small pillars. The results were used to provide a basis for studying the effect of TSL confinement to the rock or coal pillar.

In this study, a polymeric TSL material developed at the University of Wollongong was used to coat three types of rock, siltstone, sandstone and granite. The sample preparation, mechanical properties of rock, TSL properties and the loading rate are described in detail and the testing procedure is presented here. The failure mechanism of TSL coated rock samples was analysed and the comparison between rock samples with and without TSL material reinforcement were made.

6.2 Description of sample preparation, apparatus and testing procedures

In this study, three types of rock, siltstone, sandstone and granite were used to conduct the tests. The mechanical properties of these specific rocks were tested in the laboratory and are presented in Table 6.1.

Table 6.1 Mechanical properties of rock used for testing

Rock Type	Uniaxial Compressive Strength (MPa)	Tensile Strength (MPa)	Young's Modulus (GPa)	Friction Angle (^{0})	Poisson Ratio	Cohesion (MPa)
Siltstone	26.22	2.87	9.27	33	0.24	2.60
Sandstone	41.58	3.92	11.08	35	0.25	3.27
Granite	73.56	6.39	17.06	38	0.28	5.67

The rock samples diameter and length was 54 mm and 110 mm respectively as shown in Figure 6.1a. All the rock samples were cored and prepared for testing using the ASTM D7012-10 (2010) procedures. Rock samples were coated with the 5 mm thick unreinforced polymeric layer (representing TSL) using a specially made mould arrangement. The outer and inner diameters of the mould were 70 mm and 64 mm respectively. The length of the mould was 110 mm to accommodate the rock samples as illustrated in Figure 6.1b.

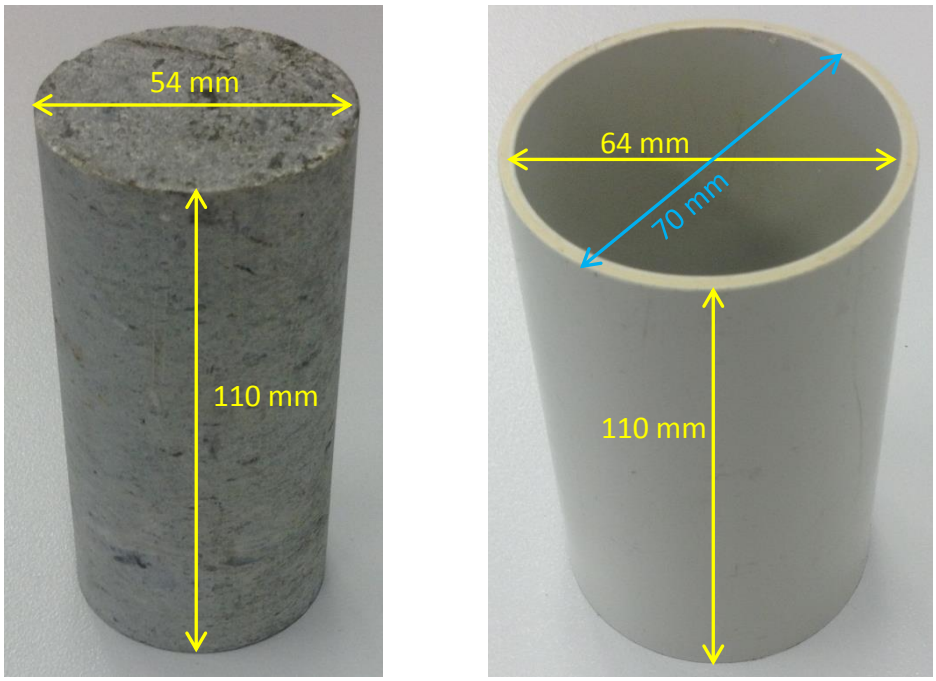

(a) (b)

Figure 6.1 Dimensions of rock sample (a), mould for TSL coating preparation (b)

6.2.1 Sample preparation

The plastic mould and rock samples were cleaned using acetone. A thin film of vaseline was used to grease the moulds for easy removal of the cured samples. The rock samples were placed on the bench as shown in Figure 6.2a, and then the plastic mould was positioned centrally around the rock sample as presented in Figure 6.2b. Thus there was a 5 mm annular gap between the rock and plastic mould to accommodate the TSL material. The bottom of the plastic mould was sealed using vaseline to prevent leakage. After that, the polymer components were mixed evenly according to the research chemist's recommended ratio using a plastic cup and a wooden spatula. The hardener was added and mixed evenly until the mixture changed its colour. To simplify the TSL pouring procedure, a large syringe was used to inject the TSL material into the space between the rock core and plastic mould as illustrated

in Figure 6.2c. After that, the coated specimen was left to cure for one hour (Figure 6.2d), and the plastic mould was removed. The coated sample (Figure 6.2e) was cured for a further 7 days under laboratory conditions at the temperature of approximately 20 ˚C and humidity of less than 60%. The TSL pour was completed within 10 minutes after the TSL mixing began. Before testing started, both ends of the coated sample were polished to make flat surface as shown in Figure 6.2f, to ensure an even distribution of the load. The tested properties of the TSL material are presented in Table 6.2.

Table 6.2 TSL properties

Material type	Tensile Strength (MPa)	Young's Modulus (GPa)	Poisson's Ratio
Unreinforced polymer	13.9	1.95	0.35

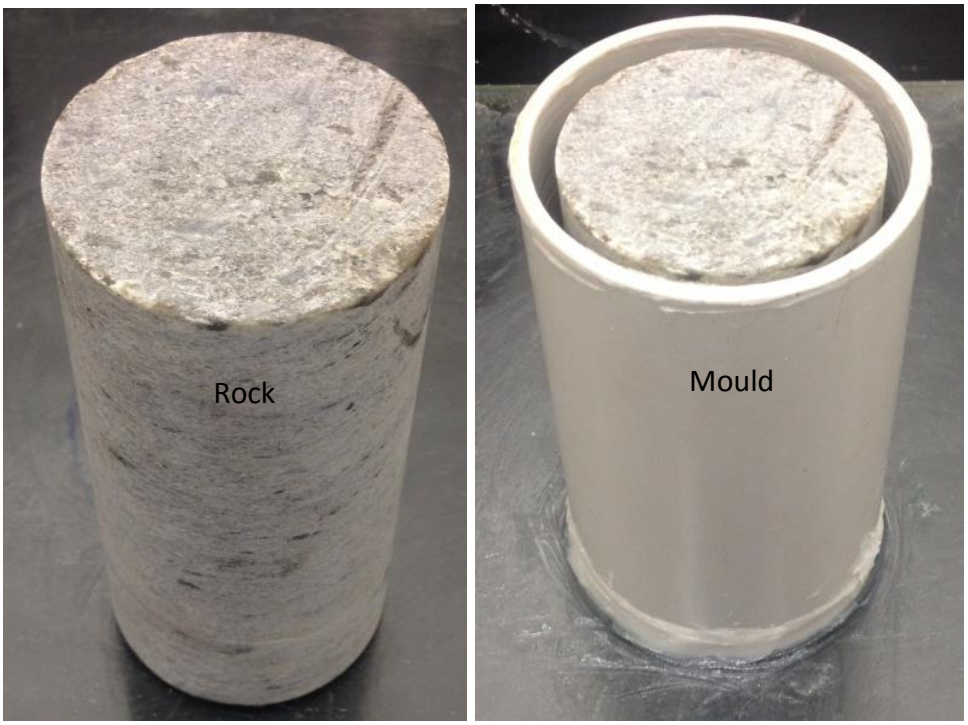

(a) (b)

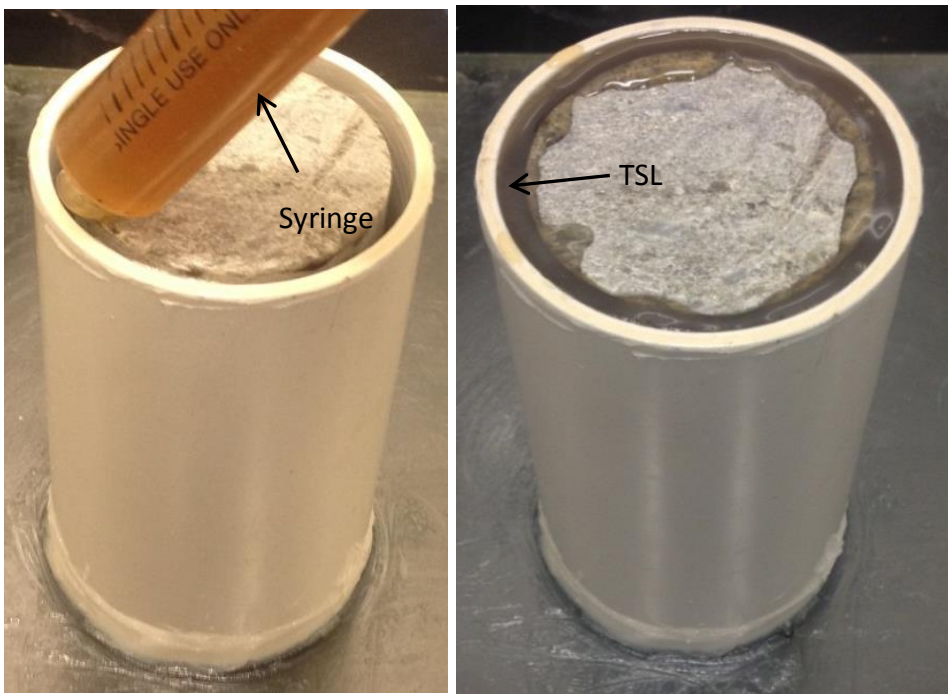

(c) (d)

(e) (f)

Figure 6.2 Steps for sample preparation

6.2.2 Testing apparatus and procedures

The test setup is shown in Figure 6.3. An Instron machine was used to conduct the compressive test. The spherical seat was utilised to ensure evenly distributed load. A steel plate was placed between the sample and the top platen of the Instron machine.

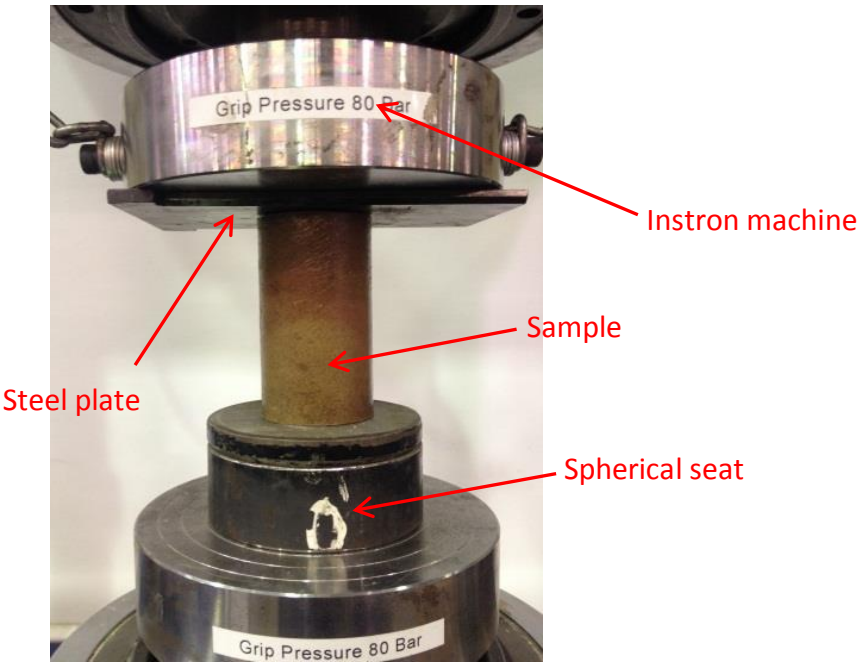

Figure 6.3 Testing setup

The displacement control mode at a rate of 0.5 mm/min was selected to load the samples. At this speed, the tests were completed within approximately two minutes. The loads and displacements were recorded for each test.

The compressive strength can be calculated using Equation (6.1). The strength can be obtained by dividing the force at failure by the contact area.

$$\sigma_c = \frac{F}{A} = \frac{4F}{\pi d^2} \tag{6.1}$$

Where F = the applied force,

σ_c = the compressive strength of the sample,

d = the diameter of the sample,

A = the contact area.

6.3 Results and discussion

The test results indicate that the cylindrical rock samples reinforced with the 5mm thick TSL material are significantly stronger than the unreinforced samples. The summary of compressive tests presented in Figure 6.4 clearly shows this relationship. The details of test results are also summarised in Table 6.3.

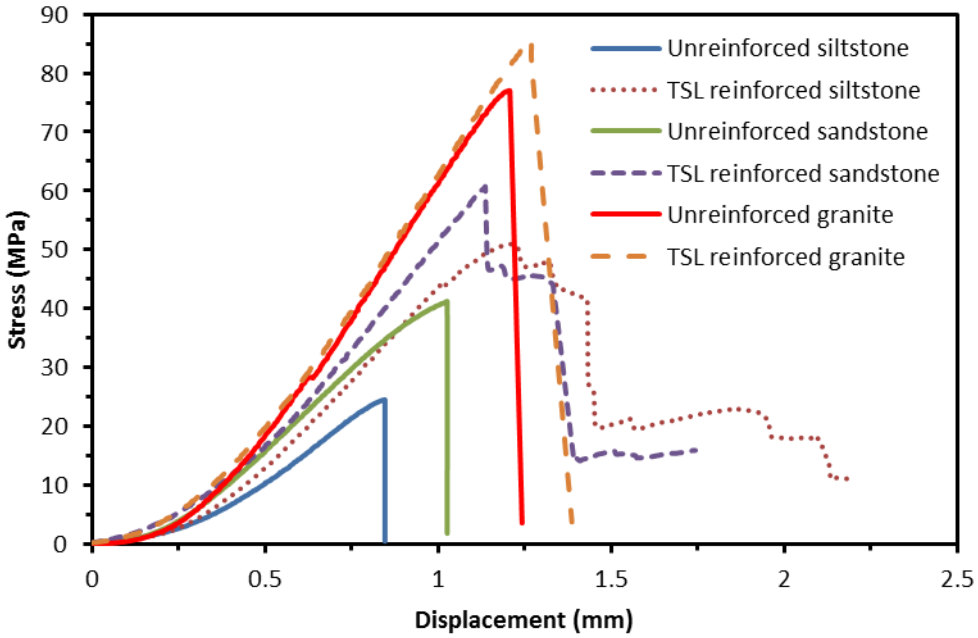

Figure 6.4 Three types of cylindrical rock samples unreinforced and reinforced with TSL material tested to failure

It can be seen that the compressive strength of the rock samples reinforced with TSL are significantly stronger than the samples without TSL. The unreinforced siltstone samples reached their average compressive strength of 26.2 MPa, while the TSL

reinforced samples failed on average at twice the load of 51.9 MPa. The TSL reinforced sandstone samples failed at 61.0 MPa, while the non-reinforced samples failed at 41.6 MPa. The reinforced granite rock samples failed at 85.3 MPa while the unreinforced samples reached failure at 73. 6 MPa. For all unreinforced rock samples, abrupt failure occurred showing no residual strength. In contrast, the reinforced samples showed various degree of post failure strength.

Table 6.3 Summary of compressive test results

Sample Type	Test Number	Compressive strength (MPa)	Mean strength (MPa)	STDEV (MPa)
Siltstone	1	27.43	26.22	1.40
	2	24.68		
	3	26.54		
TSL coated siltstone	1	53.60	51.85	1.77
	2	49.51		
	3	52.74		
	4	51.53		
Sandstone	1	41.22	41.58	2.11
	2	43.85		
	3	39.67		
TSL coated sandstone	1	60.74	60.96	1.98
	2	58.46		
	3	63.25		

	4	61.39		
Granite	1	70.50	73.56	3.26
	2	76.99		
	3	73.20		
TSL coated granite	1	85.27	85.27	1.40
	2	83.56		
	3	85.25		
	4	86.99		

6.3.1 Failure modes

Figure 6.5 shows the failure modes of the three types of rock samples used for testing. All unreinforced rock samples showed a typical shear failure while for the TSL encapsulated rock samples, the failure mode varied with the rock type. The failure modes for the soft rock with and without TSL reinforcement were different. During loading, the TSL reinforced siltstone samples failed before failure occurred within the TSL material. This can be seen in Figure 6.4 showing that after the peak strength was reached, the TSL could still provide confinement to the fractured siltstone sample that retained a significant portion of its post failure strength over a large displacement. The failure mechanism of TSL reinforced sandstone samples was similar to the siltstone failure mode. However, for the TSL reinforced granite, an abrupt failure occurred simultaneously within the granite and TSL material that was similar to the shear failure observed in the unreinforced samples. There was no post failure strength observed. It can be concluded that the TSL reinforcement of soft rock was better than of hard rock.

As can be seen in Figure 6.5, the TSL material failed in tension; therefore, the tensile strength of TSL plays an important role in the failure mechanism of TSL coated rock samples.

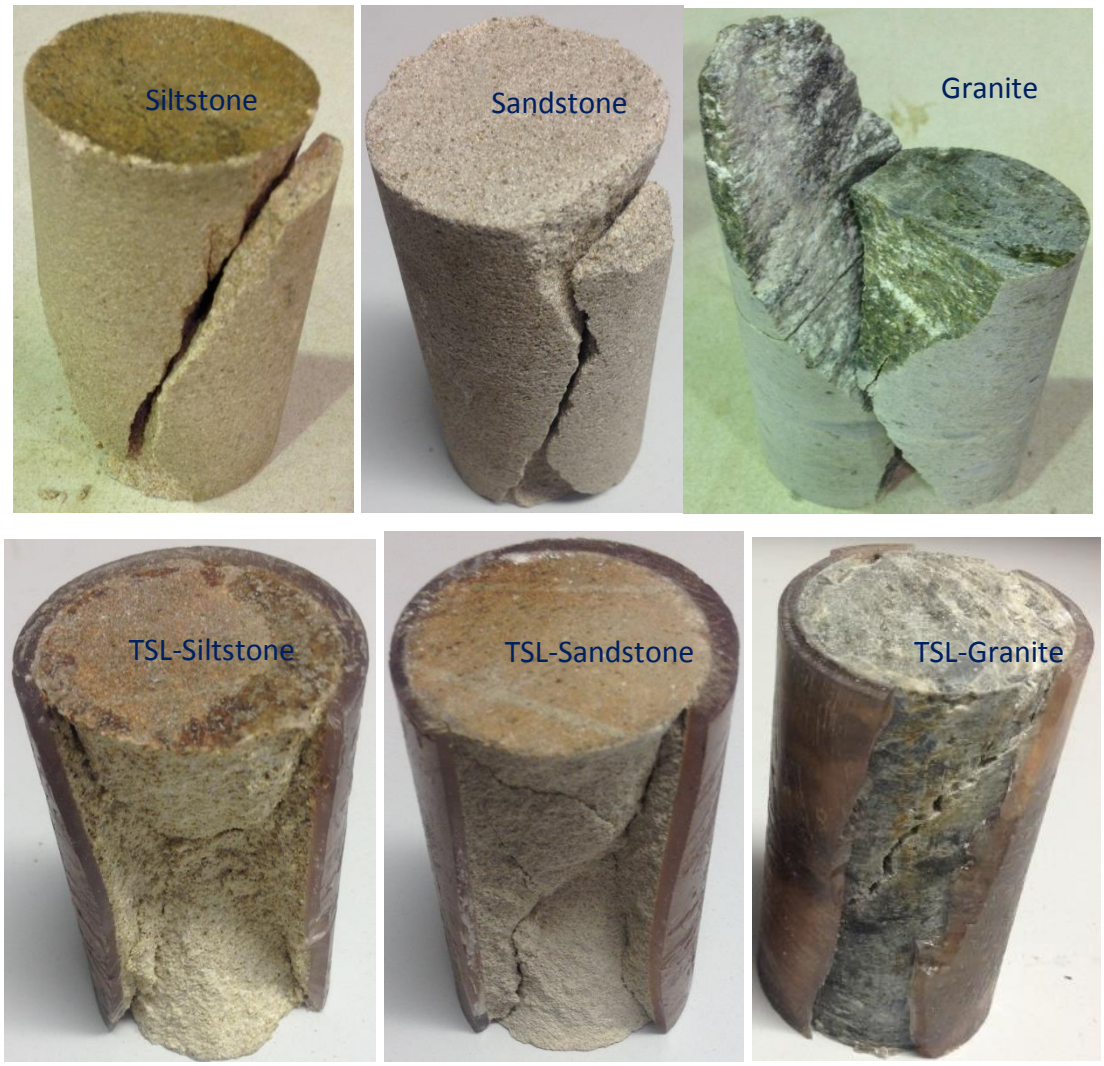

Figure 6.5 Typical failure modes for the three types of rock samples used for testing

6.4 Summary

Three types of weak siltstone, sandstone and granite rock with and without the TSL encapsulation were tested in compression. Results of rock failure tests indicated that significant strength improvement and enhancement of post failure characteristics

developed for the TSL encapsulated samples. It can be concluded that the TSL material can be used to effectively reinforce the modelled rock samples. While the rock has failed predominantly in shear, the TSL material failed in tension due to the lateral expansion of the failed samples. The tests indicate that the effectiveness of the TSL reinforcement varies with the rock type. The TSL reinforcement of the weaker rocks appears to be better than reinforcement of the stronger rocks. It is concluded that the case when the tensile strength of the TSL material is greater than the tensile strength of rock leads to an effective rock reinforcement. In contrast, the TSL reinforcement of stronger rock types may not be as effective. Therefore, the TSL material is more appropriate to reinforce the weaker rock with low compressive and tensile strength. Typically, the sedimentary strata found in underground coal mines are best suited for TSL applications to control the rock surface failure. The size of tested samples may not represent the large scale behaviour experienced underground however the support mechanism of TSL coated materials indicates the TSL benefits.

The TSL bonded to the rock skin forms a strong composite layer together with the fractured rock surface. This composite material provides a strong and effective coating system of fractured rock surface leading to improved conditions in underground excavations. Significant improvements can be expected in roof and rib stability, small pillar strength, stability of pillar corners to minimise roof spans at the roadway intersections and thus improve intersection stability and improve safety in mines.

At the time of writing the tested TSL material was not approved for use in underground mines therefore regrettably no *in situ* tests were performed. It is recommended to resume underground *in situ* tests to verify the laboratory results as soon as the approvals are finalised.

CHAPTER 7 NUMERICAL STUDY ON THE COAL PILLAR ROADWAY CORNER REINFORCED WITH GLASS FIBRE THIN SPRAY ON LINER

7.1 Introduction

In the process of coal mine extraction, the coal pillars are designed to support the overburden strata and maintain the stability of the roadways. It is a fact that wider coal pillars provide better stability of underground roadways however coal resources may be wasted, reducing the coal recovery. Therefore, researchers are looking for a method that can not only recover maximum coal, but also guarantee the support capacity of the pillar. A good pillar design is one of the most important issues in controlling ground stability in underground coal mines. To ensure safe roof conditions at roadway intersections, minimum roadway spans are essential. Despite rib bolting, substantial yield of the coal pillar corners is often experienced resulting in poor roof support above each roadway corner.

TSL bonded to the roof strata and coal pillar surfaces forms a strong composite layer with the substrate that can significantly improve roof and rib stability. The experimental results indicate that this composite layer provides a strong and effective coating system stabilising fractured roof and coal surfaces and leading to a safer working environment in coal mines. The composite layer formed by TSL adhesion is ideal to provide increased rib stability at the roadway corners.

This chapter presents the numerical modelling study using *3DEC* (Itasca 2007) of the coal pillar corners reinforced with TSL material. The roadway pillar corner *3m x 3m x 3m* in size was modelled with and without the TSL reinforcement.

7.2 Description of 3DEC and selected constitutive model

3 Dimensional Distinct Element Code (3DEC) is a three-dimensional numerical program based on the distinct element method for discontinuum modelling. Among many, this software includes a Mohr-Coulomb strain softening model (Itasca 2007) that was chosen for this work. In the strain softening model, rock exhibits a linear elastic behaviour when loaded until the peak strength is reached, followed by a strain softening phase.

The Mohr-Coulomb strain softening constitutive model uses a strain function series that changes with the Mohr-Coulomb model properties (cohesion, friction and dilation) in the phase of plastic deformation. The plastic shear strain is determined by the shear softening parameter e^{ps}, and the following equation is used to calculate the incremental form of the shear softening parameter e^{ps} where:

$$\Delta e^{ps} = \left\{\frac{1}{2}(\Delta e_1^{ps} - \Delta e_m^{ps})^2 + \frac{1}{2}(\Delta e_m^{ps})^2 + \frac{1}{2}(\Delta e_3^{ps} - \Delta e_m^{ps})^2\right\}^{\frac{1}{2}}$$

and

$$\Delta e_m^{ps} = \frac{1}{3}(\Delta e_1^{ps} + \Delta e_3^{ps})$$

Δe_j^{ps} $\quad where\ j = 1,3$ are the principal plastic shear strain increments.

The Mohr-Coulomb strain softening model includes three deformation phases. The initial phase is the elastic deformation phase before the peak strength is reached. The second phase is the strain softening deformation phase where the cohesion and the friction angle can be adjusted to soften the material after the onset of plastic yielding by employing a user-defined piecewise linear function (Itasca 2007). In the standard Mohr-Coulomb model, these properties remain constant. The last phase is the plastic deformation phase.

7.3 Material properties

The mechanical and physical properties of coal are presented in Table 7.1. The strain softening properties of coal are provided in Table 7.2. The mechanical and physical properties of joints are summarized in Table 7.3 and properties of the TSL material used are given in Table 7.4.

Table 7.1 Coal properties

Density (kg/m^3)	1400
Bulk modulus (GPa)	3.6
Shear modulus (GPa)	2.0
Cohesion (MPa)	1.0
Internal friction angle (^{o})	32
Tensile strength (MPa)	0.13

Table 7. 2 Stain softening properties of coal

Plastic Strain	Cohesion (kPa)	Internal Friction Angle (^{o})
0.0000	1000	32

0.0015	800	28
0.0050	600	26
0.0100	0	24
1.0000	0	24

Table 7. 3 Joints properties

Normal stiffness (GPa)	3.6
Shear stiffness (GPa)	2.0
Friction angle (°)	25
Cohesion (MPa)	0
Dilation (°)	5
Tensile strength (MPa)	0

Table 7. 4 TSL properties (Presentation by Nemcik to ACARP 2014)

Normal stiffness (GPa)	10
Shear stiffness (GPa)	3.3
Friction angle (°)	45
Cohesion (MPa)	2
Poisson's ratio	0.35
Young's modulus (GPa)	9
Tensile strength (MPa)	30
Thickness (m)	0.005
Yield strain	>5%
Ultimate strain	>10%

7.4 Model development

The selected geometry of the model was *3 m* in length, *3 m* in width and *3 m* in height. It is commonly known that there are numerous bedding planes and cleats that exist in coal pillars. To simulate this situation, the original model was split into small blocks with joint spacing 0.1 m in length and width, and joint spacing 0.1 m in height.

However, this model was too large exceeding the memory of the system that was available. The only way to fix this problem was to reduce the block zones by increasing the joint spacing. After a few trials, the new model was split into small blocks with joint spacing 0.3 m in length and width, and joint spacing 0.5 m in height. Two models were developed. The first model was not reinforced as shown in Figure 7.1(a) and the second was supported with 5 mm thick glass fibre reinforced TSL material as shown in Figure 7.1(b). The left side ($x=0\ m$) was fixed in the x direction, and the back side ($y=3\ m$) was fixed in the y direction. The top ($z=3\ m$) and bottom ($z=0\ m$) sides were fixed in the x and y directions. The velocity of 1×10^{-5} m/step was applied on both the top and bottom to symmetrically compress the pillar.

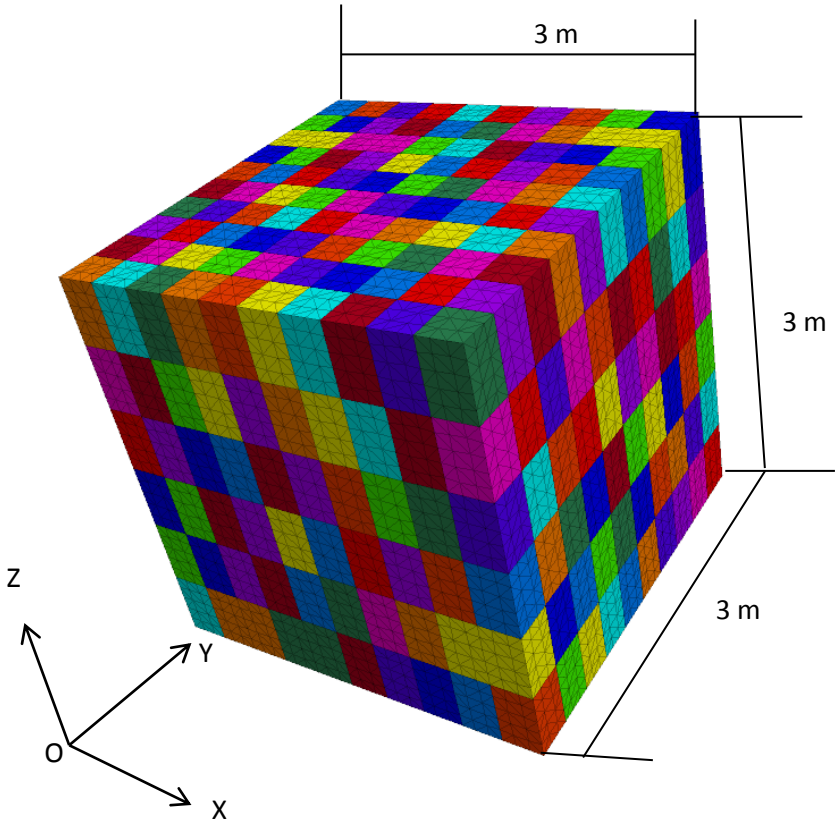

(a)

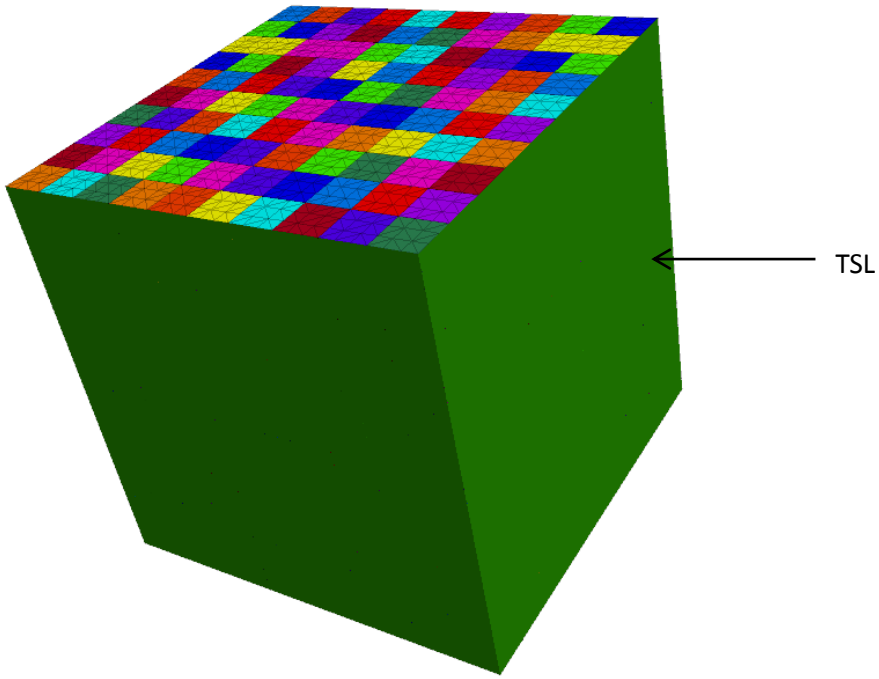

(b)

Figure 7. 1 Models without (a) and with (b) TSL reinforcement

7.5 Results

7.5.1 Displacement component in x the direction

To simulate heavy pillar loads often experienced in the tailgate roadways, the program was stopped and examined when the pillar corner model was compressed by 200 mm. The displacement component contours in the x direction along the cross-section y=1.5 m for models with and without TSL reinforcement were plotted in Figure 7.2. It can be clearly seen that without TSL reinforcement, the maximum displacement in the x direction was approximately 137 mm, while with TSL reinforcement the maximum displacement in the x direction was reduced to approximately 57 mm which was less than half the x displacement of the unreinforced pillar. In addition, the maximum displacement in the x direction slightly increased from the free corner towards the fixed sides, as shown in Figure 7.3.

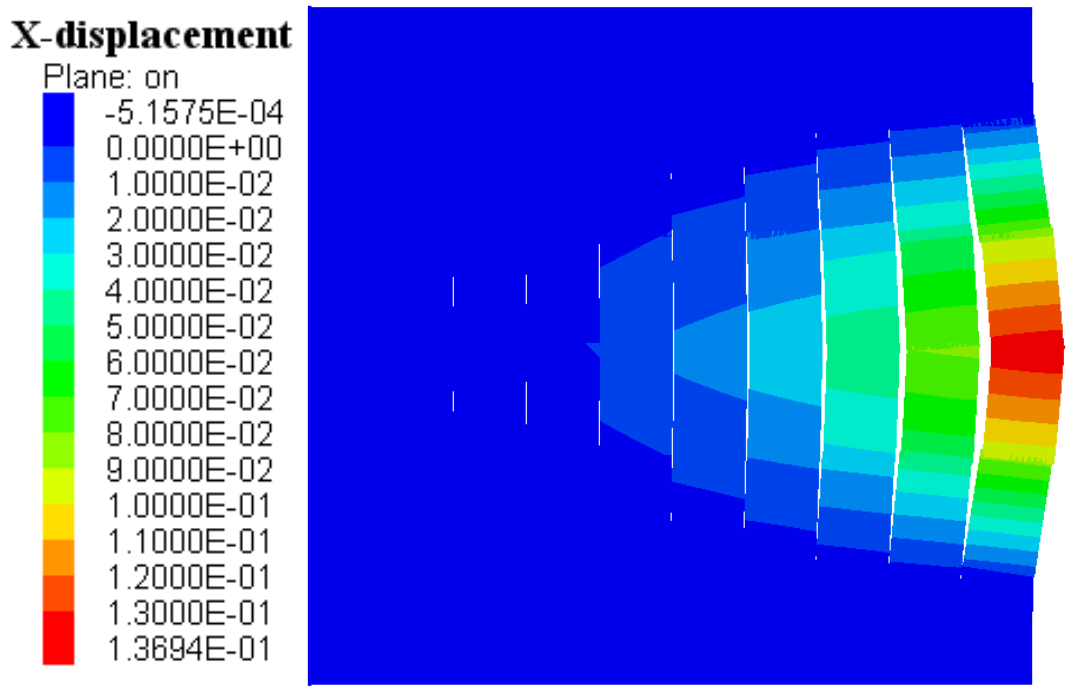

(a) Without TSL

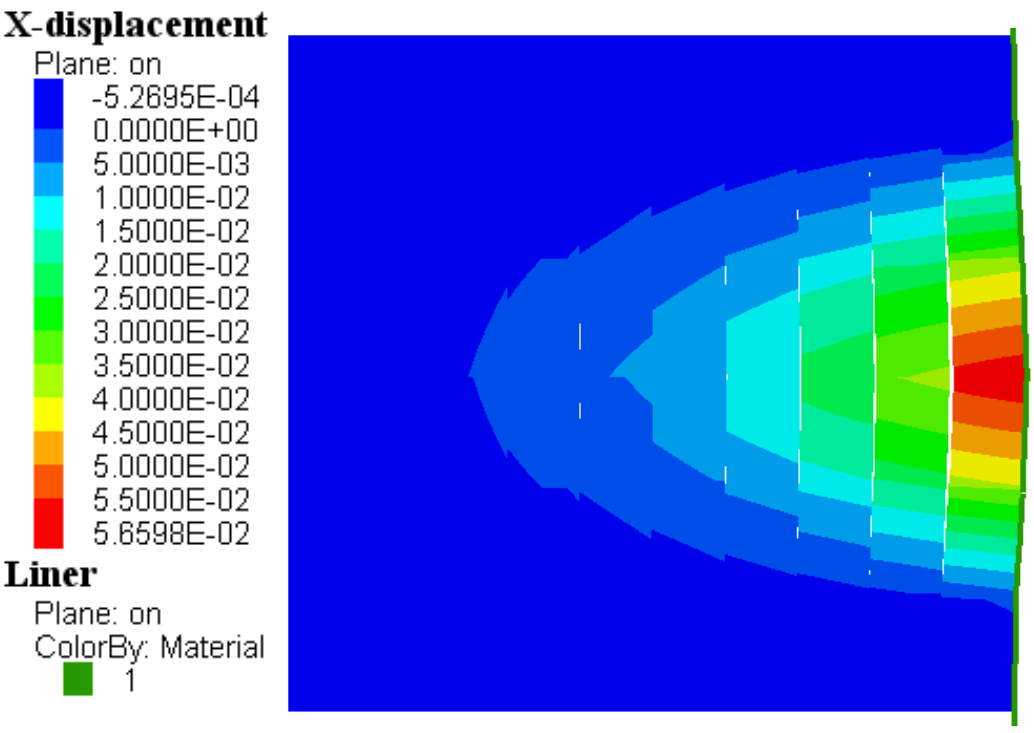

(b) With TSL

Figure 7. 2 The x displacement contours for model without TSL reinforcement (a), and with TSL reinforcement (b).

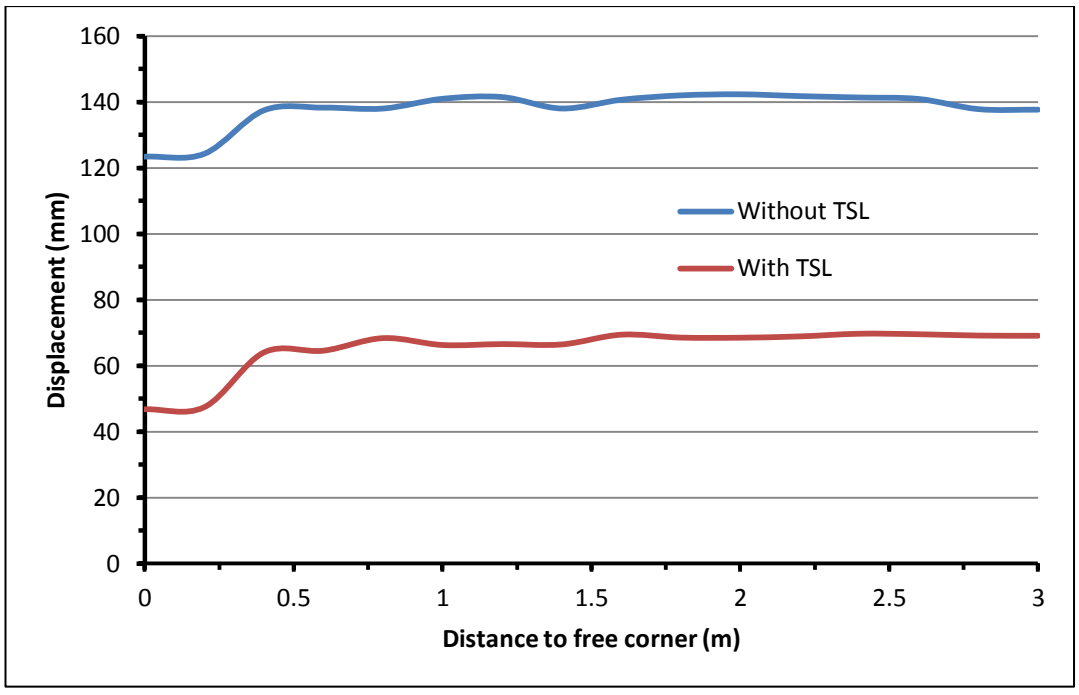

Figure 7.3 X displacement versus distance to the free corner at $x = 3$ m

7.5.2 Interpretations of modelled coal rib displacements

The displacement magnitude contours for models with and without TSL reinforcement are shown in Figure 7.4 where only the middle 1 m thick sections of each model are shown. It can be seen in Figure 7.4 that without TSL reinforcement, the maximum displacement at the pillar corner was approximately 178 mm, while with TSL reinforcement the maximum displacement was much lower at approximately 66 mm.

Form Figure 7.4(a), it is clear that the largest displacement occurred at the free unreinforced corner (shown in colours at the front of the cube) and as expected, the displacements gradually reduced towards the cube sides that were partially fixed in either *x* or *y* directions as shown in Figure 7.5(a) and (b). In contrast, it can be seen in Figure 7.4b that in the TSL reinforced pillar the largest displacement did not occur at the free corner or fixed sides but adjacent to the pillar corner. This effect occurred due to the confinement provided by TSL. The effect can be explained as follows: As the vertical stress σ_v increases, the pillar begins to deform.

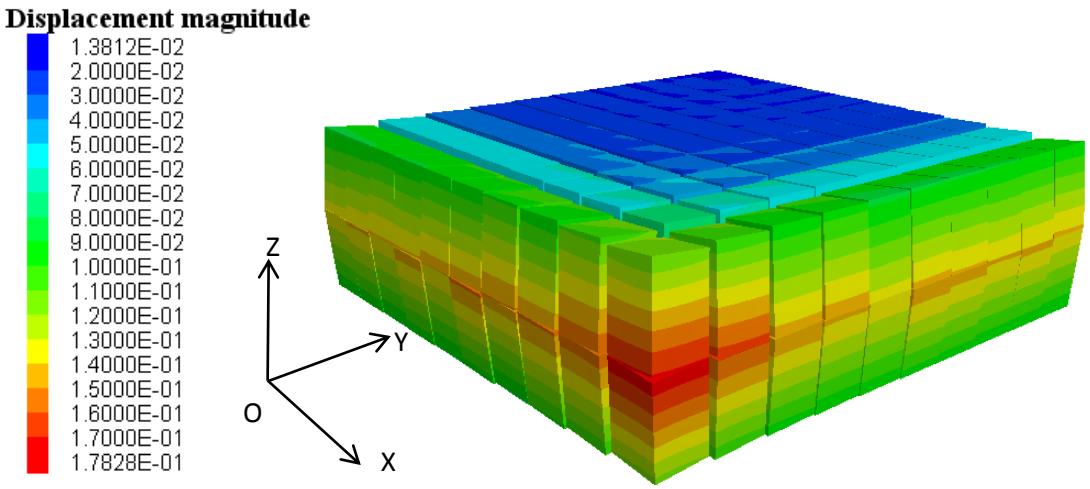

(a) Without TSL (z=1 to 2)
(x-fixed at x=0, y fixed at y=3)

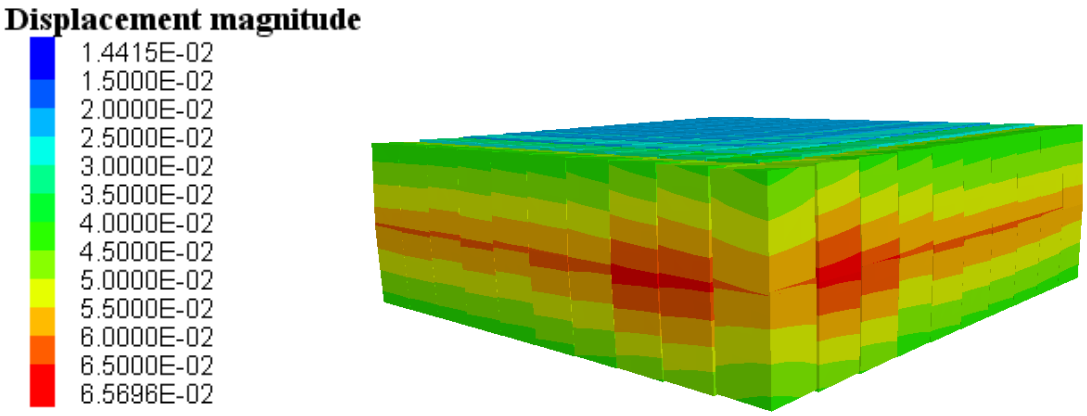

(b) With TSL (z=1 to 2)
(x-fixed at x=0, y fixed at y=3)

Figure 7.4 Modelled displacement contours without TSL reinforcement (a), and with TSL reinforcement (b)

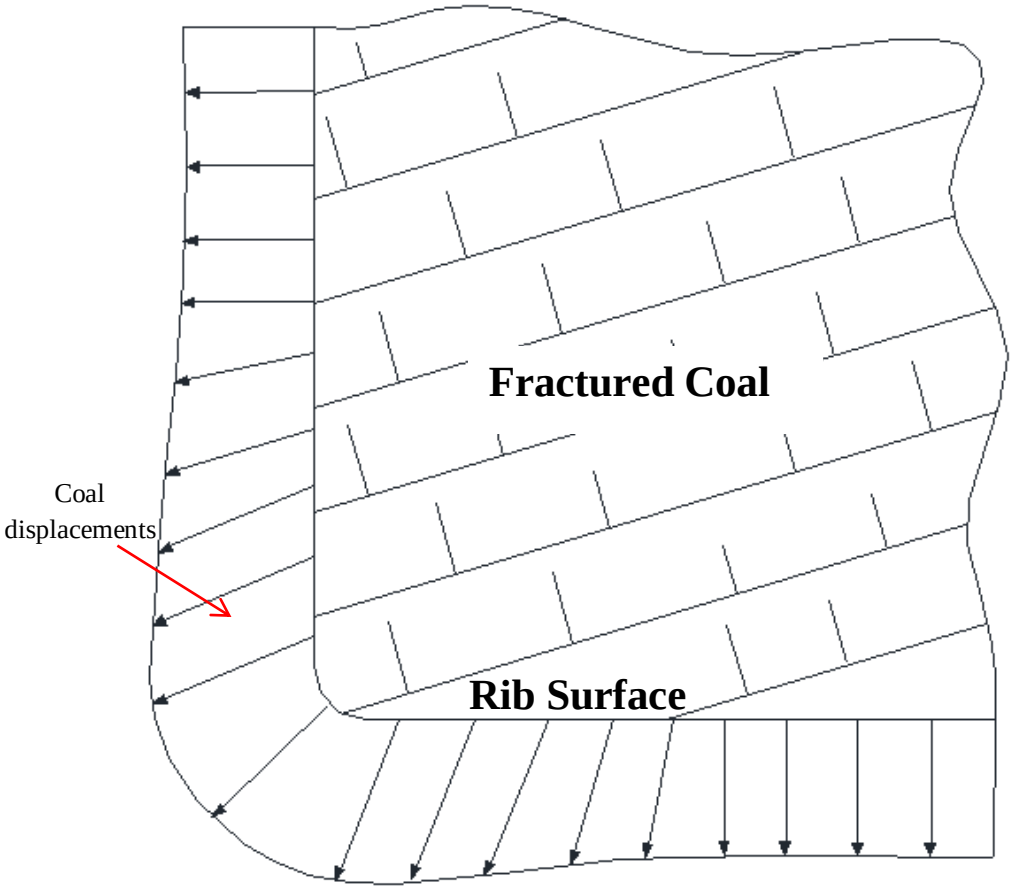

(a) Plan View

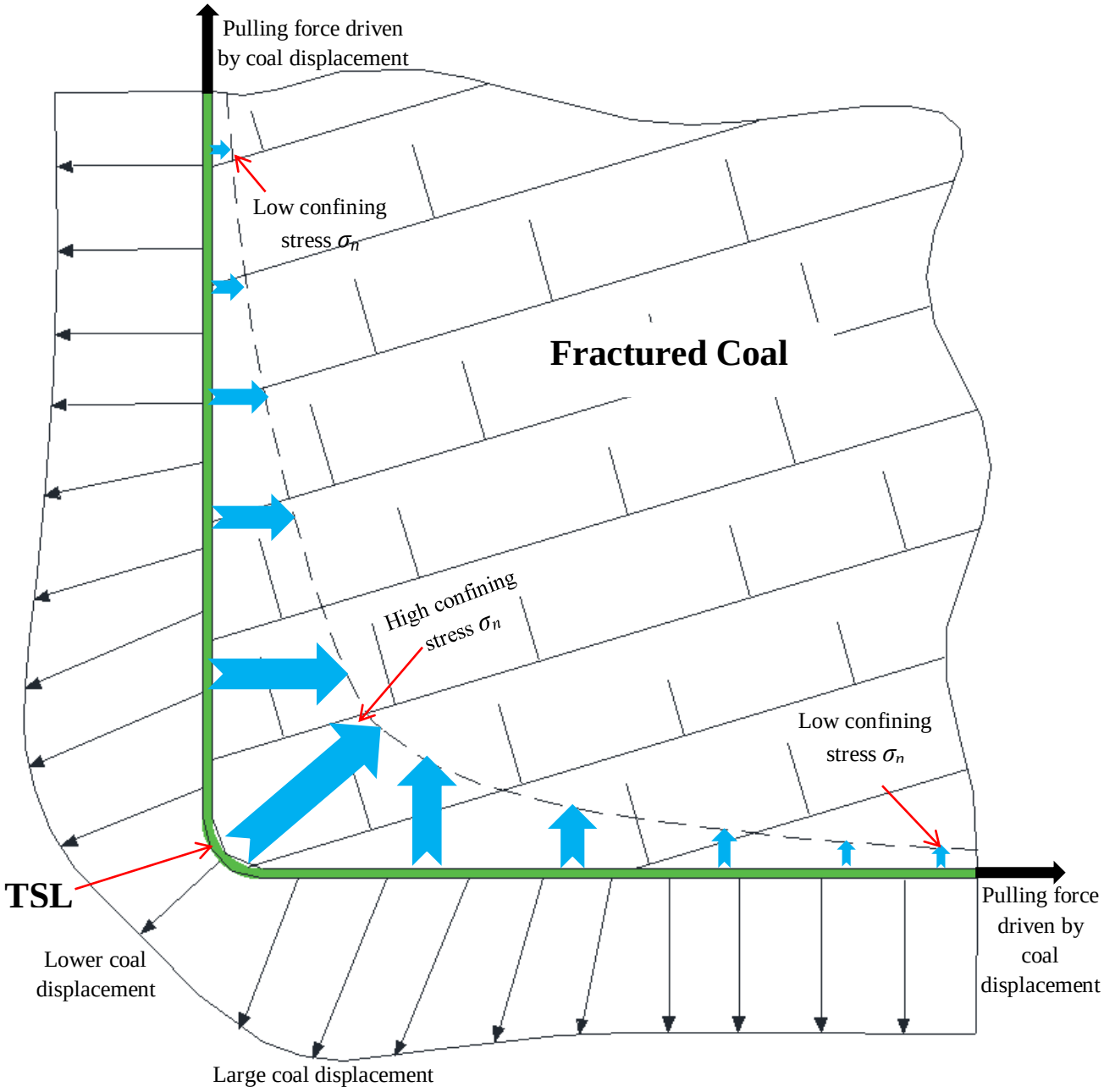

(b) Plan View

Figure 7.5 Schematic view of exaggerated rib displacements at the pillar corner (a) without TSL and (b) with TSL

At a considerable distance from the pillar corner the TSL material cannot effectively provide confinement to the coal rib that is being displaced at right angle to the rib surface. However, at the pillar corner the lateral stretching of the TSL at right angles can provide a significant normal stress σ_n to the coal surface thus reducing the amount

of coal displacement. The largest confining stress σ_n perpendicular to the TSL reinforced rib surface occurs at the corner and gradually reduces away from the corner as shown in the schematic diagram Figure 7.5(b). The modelled maximum displacement perpendicular to the coal rib shown in Figure 7.6 occurred within 0.5m-0.8m from the pillar corner.

The graphs plotted in Figure 7.7 and Figure 7.8 compare the *x*-displacements and the total displacements versus distance from the free corner without and with TSL reinforcement. The total displacement was approximately 1.4 times the x or y displacements at the free corner. Note that the maximum displacement vectors at the pillar corner rotate between the x and y axis (Figure 7.5) because total displacements are primarily made up of both x and y displacements that are symmetrical in both the x and y directions.

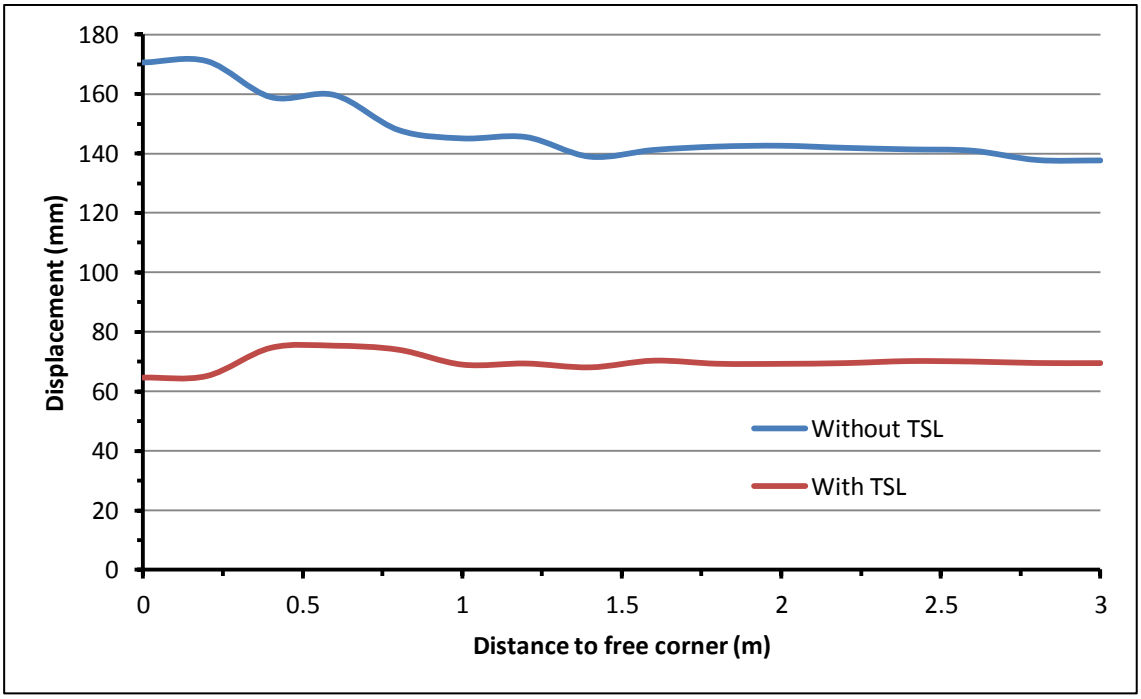

Figure 7.6 Rib displacements versus distance from free pillar corner

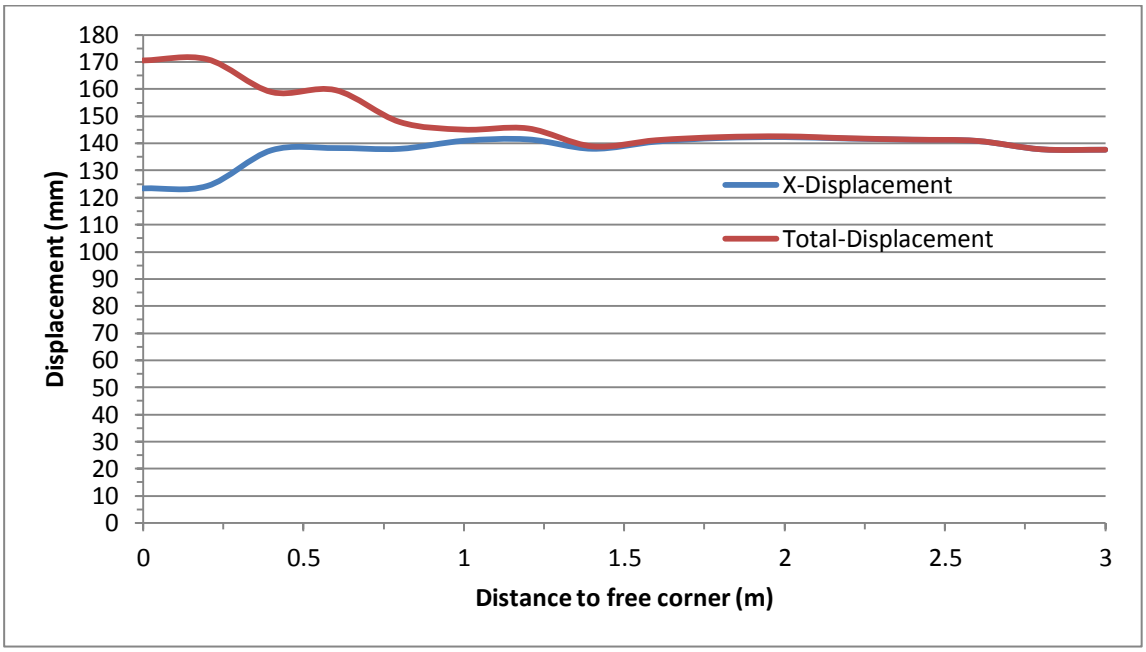

Figure 7.7 Comparison of *x* -displacement and total displacement at the rib side versus distance from free corner (without TSL reinforcement)

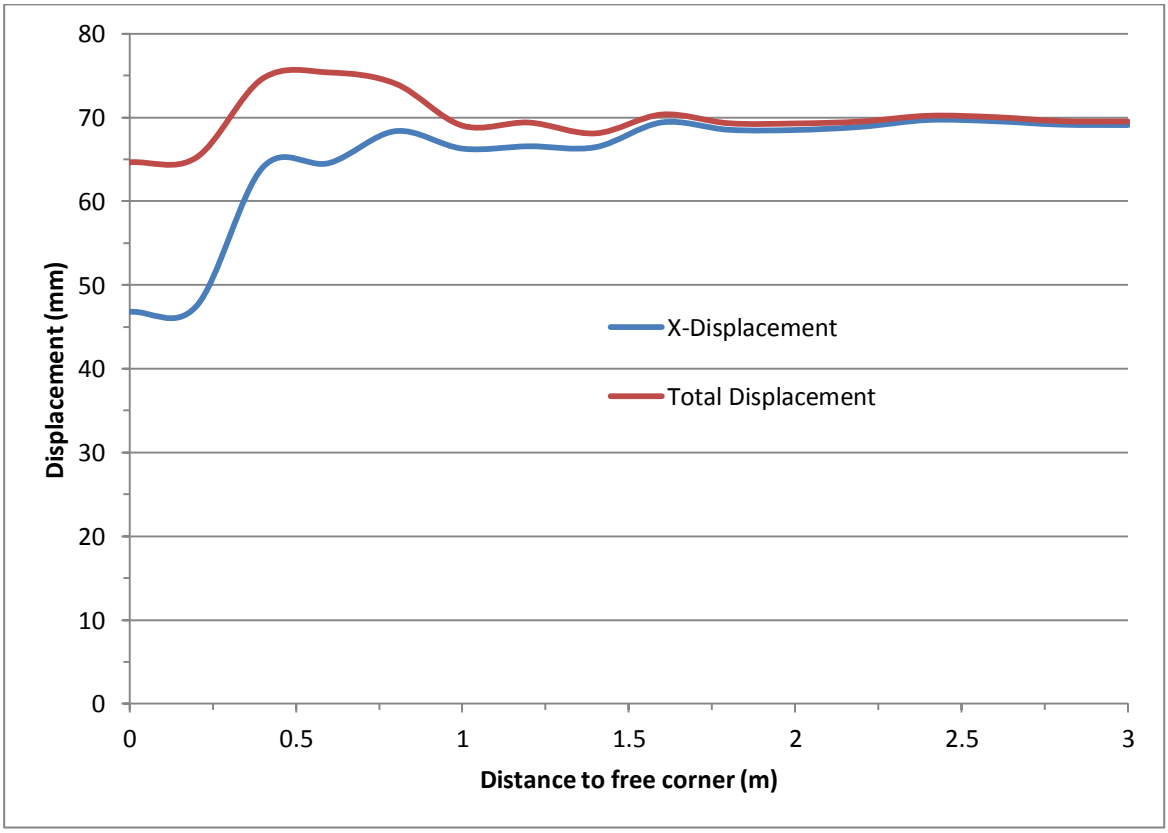

Figure 7.8 Comparison of *x* -displacement and total displacement at the rib side versus distance from free corner (with TSL reinforcement)

7.5.3 Stress Analysis

The modelled vertical stress σ_v along the diagonal between the free corner and the inner pillar (*x=0 m, y=3 m, z=1.5 m* to *x=3 m, y=0 m, z=1.5 m*) is plotted in Figure 7.9. Vertical stress (σ_v) in the model reinforced with TSL was higher than the (σ_v) without TSL reinforcement. This is due to TSL providing confining stress (σ_n) to the pillar surface, and thus TSL makes the pillar corners significantly stronger. At the pillar corner without TSL reinforcement, the vertical stress (σ_v) was around 1.3 MPa, while with TSL reinforcement the (σ_v) was higher at 20.3 MPa. The vertical stress (σ_v) distribution along the cross-section 1.5 m away from the corner is also presented in Figure 7.10.

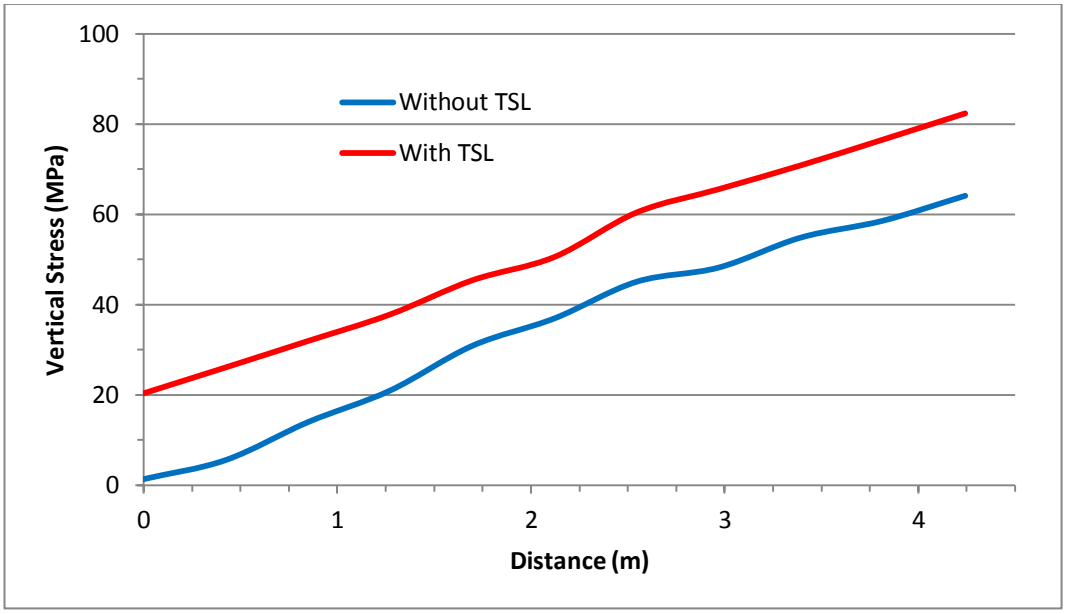

Figure 7. 9 Vertical stress (σ_v) distributions along diagonal between free pillar corner and the inner pillar

In this case the modelling results also show a similar trend to the previous case shown in Figure 7.9. At the unreinforced pillar surface 1.5m away from the corner the vertical stress (σ_v) was around 2.1 MPa while with TSL reinforcement the (σ_v) increased to 18.5 MPa. Therefore, from the modelling results it can be concluded that the TSL

material bonded to the coal pillar provides a very effective reinforcement especially at the corner of the coal pillar. This may minimise the roadway roof intersection spans and thus improve roof stability.

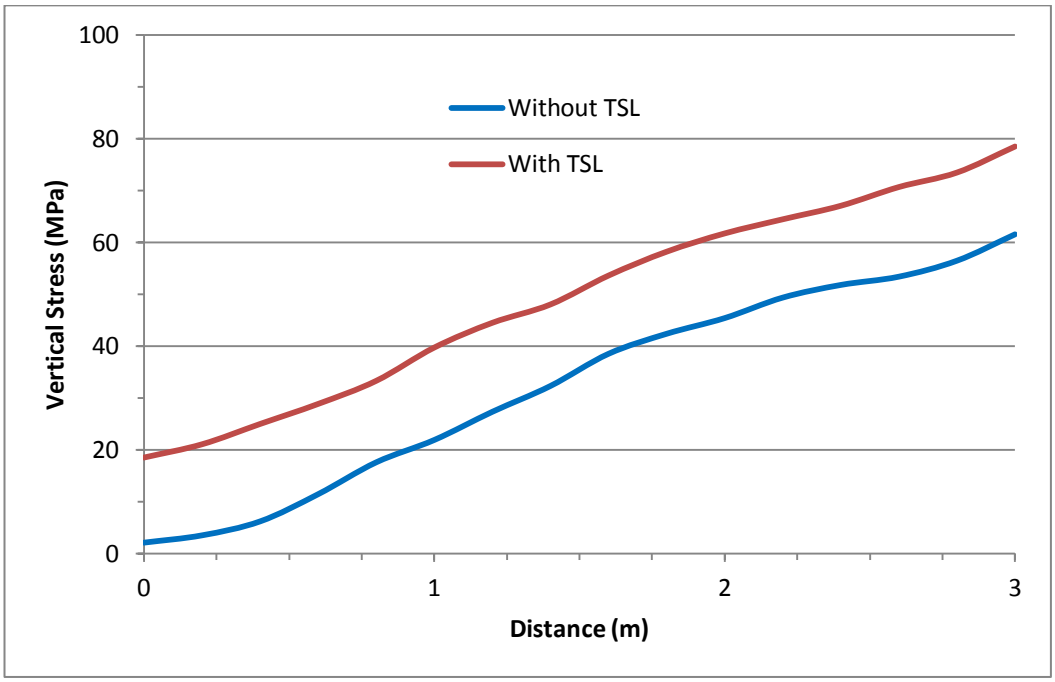

Figure 7.10 Vertical stress (σ_v) distributions along the cross-section 1.5 m away from the corner

7.6 Summary

With TSL reinforcement, the maximum displacement of the rib surface in the x direction 1.5 m away from the pillar corner was less than half the displacement at the same location of the unreinforced pillar rib. In addition, the maximum displacement in the x direction was reduced at the TSL reinforced pillar corner due to higher lateral confinement. The modelled maximum rib displacement (178 mm) in the diagonal direction at the unreinforced pillar corner was almost three times higher than that observed at the reinforced corner.

Vertical stress (σ_v) in the yielded part of the coal pillar reinforced with TSL was significantly higher than the (σ_v) in the unreinforced pillar. This is due to the effectiveness of the TSL generating confining stress at the pillar surface. Thus TSL makes the pillar significantly stronger especially at the pillar corner. This is important not only for pillar design and rib stability but also for minimising the roadway intersection spans and thus providing better roof stability above the intersections.

CHAPTER 8 CONCLUSIONS AND RECOMMENDATIONS

The following conclusions of the experimental and numerical analysis of TSL materials for use in underground mines were drawn:

8.1 Compressive strength testing of TSL materials

Currently there is no standard testing method to determine the compressive strength of TSL materials. A suitable comparative method of TSL compressive tests using cube samples 40 mm in size was developed for low glass fibre content as discussed in Chapter 3. Although suitable, this method needs to be revised to enable testing the sprayed product with higher fibre content.

8.2 Shear strength testing of TSL materials

A shear punch strength testing method was developed to determine the glass fibre reinforced TSL materials' shear strength with details presented in Chapter 3. Adopted from the commonly used fast resin strength testing method, this testing procedure is simple allowing easy preparation of TSL samples with fast testing procedure and cost reduction. In addition, it can ensure stable and symmetrical loading thereby improving the accuracy of testing results. This test is an essential part in determining the overall TSL strength and therefore is recommended to be used as one of the standard procedures in future developments and routine testing of TSL products.

8.3 Shear bond strength testing of TSL materials

Numerous TSL shear bond strength testing procedures have been developed and reported in the past. Most of these tests did not provide the unconfined strength of the

shear bond values. In this research detailed in Chapter 4, three new testing methods were trailed in order to develop an easy and quick method of testing to evaluate the unconfined shear bond strength of TSL materials. The first was the double sided shear test where the 5 mm thick TSL layer was bonded between three rock cubes 40 mm in size. The outside cubes were fixed while the central cube was loaded until the sample failed in shear. In the second test a 5 mm thick TSL ring was bonded to the cylindrical rock sample and stripped using a steel cylindrical sleeve. The third test was similar to the second test except that the TSL was partitioned into four segments. The first test failed to deliver the unconfined shear bond strength of the TSL as the TSL bond was too strong and in most cases the shear failure propagated through the rock. All double shear test results were inconclusive. In the TSL full ring shear tests, the polymer always failed in tension caused mainly by resin shrinkage during the curing process and partly due to the Poisson's ratio effect when loaded. The tension that developed within the TSL rings applied a normal stress to the bond interface and therefore would have increased the measured shear stress. For this reason this test failed to give the true unconfined shear bond strength and therefore is not recommended. In the third test where the partitioned TSL ring was sheared off the cylindrical sample, reliable shear bond results were obtained. This shear bond procedure has proven to be consistent producing true unconfined shear bond strength for all tested rock types. The test results indicate that the third testing method is an effective testing approach that has a lot of advantages including simple, quick and repeatable tests and calculations and therefore is recommended as a future TSL testing procedure.

8.4 Tensile bond strength testing of TSL materials

The modified TSL tensile bond test used for this research involved pulling the bonded TSL material directly from the rock surface. This procedure detailed in Chapter 4 was based on earlier tests used by other researchers. The test results indicate that for lower loading rates from 0.5 mm/min to 2 mm/min, the effect of loading rates can be ignored while for higher loading rates of up to 10 mm/min, the tensile bond strength increased with the increase of loading speed. The data indicate that the tensile bond strength of the polyester-based TSL material is inversely proportional to the square root of the TSL material thickness. The results indicated that the two TSL prototypes developed at the University of Wollongong bonded strongly to the substrate materials under wet, dry or dirty bond surface conditions. On the whole, these results indicate quick, consistent and repeatable results and therefore this procedure of testing is recommended for future studies.

8.5 Direct shear tests of joints infilled with TSL

The direct shear test procedure using the constant normal stiffness method of loading and shearing TSL infilled planes with casted asperities in high strength plaster (60 MPa) as described in Chapter 5. The method was based on the numerous rock joint studies conducted at the University of Wollongong laboratory. The TSL material was bonded to the high strength plaster asperities prior to shearing. The tests showed that the TSL-plaster interface did not debond but failure propagated through the high strength plaster material at a low angle of approximately 30° to the shear load direction. The data show that despite the failure within the plaster, the angle of the TSL infilled asperities affect the behaviour of the samples. The results presented in this study reveal

that as expected the shear strength of the polymeric TSL - plaster composite increased with the applied normal stress for the three asperity types used. The shear strength decreased with the increase of the TSL infill thickness to asperity height ratio. The investigation also shows that the increase in shear rate decreased the shear strength but that may not be an issue in Australian underground coal mines with predominantly low shear displacement rates. When subject to high normal loads the joint roughness had little effect on the shear stress while for lower confinement the difference in roughness provided slightly higher shear strength of the TSL-plaster composite.

Future studies using rock material should be undertaken to confirm the results presented here. This study has measured shear strength of the TSL-plaster composite subject to changes in joint properties. Understanding of joint reinforcement is essential in future studies of the TSL material reinforcing the fractures within the rock skin.

8.6 Pillar rib reinforcement with TSL

The detailed procedure of this test involving TSL coating of the cylindrical sample and loading procedures are presented in Chapter 6. The size of tested samples may not represent the large scale small pillar behaviour experienced underground however, the support mechanism of TSL coated materials are similar. Three types of typical rock with and without the TSL encapsulation were tested in compression. Results of rock failure tests indicated that significant strength improvement and enhancement of post failure characteristics developed for the TSL encapsulated samples. It can be concluded that TSL material can be used to effectively reinforce the modelled rock samples. While the rock has failed predominantly in shear, the TSL material failed in tension due to the lateral expansion of the failed samples. The tests indicate that the

effectiveness of the TSL reinforcement varies with the rock type. The TSL reinforcement of the weaker rocks appears to be better than reinforcement of the stronger rocks. Therefore, the TSL material is more appropriate to reinforce the weaker rock with low compressive and tensile strength. Typically, the sedimentary strata found in underground coal mines are best suited for TSL applications to control the rock surface failure.

Significant improvements can be expected in roof and rib stability, pillar strength, stability of pillar corners to minimise roof spans at the roadway intersections and thus improve intersection stability. TSL applications in underground mines are needed to monitor the TSL performance to verify the outcomes of this research. At the time of writing the tested TSL prototypes were not approved for underground use therefore the *in situ* TSL effectiveness to support the pillar ribs could not be tested. It is recommended that this be done once the TSL material is approved.

8.7 Numerical study on the coal pillar roadway corner

A 3-dimensional numerical model was used to simulate the TSL reinforcement of coal pillar corner with and without the TSL reinforcement. The simulations show that the modelled maximum displacement of the unreinforced pillar corner was almost three times higher than that observed at the TSL reinforced corner. In contrast, in the TSL reinforced pillar the largest displacement did not occur at the pillar corner but adjacent to the corner. This effect occurred due to the confinement provided by TSL. The effect can be further explained as follows: As the vertical stress increased, the pillar began to deform. At a considerable distance from the pillar corner the TSL material cannot effectively provide normal confinement to the coal rib that is being displaced at right

angle to the rib surface. However, at the pillar corner the lateral stretching of the TSL at right angles can provide a significant normal stress to the coal surface thus reducing the amount of coal displacement.

Vertical stress in the yielded part of the coal pillar reinforced with TSL was significantly higher than vertical stress in the unreinforced pillar. This is due to the effectiveness of the TSL generating confining stress at the pillar surface. Thus TSL makes the pillar rib significantly stronger especially at the pillar corner. This is important not only for the pillar design and rib stability but also for minimising the roadway intersection spans and thus providing better roof stability above the intersections.

8.8 Recommendations for future research

Suggested future research can focus on the following aspects:

(a) A revised compressive strength testing method needs to be developed to enable test the sprayed product with higher fibre content.

(b) Underground spray test needs to be conducted to determine the *insitu* tensile bond strength of TSL to coal or rock after sprayed.

(c) TSL applications in underground mines are needed to monitor the TSL performance to verify the outcomes of pillar reinforcement.

REFERENCES

ACARP (2012) ToughSkin Project Review Meeting.

ACARP (2014) ToughSkin Project Review Meeting.

Archibald J. (1992) Assessment of wall coating materials for localized wall support in underground mines. Report of Phase 4 Investigations for the Mining Industry Research Organization of Canada. 34 pp.

Archibald J. (2004) Canadian laboratory and field testing. In: Potvin Y, Stacey TR and Hadjigeorgiou J (eds). Surface Support in Mining. Australian Center for Geomechanics. pp: 135-139.

Archibald J. (2001) Assessing acceptance criteria for and capabilities of liners for mitigating ground falls. Mining Health and Safety Conference, Sudbury, Ontario, 31 pp.

ASTM D412-06a. (2013) Standard Test Methods for Vulcanized Rubber and Thermoplastic Elastomers—Tension, ASTM International, West Conshohocken, PA.

ASTM D638-14. (2014) Standard Test Method for Tensile Properties of Plastics, ASTM International, West Conshohocken, PA.

ASTM D7012-10. (2010) Standard Test Method for Compressive Strength and Elastic Moduli of Intact Rock Core Specimens under Varying States of Stress and Temperatures, ASTM International, West Conshohocken, PA.

Coates, DF. (1970) Rock Mechanics Principles, Mines Branch Monograph 874 (Revised 1970), Department of Energy, Mines and Resources, Canada.

Dear, AW. (2010) Analysis of the mechanical properties of Polymer Thin Spray on Liners and their effective support in underground mining. BE Mining Thesis, University of Wollongong, New South Wales, Australia.

Espley-Boudreau SJ. (1999) Thin spray-on liner support & implementation in the hard rock mining industry. M.Sc Thesis, Laurentian University, School of Engineering, Sudbury, Ontario.

Finn D, Teasdale P and Windsor C. (1999) *In situ* trials and field testing of two polymer restraint membranes. Rock support and reinforcement practice in mining, Balkema, Rotterdam. pp:139-153.

Fowkes N, de Freitas JAT and Stacey R. (2008) Crack repair using an elastic filler. Journal of the Mechanics and Physics of Solids. 56(9):2749-2758.

Hadjigeorgiou J and Grenon M. (2002) Towards a rational design methodology for thin sprayed on liners. Proceedings of 2nd International Seminar on Surface Support Liners: Thin Sprayed Liners, Shotcrete, Mesh. Sandton, South Africa, Section 12; pp. 1-16.

Hoek E and Brown ET. (1980) Underground excavations in rock. Institute on Mining and Metallurgy, London, England.

Itasca (2007). 3DEC - 3 Dimensional Distinct Element Code. Version 4.10, Itasca Consulting Group, Inc.

Jaeger JC, Cook NG and Zimmerman R. (2009) Fundamentals of rock mechanics: John Wiley & Sons.

Kendall K. (1971) The adhesion and surface energy of elastic solids. Journal of Physics D: Applied Physics. 4(8):1186-1195.

Kuijpers J. (2004) Evaluation of thin spray-on liners support behaviour. In: Potvin Y, Stacey TR and Hadjigeorgiou J (eds). Surface Support in Mining. Australian Center for Geomechanics. pp:103-112.

Kuijpers J and Toper A. (2004) Model of TSL behaviour under punch-through conditions. In: Potvin Y, Stacey TR and Hadjigeorgiou J (eds). Surface Support in Mining. Australian Center for Geomechanics. pp:113-118.

Lacerda L and Rispin M. (2002) Current ground support membrane applications in North American underground mines. 2nd International Seminar on Surface Support Liners: Thin Sprayed Liners, Shotcrete, Mesh. Sandton, South Africa, Section 7.

Lau V, Saydam S, Cai Y and Mitra R. (2008) Laboratory investigation of support mechanism for thin spray-on liners. The 12th Int Conf of International Association for Computer Methods and Advances in Geomechanics (IACMAG). Goa, India. pp. 1381-1388.

Mason D, Stacey T. (2008) Support to rock excavations provided by sprayed liners. International Journal of Rock Mechanics and Mining Sciences. 45(5):773-88.

Mirsepassi, N. (2013) Roof and rib buckling experiment of fibre reinforced polymer lining for use in underground coal mines. Master Thesis, University of Wollongong, New South Wales, Australia.

Mirzaghorbanali A, Nemcik J, Aziz N. (2014a) Effects of cyclic loading on the shear behaviour of infilled rock joints under constant normal stiffness conditions. Rock mechanics and rock engineering. 47(4):1373-91.

Mirzaghorbanali A, Nemcik J, Aziz N. (2014b) Effects of shear rate on cyclic loading shear behaviour of rock joints under constant normal stiffness conditions. Rock Mechanics and Rock Engineering. 47(5):1931-8.

Nemcik J, Porter I, Baafi E. (2013a) Tear tests of glass fibre reinforced polymer skin spray-on liner. Proceedings of 13th Coal operator's Conference. Wollongong, Australia, pp. 170-175.

Nemcik J, Baafi E and Porter I. (2013b) Stabilising rock surfaces with a glass reinforced polymer skin. Acta Geodyn Geomater. 10(2):207-13.

Nemcik J, Porter I, Baafi E and Towns J. (2011a) Bearing capacity of a glass fibre reinforced polymer liner. Proceedings of 11th Coal operator's Conference. Wollongong, Australia, pp. 148-153.

Nemcik J, Porter I, Baafi E and Navin J. (2011b) Determining the ultimate strength of'tough skin', a glass fibre reinforced polymer liner. Proceedings of 11th Coal operator's Conference. Wollongong, Australia, pp. 154-158.

Nemcik, J. (2014) Stress in Underground Mines. Lecture notes distributed for MINE323 Mining GeoMechanics.

Ozturk H. (2012) Work of adhesion of thin spray-on liners. Rock mechanics and rock engineering. 45(6):1095-102.

Ozturk H. (2012) Fracture mechanics interpretation of thin spray-on liner adhesion tests. International Journal of Adhesion and Adhesives. 34:17-23.

Ozturk H and Tannant D. (2004) Influence of rock properties and environmental conditions on adhesive bond to a thin liner. In: Potvin Y, Stacey TR and Hadjigeorgiou J (eds). Surface Support in Mining. Australian Center for Geomechanics. pp:135-9.

Ozturk H and Tannant D. (2010) Thin spray-on liner adhesive strength test method and effect of liner thickness on adhesion. International Journal of Rock Mechanics and Mining Sciences. 47(5):808-15.

Ozturk H and Tannant D. (2011) Influence of rock properties and environmental conditions on thin spray-on liner adhesive bond. International Journal of Rock Mechanics and Mining Sciences. 48(7):1196-8.

Peng SS. (1978) Coal mine ground control.

Saiang D, Malmgren L and Nordlund E. (2005) Laboratory tests on shotcrete-rock joints in direct shear, tension and compression. Rock mechanics and rock engineering. 38(4):275-97.

Saydam S, Yilmaz H and Stacey T. (2003) A new testing approach for thin spray-on liners: double-sided shear strength (DSS) test. The 3rd International Seminar on Surface Support Liners: Thin Spray-On Liners, Shotcrete and Mesh. SAIMM, Sandton, South Africa, Section 18.

Shan Z, Porter I, Nemcik J and Baafi E. (2014a) Comparing the reinforcement capacity of welded steel mesh and a thin spray-on liner using large scale laboratory tests. International Journal of Mining Science and Technology. 24(3):373-7.

Shan Z, Porter I, Nemcik J and Qiao Q. (2014b) Effect of different curing conditions on the compressive and flexural properties of Plaster of Paris. Proceedings of 14th Coal operator's Conference. Wollongong, Australia, pp. 103-108.

Singh RN and Ghose AK. (2006) Engineered rock structures in mining and civil construction: CRC Press.

Spearing A and GelsonJ. (2002) Developments and the future of thin reactive liners since the previous conference in Australia. The 2nd International Seminar on Surface Support Liners: Thin Sprayed Liners, Shotcrete, Mesh. SAIMM, Sandton, South Africa, Section 13.

Rolls, B. (2008) Polymer based alternatives to skin reinforcement in underground excavations, BE Mining Thesis, University of Wollongong, New South Wales, Australia.

Stacey T. (2001) Review of membrane support mechanisms, loading mechanisms, desired membrane performance, and appropriate test methods. JOURNAL-

SOUTH AFRICAN INSTITUTE OF MINING AND METALLURGY. 101(7):343-52.

Stacey T and Yu X. (2004) Investigations into mechanisms of rock support provided by sprayed liners. Ground support in mining and underground construction London: Taylor and Francis. pp:563-569.

Swan G and Henderson A. (1999) Water-based Spray-on liner implementation at Falconbridge Limited. Proceedings CIM/AGM, Calgary.

Tannant D. (1995) Load capacity and stiffness of welded-wire mesh. Proceedings of the 48th Canadian Geotechnical Conference.

Tannant D. (2001) Thin spray-on liners for underground rock support—testing and design issues. The 1st International seminar and field trials on surface support liners: membrane, shotcrete and mesh, Perth, Australia, Section 27, Australia Centre for Geomechanics, 22p.

Tannant D, Kaiser P and Maloney S. (1997) Load—displacement properties of welded—wire, chain—link and expanded metal mesh. International symposium on rock support: applied solutions for underground structures, Lillehammer, Norwegian Society for Charted Engineers, Norway. pp: 651-659.

Tannant D and Ozturk H. (2003) Evaluation of test methods for measuring adhesion between a liner and rock. Proceedings of 3rd international seminar on surface support liners: Thin Spray-On Liners, Shotcrete and Mesh. Quebec City, Canada, Section 13.

Tannant D, Swan G, Espley S and Graham C. Laboratory test procedures for validating the use of thin sprayed-on liners for mesh replacement. Canadian Institution of Mining and Metallurgy Annual Meeting, Calgary, published on CD-Rom, 8p.

Villaescusa, E. (2004) Weld mesh for static rock support in Australia. Surface Support in Mining, by Australia Centre for Geomechanics, Chapter 44, pp: 385-390.

Yang F and Li J. (2001) Adhesion of a rigid punch to an incompressible elastic film. Langmuir. 17(21):6524-9.

Yilmaz H. (2007) Shear-bond strength testing of thin spray-on liners. Journal of the South African Institute of Mining and Metallurgy. 107(8):519-30.

Yilmaz H. (2009) Comparison of mechanical properties of shotcrete and thin spray-on liner (TSL). ITA, SAIMM, and SANCOT:'Shotcrete for Africa'2nd. pp:251-65.

Yilmaz H. (2013) Comparison of tensile-bond strength of thin spray-on liners. International Journal of Mining, Reclamation and Environment. 27(1):56-71.